Investigating genetic modifiers of Huntington's disease using *Drosophila melanogaster*

Freja Mae Sadler

A thesis submitted to Cardiff University for the degree of
Doctor of Philosophy

June, 2022

Acknowledgements

I would like to sincerely thank my amazing team of supervisors; Lesley Jones, Gaynor Smith and Thomas Massey. Gaynor, your energy and enthusiasm for science is contagious and kept me going over the years. Tom, I have really valued your guidance and your never-ending list of interesting ideas which I wished I had the time to complete. Lesley, I have truly appreciated your support throughout my PhD, especially during the hard months of the national lockdown and some really tough times, you will be sorely missed.

I would also like to thank the UK Dementia Research Institute for funding my PhD studentship and for the opportunities to present my research across the centres at Connectome and ECR events. There are so many people in the Cardiff UK DRI that have made my experience unforgettable, but to keep it brief I want to thank Florence and Emma for always bringing out my loudest laughs.

Leo, you know I wouldn't have gotten to the stage I did without all of your help in the lab, I am extremely grateful for your invaluable help and advice. A special thank you to everyone else in the fly lab (past and present) for listening to my silly rants; Freya, Eilish, Andrew, Hannah, Dan, Uroosa, Peta, Louise and Bilal. A big thank you goes to the members of the Jones/Massey lab (past and present), for all of the help finding reagents and teaching me so much over the years; Joe, Jasmine, Lyn, Bran, Laura, Caroline, Ant and Sergey.

Special thanks to all of my friends and family near and far for the support and fun distractions from thesis-writing. A massive thank you to my parents for always believing in me and most importantly, for letting me move back in with them when my funding ran out. Finally, the biggest thank you goes to my Tom. Despite the pandemic and long-distance you have been a constant source of love and support which I couldn't have managed without. Thank you for everything.

Thesis summary

Huntington's disease is an autosomal dominant neurodegenerative disease which is caused by the pathological expansion of the CAG repeat tract in the huntingtin gene (*HTT*). The age at which symptoms onset is inversely correlated with the CAG repeat tract length, but other factors such as genetic variation can also influence the onset. Genome-wide association studies have identified genetic variants in the loci of genes that function in DNA damage responses. Specifically, genes associated with the DNA mismatch repair pathway and DNA interstrand cross-link repair are thought to affect the age of onset by somatically expanding the CAG repeat tract. However, CAG repeat expansion is not the only driver of disease progression with other potential modifiers being missed by the GWAS.

This thesis demonstrates that *Drosophila melanogaster* pan-neuronally expressing mutant human *HTT* exhibit shortened lifespans, locomotor deficits, HTT aggregation and neurodegeneration. There was no evidence of somatic instability of the CAG repeat tract in *HTT* expressed in *Drosophila* neurons, which meant potential modifiers of HD could be investigated without the having to consider CAG repeat instability. Potential genetic modifiers of the locomotor phenotype were screened and *Parp* knockdown significantly improved the locomotor performance of mutant *HTT* expressing flies. Parp knockdown and inhibition was characterised further in the different *Drosophila* models of HD it was established that reducing *Parp* expression and inhibiting Parp with pharmacological inhibitors ameliorated lifespan, locomotor and HTT aggregation phenotypes. The results suggest a potentially promising future for PARP1 inhibition in HD treatment.

List of abbreviations

AD – Alzheimer's disease

AGO2 – Argonaute 2

AIF – apoptosis inducing factor

AMO – age at motor onset

AMPAR - α-amino-3-hydroxy-5-methyl-4-isoxazole-propionic acid receptors

ASO – Antisense oligonucleotide

ATM – ataxia-telangiectasia mutated

ATP – adenosine triphosphate

BDNF – brain derived neurotrophic factor

BER – Base excision repair

Ca^{2+} – calcium ions

CAA – cytosine-adenine-adenine trinucleotide

CAG – cytosine-adenine-guanine trinucleotide

CBP – CREB binding protein

CFP – cerulean fluorescent protein

CREB – cAMP response element-binding protein

CSF – cerebrospinal fluid

DDR – DNA damage response

DNA – deoxyribonucleic acid

DPE – days post eclosion

DSB – DNA double strand break

ER – Endoplasmic reticulum

EXO1 – exonuclease 1

FANCD1 – Fanconi anaemia complementation group D1

FAN1 – FANCI associated nuclease 1

GABA – Gamma Aminobutyric Acid

GFP – green fluorescent protein

GPe – external globus pallidus

GPi – internal globus pallidus

GWAS – genome-wide association study/studies

HAT – histone N-acetyltransferase

HD – Huntington's disease

HEAT – Huntingtin, elongation factor 3, protein phosphatase 2A and TO1

HTT – human huntingtin gene

HTT – human huntingtin protein

Htt – Drosophila huntingtin gene

Htt – Drosophila huntingtin protein

*HTT*16QFL – full-length human huntingtin transgene with 16 CAGs

*HTT*128QFL – full-length human huntingtin transgene with 128 CAGs

*HTT*0Qtrunc – truncated human huntingtin transgene with 0 CAGs

*HTT*128Qtrunc – truncated human huntingtin transgene with 128 CAGs

*HTT*25QCFP – truncated human huntingtin transgene with a cerulean fluorescent tag and 25 CAGs

*HTT*96QCFP – truncated human huntingtin transgene with a cerulean fluorescent tag and 96 CAGs

*HTT*15QmRFP – truncated human huntingtin transgene with a monomeric red fluorescent tag and 15 CAGs

*HTT*138QmRFP – truncated human huntingtin transgene with a monomeric red fluorescent tag and 138 CAGs

ICC – immunocytochemistry

IHC – immunohistochemistry

iPSCs – induced pluripotent stem cells

LIG1 – DNA ligase 1

LIG3 – DNA ligase 3

m*HTT* – mutant huntingtin gene

mHTT – mutant huntingtin protein

MIF – migration inhibitory factor

MLH1 – MutL homolog 1

MLH3 – MutL homolog 3

MMR – Mismatch repair

MRE11 – meiotic recombination 11

mRFP – monomeric fluorescent protein

MRI – Magnetic resonance imaging

MSH2 – MutS homolog 2

MSH3 – MutS homolog 3

MSH6 – MutS homolog 6

MSN – medium spiny neuron

NAD$^+$ – nicotinamide adenine dinucleotide

NER – nucleotide excision repair

NHEJ – non-homologous end-joining

NMDA – N-methyl-D-aspartate

Ns – not significant

PAR – poly ADP ribose

PARP1 – poly ADP ribose polymerase 1

PARG – poly ADP ribose glycohydrolase

PCM1 – pericentriolar material 1

PCNA – proliferating cell nuclear antigen

PD – Parkinson's disease

PGC1α - peroxisome proliferator-activated γ-coactivator 1α

PMS1 – protein homolog 1

PMS2 – protein homolog 1

Poly-Q – poly-glutamine

Polβ - DNA polymerase β

Polδ – DNA polymerase δ

Polϵ – DNA polymerase ϵ

PRD – proline rich domain

PTM – post-translational modification

PTP – permeability transient pores

Q – glutamine

RING – rapid iterative negative geotaxis

RIPK – receptor-interacting kinase

RNA – ribonucleic acid

RNAi – RNA interference

ROS – reactive oxygen species

RPA – Replication protein A

SCA3 – spincerebellar ataxia 3

SH3 domain

SNP – single polynucleotide polymorphisms

SNpc – substantia nigra pars compacta

SNpr – substantia nigra pars reticular

SSB – DNA single strand break

TLR – toll-like receptor

TOP1 – topoisomerase 1

TRIAD – transcriptional repression-induced atypical death

UAS – upstream activating sequence

Ub – ubiquitin

UPS – ubiquitin proteasome system

WT – wild-type

WW-domain

XRCC1 – X-ray repair cross-complementing protein 1

YAP – Yes-associated protein

YAP_N – neuron-specific Yes-associated protein

ZF – Zinc finger domain

Table of Contents

List of Figures

List of Tables

1. General Introduction

1.1 Background

1.1.1 History

Huntington's disease (HD) was first fully described by George Huntington in 1872, who detailed the "chorea" and hereditary nature of the disease (Huntington 1872). He described the progressive nature of the disease, initially starting with "slight twitchings" in the face muscles that increases with intensity and variety over time. He also referenced the changes to a patient's mental health as "insanity that leads to suicide", connecting the disease progression with depression and mood changes. A more detailed description was published by Charles Davenport in 1916, in a report for the US eugenics office (Davenport and Muncey 1916). It contained complete descriptions of the traits and symptoms of the disease, as well as referencing that "half the children" inherit the disease (autosomal dominance). He also described that behavioural changes often occurred prior to the motor symptoms. While it had been described in these reports, the autosomal dominant nature of the disease was confirmed over 50 years later (Hayden 1983) along with the mapping of the disease-causing gene (Gusella et al. 1983). It was mapped to the short arm of chromosome 4, but the exact sequence was unknown. It was 10 years later and with a massive communal effort that the huntingtin gene (*HTT*) and its CAG repeat tract was fully identified (The Huntington's Disease Collaborative Research Group 1993). This exciting new finding meant that people at risk could be given a pre-manifest diagnosis. The discovery of the *HTT* sequence instigated the beginnings of a new avenue of HD research that would become the work that we know of today.

1.1.2 Epidemiology

Huntington's disease proportionally affects European/Caucasian populations at higher frequencies than Asian and African populations. Data from a meta-analysis estimated that HD had a prevalence of 5.7 diagnoses per 100,000 people in European, North American and Australian populations in comparison to 0.40 per 100,000 in Asian populations (Pringsheim et al. 2012). The length of the CAG repeat tract in the *HTT* gene on average is longer in the European populations in comparison to the Asian and African populations (Squitieri et al.

1994). However, there are areas of the world which have a particularly high prevalence of HD, such as in Venezuela where hundreds of patients can be related to one ancestor (Wexler et al. 2004). The UK has a higher HD diagnosis frequency than average with a prevalence of 12.3 diagnoses per 100,000 (Evans et al. 2013), as does the US with prevalence of 12.7 diagnoses per 100,000 (Yohrling et al. 2020). The frequency of HD diagnoses has increased with time. In the UK alone the number of HD diagnoses doubled from 5.4 per 100,000 in 1990 to 12.3 per 100,000 in 2010 (Evans et al. 2013). This could be due to multiple factors such as the availability of diagnostic testing, physicians' awareness of the disease, de-stigmatisation of disease diagnosis, increased population survival and possibly increased mutation rates.

1.1.3 Clinical symptoms and diagnosis

1.1.3.1 Disease overview

HD is an autosomal dominant genetic condition that results in progressive neurodegeneration and ultimately death (Bates et al. 2015). It has a 50% chance of being passed down from parent to child making it a devastating disease for patients and their families. *HTT* contains an expanded CAG repeat tract within exon1 that encodes a poly-glutamine (poly-Q) tract (Stamatakou et al. 2018). The mean age of disease onset is 45 years old, although clinical onset is very variable, ranging from early childhood to over 80 years of age (Bates et al. 2015). The number of repeats is inversely correlated with age at disease onset, although there is considerable variation. A CAG repeat tract containing 36-39 CAGs incurs partial penetrance and 40 CAGs or more repeats causes disease onset (Quarrell et al. 2007). Huntingtin protein (HTT) with a poly-Q tract above 40 is thought to be toxic and it self-aggregates within neurons into fibrillar structures (Wagner et al. 2018). HTT aggregates form within the cytoplasm and the nucleus (DiFiglia et al. 1997). Evidence suggests that aggregated HTT within the nucleus is toxic, but the effect of mutant HTT in the cytoplasm is still debated (Chen et al. 2001; Yang et al. 2002). The medium spiny neurons of the striatum are particularly sensitive to the toxicity of HTT and this is where the neurodegeneration is first observed. Throughout disease progression, other areas of the brain become affected by mutant HTT either through prion-like spreading of the mutant protein or due to inherent

biological features which make them more susceptible to mutant HTT toxicity. This includes the cortex which also degenerates as the disease progresses (Hsu et al. 2018).

1.1.3.1 Motor symptoms

The chorea is one of the prominent behavioural hallmarks of HD. It is an uncontrolled dance-like movement that was first described by George Huntington (Huntington 1872). The onset of motor symptoms is commonly used to diagnose HD with genetic tests confirming the diagnosis. Initially patients experience restlessness, muscle spasms, face grimaces and difficulties with coordination. As the disease progresses they can experience the involuntary chorea but they also have issues with speech, balance and walking (Kirkwood et al. 2001). Dystonia of the face and back muscles and issues swallowing also onset during the middle stages of disease. At later stages of disease progression, patients are unable to walk, talk and look after themselves, and the swallowing problems worsen, increasing the likelihood of choking (Smith et al. 2000; Bates et al. 2015). These symptoms change and progress over the 10-20 years of their life. It is not clear what causes the motor symptoms, but the striatum is involved in the coordination of movement (Graybiel and Grafton 2015) so potentially the degeneration of the striatum yields these symptoms.

1.1.3.2 Psychiatric symptoms

Along with the chorea, George Huntington also described patients with HD as having "a tendency to insanity and suicide" implicating mood disorders in the disease (Huntington 1872). There have been reports detailing case studies of HD patients with extremely severe psychiatric manifestations (Jauhar and Ritchie 2010; Kachian et al. 2019), but not all HD patients experience such severe symptoms. There have been reports of depression, anxiety and hostility having higher incidences in HD patients than people without an expanded repeat tract (Paulsen et al. 2001; Duff et al. 2007). There is mounting evidence which suggests that psychiatric symptoms precede the onset of motor symptoms which is how disease onset is usually defined (Brandt et al. 2002; Paulsen et al. 2008; Stout et al. 2011; Paulsen et al. 2013; Tabrizi et al. 2013; McAllister et al. 2021). This research implies that disease onset could be occurring as early as 10 years prior to motor onset.

1.1.3.3 Diagnosis

When a person presents with chorea-like symptoms HD diagnosis is confirmed with a genetic test which usually involves taking a blood sample to ascertain the presence or absence of a pathological expansion in the *HTT* gene (Stoker et al. 2022). Motor and neuropsychological assessments are performed to confirm the presence of the chorea. Magnetic Resonance Imaging (MRI) can be performed to identify any changes to the striatum and surrounding areas. As with the motor and neuropsychological assessments, MRI scans help confirm the symptoms being presented are due to the onset of HD. If a patient has a family history, (i.e. a parent who is afflicted with HD), they may request a genetic test prior to the onset of any symptoms. There is still some stigma surrounding this, and the choice to assess your *HTT* CAG repeat tract length is a stressful decision to make because there are currently no treatments that would alter the course of the disease if they have a pathological expansion in the *HTT* gene. Proper counselling should be given to the patient and potentially their family prior to testing (Migliore et al. 2019).

1.1.3.4 Current therapies

Currently the only treatments available for HD patients are therapies that target symptoms rather than the cause. The chorea is believed to be caused by an imbalance in dopamine signalling (Cepeda et al. 2014; Koch and Raymond 2019). The mechanism for the drug used to treat the chorea is a vesicular monoamine transporter blocker (Tetrabenazine), which inhibits the reuptake of dopamine and other neurotransmitters into neurons (Chen et al. 2013; Frank 2014). Physical therapy, occupational therapy and speech therapy are also used to help patients improve their motor skills, coordination and communication skills.
For treatment of the psychiatric symptoms anti-depressants and anti-anxiety medication is usually prescribed. Researchers suggest that a shift should be made in the treatment of the disease as non-motor symptoms of the disease have a great impact on the patients' quality of life (Snowden 2017).

There are currently no disease-modifying treatments for HD, although some therapies which reduce the levels of mutant huntingtin RNA in the cerebrospinal fluid (CSF) are in clinical trials (Tabrizi et al. 2022). Antisense oligonucleotides (ASOs) and RNA interference (RNAi) are two mechanisms which researchers are currently testing to lower mutant RNA levels in

various neurodegenerative disorders, but in the case of HD these therapies target mutant

HTT RNA (Wild and Tabrizi 2017; Lane et al. 2018; Tabrizi et al. 2019a; Aslesh and Yokota

2020; Silva et al. 2020). ASOs are synthetic single-stranded nucleotides which are designed

to hybridise to the RNA strand of a gene of interest by Watson-Crick base pairing (Chery

2016). Once the ASO has bound to the RNA it inhibits ribosomes from translating the strand

and triggers the degradation of the RNA transcript thus reducing expression of the targeted

gene (Di Fusco et al. 2019). RNAi are double-stranded nucleotides that require RNA silencing

complexes to regulate expression. Argonaute 2 (AGO2) is part of an RNA silencing complex

which takes up double-stranded RNAi, removes the passenger strand and mediates the

binding of the newly single-stranded RNAi to the RNA transcript of the gene of interest

(Schuster et al. 2019). The guide RNAi strand is complementary to the RNA transcript and

similarly to ASOs, it hybridises to the strand using Watson-Crick base pairing. Likewise, when

the RNAi strand is bound to the target RNA transcript it cannot be translated and the duplex

is degraded (Watts and Corey 2012).
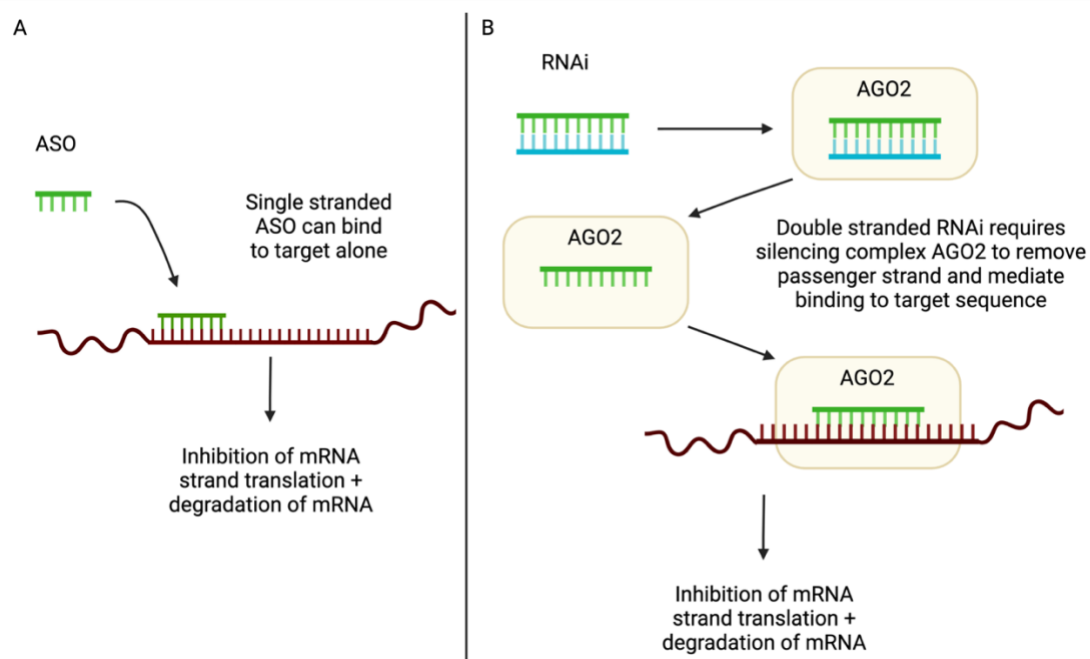
Figure 1.1 - ASO vs RNAi Mechanism (Created with BioRender.com)

In HD, ASOs and RNAi are synthesised to target the *HTT* gene to prevent its translation into

HTT protein. Some compounds are solely targeting the mutant *HTT* RNA, and some are

targeting both mutant and healthy RNA (Tabrizi et al. 2019b). While there are multiple *HTT*

lowering therapies in various stages of clinical trials, applying these techniques has not been

without its difficulties with a couple of clinical trials being halted in recent years (Kingwell 2021).

1.1.4 Juvenile HD

5-10% of HD cases occur in patients before the age of 21 (Lesinskienė et al. 2020). The symptoms that manifest in Juvenile HD are seizures, rigidity, ataxia, bradykinesia and behavioural problems (Ruocco et al. 2006; Stoker et al. 2022). In contrast to the disease in adults, there is less prominent chorea in the symptoms of Juvenile HD. The CAG repeat tracts in the pathological *HTT* allele in patients with Juvenile HD typically exceeds 60 CAGs, but there are cases where the repeat tract has surpassed 100 CAGs (Quarrell et al. 2013). Juvenile HD progresses quickly and as with adult HD, treatment includes symptom management rather than disease-modifying treatments.

1.2 Huntington's disease pathology

1.2.1 Huntingtin gene (*HTT*)

The human *HTT* gene is localised to chromosome 4p16.3 and it covers a region of 210kb which contains 67 exons and encodes a large 350kDa protein (HTT) which has a multitude of cellular functions that have not been fully elucidated (Saudou and Humbert 2016). The gene is well conserved, being expressed in organisms such as sea urchin, flies and non-human primates (Krench and Littleton 2013; Katow et al. 2021; Iennaco et al. 2022). These functions include, but are not limited to; vesicle trafficking, regulation of transcription and antiapoptotic activity (Schulte and Littleton 2011). The CAG repeat tract in exon 1 encodes a polyglutamine (poly-Q) tract, which may have some disease relevance as the pathological expansion of the CAG tract is translated. The normal CAG tract length is between 9 and 26 repeats with most people having between 17 and 20 repeats (Kremer et al. 1994). As mentioned previously, an abnormal expansion of the CAG tract exceeding 35 repeats will yield partial penetrance of the HD and expansions surpassing 40 repeats lead to disease onset.

1.2.2 Huntingtin protein (HTT)

HTT is expressed throughout the body, but is most highly expressed in the brain (Augood et al. 1996; Rüb et al. 2015; Uhlén et al. 2015). The N-terminus of human HTT has been well characterised due to it containing the potentially pathogenic CAG repeat tract, but there are other key structural features of HTT. These include a number of well conserved HEAT (Huntingtin, elongation factor 3, protein phosphatase 2A and TOR1) repeat domains, a proline rich domain (PRD) and an N-terminal amphipathic α-helix (Andrade and Bork 1995; Atwal et al. 2007; Tartari et al. 2008). The HEAT repeat domains are likely to aid HTT with its protein-protein interactions during its potential roles in vesicle trafficking or as a scaffolding protein (Andrade and Bork 1995; Takano and Gusella 2002). The function of the PRD is controversial. It resides adjacent to the poly-Q repeat tract and has been shown to be vital for WW-domain containing proteins and proteins containing SH3 domains (Harjes and Wanker 2003). Deletion of the PRD in yeast has been shown to increase the number of HTT foci and toxicity of HTT, however when it is knocked down *in vivo* it has no effect on the behaviour of mice (Dehay and Bertolotti 2006; Neveklovska et al. 2012). The N-terminal amphipathic α-helix consists of 17 amino acids which functions as a nuclear export signal, and also undergoes many post-translational modifications (PTMs) including, ubiquitination, acetylation and phosphorylation, that affect HTT subcellular localisation and clearance (Atwal et al. 2007; Maiuri et al. 2013). Poly-ADP Ribose (PAR) has been shown to bind to HTT (Maiuri and Truant 2018), which suggests that Poly-ADP Ribose Polymerase 1 (PARP1) interacts with HTT. The high number of protein-protein interaction regions and sites for PTMs signify the large number of cellular functions HTT has, so when the protein becomes mutated it is understandable as to why it is so damaging to neuronal health.

Functions of HTT include; vesicle trafficking, regulating transcription, mediating endocytosis, roles in autophagy, ciliogenesis among others (Saudou and Humbert 2016). HD is mostly a toxic gain-of-function disease so it is likely that these functions are all being carried out aberrantly. In the case of ciliogenesis, it requires HTT to traffic of pericentriolar material 1 protein (PCM1) from the base of the cilia in striatal neurons (Keryer et al. 2011). When HTT with an expanded poly-Q is expressed, PCM1 resides at the base to the cilia resulting in elongated, dysfunctional neuronal cilia which alter the flow of CSF. Another example of the toxic gain-of-function nature of mHTT is with its role in autophagy. WT-HTT aids p62 in

recognising cargo for autophagosomes, but mHTT interferes with this cargo recognition, resulting in empty autophagosomes (Martinez-Vicente et al. 2010). Although, mHTT does not always yield toxic gain-of-function attributes. HTT is involved in the transcription and trafficking of Brain Derived Neurotrophic Factor (BDNF) in cortical neurons which is crucial for the survival of MSNs of the striatum (Zuccato et al. 2003; Gauthier et al. 2004). Embryonic stem cells derived from HD-patients show reduced BDNF trafficking which is recovered by silencing the mutant *HTT* allele (Drouet et al. 2014). These are only a few of the pathways that HTT interacts with, which highlights the difficulties of selecting a pathway to target for treating HD. On the other hand, targeting HTT could lead to off-target side effects given the number of pathways it interacts with.

1.2.3 Striatal pathology

The striatum is the largest nucleus of the subcortical basal ganglia that mainly receives signals from the cortex and propagates signals to the other elements of the basal ganglia to coordinate motor and reward systems (Cicchetti et al. 2000; Wilson 2009; Yager et al. 2015). It is comprised of 2 structures divided into the dorsal striatum and ventral striatum. These are then divided into the compartments caudate and putamen (dorsal), and nucleus accumbens and olfactory tubercle (ventral) (Báez-Mendoza and Schultz 2013). 95% of the striatum is made up of inhibitory MSNs which at late stages of disease are almost completely ablated (Rao 2005; Morigaki and Goto 2017). Interneurons make up the other 5% of the striatum.
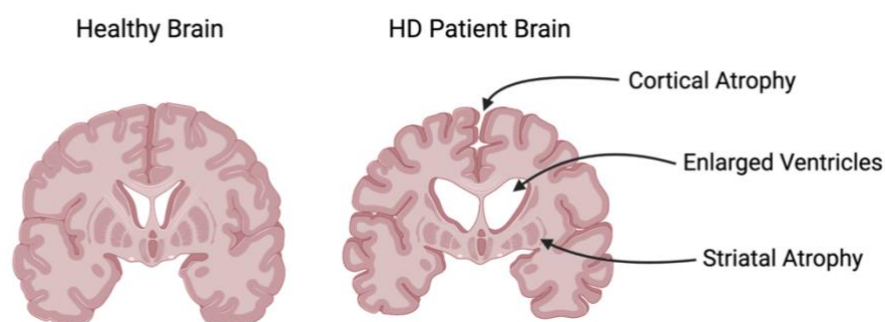
Figure 1.2 - Comparison of brain structure of a healthy brain and a HD patient brain. (Created with BioRender.com)

One study described five grades to define striatal degeneration in HD (Vonsattel et al. 1985). Grade 0 described striatum with no evidence of degeneration or abnormalities. Grade 1 was

defined by microscopic changes to the striatum, however they quantified that the caudate nucleus had already been reduced by 50% at this stage. Atrophy was macroscopically detected at Grade 2, and by Grade 4, 90% of the caudate nucleus has diminished and there was a notable increase in astrocytes and gliosis in the striatum. Figure 1.2 depicts the neurodegeneration observed in the brain of a HD patient.

1.2.4 Medium spiny neurons

Research is currently being done to assess why MSNs of the striatum are more sensitive to mutant HTT. They receive inputs from the cortex, thalamus and substantia nigra pars compacta and release the inhibitory neurotransmitter GABA to other nuclei of the basal ganglia to elicit their effect on movement control and initiation (Arama et al. 2015). There are two subtypes of MSNs, based on which nucleus of the basal ganglia they project to and the type of dopamine receptor they express (Chuhma et al. 2011). D1 MSNs project to the substantia nigra pars reticulata and internal globus pallidus, and express D1 receptors and dynorphin in the direct pathway. D2 MSNs project to the external globus pallidus and express D2 receptors and enkephalin in the indirect pathway (Gerfen et al. 1990; Ehrlich 2012; Zhou 2020). When striato-nigral D1 MSNs are activated by projections from the cortex and thalamus, they increase their output, sending inhibitory signals to the substantia nigra. However, when striato-pallidal D2 MSNs are innervated by the cortex and/or thalamus, they decrease their output. The direct pathway facilitates wanted movements whereas the indirect pathway suppresses involuntary movements, combined they regulate motor control (Figure 1.3) (Bergonzoni et al. 2021).
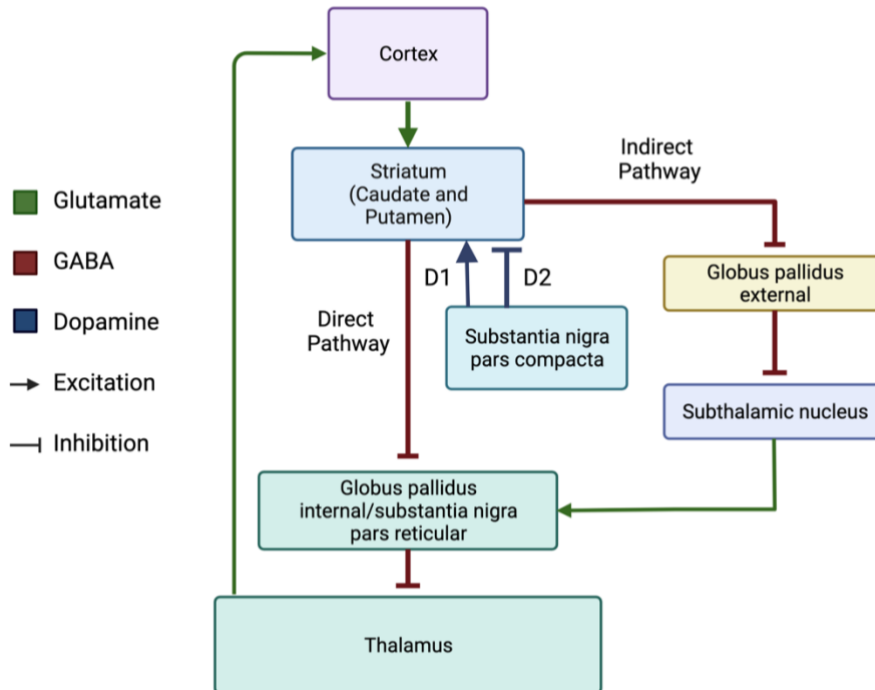
Figure 1.3 - The Direct and Indirect Striatal Pathways. The cortex releases excitatory glutamate which binds to AMPA and NMDA receptors of the MSNs. **Direct pathway**: The cortex sends glutamate to the striatum. MSNs expressing D1 dopamine receptors then send inhibitory GABA to the internal Globus pallidus (GPi) and substantia nigra pars reticular (SNpr). The GPi and SNpr usually send inhibitory GABA to the thalamus, dampening its excitation, but when the GPi and SNpr receive signals from the D1 MSNs it can no longer transmit GABA to the thalamus. Thus, the thalamus can send excitatory glutamate to the cortex. **Indirect pathway**: The cortex sends glutamate to the striatum. MSNs expressing D2 dopamine receptors project to the external globus pallidus (GPe) inhibiting the GPe. The subthalamic nucleus which is usually inhibited by the GPe becomes activated and transmits glutamate to the GPi, which in turn activates the GPi. This enables the GPi to inhibit the thalamus, thus reducing the excitatory feedback from the thalamus to the cortex. The substantia nigra pars compacta transmits dopamine to the striatum. D1 MSNs become activated by dopamine, enhancing the direct pathway. D2 MSNs are inhibited by dopamine, deactivating the indirect pathway (Chuhma et al. 2011; Bergonzoni et al. 2021). (Created with BioRender.com).

Research suggests that D2 MSNs are more susceptible to insult from mutant HTT expression with one study finding lower levels of immunofluorescence of enkephalin in post-mortem HD patient striata than in control (Sapp et al. 1995). D2 MSNs receive more input from the cortex and the synapses are larger in comparison to dendritic synapses of D1 MSNs (Lei et al. 2004), which indicates that D2 MSNs may be more sensitive to excitotoxicity (Bergonzoni et al. 2021).

1.2.5 Pathological mechanisms

1.2.5.1 Toxic HTT fragments and oligomers

Exon1 fragments of mHTT protein have been observed in disease. These can occur by translation of the full-length m*HTT* RNA which then undergoes proteolysis to become smaller mHTT peptides (Bates et al. 2015). Full-length HTT can undergo proteolytic processing by various proteases including caspases, cathepsins, metalloproteinase MMP10, and calpain (Saudou and Humbert 2016). The mutant RNA can also be aberrantly processed after transcription into a truncated fragment containing the pathological expansion, where it then undergoes translation to form mHTT exon1 peptides (Neueder et al. 2017). Both pathways result in the formation of a toxic HTT fragment which can disrupt cellular processes and seed aggregates. The fragments can co-localise from the cytoplasm into the nucleus where they interfere with transcription resulting in cell death (Saudou et al. 1998). As mentioned previously, BDNF transcription is altered by the presence of mHTT in the nucleus (Zuccato and Cattaneo 2007; Zuccato et al. 2011) which has repercussions for cell survival. R6/2 mice expressing exon1 of human *HTT* with 144 CAGs exhibit HD-like neurological phenotypes which include motor deficits, epileptic seizures, and non-movement related phenotypes (Mangiarini et al. 1996) which demonstrates the toxicity of the short HTT fragment.
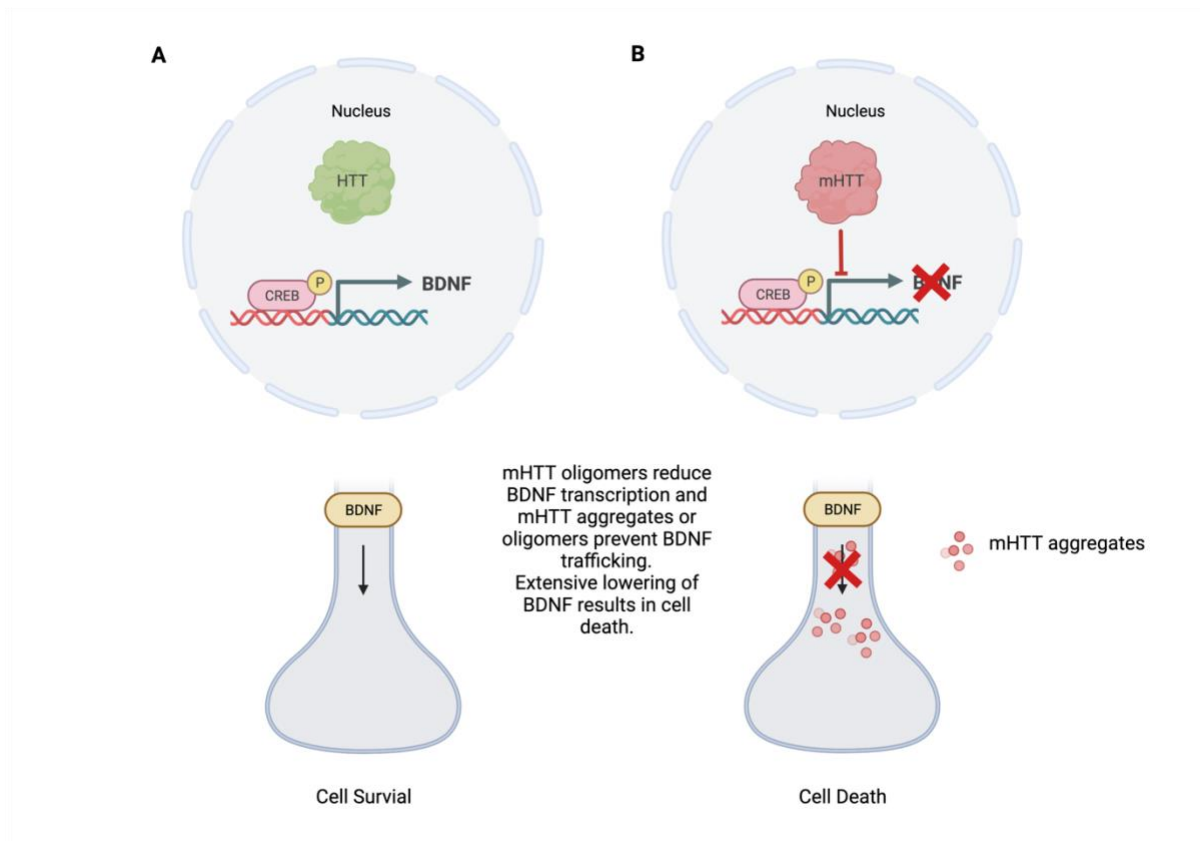
Figure 1.4 – mHTT blocks transcription of BDNF and inhibits BDNF and organelle trafficking. A) HTT aids the transcription of BDNF among other factors, and does not aggregate within neurons enabling efficient transport of organelles, BDNF and other genes around the neuron. B) mHTT oligomers enter the nucleus and inhibit the transcription of BDNF and other genes. mHTT blocks forms aggregates which block transport of proteins and organelles around the neuron (Gauthier et al. 2004; Giralt et al. 2011). (Created with BioRender.com).

Prior to forming insoluble aggregates, toxic HTT monomers/oligomers can be broken down either by macro-autophagy or the Ubiquitin Proteasome System (UPS) *in vitro* and *in vivo* (Bhat et al. 2014; Juenemann et al. 2015). Post translational modifications of HTT affect its turnover rate, with increased phosphorylation decreasing the half-life of HTT (Thompson et al. 2009). The expanded poly-Q tract of mHTT is thought to prevent or reduce phosphorylation of the mutant protein, thus reducing its risk of being cleared (Thompson et al. 2009).

While phosphorylation of mHTT may be reduced, the soluble oligomeric form of mHTT has been shown to interact with hundreds of proteins (Kim et al. 2016) in comparison to the tens of interactors that insoluble HTT aggregates have which suggests soluble HTT oligomers are more neurotoxic than the aggregates. Only 1-4% of MSNs exhibit HTT aggregates while

they are much more common in the interneurons of the striatum and also in cortical neurons which suggests that mHTT oligomers are more toxic than mHTT aggregates (Gutekunst et al. 1999; Kuemmerle et al. 1999).

1.2.5.2 HTT Aggregates

As with many other neurodegenerative disease, one of the hallmarks of HD is that soluble mHTT forms insoluble aggregates (Bates et al. 2015). HTT aggregates are formed by toxic HTT peptides that self-assemble forming β-hairpin structures, which recruit more molecules of HTT, mutant and WT, and other proteins to assemble with them forming β-sheet fibrils (Slepko et al. 2006; Stanley et al. 2011; Chen et al. 2016; Sahoo et al. 2016; Riguet et al. 2021). It is not clear whether HTT aggregates are toxic or neuroprotective (Miller et al. 2010; Shen et al. 2016), as some research has shown that blocking the formation of mHTT aggregates induces mHTT-related neuronal death (Saudou et al. 1998), but the existence of large cytoplasmic mHTT aggregates blocks axonal transport which has negative consequences for neuronal health in animal and cellular models of HD (Figure 1.4) (Li et al. 2001; Lee et al. 2004).

HTT aggregation can be mediated and accelerated by HTT exon1 fragments interacting with the plasma membrane (Atwal et al. 2007; Tao et al. 2019; Marquette et al. 2021). When truncated mutant *HTT* was expressed in HEK293 fibroblast cells and neuroblastoma cells, HTT aggregates were observed in the cytoplasm and the nucleus (Cooper et al. 1998). Intranuclear HTT aggregates have also been observed in the striatal neurons of HD patient brain tissue (DiFiglia et al. 1997; Becher et al. 1998), and some have been reported in the cytoplasm of cellular and mouse models of HD (Hackam et al. 1999). Evidence from HEK293 cells suggests these aggregates have different biochemical compositions which could indicate distinct aggregation mechanisms in the nucleus and cytoplasm, and potentially differing toxicities (Riguet et al. 2021). There is evidence that cortical neurons exhibit more HTT aggregation than the MSNs (Gutekunst et al. 1999; Kuemmerle et al. 1999), which supports the notion that aggregate formation is neuroprotective as cortical neurons are less susceptible to mHTT toxicity. The presence of HTT aggregates in neuronal cell culture promoted survival in comparison to those that did not display any inclusions (Arrasate et al.

2004) indicating that the neurons were "reducing" the levels of mHTT by being sequestered into aggregates. These data promote the concept of current therapies targeting m*HTT* RNA with antisense oligonucleotides to lower levels of soluble mHTT (Tabrizi et al. 2019a), rather than targeting the HTT aggregates.

A feature of HTT aggregates *in vivo* and *in vitro* is that they spread from cell to cell in a prion-like way, which has been observed between neurons, and between neurons and glia (Pearce et al. 2015; Pearce and Kopito 2018; Masnata et al. 2019). HTT aggregates have also been detected in the CSF of patients and mouse model (Tan et al. 2015). There is also evidence of mHTT spreading to healthy neighbouring cells and recruiting WT HTT to form aggregates, *in vitro* (Sameni et al. 2020). This could explain why at the end stage of the disease, cortical regions of HD patient brains are also atrophied and degenerated, just not to the extent of the subcortical white matter (Bates et al. 2015).
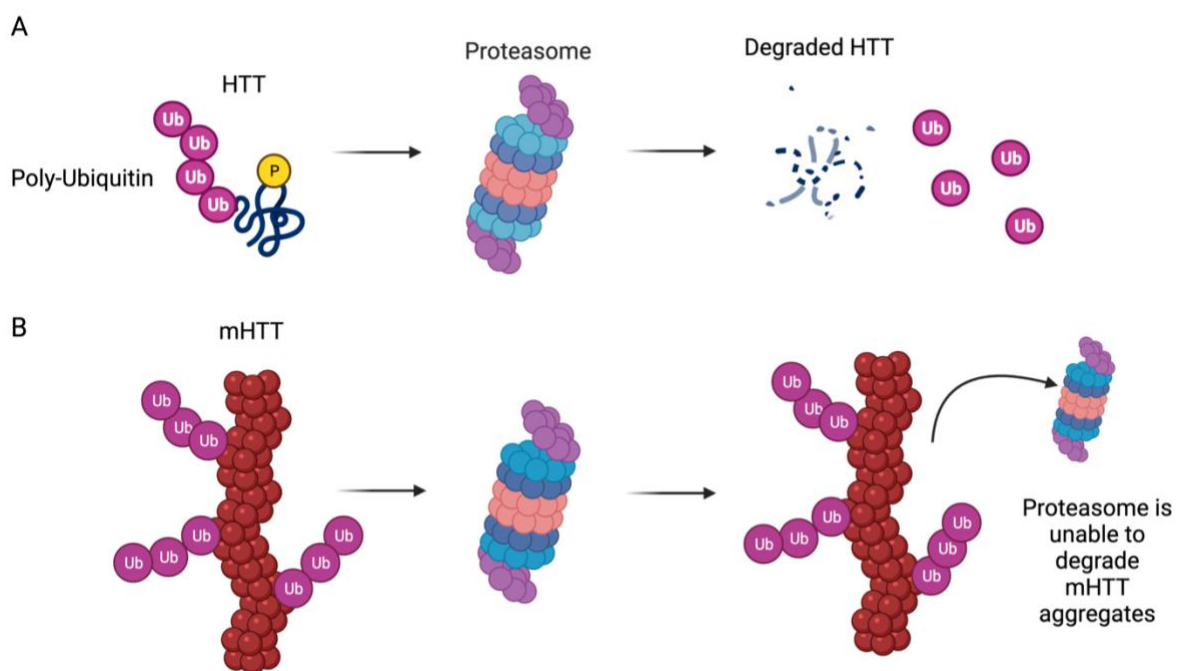
Figure 1.5 - Proteasomal breakdown of HTT. A) HTT is poly-ubiquitinated by ubiquitinating enzymes. The proteasome recognises the poly-ubiquitin tail and HTT protein is degraded by the proteasome. Phosphate (yellow) can increase the likelihood of HTT degradation. Ubiquitin is released to be recycled to bind to another protein. B) mHTT aggregates are ubiquitinated by ubiquitinating enzymes. The proteasome is recruited to the mHTT aggregate, but it is unable to degrade the aggregate so either dissociates or is recruited into the inclusion (Thompson et al. 2009; Juenemann et al. 2013; Schipper-Krom et al. 2014). (Created with BioRender.com).

HTT inclusions cannot be cleared by the ubiquitin proteasome system (UPS). There is evidence that proposes eukaryotic proteasomes cannot digest proteins with expanded polyglutamine sequences, suggesting that polyglutamine sequences prone to aggregation must undergo further hydrolysis prior to degradation (Venkatraman et al. 2004). However, this has been disputed by more recent research which shows that huntingtin fragments containing an expanded polyglutamine sequence can be degraded by the mammalian proteasome (Juenemann et al. 2013). Studies using yeast have shown that human ubiquitin-conjugating enzyme (E2) interacts with HTT (Kalchman et al. 1996) and in neuroblastoma cells, transfected with pathogenic *HTT* constructs, ubiquitin was shown to bind to HTT inclusions (Juenemann et al. 2015). Ubiquitin has also been found in the nuclear inclusions of HD patient brain tissue (DiFiglia et al. 1997). Other work *in vitro* shows that even though proteasomes are recruited to HTT inclusions, they remain catalytically active (Schipper-Krom et al. 2014) suggesting that proteasomes can recognise that the HTT aggregates are incorrectly formed and can bind to them, but they are unable to degrade them.

1.2.5.3 BDNF

MSNs rely on the synthesis and vesicle trafficking of BDNF to survive (Figure 1.4) (Zuccato et al. 2003; Gauthier et al. 2004) and both of these processes are altered by the presence of mHTT (Drouet et al. 2014). BDNF mediates the surface expression of the glutamatergic α-amino-3-hydroxy-5-methyl-4-isoxazole-propionic acid receptors (AMPARs) on MSNs in the nucleus accumbens (Reimers et al. 2014). If BDNF mediates this process in the MSNs of the striatum, mHTT could have a downstream effect of dysregulating the distribution of AMPARs in the MSNs of the striatum which could affect its ability to receive glutamatergic signals from the cortex.

It is not known why MSNs are particularly sensitive to BDNF depletion due to mHTT expression, however some research is being performed to assess the impact of increasing BDNF levels in HD models and patients. BDNF perfusion has been used to treat R6/2 mice and it ameliorated their motor coordination impairment and neuronal dysfunction (Giralt et al. 2011; Giampà et al. 2013). Overexpression of BDNF in the forebrain of YAC128 mice has also had ameliorative effects on HD-related phenotypes (Xie et al. 2010). These studies

indicate promising uses for targeting BDNF for HD treatment. However, when HD patients were treated with citalopram, which is believed to increase BDNF levels, they found no improvement of motor symptoms (Beglinger et al. 2014).

1.2.5.4 Mitochondrial Dysfunction and Oxidative Stress

mHTT has been shown to dysregulate mitochondrial function, biogenesis and fission resulting in high levels of cytoplasmic reactive oxygen species (ROS) and a neurotoxic environment in cell and animal models of HD and HD brain tissue (Panov et al. 2002; Damiano et al. 2010; Guedes-Dias et al. 2016; Carmo et al. 2018). ROS are free radicals and reactive molecules derived from oxygen which are synthesised by the mitochondria during aerobic metabolism (Ray et al. 2012; Bottje 2019). The mitochondria minimise oxidative damage by carrying out anti-oxidant redox reactions which reduce mitochondria and cellular ROS levels. Mitochondria from HD-patient lymphoblasts become fragmented and the conformation of the cristae changes, resulting in increased levels of apoptosis (Costa et al. 2010). In the nucleus, mHTT can inhibit the transcription of peroxisome proliferator-activated γ-coactivator 1α (PGC1α) which blocks the biogenesis of mitochondria (Figure 1.5) (Costa and Scorrano 2012). mHTT also inhibits PGC1α directly, preventing it from activating the ROS defence system (McGill and Beal 2006). In the cytoplasm, mHTT directly interacts with mitochondria by depleting adenosine triphosphate (ATP) levels and reducing the mitochondrial membrane which results in hyper-sensitivity to Ca^{2+} ions opening the permeability transition pore (Tang et al. 2005). This leads to the release of pro-apoptotic factors from the mitochondria and cell death (Tang et al. 2005; Zheng et al. 2018). Prior to cell death, mitochondrial dysregulation also results in an accumulation of ROS in the neurons. ROS are extremely toxic and can lead to high levels of DNA damage (Srinivas et al. 2019), which is a feature of HD. In cortical neurons, HTT aggregates block mitochondrial movement and trafficking resulting in mitochondria accumulating at HTT inclusions. Mitochondrial dysfunction has been implicated in many other neurodegenerative diseases including Parkinson's disease (PD) and Alzheimer's disease (AD) (Trushina and McMurray 2007; Sayre et al. 2008; Yu et al. 2021a). All of this evidence indicates a role for mitochondrial dysfunction in HD pathogenesis and for other neurodegenerative disorders.
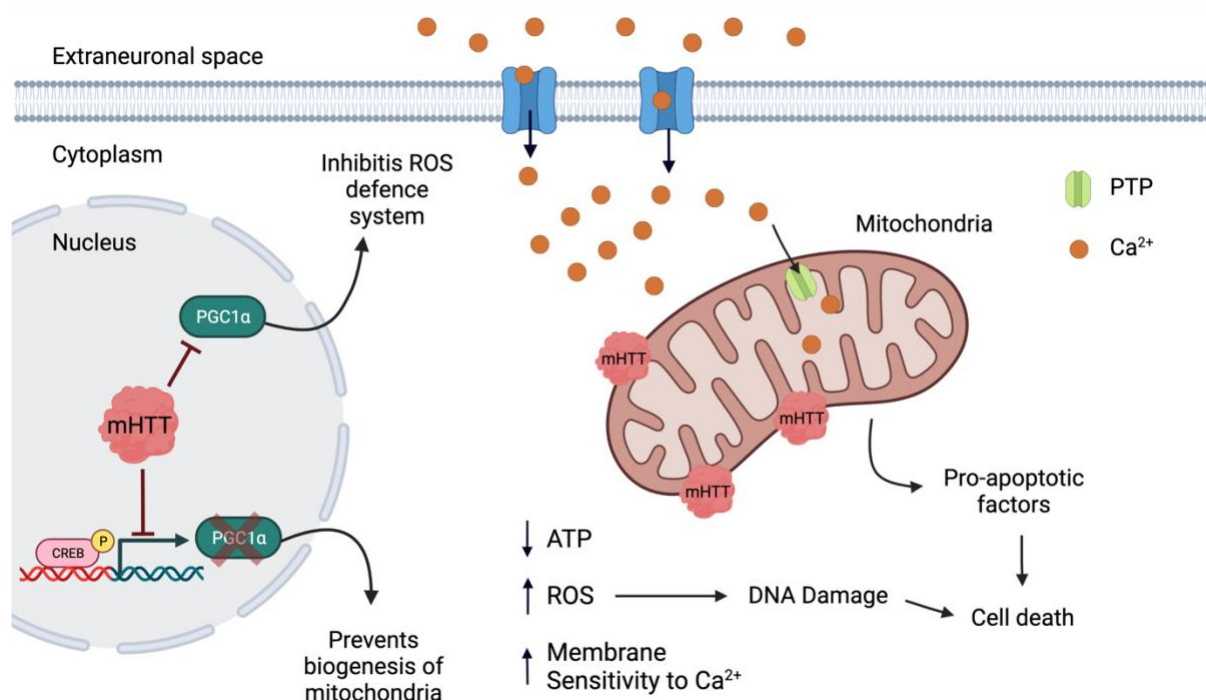
Figure 1.6 - The effects of mHTT on the mitochondria. mHTT elicits many effects on the mitochondria. It inhibits the transcription of PGC1α, and inhibits PGC1α directly to prevent mitochondrial biogenesis and inhibit the mitochondrial ROS defence system. mHTT directly interacts with the mitochondria to disrupt its membrane potential causing a calcium influx (orange dots) through permeability transient pores (PTP) within the mitochondria. This leads to the release of pro-apoptotic factors and prolonged calcium influx results in cell death. Dysfunctional mitochondria result in ATP depletion, ROS increase which increase the rate of DNA damage. This can also cause neuronal death (Costa and Scorrano 2012). (Created with BioRender.com).

Mitochondrial dysfunction leads to increased levels of ROS in the neurons, and as mentioned previously, high levels of ROS can result in high levels of DNA damage. DNA damage induced by ROS activates Poly ADP-Ribose Polymerase 1 (PARP1), a DNA damage sensor. Excessive levels of DNA damage results in hyperactivation of PARP1 which depletes cellular nicotinamide adenine dinucleotide (NAD^+) stores and activates a caspase-independent cell death pathway called Parthanatos (David et al. 2009). Upon PARP1 hyperactivation, poly ADP-Ribose (PAR) translocates from the nucleus to the cytoplasm where it interacts with the mitochondrial protein apoptosis inducing factor (AIF) (Wang et al. 2009). AIF is released from the mitochondria where it forms a complex with migration inhibitory factor (MIF) and translocates into the nucleus. Upon entering the nucleus, MIF mediates DNA fragmentation by cleaving DNA, resulting in cell death (Fatokun et al. 2014). While Parthanatos has not been explicitly observed in HD patient tissue or animal models, high levels of immunoreactivity for PARP1 has been observed in post-mortem brain tissue of

HD patients (Vis et al. 2005). Treating R6/2 mice with a PARP1 inhibitor had neuroprotective effects (Cardinale et al. 2015; Paldino et al. 2017) suggesting that PARP1 may be hyperactive in HD. PARP1 hyperactivity is being extensively studied in Parkinson's disease (PD) as PARP1 activity exacerbates α-synuclein toxicity (Kam et al. 2018; Wang and Ge 2020). As there is mitochondrial dysfunction in both PD and HD, it would only enhance the field of research by further characterising PARP1 activity in HD pathogenesis. While there is not enough evidence to convincingly implicate PARP1 and Parthanatos in the progression of HD, the ameliorative effect of PARP1 inhibitor treatment in HD models makes it an interesting pathway for further investigation.
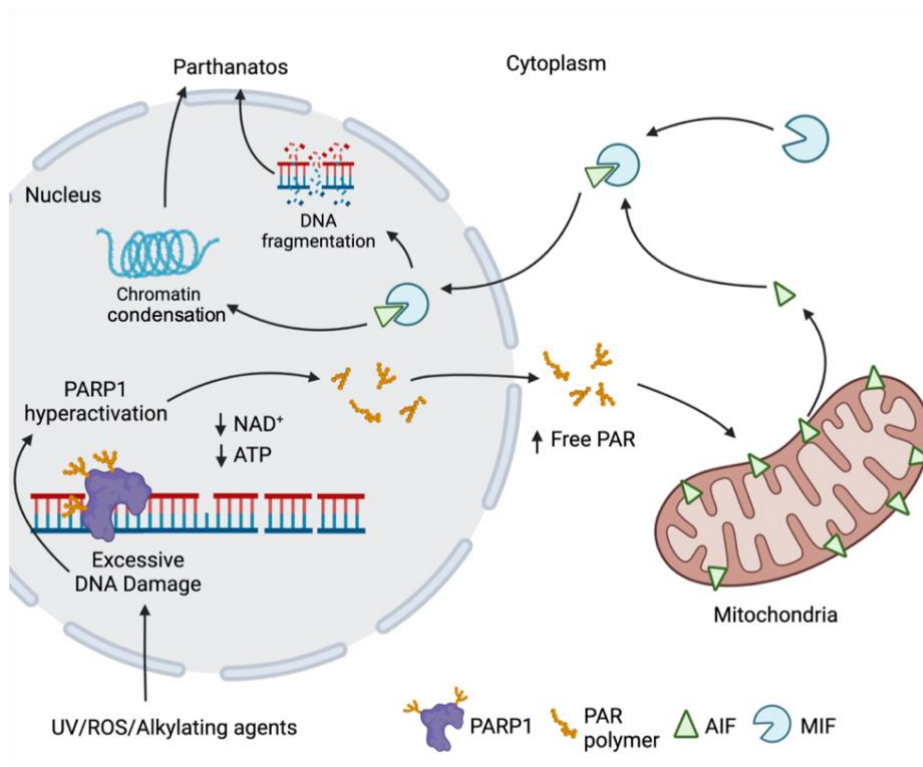
Figure 1.7 - Parthanatos - PARP1 induced cell death pathway. PARP1 becomes hyperactive in response to high levels of DNA damage which results in depleted NAD+ and ATP and translocation of PAR polymers into the cytoplasm. Free PAR polymers interact cause the depolarization of the mitochondrial membrane releasing Apoptosis Inducing Factor (AIF), but PAR can also interact directly with AIF to release it from the mitochondrial membrane. AIF forms a complex with Migration Inhibitory Factor (MIF) and translocates into the nucleus where DNA fragmentation and chromatin condensation occur resulting in cell death, Parthanatos (David et al. 2009; Wang and Ge 2020). (Created with BioRender.com).

1.2.5.5 Excitotoxicity

MSNs receive glutamatergic signals from the cortex and the thalamus and it is believed that excessive glutamatergic signalling could be contributing to HD pathogenesis (Estrada

Sánchez et al. 2008). Excitotoxicity occurs when there is aberrantly increased glutamate receptor activation which leads to high levels of Ca^{2+} influx in neurons resulting in membrane depolarization, mitochondrial failure and ultimately cell death (Sepers and Raymond 2014). Excitotoxicity is most commonly observed in patients who have experienced acute hypoxic ischemic stroke or traumatic brain injuries (Verma et al. 2022). The striata of YAC128 mice have been reported as having higher expression of glutamatergic N-methyl-D-aspartate (NMDA) receptors, specifically those containing the NR2B subunit, and having increased NMDA receptor activity in pre-manifest stages (Milnerwood et al. 2010). When YAC128 HD mice were treated with memantine, an extrasynaptic NMDA receptor antagonist, it ameliorated neuropathological and behavioural phenotypes (Okamoto et al. 2009; Milnerwood et al. 2010). When late stage symptomatic R6/2 mice were treated with the NMDA receptor agonist, quinolinic acid, they showed resistance to neurodegeneration of the striatum in comparison to wild-type (Hansson et al. 1999). However, when the R6/2 mice were treated with quinolinic acid at a pre-symptomatic age, the striatal neurons were much more sensitive to excitotoxicity induced by NMDA receptors (Hansson et al. 2001). This suggests that aberrant glutamate signalling plays a critical role in early stages of HD pathogenesis, and may contribute to early cortico-striatal synapse loss (Raymond 2003).

1.2.5.6 Apoptosis

Apoptosis is the programmed cell death pathway which is a homeostatic mechanism that occurs during development and aging that regulates cell populations in tissues (Elmore 2007). Apoptosis is a caspase-dependent biochemical process where the nucleus of the cell condenses and the cytoplasm forms vesicular "blebs" which are cleared by phagocytes (Taylor et al. 2008). Aberrant apoptosis is a feature of a multitude of human conditions such as ischemic stroke, cancers, autoimmune disorders and neurodegenerative disorders. Apoptosis can occur in response to mitochondrial dysfunction and excitotoxicity as the cell environment has become too toxic for the cell's survival. There is evidence of DNA fragmentation in the striatum of late-stage HD patients and caspase activation, both of which are indicators of apoptosis, at late stages of disease progression (Dragunow et al. 1995; Portera-Cailliau et al. 1995; Butterworth et al. 1998; Kiechle et al. 2002). *In vitro* models have shown evidence of caspase activation and apoptosis induction in HD cell

models (Saudou et al. 1998; Sawa et al. 1999; Li et al. 2000; Jana et al. 2001; Tang et al. 2005). Mouse models of HD suggest that apoptosis is upregulated due to increased NMDA receptor activation in the medium spiny neurons (Shehadeh et al. 2006) and that full-length mutant *HTT* is required to disrupt Ca^{2+} signalling that results in apoptosis induction in striatal neurons (Zhang et al. 2008). Expressing mutant *HTT* with 103Q in pigs led to DNA fragmentation, increased caspase-3 activation and apoptosis in the brains of the transgenic pigs (Yang et al. 2010). Caspase enzymes have been shown to mediate cleavage of HTT (Goldberg et al. 1996; Wellington et al. 1998) and when HTT cleavage is inhibited by expressing *HTT* with a mutant caspase-cleavage site there is a reduction of the degeneration of medium spiny neurons of the mutant YAC128 HD mice (Graham et al. 2006). Inhibitors which irreversibly inhibit caspase-3 and -6 activity have been shown to prevent HTT proteolysis in $Hdh^{111Q/111Q}$ mouse striatal cells *in vitro* and reduce neurodegeneration in rat striatal and cortical neurons expressing toxic HTT *ex vivo* (Leyva et al. 2010). All of this evidence suggests a strong role for apoptosis mediating cell death at late stages of HD.

1.2.5.7 Necrosis and Necroptosis

While there is an extensive amount of research that supports apoptosis as the pathway mediating cell death in HD, there are other pathways that should be considered as apoptosis seemed to be primarily activated at the end-stage of disease. Necrosis is a passive, unprogrammed type of cell death whereby the mitochondria become enlarged and the cell membrane ruptures due to a loss of membrane integrity (Proskuryakov et al. 2003). The contents of the cell leaks into the extracellular space where it is detected by immune cells triggering an inflammatory response (Xu et al. 2018). This typically occurs when cells are exposed to toxic insults such as reduced oxygen levels, exposure to chemical toxins and high temperatures. Researchers have discovered a type of programmed necrosis which is regulated by toll-like receptors (TLRs), death receptors, and receptor-interacting kinases (RIPKs) upon inhibition of caspase-8 in apoptosis (Yu et al. 2021b). The activation of these complexes yields membrane instability. Necroptosis progresses similarly to necrosis, displaying morphological similarities; disrupted membranes, cytoplasmic leakage into the extracellular space and swollen organelles (Pasparakis and Vandenabeele 2015). Necroptosis has been associated with stroke (Naito et al. 2020), Alzheimer's disease

(Jayaraman and Reynolds 2022) and multiple sclerosis (Picon et al. 2021) which demonstrate that neurons can undergo this process.

There is limited evidence for necroptosis or necrosis being present in HD, but one research group highlights a novel cell death pathway that is induced by the presence of mutant HTT. Transcriptional repression-induced atypical death (TRIAD) is a type of necrosis that researchers have shown to occur in HD model systems (Hoshino et al. 2006). TRIAD is associated with the Hippo pathway which regulates organ growth and size during development (Zhao et al. 2010). The cell death pathway is described as occurring slower in comparison to canonical necrosis and apoptosis. It is associated with enlarged endoplasmic reticulum (ER) and vacuoles, and the reduced expression of a cofactor of the apoptotic protein p73, Yes-associated protein (YAP). A neuron-specific YAP (YAP$_N$) isoform and activated p73 were shown to colocalise in striatal neurons in post-mortem brains of HD patients and in transgenic *HTT* mice (Hoshino et al. 2006). The expression of human YAP$_N$ was shown to rescue HTT-induced cell death in the *Drosophila* eye of a *Drosophila* model of HD (Hoshino et al. 2006). These initial results show a role for YAP and p73 in HD pathology. Later research by the same group showed morphological differences in primary cortical mouse neurons were infected with a mutant *HTT* lentivirus (HTT104Q). Over a 7-day period (7 days post-infection), these neurons adopted one of three different morphological features associated with neurodegeneration; shrinkage, rupture and ballooning (Mao et al. 2016). Cell shrinkage was associated with apoptosis and cell rupturing due to excessive cell body expansion was associated with necrosis. The ballooning type cell death involved the cell bodies changing into an elongated balloon shape, the formation of large vacuoles greater than 10μm in diameter, which resulted in rupturing the cell body in a process which took 12 hours. Live cell imaging captured these processes and found that cell shrinkage neurodegeneration took 90 minutes from the initial signs of shrinkage to cell death, and cell rupture neurodegeneration took 3 hours from the expansion and collapse of the cytoplasm. Further research by the group showed evidence of the activation of a marker of TRIAD, LATS1 kinase, and the enlargement of the ER in cortical neurons of post-mortem HD brains and HTT-knock-in mice (Yamanishi et al. 2017). They also found reduced expression of YAP isoforms in cortical neurons of post-mortem HD brains which had previously been associated with higher levels of TRIAD. As HD is associated with dysregulated transcription,

this novel cell death pathway could potentially be occurring during disease progression, although it may not be the main cause of neurodegeneration in HD.

1.3 Genetic modifiers of Huntington's disease

1.3.1 Variability of Age of Onset (AOO) and GWAS

There is an inverse correlation between the number of CAG repeats and the age of onset of motor symptoms (AMO) with a longer CAG repeat tract associated with a younger AMO (Langbehn et al. 2004; Gusella and MacDonald 2009). The extended expansion of the CAG tract reported in Juvenile HD is associated with the extremely early AMO. Some young patients have CAG repeat tracts that number 200+ CAGs (Quigley 2017). Recent studies have shown that the length of the uninterrupted CAG repeat tract is a better indicator of disease onset, with longer pure CAG repeat tracts being associated with earlier disease onset (Ciosi et al. 2019; Lee et al. 2019). Exome sequencing of HD patients revealed that the composition of the CAG repeat tract affected the onset of disease, with patients carrying a *HTT* allele with a CAG tract containing multiple CAA interruptions having later onset of disease (McAllister et al. 2022). However, CAG length only explains up to 60% of the variation in AMO observed in the HD population, leaving 40% unaccounted for. The Venezuelan kindreds (Wexler et al. 2004) show that up to 50% of this remaining 40% is heritable suggesting that there are genetic modifiers.

Genome wide association studies (GWAS) have been performed on various cohorts of HD patients and they have highlighted several key pathways that could be implicated in modifying the AMO (Lee et al. 2015; Moss et al. 2017; Lee et al. 2019). The most significant single nucleotide polymorphisms were found close to the FANCD2 and FANCI Associated Nuclease 1 (*FAN1*) loci which functions in DNA interstrand-crosslink repair (Kratz et al. 2010; MacKay et al. 2010; Thongtip et al. 2016). Different *FAN1* variants appear to have different effects on HD progression and the stability of the CAG repeat tract (Deshmukh et al. 2021; McAllister et al. 2022). A transcriptome-wide association study performed with prefrontal cortex samples from HD patients found that increased *FAN1* expression was associated with delayed onset of HD and decreased expression of *FAN1* trended to earlier onset of disease (Goold et al. 2019). The same researchers found that *FAN1* knockdown in induced

pluripotent stem cells (iPSCs) also increased the instability of the HTT CAG repeat tract (Goold et al. 2019), demonstrating the importance of functioning FAN1 for disease onset and CAG repeat stability.

The GWAS data also highlighted significant single nucleotide polymorphisms (SNPs) in several elements of the DNA Mismatch Repair (MMR) pathway or elements that interact with it: *MLH1*, *MLH3*, *MSH3*, *LIG1*, *PMS1*, and *PMS2* (Lee et al. 2015; Moss et al. 2017; Ciosi et al. 2019). MMR canonically repairs mismatched DNA bases arising from DNA replication, but has also been associated with other DNA repair functions, independent of replication. Aberrant MMR activity is thought to be one of the driving factors of the somatic expansion of the CAG repeat tract in HD (Iyer and Pluciennik 2021).

1.3.2 Somatic Instability

The CAG tract within *HTT* can change in length intergenerationally, throughout a patient's life and in different tissues, within humans and animal models (Kennedy et al. 2003; Swami et al. 2009; Jung et al. 2011). Expansions of the CAG repeat beyond the inherited length in non-germline tissues is known as somatic expansion and occurs in HD patients. Given that more somatic expansion is observed in neurons than elsewhere in the body, one hypothesis is that it drives disease onset and progression (Ciosi et al. 2019). Identifying the factors that drive somatic expansion could identify novel therapeutic targets in HD (Guillotin and Martin 2014). Instability of a non-HTT expanded CAG tract has been shown in *Drosophila* germline cells (Jung et al. 2011), but somatic instability of an expanded CAG repeat tract has not been explicitly tested in neurons or other somatic cell types in *Drosophila*.

Sequencing of HD-patient exomes implicated the FAN1 DNA-binding domains and nuclease domains in the inhibition of somatic instability, with damaging coding variants being associated with earlier onset of HD (McAllister et al. 2022). *In vitro* studies using HD patient-derived iPSCs expressing pathogenic *HTT* with *FAN1* variants associated with early onset of disease did show more instability of the CAG repeat tract of *HTT*. Endogenous *FAN1* was mutated to a nuclease-inactive form and the CAG repeat tract in these cells expanded similarly to *FAN1* knockouts (McAllister et al. 2022).

1.4 DNA Repair Pathways

1.4.1 DNA damage in HD

High levels of DNA damage have been reported in the blood of HD patient's (Askeland et al. 2018; Castaldo et al. 2018), which complements the findings from the GWAS which implicate aberrant DNA repair pathway function with the progression of the disease (Lee et al. 2015; Moss et al. 2017; Ciosi et al. 2019). The evidence of mitochondrial dysfunction and high levels of ROS indicate that DNA damage may be occurring in HD.

1.4.2 Mismatch Repair (MMR)

MMR has been implicated in somatic expansion with the hypothesis that wild-type MMR proteins such as MSH2 and MSH3 can drive expansion. The SNPs in the or near the coding region of *MSH2* and *MSH3* that were highlighted in the GWAS could affect the expression of the WT proteins rather than their function. This altered expression could modify the MMR which leads to the expansion of the CAG repeat (Figure 1.4) (Moss et al. 2017).
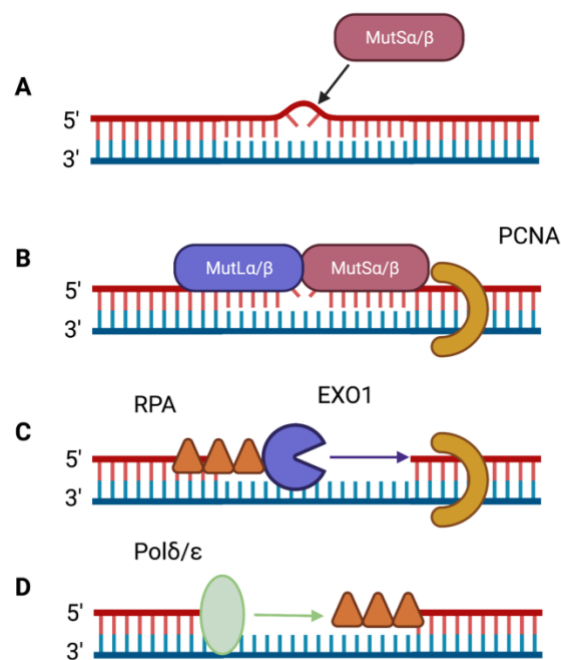
Figure 1.8 – Mammalian Mismatch Repair Pathway. A) Recognition of mismatch by MutS complex comprised of MSH2 and MSH3/MSH6. B) Recruitment of MutL complex, which contains endonuclease activity, which nicks the strand. MutL can be comprised of MLH1 and PMS1/PMS2. Proliferating cell nuclear antigen (PCNA) is also recruited and activated the endonuclease activity. C) EXO1 is recruited to the mismatch site and excises the nucleotides surrounding the mismatch, moving in a 5'-3' direction. Replication protein A (RPA) molecules prevent degradation of the single strand. D) The strand is resynthesised by DNA polymerase Polδ or Polε, which also resynthesises the strand in a 5'-3' direction. (Li 2008). (Created with Biorender).

MMR carries out three key processes to repair a mismatch; recognition of the mismatched base pairs or insertion/deletion loops, excision of part of the strand surrounding the error, and re-synthesis of the excised strand (Guillotin and Martin 2014). There are a few ways in which MMR can occur due to the number of proteins that can form the heteroduplexes MutS and MutL (Figure 1.9). The mismatched base pair or insertion/deletion loop is recognised by one of the MutS heteroduplexes (Guillotin and Martin 2014). This complex has intrinsic ATPase activity which provides the energy for the conformational change of MutS which recruits one of the MutL heteroduplexes (Li 2008). MutL recognises the mismatch and excises the strand from the mismatch. Exonuclease 1 (EXO1) is recruited and excises the lagging strand in a 5'-3' direction. DNA polymerase re-synthesises the strand and the pathway culminates with DNA ligase 1 (LIG1) ligating the newly synthesised sequence to the original strand (Hsieh and Yamane 2008). It is easy to see how alterations to this pathway could have detrimental genetic effects.

It is thought that CAG repeat instability is driven by aberrant activity of proteins in the MMR. Mismatches form when there are slippages in the DNA strand which canonically occurs during DNA replication, but in neurons most likely occurs because of errors during transcription (Lin et al. 2009; Lin and Wilson 2011; Goula et al. 2012). The slippages in the CAG repeat tract form extrahelical extrusions structures which are detected by MutSβ (Tian et al. 2009). Aberrant correction of the mismatch by the MMR machinery could be driving instability of the CAG repeat tract and thus driving disease progression (Iyer and Pluciennik 2021).
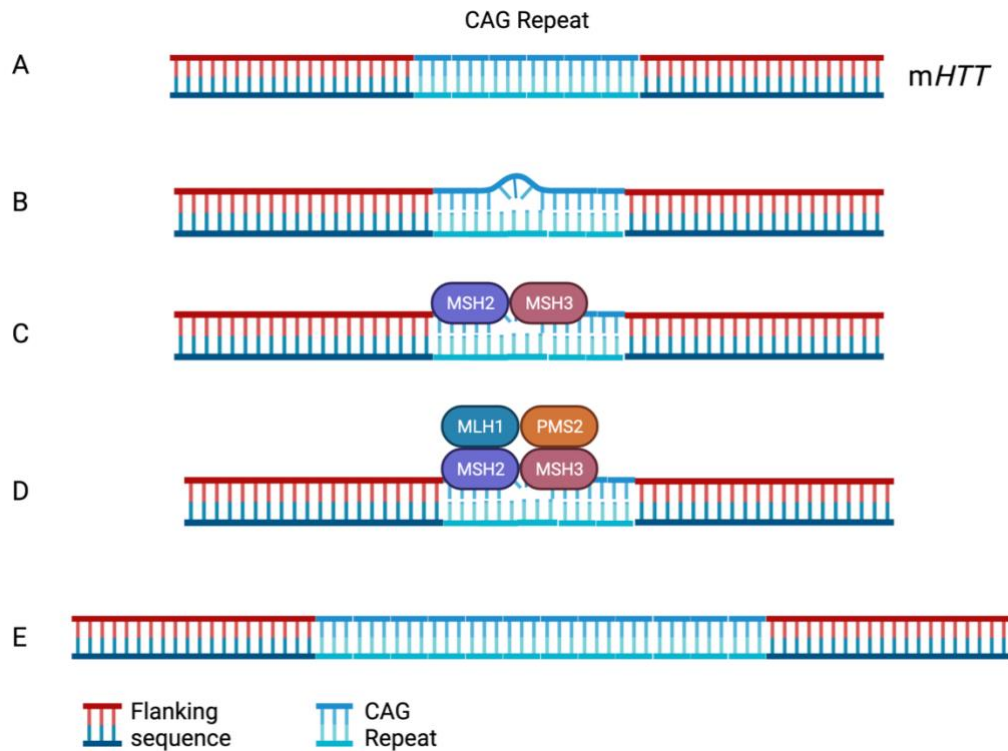
Figure 1.9 - Overactive or impaired mismatch repair mechanism yields somatic expansion of CAG repeat tract. A) m*HTT* with a CAG repeat expansion. B) CAG repeat becomes partly unwound. C) Unwound DNA is recognised by MutS duplex comprised of MSH2 and MSH3. D) The MutL duplex comprised of MLH1 and PMS2 binds to the MutS duplex and its endonuclease activity cleaves the DNA. E) The repair of the strand results in the expansion of the CAG repeat tract (somatic expansion) (Pardiñas et al. 2017). (Created with BioRender.com).

A study showed that homozygous *MLH1* knockout (-/-) mice containing human *HTT* with 111Q had lower levels of *HTT* CAG instability in the striatum and liver than the heterozygous knock-out (+/-) and control (Pinto et al. 2013). They also showed that *MLH3* -/- mice had lower levels of *HTT* CAG instability as well. This study directly implicates key components of the MMR pathway in somatic expansion of *HTT* in two tissues of a HD mouse model. Other studies have also shown that knocking down or knocking out elements of the mismatch repair pathway yields reduced somatic expansion of the CAG repeat tract (Manley et al. 1999; Dragileva et al. 2009; Tomé et al. 2013). If these components can be targeted in neurons then somatic expansion and AMO could be delayed.

1.4.3 PARP1, the DNA damage sensor

Poly ADP-Ribose Polymerase 1 (PARP1) is an enzyme that carries out the post-translational modification known as Poly ADP-Ribosylation (PARylation) which is the addition of poly ADP-ribose (PAR) to itself and target proteins. It belongs to a superfamily of PARP enzymes, containing 16 proteins, however PARP1 and PARP2 are the only members which can add PAR to targets. The other PARPs can only add monomeric ADP-Ribose to targets (Richard et al. 2022). Primarily, PARP1 PARylates proteins involved in single-strand break (SSB) and double-strand break (DSB) repair and chromatin remodelling. In order for DNA to replicate or be repair, chromatin has to be remodelled and PARP1 enables that process (Ray Chaudhuri and Nussenzweig 2017).
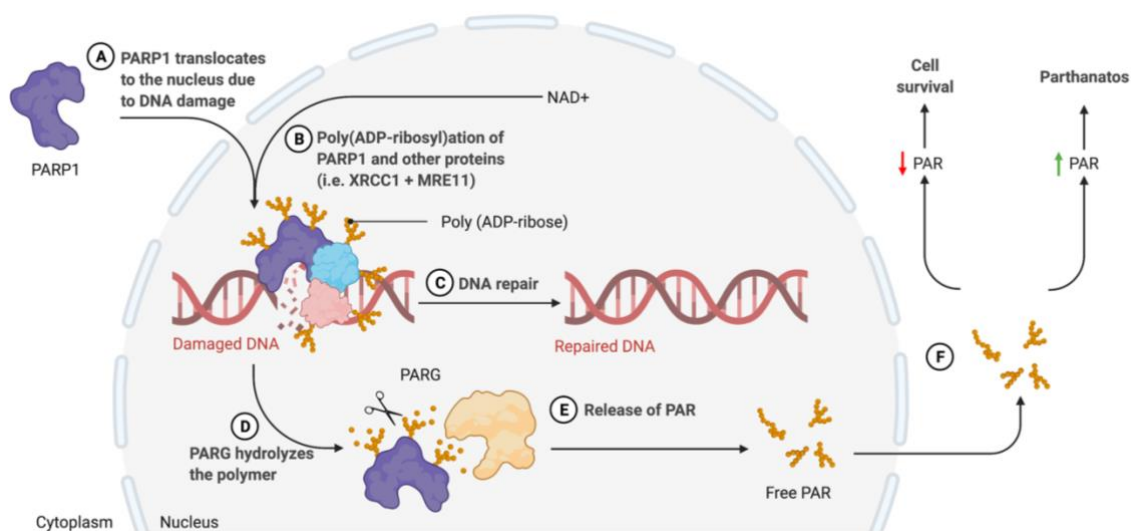
Figure 1.10 – PARP1 and DNA Repair. A) PARP1 translocates to the nucleus due to DNA damage. B) PARP1 senses DNA and PARylates itself and target proteins. C) DNA is repaired by the recruited proteins. D) PARG hydrolyses PAR polymers, removing them from PARP1 and its targets. E) PAR is released into the nucleus. F) PAR translocates to the cytoplasm. Low levels of cytoplasmic PAR enhance cell survival whereas high levels of cytoplasmic PAR are associated with Parthanatos. (Adapted from "Poly(ADP-Ribose) Metabolism in Trypanosoma Cruzi" by BioRender.com (2022). Retrieved from https://app.biorender.com/biorender-templates).

PARP1 acts as a DNA damage sensor and the PARylation recruits its targets to the site of DNA damage where it can initiate repair (Figure 1.10) (Sinha et al. 2021). PARP1 has three zinc finger domains (ZFs) which recognise sites of DNA damage (Ali et al. 2012). The mechanism of recognising single strand breaks and double strand breaks differs, with two PARP1 proteins required for recognition of an SSB, but only one PARP1 protein required for the recognition of a DSB. In SSBs, ZF1 of one PARP1 protein binds to the 3'-strand end of the

break and interacts with ZF2 of another PARP1 protein, which has bound to the other broken strand. During this process they dimerise, which could potentiate other conformational changes in the PARP1 proteins, but possibly enables the activation of PARP1's catalytic site (Ali et al. 2012). When a DSB is recognised by PARP1, ZF1, ZF3 and a WGR domain bind to the exposed strand and stabilise it prior to repair (Langelier et al. 2012; Steffen et al. 2016). Its targets include; X-ray repair cross-complementing protein 1 (XRCC1), meiotic recombination 11 (MRE11), and topoisomerase 1 (TOP1), however it does interact with a multitude of other proteins such as ataxia-telangiectasia mutated (ATM) and more importantly, HTT (Ray Chaudhuri and Nussenzweig 2017; Maiuri and Truant 2018). There is evidence of mitochondrial dysfunction and high levels of ROS in HD patient brains, which is associated with causing DNA damage that activates PARP1 (Chen et al. 2007; Johri and Beal 2012). While PARP1 did not appear in the HD GWAS, its potential interaction with HTT along with it being activated by ROS warrant more investigation into this protein and any role it might have in disease. PARP1 inhibitor treatment in R6/2 mice ameliorated HD-like phenotypes and selectively spared mouse striatal neurons, however the mechanism remains unknown (Cardinale et al. 2015; Paldino et al. 2017).

1.5 Using *Drosophila* to investigate genetic modifiers of HD

1.5.1 *Drosophila melanogaster* and its genetic tools

Drosophila melanogaster is a commonly used model system which is easy to manipulate genetically, are rapid and relatively inexpensive. They share homology with humans, with 48% of fly genes having human homologs and 31% of these genes being related to human diseases such as Leigh syndrome, Usher syndrome and Friedereich's ataxia (Yamamoto et al. 2014). Recently, researchers used *Drosophila* to investigate the molecular mechanisms of circadian rhythms and won a Nobel Prize (Huang 2018). This displays how important and relevant *Drosophila* research can be for human systems.

The *Drosophila* life cycle is temperature-sensitive meaning at higher temperatures their development speeds up and at lower temperatures it slows down. At 25°C their development from egg to eclosion spans 10 days and at 18°C this increases to 20 days. It takes 5 days for the egg to develop through the larval stages to become a pupa. At 10 days

the adult fly ecloses from the pupa. At 25°C WT flies (w[118]), live on average 60 days (Linford et al. 2013). Because their life cycle is so temperature sensitive this means it can be manipulated with genetic tools like the Gal4-Upstream Activation Sequence (UAS) system.
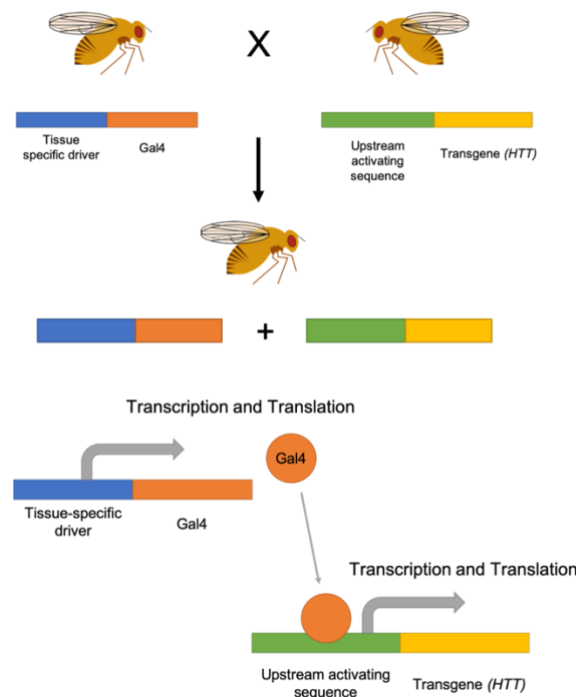
Figure 1.11 - The Gal4-UAS System of gene expression in *Drosophila melanogaster.*

The Gal4-UAS system is utilised to express a gene of interest, an RNAi, a reporter and/ or fluorophore in a specific tissue. The components of the Gal4-UAS system are; a tissue specific driver/enhancer that promotes the expression of Gal4, Gal4, an upstream activating sequence (UAS) and a gene of interest (Greenspan 1997; Kelly et al. 2017). The tissue specific enhancer drivers the transcription of Gal4 which culminates in its translation (Brand and Perrimon 1993). Gal4 protein binds to the UAS sequence which activates the expression of the gene of interest (Figure 1.11). A fly with the tissue-specific driver and Gal4 within its genome will be crossed with a fly that contains the UAS and gene of interest so their offspring contain all four elements. In the case of this project, the pan-neuronal driver ELAV-Gal4 and glutamatergic neuronal driver OK371-Gal4 were used to drive human *HTT* transgenes.

Gal4 protein may be supressed to limit expression or knockdown of the target genes during development. This can be done using a temperature-sensitive Gal80 (Tubulin Gal80[TS]),

which is a tissue specific promoter, like Gal4, but at lower temperatures (19°C) it is able to prevent Gal4 from binding to a UAS. (McGuire et al. 2003). At higher temperatures (30°C) Tubulin Gal80^{TS} is no longer active allowing Gal4 to activate the transcription of the gene of interest. Gene switch is another method to limit expression during development (Robles-Murguia et al. 2019). It is a modified Gal4/UAS system which induces the expression transgene upon feeding flies a drug, RU486. These techniques are particularly important when studying age-related diseases, such as Alzheimer's disease, as tau and Aβ/APP can be expressed later on in the flies' lifespan to more accurately depict the disease progression (Purice et al. 2016).

RNA interference (RNAi) facilitates the knock-down of a gene of interest within the *Drosophila* genome (Fire et al. 1998; Hannon 2002; Ma et al. 2006; Ravi et al. 2009). They are used to help to study genes where heterozygous or homozygous knockout would be lethal. The RNAis have a UAS so they can be driven by the same Gal4 drivers to give tissue specificity.

1.5.2 Modelling HD in *Drosophila*

Although *Drosophila* have a conserved *Htt* gene, the CAG repeat tract in exon1 of *HTT* is not well conserved and is absent, however *Drosophila* Htt contains homologous HEAT repeat regions which are crucial for Htt protein-protein interactions (Li et al. 1999). Full-length and truncated human *HTT* (truncated: transgenes containing the first 12 exons) can be successfully introduced to the *Drosophila* genome and used to synthesise HTT protein (Lee et al. 2004; Romero et al. 2008; Weiss and Littleton 2016; Rosas-Arellano et al. 2018). The reason for expressing the first 548 amino acids is due to a lack of homology between *Drosophila* and human huntingtin within the N-terminal region (Lee et al. 2004). Table 1.1 shows some of the common phenotypes in *Drosophila* models of HD.

HD Phenotype	Model and Driver	Reference
Reduced lifespan	Elav-Gal4 – Pan-neuronal: • *HTT*93Q • *HTT*128Qtrunc • *HTT*200QFL • *HTT*103Q nSyb-Gal4 – Pan-neuronal: • *HTT*103Q::mCherry C164-Gal4 – Motor neurons: • *HTT*128QFL OK6-Gal4 – Motor neurons: • *HTT*103Q Ple-Gal4 – Dopaminergic neurons: • *HTT*103Q Cha-Gal4 – Cholinergic neurons: • *HTT*103Q Gem-Gal4 – Early development glia: • *HTT*103Q Repo-Gal4 – Adult glia • *HTT*103Q	(Steffan et al. 2001; Lee et al. 2004; Al-Ramahi et al. 2006; Kaltenbach et al. 2007; Romero et al. 2008; Shiraishi et al. 2014; Besson et al. 2015; Pocas et al. 2015; Yao et al. 2015)
Locomotor deficits	Elav-Gal4 – Pan-neuronal: • *HTT*93Q • *HTT*128Qtrunc • HTT103Q C164-Gal4 – Motor neurons: • *HTT*128QFL OK6-Gal4 – Motor neurons: • *HTT*103Q Ple-Gal4 – Dopaminergic neurons: • *HTT*103Q Cha-Gal4 – Cholinergic neurons: • *HTT*103Q Gem-Gal4 – Early development glia: • *HTT*103Q Repo-Gal4 – Adult glia • *HTT*103Q	(Steffan et al. 2001; Lee et al. 2004; Al-Ramahi et al. 2006; Kaltenbach et al. 2007; Romero et al. 2008; Shiraishi et al. 2014; Besson et al. 2015; Yao et al. 2015)
HTT Aggregation	CCAP-Gal4*/Tubulin Gal80^{TS} – small subset of neurons: • *HTT*138Q::mRFP Or67d-QF – small subset of olfactory neurons: • *HTT*91Q::mCherry TH-Gal4 – Dopaminergic neurons: • *HTT*103Q::mCherry	(Al-Ramahi et al. 2006; Weiss et al. 2012; Babcock and Ganetzky 2015; Pearce et al. 2015; Pocas et al. 2015; Lin et

	Orb83-Gal4 – subset of olfactory neurons: • _HTT_138Q::mCherry Hml-Gal4 – Haemolymph: • _HTT_93Q <u>GMR-Gal4 – eye:</u> • _HTT_128Qtrunc	al. 2019; Donnelly et al. 2020)
Photoreceptor degeneration	<u>Elav-Gal4 – Pan-neuronal:</u> • _HTT_93Q • _HTT_128Qtrunc • _HTT_200QFL <u>GMR-Gal4 – eye:</u> • _HTT_128Qtrunc • _HTT_108Q • _HTT_103Q::mCherry • _HTT_120Q • _HTT_93Q • _HTT_128QFL <u>Rh-Gal4 – photoreceptor neurons:</u> • _HTT_108Q	(Jackson et al. 1998; Steffan et al. 2001; Lee et al. 2004; Sang et al. 2005; Al-Ramahi et al. 2006; Kaltenbach et al. 2007; Romero et al. 2008; Besson et al. 2015; Jimenez-Sanchez et al. 2015; Pocas et al. 2015)
Axonal degeneration	<u>C380-Gal4 – motor neurons:</u> • _HTT_138Q::mRFP	(Weiss and Littleton 2016)
Glial engulfment of mHTT	<u>Or67d-QF – small subset of olfactory neurons:</u> • _HTT_91Q::mCherry	(Pearce et al. 2015; Donnelly et al. 2020)

Table 1.1 – _Drosophila_ models of Huntington's disease. *Expressed in Crustacean cardioactive peptide-secreting cells of the ventral ganglion and brain.

When hu_HTT_ with a pathological repeat is expressed in a subset (dopaminergic/motor/cholinergic/olfactory/photoreceptor) or all neurons of the fly, it can result in reduced survival, locomotor deficits, neurodegeneration and aggregation (Table 1.1) (Weiss et al. 2012; Lewis and Smith 2016). Utilising the Gal4-UAS system, a small subset of neurons can be specifically targeted in order to visualise a localised effect of hu_HTT_ expression. GMR-Gal4 is a tissue-specific driver that yields expression of a transgene in all cells of the _Drosophila_ eye. When a truncated hu_HTT_ transgene containing 128 CAGs (_HTT_128Qtrunc) was expressed in the eyes it caused a rough-eye phenotype with corresponding photoreceptor degradation (Lee et al. 2004). When the same construct was expressed, containing 0 CAGs (_HTT_0Qtrunc), there was no evidence of degeneration.

Electroretinograms have been performed to assess how the neurons in the fly eye respond to a flash of light (Vilinsky and Johnson 2012). They demonstrated that flies expressing *HTT*128Qtrunc, under GMR-Gal4 control, had reduced photoreceptor depolarization and abolishment of synaptic transmission in response to light stimulus in comparison to flies carrying *HTT*0Qtrunc. This was evidence enough to show that the *HTT*128Qtrunc transgene was causing neurodegeneration.

The development of the *Drosophila* eye requires roughly 60% of vital genes (Thaker and Kankel 1992) which is one of the reasons why it has been used for genetic screens. The *Drosophila* eye is a highly structured organ made up of 750 ommatidia which contain 8 photoreceptors that form a trapezoid shape (Thomas and Wassarman 1999). Changes in gene expression can yield physiological changes that include changes to the shape that the photoreceptors form, the number of photoreceptors within each ommatidia and the number of ommatidia in the eye (Iyer et al. 2016). In the realms of HD research these changes have been detected by light, confocal or scanning electron microscopy (Romero et al. 2008) and have shown the detrimental effects of expressing human mutant *HTT* at a cellular level. Romero et al. used a combination of experiments utilising GMR-Gal4 which yields expression in the eye to capture a neurodegeneration phenotype. Romero et al. noted decreased levels of eye pigmentation and lower numbers of ommatidia when *HTT*128QFL was expressed, in comparison to when *HTT*16QFL was expressed under the control of GMR-Gal4. Romero et al. also quantified the number of neuronal projections to the indirect flight muscles which expressed expanded and unexpanded full-length human *HTT* under the control of C164-Gal4. The number of projections decreased with time in flies that expressed *HTT*128QFL (Romero et al. 2008).

HTT aggregate spreading has also been modelled in *Drosophila* models of HD with studies showing fluorescently tagged HTT aggregates localising at synaptic terminals of a defined subset of neurons which gradually spread throughout the brain (Babcock and Ganetzky 2015). When synaptic protein N-ethylmaleimide-sensitive fusion protein 1 was inhibited HTT aggregate uptake and release were impaired. It is thought that phagocytic glia contribute to the transmission of mutant HTT throughout the brain of Drosophila models of HD. They

have been shown to mediate the transmission of soluble and aggregate HTT between neuronal synapses (Pearce et al. 2015; Donnelly et al. 2020).

While somatic instability of CAG repeats has not been investigated in a fly model, intergenerational instability of a CAG repeat tract has been reported. Researcher's inserted a pure noncoding CAG repeat tract of 270 CAGs (UAS-CAG270) to assess if proteins containing a pathogenic glutamine expansion could modify the noncoding CAG repeat tract (Jung et al. 2011). Similarly, to *HTT*, the spinocerebellar ataxia 3 gene (*SCA3*) also contains a CAG repeat tract which when expanded can cause disease. In this study they demonstrated that the coexpression of *SCA3* with a pathological expansion yielded a 20% increase in the likelihood of a +1 expansion of the noncoding CAG repeat tract in female germline cells, in comparison to a 10%-13% likelihood when SCA3 with a shorter CAG repeats were expressed (Jung et al. 2011). This work showed that the expression of a pure CAG repeat tract in germline tissue without the presence of a pathological polyQ protein would incur some instability between generations, but the expression of a pathological polyQ protein exacerbates the likelihood of expansion. They have previously linked the expansion properties of pathological polyQ proteins with the expression of CREB-binding protein (CBP) and histone N-acetyltransferase (HAT) protein, showing that inhibition of these two proteins yields higher degrees of intergenerational repeat instability in the presence of a pathological polyQ protein (Jung and Bonini 2007). *Drosophila* lack homologs for *MSH3* and *FAN1* which suggests that unlike in human disease, CAG repeat instability may not be related to the MMR pathway in *Drosophila* (Wheeler and Dion 2021).

1.6 Project Aims

Human genetic data have suggested the importance of DNA damage repair pathways in determining the age-of-onset of HD. The ability of these genes, and those in related pathways to modify hallmark features of the disease has yet to be determined. *Drosophila* are a useful model for HD research and can be used to screen for modifying genes relevant to behaviour and molecular changes seen in the human condition. If modifying genes are found they could potentially indicate a new therapeutic target for HD.

Primary Aims:

1. Characterise several *Drosophila* models of HD to select a suitable model and phenotype for screening. We will also determine a new way to assess neurodegeneration using the *Drosophila* wing system.

2. Assess whether the CAG repeat tract of human *HTT* can undergo somatic instability in aged *Drosophila* neurons

3. Screen for genetic modifiers of a Drosophila HD model using the locomotion assay.

4. Determine the effect of Parp inhibition on longevity, mutant *HTT* toxicity, locomotion and neurodegeneration.

2. Materials and Methods

2.1 Drosophila Husbandry

2.1.1 Stock maintenance and food

Fly stocks were stored at 18°C and crosses were stored at 25°C in a 12-hour light/dark cycle. Stocks were flipped every 3-4 weeks. Crosses were flipped every 2-3 days.

Ingredient	Volume/weight for 43L of food	Source and Catalogue Number
Deionized water	~42 L	
Agar	300 g	BTP Drewitt, Min Gel 920
Brewers yeast	1000 g	MP biomedical, 903312
Cornmeal	2500 g	MP biomedical, 901411
Molasses	2.5 L	Flystuff SLS, 62-118
Methyl-p-Hydroxybenzoate (Tegosept)	56 g	MP biomedical, 102341
Ethanol absolute	280 mL	Fisher Scientific, E/0600DF/21
Acid mix:	168 mL	
- Propionic Acid	250 mL	Acros Organic, 220130025
- Phosphoric Acid	25 mL	Acros Organic, 201140010
- Deionized water	325 mL	

Table 2.1 - Fly food ingredient list, their volume/weight and their source and catalogue number.

The recipe for it is based off the recipe listed on the Bloomington Drosophila Stock Centre website (Bloomington Drosophila Stock Center. [no date]). The agar (BTP Drewitt, Min Gel 920) was added to ~32 L of hot deionised water and heated to 60°C. 10 L of boiled deionised water was added to the cornmeal (MP biomedical, 901411) and once it is combined it is added to the agar solution. The molasses (Flystuff SLS, 62-118) and brewers yeast (MP biomedical, 903312) were then added to the solution and it is left to cook for 3 hours at ~80°C. During this time the acid mix was prepared and the Tegosept (MP biomedical, 102341) was dissolved in the ethanol (Fisher Scientific, E/0600DF/21). Once the temperature had dropped to 70°C the acid mix and Tegosept were added and the solution was mixed. The food solution was dispensed into plastic vials using the Droso-Filler (FlyTabs/Genesse).

2.1.2 Stock list

Driver	Genotype	Stock Number
Elav-Gal4	*P{w[+mW.hs]=Gaw}elav[C155]*	BDSC - 538
Elav-Gal4; Tubulin-Gal80^{TS}	*P{w[+mW.hs]=Gaw}elav[C155]; P{tubP-GAL80^{ts}}20*	
OK371-gal4	*w[1118]; P{w[+mW.hs]=GawB}VGlut[OK371]*	BDSC - 26160
OK371::mCD8GFP	*w[1118]; OK371-gal4/5xUAS-mCD8::UAS-GFP*	
Transgenes and Markers	**Genotype**	**Stock Number**
GFP	*w[1118]; P{w[+mC]=UAS-GFP.nls}14*	BDSC - 4775
HTT16QFL	*w[1118]; P{w[+mC]=UAS-HTT.16Q.FL}F24/CyO*	BDSC - 33810
HTT128QFL	*w[1118];; P{w[+mC]=UAS-HTT.128Q.FL}f27b*	BDSC - 33808
HTT25QCer	*w[*]; P{w[+mC]=UAS-HTT.25Q.Cerulean}2*	BDSC - 58360
HTT96QCer	*w[*]; P{w[+mC]=UAS-HTT.96Q.Cerulean}2*	BDSC - 56771
HTT15Q::mRFP	*w[1118]; P{UAS-HTT.Q15.mRFP}*	Kindly donated by Troy Littleton
HTT138Q::mRFP	*w[1118]; P{UAS-HTT.Q138.mRFP}*	Kindly donated by Troy Littleton
RNAi	**Genotype**	**Stock Number**
Spelchecker1 / MSH2	*y1 sc* v1 sev21; P{TKO.GS00581}attP40*	BDSC - 76412
Msh6 / MSH6	*y1 sc* v1 sev21; P{TKO.GS01801}attP40*	BDSC - 79765
Tosca / EXO1	*y1 sc* v1 sev21; P{TRiP.GL00443}attP40*	BDSC - 35603
Pms2 / PMS2	*y1 sc* v1 sev21; P{TRiP.HMC03753}attP40*	BDSC - 55614
Parp (2) / PARP1	*y1 sc* v1 sev21; P{TRiP.HMC04658}attP40*	BDSC - 57265
Parp (3) / PARP1	*y1 sc* v1 sev21; P{TRiP.GL00229}attP2/TM3, Sb1*	BDSC - 35792
Parg / PARG	*y1 v1; P{TRiP.HMJ23169}attP40*	BDSC - 61333
Mre11 / MRE11	*y1 v1; P{TRiP.HMS01947}attP40*	BDSC - 39028
Xrcc1 / XRCC1	*y1 v1; P{TRiP.HMJ23251}attP40*	BDSC - 61359
Null mutant	**Genotype**	**Stock Number**
Mre11 / MRE11	*y1 w*; P{EP}mre11G6145/CyO*	BDSC - 26917

Table 2.2 – List of fly stocks used, their genotypes and their stock numbers. BDSC = Bloomington Drosophila Stock Centre. Troy Littleton (Krench and Littleton 2013).

2.1.3 PARP1 Inhibitor Food Prep

In order to assess whether PARP1 inhibitors could affect the locomotor phenotype and Htt aggregate phenotype of the HTT96QCer flies, food treated with PARP1 inhibitors had to be made. 5 mg of Niraparib was dissolved reconstituted in DMSO based on the producers instructions, and further diluted with PBS to a 100 μM stock solution. Veliparib was diluted from 10 mM/mL in DMSO to 100 μM using PBS. DMSO was diluted 1:1000 in PBS (vehicle). 200 mL of 70°C water was added to 36 g of pre-mixed fly food (NUTRI-fly, #66-113) and was

mixed to combine. 2.8 mL of diluted Tegosept (MP biomedical, 102341) as added once the temperature of mixture sunk below 70°C. The inhibitors and DMSO (vehicle) were added once the temperature of the mixture had dropped below 60°C. 1.25 μL of 100 μM Veliparib stock was added to the food to make a final concentration of 5 nM. 12.5 μL of 100 μM Niraparib was added to the food to make a final concentration of 50 nM. 10 μL of diluted DMSO was added to the 200 mL of pre-mixed fly food. The food was mixed well and dispensed into plastic vials. Vials were left covered to set overnight and cotton wool stoppers were individually placed in each vial. Crosses were set up on normal food (described in 2.1.1), after 24 hours the flies were transferred to inhibitor treated food.

Reagents	Supplier and Catalogue Number
Nutri-fly, pre-mixed fly food	Genesee Scientific, 66-113
Tegosept	MP biomedical, 102341
Dimethly sulfoxide	Sigma Life Science, D2438
Veliparib	Selleckchem/Stratech, ABT-888/S1004-SEL-10mM/1mL
Niraparib	Selleckchem/Stratech, MK-487/S2147-SEL-5mg

Table 2.3 – List of reagents used in the preparation of PARP1 inhibitor treated food.

2.2 *Drosophila* Assays to characterise HD-related phenotypes

2.2.1 Lifespan

Linford's protocol for measuring *Drosophila* lifespans (Linford et al. 2013) was referenced in the design of the lifespan experiment to assess whether hu*HTT* or the Parp RNAi had an effect on the lifespan of the flies. Crosses were set and flies eclosing had their genotype assessed. Flies with the correct genotype that eclosed on the same day were transferred to a vial. Only females were used. Vials contained 3-12 flies, with an average of 8 flies per vial. In most cases around 100 flies were assayed. Flies were transferred into new vials every 2-3 days and the number of dead flies was recorded. This continued until all the flies had died. Survival was plotted on Kaplan Meier.

2.2.2 Rapid Iterative Negative Geotaxis (RING) Assay

In order to assess locomotor function of flies expressing hu*HTT*, Gargano's protocol for assessing the effect of age on motor function (Gargano et al. 2005) was used. The RING assay apparatus was designed by Eilish Mackinnon and built by Mr. Mackinnon imaged below.

Figure 2.1 – A photo of the rapid iterative negative geotaxis apparatus.

Flies were transferred into empty plastic vials and then loaded into the RING apparatus. The escape response of the flies was triggered by dropping the apparatus from a height of 20cm. 10 photos were taken over 10 seconds after the apparatus was dropped. The distance climbed by each fly at 4 seconds was calculated in ImageJ, the macros are found in Table 2.

2.2.3 Wing dissections

Flies were anaesthetised and their wings were dissected (Smith et al. 2019) at the hinge of the wing and place onto a Superfrost microscope slide (Epredia, ISO 8037/1) coated in Halocarbon oil (Sigma-Aldrich, H8773) and a glass cover slip (Academy, 400-01-20) was placed on top of the wings. They were imaged using the Zeiss Spinning Disk Confocal microscope, details found in Section 2.5. Cell body number was counted manually. Cell body fluorescence was measured with the Mean Grey Value tool in ImageJ. The background Mean Grey Value was subtracted from each cell body fluorescence measurement. One cell body per wing was quantified (Figure 2.1).
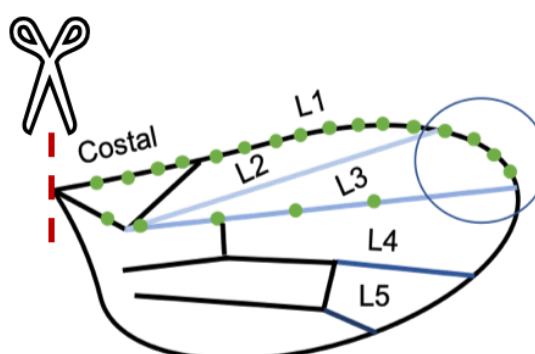
Figure 2.2 – Diagram of the Drosophila wing. The wing is dissected at the hinge by the costal vein. The tip of the L1 vein is imaged (circled in blue). The green dots symbolise the sensory neurons projecting their axons toward the fly body.

2.2.4 Single-cell resolution imaging of neurons in the *Drosophila* wing

Wings were imaged using Laser Scanning Confocal Microscopy (Zeiss Cell Observer), using the Zen software. A z-stack composed of five 1 μm slices was taken of the tip of the L1 vein at 63X magnification with the following settings:

Imaging Set-Up	Setting
SD Laser 488nM	100.0%
Black	35
Gamma	1.00
White	255

2.2.5 Brain dissections

Flies were anaesthetised and their heads were removed from their bodies and fixed in cold 4% PFA for 16 minutes at room temperature. The heads were washed in 0.1% PTx for 30

minutes. Dissected heads were transferred to ice-cold 0.1% PTx. Transfer dissected brains to ice-cold 4% PFA and fix the brains for a second time for 16 minutes at room temperature. The brains were washed in 0.1% PTx for 30 minutes. The brains were mounted on a microscope slide in between two pieces of double-sided tape. The brains were covered with a coverslip and pipette mounting medium into the gap, encasing the brains. They were stored at 4°C. They were imaged using the Zeiss Spinning Disk Confocal microscope, details found in Section 2.5.

Reagents	Ingredients
4% Paraformaldehyde (PFA)	250μL 16% paraformaldehyde in 750μL 1X PBS
0.1% PTx	500uL 10% Triton X-100 in 50mL 1X PBS
1X Phosphate Buffered Saline (PBS)	50mL 10X PBS in 450mL distilled H_2O
Reagents	**Supplier and Catalogue Number**
16% PFA	Thermo Scientific, 11586711
PBS pH 7.4 (10X)	Gibco, 70011-036
Triton-X100	Thermo Scientific, ACROS Organics, 9002-93-1/10591461
Mounting medium	Vectashield Antifade Mounting Medium (H-1000)

Table 2.4 – List of reagents used in the dissection of fly brains.

2.2.6 HTT aggregate imaging

HTT aggregates were imaged using Laser Scanning Confocal Microscopy (Zeiss Cell Observer). To visualise the whole *Drosophila* brain, 60 x 1 μm slices were imaged to form Z-stacks at 10X magnification. To visualise HTT aggregates for quantification, 80 x 1 μm slices were imaged to form Z-stacks at 63X magnification, from each side of the central brain. These imaging settings were used:

Imaging Set-up	Setting
SD Laser 405nm	50.0%
Black	0
Gamma	1.00; 0.45; 1.0
White	2144

2.2.7 Image processing and Htt aggregate analysis

Orthogonal projections of the 80 x 1 μm-slice Z-stacks at 63X magnification were created. Htt aggregate number and area were calculated using ImageJ. The macro can be found in Table 2.7. During this process, obvious trachea were removed, the threshold of the images were altered and the aggregates were counted (Figure 2.2).
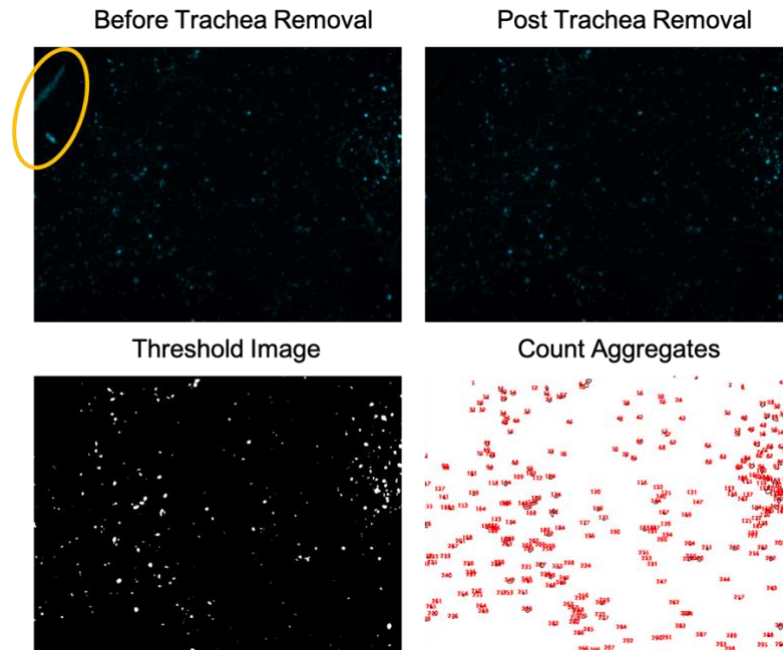
Figure 2.3 – The processing of brain images for HTT aggregate analysis.

2.3 Assessing CAG repeat tract length stability

2.3.1 Genomic DNA extraction – Squish Buffer DNA Extraction

Squish buffer was created by dissolving Tris into 400 mL of distilled water. 5 M HCl was added dropwise until a pH of 8.2 was reached. EDTA and NaCL were added and dissolved into the Tris solution. Once the reagents had dissolved the squish buffer was topped up to 500 mL with distilled water. This solution was dispensed into 50 mL falcon tubes and autoclaved. Concentrations and volumes for the squish buffer reagents can be found in the table below.

Reagent	For 500 mL Squish Buffer	Final concentration
Tris	0.61 g	10 mM
EDTA	0.19 g	1 mM
NaCL	0.73 g	25 mM

Tissue was homogenised with a motorized pestle for 30-60 seconds in 50 μL of squish buffer. An additional 100 μL of squish buffer was added, in addition to 1 μL of Proteinase K 4 μg/mL. Homogenates were incubated at 37°C for 60 minutes, then 85°C for 10 minutes. DNA was quantified by the NanoDrop. DNA was diluted and kept at -20°C.

2.3.2 gDNA purification

DN-easy purification kit (QIAGEN) was used to purify the genomic DNA (gDNA) extracted from the flies (2.3.1). The manufacturer's protocol was followed.

2.3.3 Primer list

Gene	Purpose	Forward (F)/ Reverse(R)	Sequence 5'-3'	Annealing Temperature
HTT	Sequencing	F	GACCCTGGAAAAGCTGATGA	58°C
HTT	Sequencing	R	GGCTGAGGAAGCTGAGGAG	58°C
HTT	GeneScan	F	FAM-ATGAAGGCCTTCGAGTCCCTCAAGTCCTTC	65°C
HTT	GeneScan	R	GGCGGCTGAGGAAGCTGAGGA	65°C
Parp	qRT-PCR	F	GAAGTACGGAGGCCAACCTTT	61°C
Parp	qRT-PCR	R	TATCTTCACCTGACGCAAACC	61°C
GAPDH	qRT-PCR	F	TAAATTCGACTCGACTCACGGT	61°C
GAPDH	qRT-PCR	R	CTCCACCACATACTCGGCTC	61°C
RP-49	qRT-PCR	F	AGCATACAGGCCCAAGATCG	61°C
RP-49	qRT-PCR	R	TGTTGTCGATACCCTTGGGC	61°C

2.3.4 Polymerase Chain Reaction (PCR)

To confirm the presence of the hu*HTT* transgene in the flies and assess the length of the CAG repeat tract, PCRs using primers that amplified hu*HTT* exon1 were performed. Genomic DNA was extracted from individual flies (2.3.1). LA Taq Polymerase with GC Buffers were used for the PCRs as they are ideal for the amplification of GC-rich regions. PCR reactions included:

Reagent	Volume (μL)
TaKaRa LA Taq (5 U/μL)	0.1
GC1 Buffer (1X)	5
dNTP mixture 2.5 mM	1.6
Forward primer 10 pmol/μL	0.5
Reverse primer	0.5
Nuclease free water	0.3
Sample DNA 30 ng/μL	2
Total	10

Reactions were vortexed and centrifuged before being placed in a T100 Thermal-Cycler. The following PCR conditions were used:

Cycles	Temperature	Time
1	94°C	3 minutes
35	94°C	30 seconds
	58/65°C	30 seconds
	72°C	90 seconds
1	72°C	5 minutes
	4°C	Forever

2.3.5 Gel Electrophoresis

PCR products were run on 1.8% agarose gels made with 0.5% TBE. A volume of DNA Gel Loading Dye (Thermo Scientific) that equated to 10% of the volume of the PCR product was added to each PCR product. 2.5uL of HyperLadder™ 100bp (Bioline) was loaded into the first lane of each gel. 10-15 μL of PCR product and loading dye was loaded into each lane. Gels were electrophoresed at 100 V for 2 hours. Bands were visualised with the Gel Doc XR+ Imaging System (Bio-Rad).

2.3.6 Gel DNA extraction

A DNA gel extraction kit was used to extract DNA from an agarose gel for sequencing. The Monarch DNA Gel Extraction Kit was used (New England BioLabs Inc) and the manufacturer's instructions were followed. DNA bands were visualised with the BluPAD (Bio-Helix).

2.3.7 GeneScan

In order to assess whether the CAG repeat tracts present in the hu*HTT* could undergo expansion when expressed in *Drosophila* neurons, GeneScan was performed. Fluorescently labelled (FAM) forward primer and a reverse primer were used to amplify the exon1 fragment of HTT. The PCR generated fluorescently tagged PCR products which are separated by capillary electrophoresis (GeneScan). PCR products were mixed with Hi-Di^{TM} Formamide (Applied Biosystems) and a GeneScan^{TM}-600 LIZ size standard (Applied Biosystems).

	Volume (µL)
PCR product	0.5
Hi-Di formamide	9.1
GeneScan-600 LIZ size standard	0.4
Total	10

Reactions were centrifuged then subjected to a denaturation step.

Cycles	Temperature	Time
1	95°C	4 minutes
1	4°C	3 minutes

Samples were added to the GA3130xL Genetic Analyser (Applied Biosystems) and a run module was created according to the manufacturer's recommendations. Peak scanner v2.0 and GeneMapper software were used to view the CAG repeat size distribution traces of the HTT gene. They were also used to determine the CAG repeat tract length. CAG repeat tract length was determined from the size of the modal peak in the trace:

$$HTT\ CAG\ repeat\ length = \frac{size\ of\ modal\ peak - 80}{3}$$

2.3.8 Sanger sequencing

Sanger Sequencing was used to assess the composition of the CAG repeat tracts in the *Drosophila* HD models. Genomic DNA was extracted (2.3.1) and purified (2.3.2). PCRs were performed with the relevant primers at the relevant settings (2.3.3 and 2.3.4) with 30 ng of DNA. In some cases, DNA had to be extracted from a gel (2.3.6). PCR products were purified using the Monarch PCR and DNA kit (New England BioLabs Inc). Purified PCR product was eluted in XμL of nuclease-free water. 5 μL of purified PCR product (≈20 ng/μL) were added to an eppendorf with 2.5 μL of the forward primer and 2.5 μL of the reverse primer (5 pmol/μL) that was used in the PCR. This sequencing was performed by Source BioSciences. SnapGene Viewer was used to assess the CAG repeat tract length and composition.

2.4 Assessing Parp expression levels

2.4.1 RNA extraction

Fly heads were removed from the flies and 8 heads from each genotype was added to 250 μL of TRIZOL (brand). They were homogenised using a motorised pestle for 1 minute. 250 μL was added to the homogenates and they were incubated for 5 minutes at room temperature. The samples were centrifuged for 5 minutes at 10,000 x g (4°C) to pellet undissolved tissue. The supernatant was transferred to an eppendorf and 100 μL of chloroform (brand) was added to the supernatant and it was shaken vigorously for 15 seconds. The supernatant was then incubated at room temperature for 5 minutes. Following incubation, the samples were centrifuged for 15 minutes at full speed (4°C). The upper aqueous phase was transferred to a RNase-free tube. A volume of isopropanol (brand) equal to the aqueous phase was added to the aqueous phase and mixed by inversion and incubated at room temperature for 10 minutes. Following incubation, the samples were centrifuged at full speed for 10 minutes (4°C). following centrifugation, the samples were washed with 70% ethanol (in RNase free water). The pellet was disrupted in ethanol then centrifuged again at full speed for 3 minutes (4°C) and the supernatant was removed. This washing step was repeated. The RNA pellet was left to dry for 10-30 minutes until it goes from white to a colourless gel. The RNA was resuspended in 20 μL RNase-free water. RNA concentration and quality were checked by the Nanodrop. RNA samples were diluted to 600 ng/μL then stored at -80°C.

2.4.2 RNA purification

The TURBO DNA-free kit (Invitrogen) was used to remove contaminating DNA from the RNA samples. The manufacturer's instructions were followed.

2.4.3 Reverse transcription

RNA was converted into cDNA using the Quantitect Reverse Transcription Kit (Qiagen). The manufacturer's instructions were followed.

2.4.4 SYBR Green qRT-PCR

Nuclease free water (40 μL) was added to each cDNA sample and control to make a total volume of 60 μL. Table 2.5 depicts the composition of each qRT-PCR reaction. QuantStudio7 was used to determine the amount of PCR product at a given cycle.

Component	Final concentration	1 Reaction in 384 well plate (μL)
SYBR (2X)	1X	5
Forward Primer (10μM)	0.3 μM	0.3
Reverse Primer (10μM)	0.3 μM	0.3
ROX solution (5μM)	10 nM	0.02
Template DNA	< 500 ng	3
Water		1.38
Total		10

Table 2.5 - Reaction volumes for SYBR Green qRT-PCR.

2.4.5 qRT-PCR Analysis

The amplification efficiency of each reaction was calculated using the qPCR package in R Studio by fitting sigmoidal curves to fluorescence intensity using the *pcrbatch* function. The *ratiobatch* function was used to calculate the fold-change ratio. The *ratiobatch* calculation can be found below:

$$\frac{E(gc)^{cp(gc)}}{E(gs)^{cp(gs)}} / \frac{E(rc)^{cp(rc)}}{E(rs)^{cp(rs)}}$$

Symbol	Definition
E	Amplification efficiency
cp	Crossing point
gc	Target gene experimental samples
gs	Target gene of control samples
rc	Reference gene of experimental samples
rs	Reference gene of control samples

Statistical significance was calculated by pairwise fixed random reallocation test, similar to the REST software (Pfaffl et al. 2002). Amplification efficiency values are connected to cp values and are randomly mixed between experimental and control samples for 1000 permutations. For each permutation a fold-change value is calculated and compared to the original value that was generated. The number of permutations which produce a fold-

change greater than, less than or equal to the original value is used to produce a p value which represents the probability that the fold-change calculated from the original value was due to chance.

2.4 iPSC Culture

2.4.1 Cell culture reagents

Cell culture reagent	Supplier	Catalogue Number
Essential 8 Flex Medium Kit	Life Technologies	A2858501
Advanced DMEM/F-12	Life Technologies	12634028
Knockout DMEM/F-12	Life Technologies	12660012
Glutamax	Thermo Fischer	35050-038
Penicillin/Streptomycin (5000U/5000μg)	Gibco	15070063
CryoStor CS10	Stem Cell Technologies	07931
ReLeSR	Stem Cell Technologies	05873
D-PBS	Life Technologies	14190250
Y-27632 dihydrochloride (ROCK Inhibitor)	Tocris	1254
Paraformaldehyde (4%)	Sigma-Aldrich	1.00496
KBrO$_3$	VWR International Ltd	1099250001

Table 2.6 - List of reagents used for stem cell culture and differentiation.

2.4.2 iPSC maintenance

Human Q109 and isogenic controls Q22 induced pluripotent stem cells (iPSCs) were kindly donated by Jasmine Donaldson (Donaldson 2019). The Q109 cells (11b11) contained an expanded CAG *HTT* allele of 109 repeats and the Q22 cells (2h1) contained the corrected CAG *HTT* allele with 22 repeats (Donaldson 2019). The iPSCs were cultured on vitronectin-coated plated (0.5 μg/cm^2) (Life Technologies) in Essential 8 Flex medium (E8 Flex) (Life Technologies) and 0.1% Penicillin/Streptomycin (Gibco) under standard culturing conditions (37°C, 5% CO$_2$).

Cells were passaged every 3-4 days after reach ~70% confluency. When passaging cells, they were incubated with ReLeSR (Stem Cell Technologies) for 1 minute at 37°C. After aspirating the ReLeSR (Stem Cell Technologies), cells were dissociated into small groups in fresh warmed media, and were seeded into a new plate at a density of 1:10.

When freezing the iPSCs, the cells were dissociated as described above, centrifuged at 1000rpm for minutes and then resuspended in CryoStor CS10 (Stem Cell Technologies) with

approximately 1×10^6 cells/0.5 mL CryoStor CS10. Cryovials containing the cell suspension were transferred to a Cool Cell Freezing Container (Corning) and placed at -80°C where cells were frozen at a rate of -1°C/minute.

For thawing the iPSCs, cryovials were warmed to 37°C in a water bath for 1-2 minutes until partially thawed. 1 mL of Advanced DMEM/F-12 (ADF) (Life Technologies) was added to the thawed cell suspension dropwise. The cell suspension was transferred to an eppendorf, then centrifuged at 1000 rpm for 3 minutes, then resuspended in warmed E8 Flex Media containing 10 μM Y-27632 dihydrochloride (Rock Inhibitor).

2.4.3 Reactive Oxygen Species (ROS) treatment

iPSCs were seeded at a density of 1:10 and incubated at 37°C for 2 days until the wells met ~70% confluency. The cells were treated with either E8 Flex media, or 1 mM/10 mM $KBrO_3$ (VWR International Ltd) in E8 Flex Media for 2 hours. Cells were washed in D-PBS (Life Technologies) then fixed in 4% PFA (Sigma-Aldrich) for 15 minutes, washed again and stored in DPBS at 4°C.

2.4.4 Immunocytochemistry

Following fixation, the cells were permeabilised using 0.1% triton-X (Sigma-Alrdich) in PBS for 30 minutes. The cells were washed gently 3 times with PBS. Cells were blocked with 1% BSA in PBS at room temperature for 1 hour, to prevent non-specific binding. The cells were then incubated with primary antibody at the appropriate dilution (Table 2.7), overnight at 4°C. Following 1° antibody incubation the cells were washed in 3 x 20-minute washes in PBS. The cells were incubated with the appropriate secondary antibodies (Table 2.7) in a humidified chamber for 1 hour. Following 2° antibody incubation the cells were washed in PBS (3 x 20 minutes). The nuclear stain Hoechst was subsequently added to the wells for 10 minutes at room temperature. The cells were washed again in PBS (3 x 20 minutes) then the plate was covered in parafilm and tin foil then stored at 4°C for at least 24 hours before imaging.

1° Antibody	Dilution	Supplier	Catalogue Number
PAR	1:200	Sigma Aldrich	MABE1016
γ-H2AX	1:250	Abcam	ab11174
Stain	**Dilution**	**Supplier**	**Catalogue Number**
Hoechst 33342 (12.3mg/mL)	1:12,000	Thermo	62249
2° Antibody	**Dilution**	**Supplier**	**Catalogue Number**
Alexa Fluor 488 Goat anti-rabbit	1:400	Invitrogen	A11001
Alexa Fluor 568 Donkey Anti-mouse	1:400	Invitrogen	A21202

Table 2.7 - List of antibodies and dilutions.

2.4.5 Cell imaging and analysis

Cells were imaged using the Leica DM6000B inverted fluorescence microscope. 3 representative images were taken from each well. Colonies were imaged at 20X magnification. 10 x 1 μm sliced z-stacks were imaged. The z-stacks were converted into orthogonal projections. Nuclear PAR and γ-H2AX signal were analysed with ImageJ, macro described in Table 2.8.

2.6 Macros and Statistics

2.6.1 ImageJ Macros

Macro Name	Macro Instructions

Image Crop	run("Crop");
	
	run("8-bit");
	
	run("Subtract Background...", "rolling=30 light");
	
	setAutoThreshold("Default");
	
	//run("Threshold...");
	
	//setThreshold(0, 203);
	
	setOption("BlackBackground", true);
	
	run("Convert to Mask");

Particle Analysis	run("Set Scale...", "distance=2012 known=8.0 pixel=1 unit=cm");
	
	run("Analyze Particles...", "size=0.010-Infinity show=Outlines display");
	
	run("script:Analyse Particles.ijm.ijm");

HTT Aggregate Analysis	run("Enhance Contrast...", "saturated=0.3");
	
	//run("Threshold...");
	
	setThreshold(0, 1000);
	
	run("Convert to Mask");
	
	setOption("BlackBackground", true);
	
	run("Convert to Mask");
	
	run("Set Measurements...", "area mean min center perimeter shape
	
	redirect=None decimal=3");
	
	run("Analyze Particles...", "size=0-50 show=Outlines display include");

Nuclear PAR Analysis	name=getTitle()
	
	roiManager("reset");
	
	run("Split Channels");
	
	selectWindow("C1-"+name);
	
	setAutoThreshold("Default dark");
	
	//run("Threshold...");
	
	setThreshold(450, 1250);
	
	setOption("BlackBackground", true);
	
	run("Make Binary", "method=Default background=Dark calculate black");
	
	run("Watershed", "stack");
	
	//run("Threshold...");
	
	run("Analyze Particles...", "size=100-2000 pixel circularity=0.01-1.00
	
	show=Outlines add");

	selectWindow("C2-"+name);
	roiManager("measure");
	run("Summarize");
	IJ.renameResults(name);
Nuclear γ-H2AX Analysis	roiManager("reset");
	run("Split Channels");
	selectWindow("C1-"+name);
	setAutoThreshold("Default dark");
	//run("Threshold...");
	setThreshold(750, 65535);
	setOption("BlackBackground", true);
	run("Make Binary", "method=Default background=Dark calculate black");
	run("Watershed", "stack");
	//run("Threshold...");
	run("Analyze Particles...", "size=100-2000 pixel circularity=0.01-1.00 show=Outlines add");
	selectWindow("C3-"+name);
	roiManager("measure");
	run("Summarize");
	IJ.renameResults(name);

Table 2.8 – ImageJ Macros for quantifying the negative geotaxis, H*TT* aggregate number, nuclear PAR intensity and nuclear y-H2AX intensity. Yellow highlight indicates scale that could change depending on camera position in RING Assay.

2.6.2 Statistics

The data was checked to see if it was normally distributed in order to choose a parametric or non-parametric test. In order to calculate significance in each data set a combination of t-tests, One-way ANOVA and Two-way ANOVA with post hoc multiple comparisons were used based on the type of data. All data were analysed and plotted in Graph Pad Prism 9.

3. A characterisation of *Drosophila* models of Huntington's disease.

3.1 Introduction

Prior to investigating the effect of potential genetic modifiers in *Drosophila* models of HD, an in-depth characterisation was necessary to choose the most suitable and robust system, to cover a range of experiments including lifespan, locomotion assays and to measure aggregate formation. The models sourced for future experiments are represented in Table 3.1. Models containing various human *HTT* transgenic constructs were characterised. *HTT* contains a CAG repeat tract in exon 1, whereas *Drosophila Htt* does not contain this region (Li et al. 1999). Lifespan and locomotion assays are the gold standard when characterising the effect of neurodegenerative disease-causing genes in *Drosophila* as they indicate CNS function. The Longevity Assay (Linford et al. 2013) and the RING Assay (Gargano et al. 2005) were used to measure lifespan and locomotive function respectively.

Model	*HTT* gene length	Fluorescent Tag	Reported CAG Length	Reference
*HTT*128Q (*UAS-HTT.128Q.FL*)	Full-length	No	128 CAGs	(Romero et al. 2008)
*HTT*16Q (*UAS-HTT.16Q.FL*)	Full-length	No	16 CAGs	(Romero et al. 2008)
*HTT*96QCer (*UAS-HTT.96Q.Cerulean*)	First coding exon	Cerulean fluorescent protein (CFP)	96 CAGs	(Quinn, 2014)
*HTT*25QCer (*UAS-HTT.25Q.Cerulean*)	First coding exon	CFP	25 CAGs	(Quinn, 2014)

Table 3.1 – The *Drosophila* models of HD that were characterised in this results chapter.

Previous studies have shown that expressing *HTT* with an expanded CAG tract in all or a subset of neurons leads to a shortened lifespan of *Drosophila* (Rosas-Arellano et al. 2018). Locomotor defects have also been observed in *Drosophila* expressing mutant *HTT* (Lee et al. 2004; Liévens et al. 2008; Tamura et al. 2011). Aggregation of mutant human HTT occurs in *Drosophila* depending on the cell-type expression and the transgene expressed. GMR-gal4 yields expression of *HTT* in the photoreceptors of the eye which produces eye degeneration

phenotypes and aggregation of mutant HTT, whereas ELAV causes a wider level of expression in all neurons of the fly (Babcock and Ganetzky 2015). Fluorescently tagged *HTT* transgenes are preferable for visualising aggregates as it negates the need for aggregate staining. These studies demonstrate that the hallmark features of mutant *HTT* toxicity can be efficiently modelled in the fly and capture the pathological state of HD. However, it is clear that studies to visualise and quantify neuronal degeneration beyond the eye are currently lacking.

There is a plethora of causes of cell death related to the expression of mutant HTT ranging from programmed apoptosis during development to glutamate-induced excitotoxicity, but it is not fully understood how neurons die in HD (Sawa et al. 2003; Fricker et al. 2018). HTT protein has several functions in neurons although not all of them are comprehensively described. We do know that it is essential for neurodevelopment (Ma et al. 2010; Bates et al. 2015) and that it has been implicated in transcription, cellular homeostasis, autophagy, endocytosis and RNA splicing (Schulte and Littleton 2011; Dé Ric Saudou and Humbert 2016). From this extensive list of associated pathways we can predict that when *HTT* becomes mutated it may have a detrimental effect on several cellular pathways, which all likely play a role in neurodegeneration. For example; mutant *HTT* mRNA fragments have been shown to interfere with mitochondrial protein transport and cause alterations in mitochondrial dynamics which make neurons more susceptible to excitotoxicity (Panov et al. 2002; Costa et al. 2010; Yano et al. 2014; Carmo et al. 2018). Apoptosis, axonal degeneration and necrosis have also been implicated as cell death pathways activated in HD (Portera-Cailliau et al. 1995; Li et al. 2001; Tang et al. 2005; Vis et al. 2005; Mao et al. 2016; Ramdzan et al. 2017). We propose an assay that can investigate neurodegeneration and the mechanisms active prior to it by observing the neuronal survival in the *Drosophila* wing. Using this *in vivo* assay to visualise neurons dying we aim to associate neuronal loss with behavioural changes.

There is a set of sensory glutamatergic neurons that are activated by the bristle hairs of the wing and their cell bodies project from the tip of the wing down the L1 vein, through the costal vein and into the body of the fly (Fig 3.5A). The Gal4-UAS system can be used to yield expression of fluorescent proteins in this subset of neurons so they can be viewed by

fluorescent microscope at single neuron resolution (See Chapter 1.5.1). This system was used to characterise Wallerian degeneration in *Drosophila* although the assay we used was an adaptation of previously published assays (Coleman and Freeman 2010). In previous experiments used to investigate axonal injury, the fluorescently labelled axons of the costal vein are injured by a small cut. Axonal degeneration was observed by the fragmenting of the fluorescent axons, general loss of fluorescence in the injured area and loss of visible cell bodies in the L1 vein (Soares et al. 2014; Fang and Bonini 2015). In addition to injury the wing system can be used to study mechanisms of neurodegeneration associated with mitochondrial dysfunction and neuronal ageing (Vagnoni and Bullock 2016; Vagnoni and Bullock 2018; Smith et al. 2019; Lin et al. 2021). The tip of the L1 vein was imaged and the number of cell bodies and fluorescence of those cell bodies were quantified to determine whether neurodegeneration was occurring as a result of mutant *HTT* expression. This method created a quick way to test for neurodegeneration without use of antibody staining. The combination of the standard locomotion and lifespan assays with the wing neurodegeneration assay provided insights into the effect of m*HTT* expression in *Drosophila* neurons.

3.1.1 Aims and Hypothesis

I hypothesised that flies expressing mutant *HTT* in neurons would induce deficits in lifespan, locomotion and neuronal survival which could be used to model aspects of HD.

Aim 1) Compare humanised transgenic HD fly models with varying CAG repeat tract lengths, for their ability to induce widely used deficits in locomotion and lifespan.

Aim 2) Visualise mutant HTT induced neurodegeneration and aggregate formation directly using fluorescent neuronal markers and tagged versions of the *HTT* transgene.

Aim 3) Investigate how neurons are dying i.e. a gradual die-back (axons then cell body) or a ubiquitous profile of neurodegeneration.

Aim 4) Choose an appropriate model and assay to use for a screen to investigate genetic modifiers of mutant *HTT* (for Screen see Chapter 6).

3.1.2 Experimental Design

In order to measure the effect of *HTT* on the lifespan, locomotion and neurodegeneration of *Drosophila melanogaster*, *HTT* transgenes containing different CAG repeat lengths were expressed in different populations of neurons (Table 2). For lifespan and locomotion experiments, full-length *HTT* with 128 or 16 repeats were expressed pan-neuronally by the driver ELAV-Gal4 (Koushika et al. 1996), (Crossing Scheme 3.1). The lifespan and locomotor function of the flies' pan-neuronally expressing the cerulean fluorescently tagged HTT were also measured. The flies expressing full-length *HTT* with 16 CAGs was used as an expression control for the flies expressing full-length *HTT* with 128 CAGs. The protocols for Linford method was followed for the measurement of lifespan (Linford et al. 2013) and the RING Assay was used for the measurement of locomotive function (Gargano et al. 2005) (See Methods 2.2.1 and 2.2.2). The RING Assay was performed at 1 dpe, 7 dpe and then every 7 days until the end of the lifespan of the flies expressing *HTT* with 128 CAGs. This enabled 4 measurements throughout the flies' lifespan and enough time to produce a phenotype. The flies were measured climbing for four seconds as it was enough time for the best-performing control flies to reach to the top of the vial, but not enough time for them to be able to climb or fly back down the vial again.
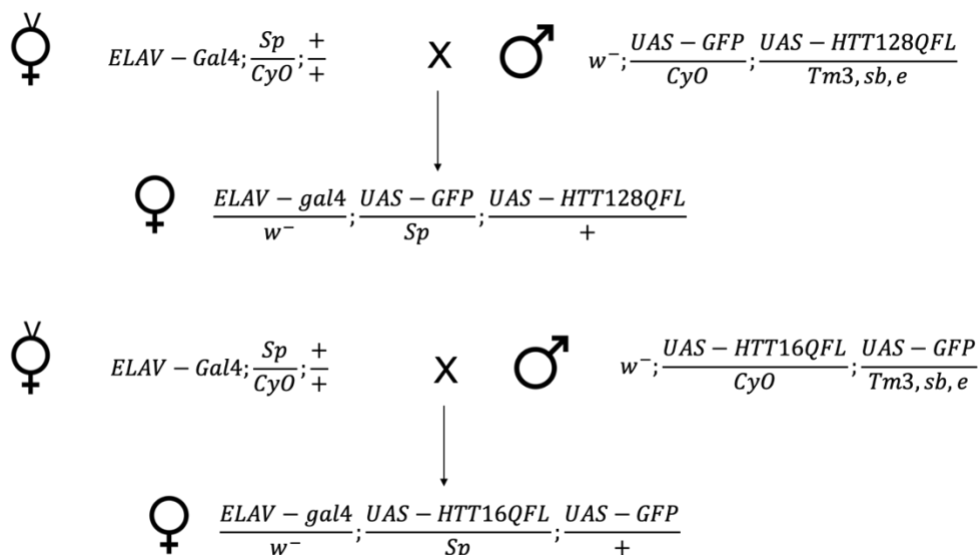
Crossing Scheme 3.1 – Pan-neuronal driver (ELAV-Gal4) carrying virgins are crossed with males carrying UAS-GFP and UAS-*HTT* with either 16 or 128 CAGs. The resulting progeny express GFP and full-length human *HTT* in all neurons.

To make it easier to visualise *HTT* within the fly, fluorescently tagged *HTT* transgenes were crossed with ELAV-Gal4 (Crossing Scheme 2). These flies were used to assess HTT aggregation in the brain.

$$\female \quad ELAV-Gal4; \frac{Sp}{CyO}; \frac{+}{+} \qquad X \qquad \male \quad w^-; \frac{UAS-HTT96QCer}{CyO}; \frac{Dr}{Tm3,Sb,e}$$

$$\downarrow$$

$$\female \quad \frac{ELAV-gal4}{w^-}; \frac{UAS-HTT96QCer}{Sp}; \frac{+}{Tm3,Sb,e}$$

$$\female \quad ELAV-Gal4; \frac{Sp}{CyO}; \frac{+}{+} \qquad X \qquad \male \quad w^-; \frac{UAS-HTT25QCer}{CyO}; \frac{+}{+}$$

$$\downarrow$$

$$\female \quad \frac{ELAV-gal4}{w^-}; \frac{UAS-HTT25QCer}{Sp}; \frac{+}{+}$$
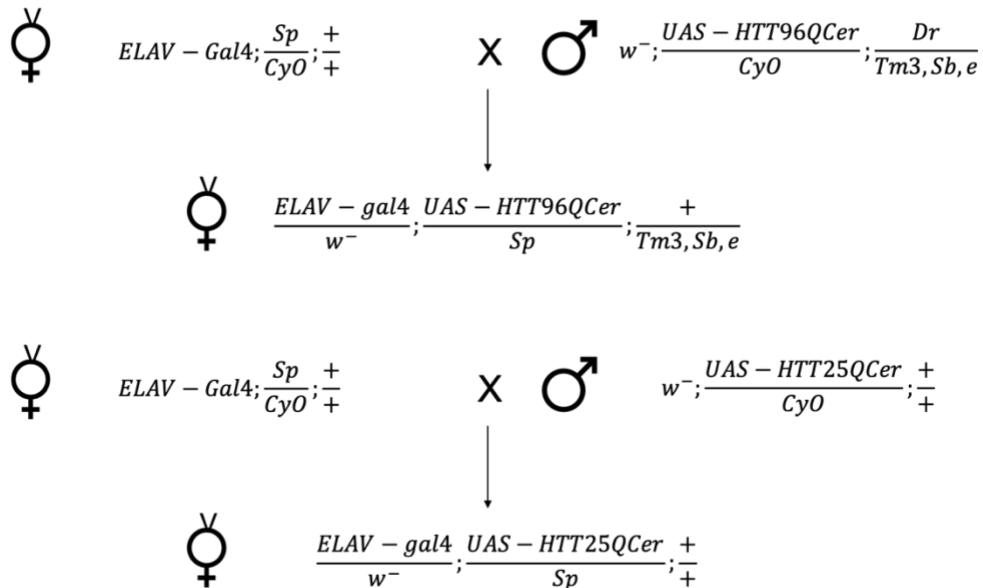
Crossing Scheme 3.2 – Virgin flies carrying the pan-neuronal driver ELAV-Gal4 were crossed with male flies carrying a human HTT construct tagged with a C-terminal Cerulean Fluorescent Protein, with either 96 or 25 CAG repeats. The resulting progeny expressed this human HTT construct in all neurons.

Canonically neurodegeneration has been judged by the mass of brain regions expressing human mutant genes and comparing to control. This process is time-consuming and a quicker single-neuron resolution protocol was desired. The neurodegeneration assay was inspired by assays usually used to investigate axonal injury (Llobet Rosell and Neukomm 2019). The glutamatergic neuronal driver OK371-gal4 was used to drive the expression of GFP and the full-length hu*HTT* constructs in the mechano-sensory neurons of the L1 vein, (Crossing Scheme 3.3).

Female $w^-; \dfrac{UAS-GFP}{CyO}; \dfrac{UAS-HTT128QFL}{Tm3,sb,e}$ X Male $w^-; \dfrac{OK371-gal4}{CyO}; \dfrac{+}{+}$

Female + Male $w^-; \dfrac{UAS-GFP}{OK371-gal4}; \dfrac{UAS-HTT128QFL}{+}$

Female $w^-; \dfrac{UAS-HTT16QFL}{CyO}; \dfrac{UAS-GFP}{Tm3,sb,e}$ X Male $w^-; \dfrac{OK371-gal4}{CyO}; \dfrac{+}{+}$

Female + Male $w^-; \dfrac{UAS-HTT16QFL}{OK371-gal4}; \dfrac{UAS-GFP}{+}$
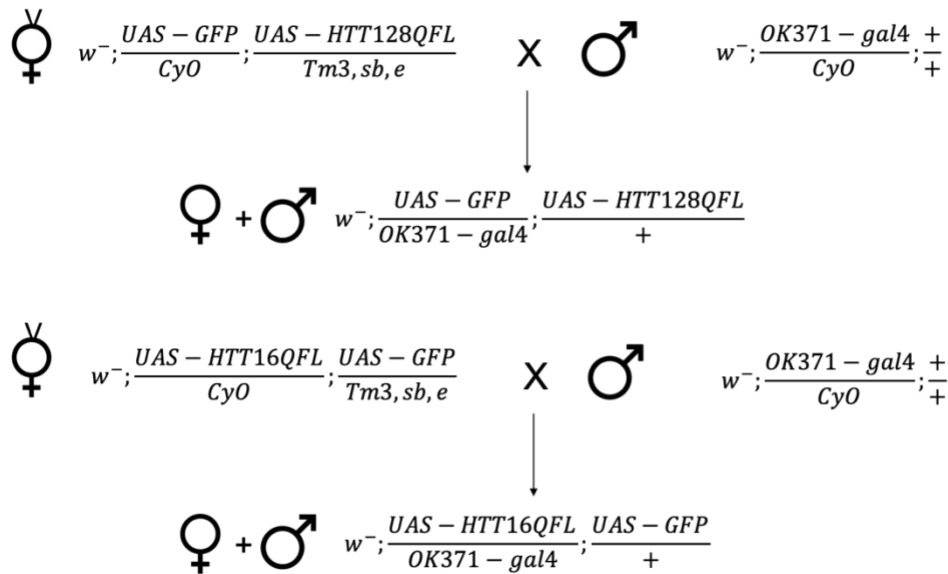
Crossing Scheme 3.3 – Glutamatergic neuronal driver (OK371-Gal4) males were crossed with virgin flies that carried UAS-GFP and UAS-*HTT* with either 16 or 128 repeats. The resulting progeny express GFP and human *HTT* in glutamatergic neurons.

Single neurons at the tip of the L1 vein were imaged using the driver OK371-gal4 which drove the expression of GFP and *HTT* in glutamatergic neurons (Mahr and Aberle 2006). In the wing this expression is specific to sensory neurons that receive input from the hairs on the wing (Neukomm et al. 2014). GFP was expressed in the neurons which were viewed with Spinning Disc Confocal Fluorescent Microscopy. In this procedure the wings were removed and the green fluorescence was maintained for up to an hour after dissection. It was not as invasive as a brain dissection and created a quick way to check the viability of the neurons. The tip of the L1 vein is known to have 3-4 defined cell bodies, so any changes in number, morphology or fluorescence of the cell bodies would be easy to detect (Soares et al. 2014).

3.2 Results

3.2.1 Longevity assay shows flies with longer CAG length live shorter lifespan

Previous research has shown that flies expressing full-length mutant hu*HTT* with an expanded CAG repeat in dopaminergic neurons results in shorter lifespans (Romero et al. 2008), but it was important to assess this pan-neuronally. It was also important to assess the effect of pan-neuronal expression of the cerulean fluorescent constructs on the lifespan as it has not been published.
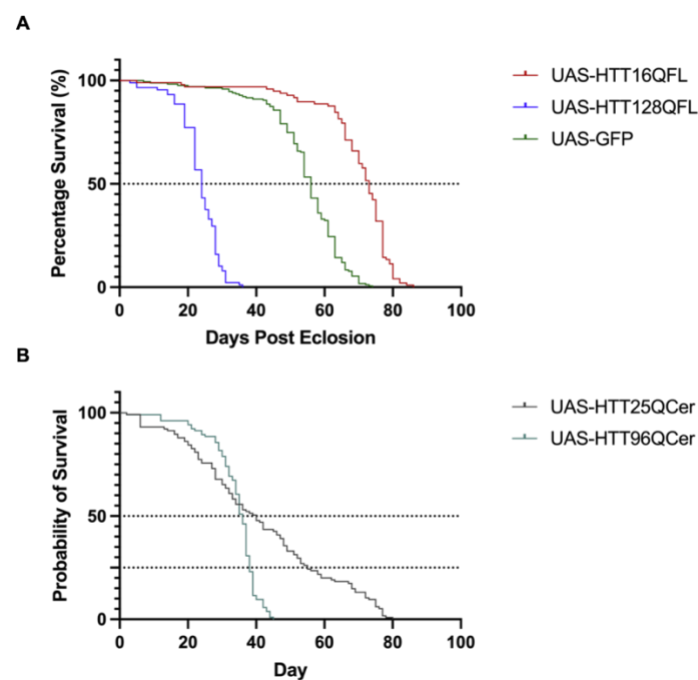
Figure 3.1 – Expression of pathological hu*HTT* reduces lifespan. (A) Kaplan Meier Plot displaying the percentage survival of flies pan-neuronally expressing *HTT*128QFL and *HTT*16QFL, as well as flies pan-neuronally expressing GFP (GFP n=167, *HTT*16QFL n=156, *HTT*128QFL n=182). (B) Kaplan Meier Plot displaying the percentage survivorship of flies' pan-neuronally expressing HTT96QCer and *HTT*25QCer. (*HTT*96QCer n=104, *HTT*25QCer n=115). Data were plotted as percentage survival, and significance was calculated by the Mantel-Cox Test.

Two models were used to investigate the effect of pan-neuronal expression of *HTT* on the lifespans of *Drosophila melanogaster*. The flies expressing full-length *HTT* with a longer CAG repeat had a shorter lifespan, with the *HTT*128QFL expressing flies having a median lifespan of 24 days (Figure 3.1A). The flies expressing *HTT*16QFL had a median lifespan of 68 days and the flies expressing only GFP had a median lifespan of 56 days. The Log-rank (Mantel-Cox) Test showed a significant difference between the longevity curves of the fly models,

with the lifespan of *HTT*128QFL being significantly shorter than the controls (df = 1, p<0.0001) which is consistent with previous reporting of the model (Romero et al. 2008).

The Log-rank (Mantel-Cox) test also showed a significant difference between the median lifespan of the GFP expressing flies and the *HTT*16QFL expressing flies (df = 1, p < 0.0001). These results showed that flies expressing *HTT* with a non-pathogenic CAG repeat tract have a significantly longer lifespan than those expressing GFP, and that expressing non-pathogenic full-length *HTT* has no damaging effect on the lifespan of the fly.

The median lifespan of the flies expressing *HTT*96QCer and *HTT*25QCer were similar. The *HTT*25QCer expressing flies had a median lifespan of 40 days which was only 4 days longer than the *HTT*96QCer expressing flies, which had a median lifespan of 36 days. However, their survival curves differ in shape. The remaining *HTT*96QCer flies died within 7 days of the median survival time point with the last fly dying at 43 days. However, the remaining *HTT*25QCer flies died within 40 days with the last fly dying at 80 days. Log-rank (Mantel-Cox) test showed there was a highly significant difference between the survival curves of the CFP-tagged *HTT* flies (df = 1, p < 0.0001). This shows that while the median lifespans of the CFP-tagged *HTT* flies may be similar, *HTT* with a pathological expansion is still having a detrimental effect on the flies' lifespan.

The median lifespan of the *HTT*96QCer flies was longer than the lifespan of the *HTT*128QFL flies, at 40 and 24 days respectively. The *HTT*128QFL construct has ~30 more CAGs in the repeat tract in comparison to the *HTT*96QCer construct. This suggests that expressing hu*HTT* with a longer pathological expansion is more toxic than a *HTT* construct with a shorter pathological CAG repeat tract.

3.2.2 Longer CAG tract leads to increased locomotive deficits in ageing *HTT* flies

Motor deficits are a hallmark of HD with most patients presenting the characteristic chorea during the course of their disease (Kremer et al. 1994). The RING assay measures a fly's innate escape response which in turn is its ability to climb up the side of the tube (Gargano et al. 2005). Previous research has shown that expressing full-length pathological human *HTT* in dopaminergic neurons negatively affects a fly's climbing ability and flying ability (Romero et al. 2008), so it was important to assess the locomotor performance of flies expressing these constructs pan-neuronally. As with the lifespan, it was important to assess the effect of pan-neuronal expression of the cerulean fluorescent constructs on the locomotor function of the flies as it has not been published.
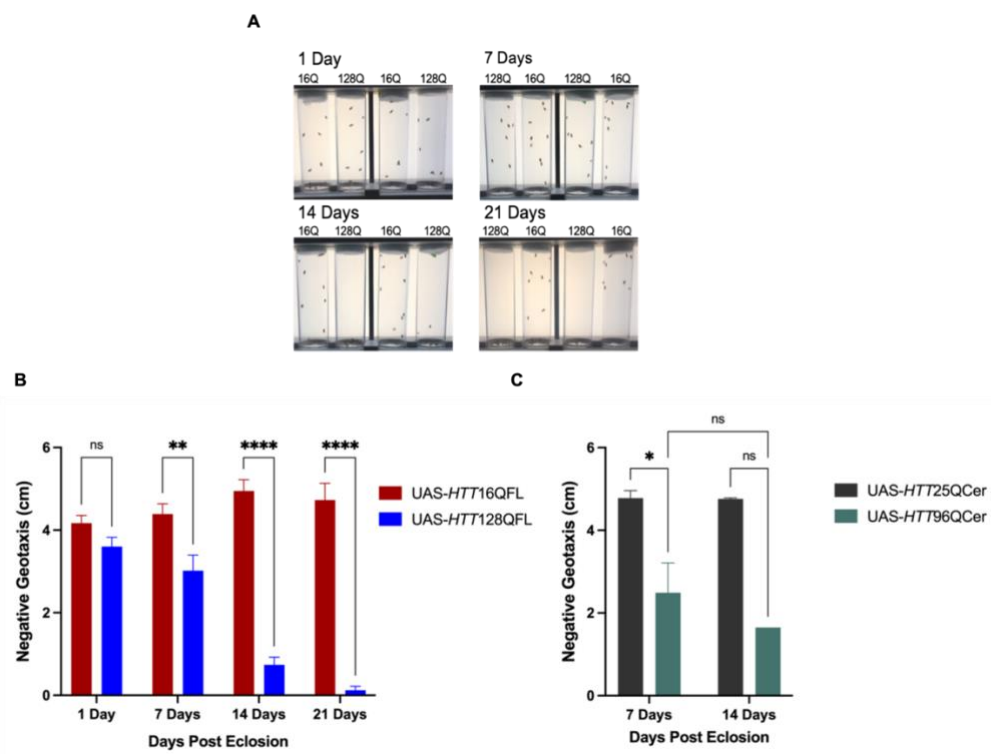
Figure 3.2 – Locomotor deficits occur with increased CAG repeat size as the flies age. (A) Images depicting the climbing position of flies pan-neuronally expressing *HTT* with different repeat sizes at increasing time points. (B) Average distance climbed by flies expressing full-length *HTT* after 4 seconds at 1, 7, 14 and 21 dpe. (C) Average distance (cm) climbed by flies expressing cerulean fluorescently tagged *HTT* after four seconds at 7 and 14 dpe. (*HTT*16QFL n = 2-11, *HTT*128QFL n=2-10, *HTT*25QCer n=2-6, *HTT*96QCer n=1-4, n=1 the average distance climbed by flies within 1 vial averaged over 5 technical replicates). Data were plotted as Mean $\pm$ SEM and statistical significance was calculated by two-way ANOVA and Tukey's multiple comparisons test.

The climbing ability of the flies expressing the full-length *HTT* constructs did not differ significantly at 1 dpe. The flies expressing *HTT*128QFL started developing significant locomotor deficits at 7 dpe with an average climbing distance of 3 cm, whereas the *HTT*16QFL flies had an average climbing distance of 4.4 cm. This deficit increased as the *HTT*128QFL flies aged with their average climbing distance significantly decreasing to 0.74 cm at 14 dpe and 0.12 cm at 21 dpe. This was significantly lower than the distance climbed by *HTT*16QFL flies at those time points. A two-way ANOVA showed that age and genotype significantly affected the locomotor ability of the flies ($F_{3, 49}$ = 7.461, p = 0.0003); ($F_{1,49}$ = 106.4, p < 0.0001). Post hoc Tukey's multiple comparisons test revealed *HTT*128QFL flies climbed worse than *HTT*16QFL flies at 7 (p = 0.0062), 14 (p < 0.0001) and 21 dpe (p < 0.0001).

The *HTT*128QFL flies have a median lifespan of 24 days so it is of little surprise to observe their climbing ability so low at the end of their lifespan. The flies expressing *HTT*16QFL were able to maintain their locomotor function and were able to climb to an average of 4.9 cm at 14 dpe and 4.7 cm at 21 dpe. The *HTT*96QCer flies exhibited a climbing deficit, which was significantly different to the *HTT*25QCer flies at 7 dpe. A two-way ANOVA showed the genotype of the flies significantly affected the locomotor ability of the flies ($F_{1, 9}$ = 19.03, p = 0.0018). Post hoc tests showed a significant difference in the climbing ability of *HTT*96QCer and *HTT*25QCer flies at 7 dpe (p = 0.0142), but not at 14 dpe (p = 0.0764), this is potentially due to the number of the flies that were assayed at 14 dpe. These findings show that as flies expressing pathological *HTT* age, they develop more severe motor deficits, and expressing the non-expanded *HTT* transgene does not impede climbing ability. Both flies expressing 128 and 96 CAGs showed a similar level of climbing deficit at 14 dpe, indicating that different lengths of *HTT* CAG expansion affects locomotor phenotypes similarly in the *Drosophila* nervous system.

3.2.3 Expressing human *HTT* with an expanded repeat causes HTT aggregate formation

A hallmark of HD is the formation of HTT aggregates throughout the brain. It was important to assess whether this could be modelled in *Drosophila* brain. It was decided that fluorescently tagged *HTT* constructs would be expressed pan-neuronally to visualise HTT protein in the brain. Fluorescently tagged *HTT* was also expressed in glutamatergic neurons in order to visualise HTT at a single-cell level in the mechano-sensory neurons of the wing.
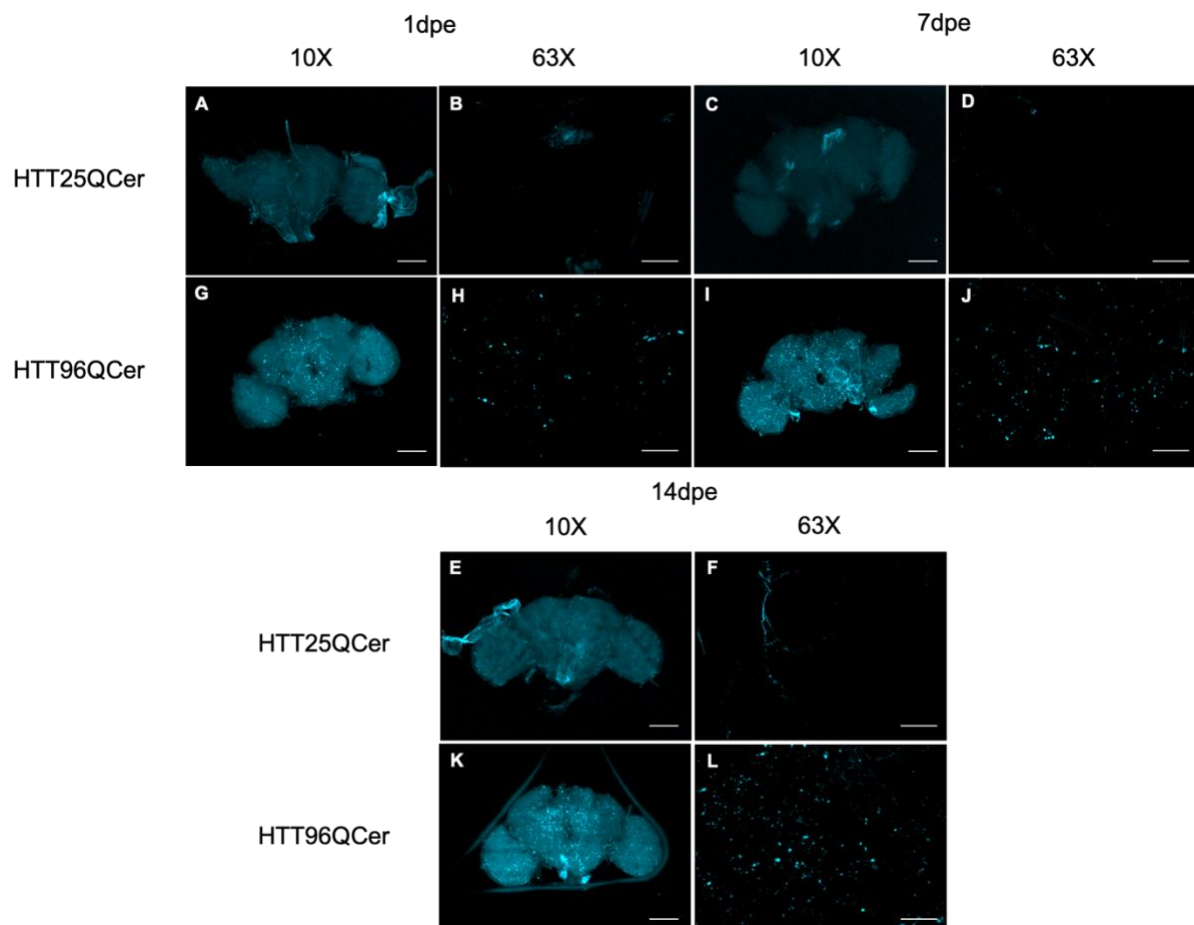
Figure 3.3 - Expressing *HTT* with an expanded repeat leads to HTT aggregate formation in the brain. (A-F) Orthogonal projections of *Drosophila* brains expressing *HTT*25QCer at 1, 7 and 14 d.p.e at 10X and 63X magnification. (G-L) Orthogonal projections of *Drosophila* brains expressing *HTT*96QCer at 1, 7 and 14 d.p.e at 10X and 63X magnification. Scale bar 100μm at 10X, 20 μm at 63X.

When *HTT*96QCer was expressed pan-neuronally using the Gal4-UAS system, HTT aggregates formed in the brain (Figure 3.3G-L) as early as 1 dpe. The number of aggregates appeared to increase as the flies aged, but this was not quantified. However, when *HTT*25QCer was pan-neuronally expressed there was no indication of aggregate formation (Figure 3.3A-F). This method did not display where in the neuron they were located. Under OK371-gal4 control, cerulean fluorescent-tagged HTT was imaged in glutamatergic neurons

of the wing (Figure 3.4). GFP was also expressed by OK371-gal4 which resulted in the cytoplasm of the neurons fluorescing green. Once again there was no evidence of HTT aggregation when *HTT*25QCer was expressed in the peripheral glutamatergic neurons in the wing (Figure 3.4A-C). When *HTT*96QCer was expressed in this subset of neurons, HTT aggregates were observed (Figure 3.4D-G). The aggregates appeared to be situated within the cell bodies of the glutamatergic neurons, at the perinuclear position. The nucleus of the neurons did not display any GFP signal and the magenta signal from the HTT aggregates always overlapped with GFP signal. Aggregates were also seen in the axons of the flies, occasionally at sites where axons were showing signs of axonal-swelling. These results show that expressing fluorescently tagged pathological *HTT* in peripheral glutamatergic neurons yields intracellular HTT aggregate formation.
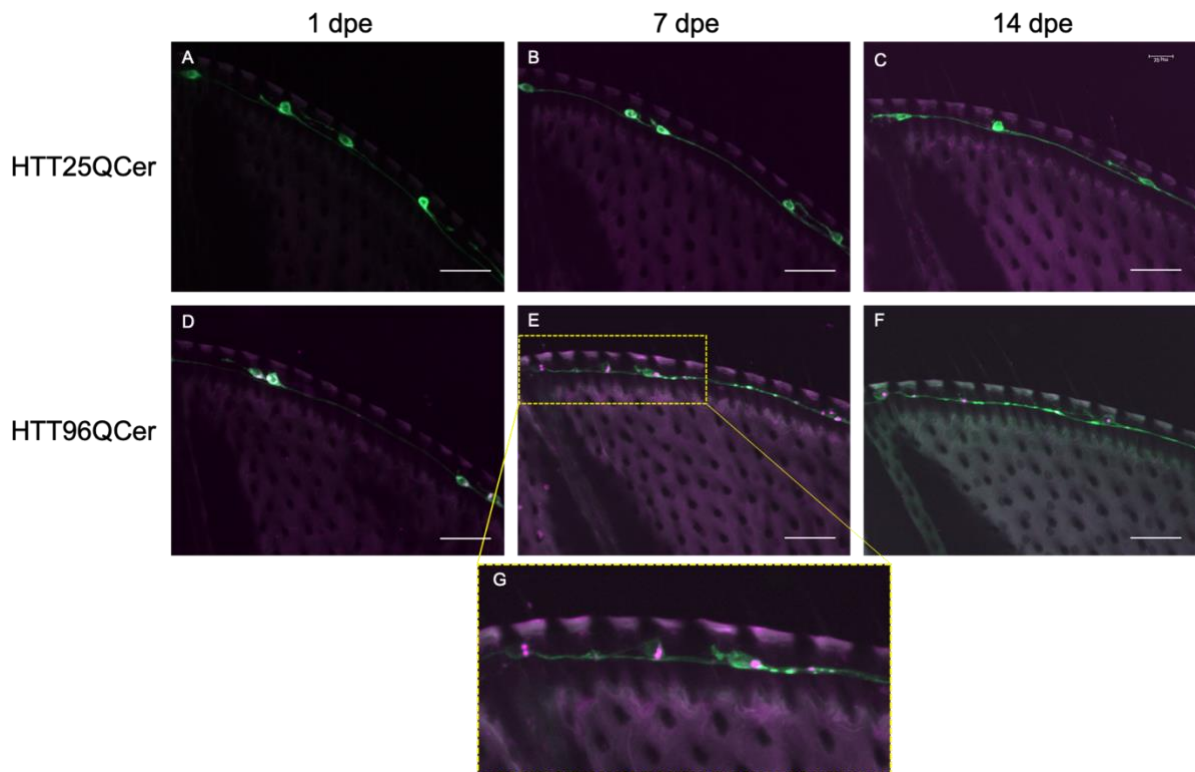
Figure 3.4 – HTT aggregates form in the cytoplasm and axons, but not the nuclei. (A-C) Orthogonal projections of wings from flies expressing *HTT*25QCer and GFP at 1, 7 and 14 dpe at 63X magnification. (D-F) Orthogonal projections of wings from flies expressing *HTT*96QCer and GFP. Neurons are labelled green, HTT is labelled magenta. (G) Zoomed in image of 3.4E to illustrate localisation of HTT aggregates. *HTT* and GFP were expressed by the glutamatergic neuronal driver OK371-Gal4. Scale bar = 20 μm.

3.2.4 Increased CAG repeat length yields neurodegeneration originating at the cell body

The *Drosophila* wing has been used to investigate axonal degeneration, and advances were made by Marc Freeman's lab in determining factors integral for Wallerian degeneration (Coleman and Freeman 2010; Neukomm et al. 2014; Soares et al. 2014; Llobet Rosell and Neukomm 2019). We modified this approach to test the effects of expressing mutant hu*HTT* in the neurons of the wing.
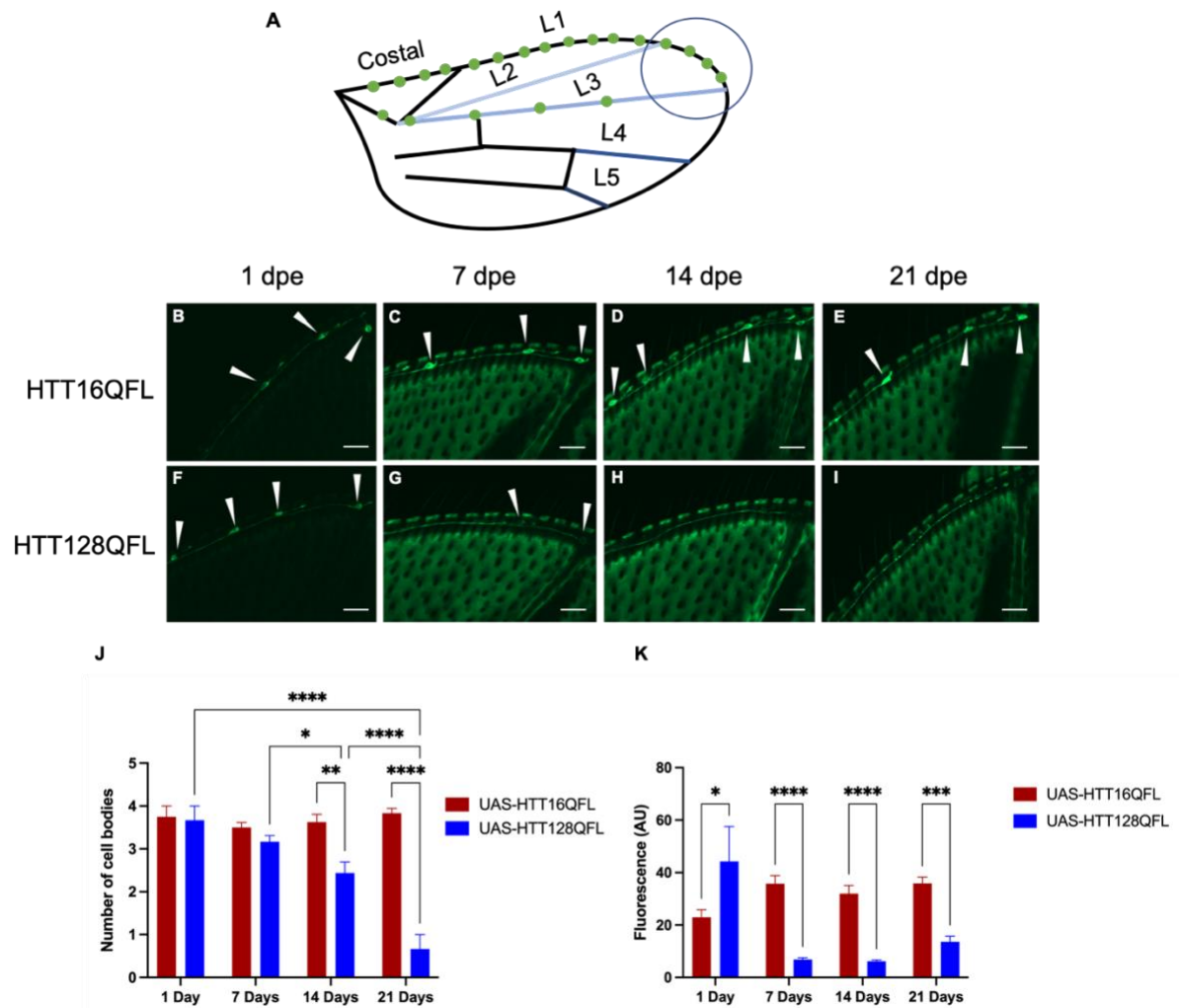
Figure 3.5 – Expanded CAG tract yields neurodegeneration originating at the cell body. (A) Illustration of Drosophila melanogaster wing with the tip of the L1 vein circled. The green circles indicate cell bodies that project through the costal vein into the body of the fly. (B-E and F-I) Images of sensory neurons in Drosophila wings from flies carrying *HTT*16QFL and *HTT*128QFL respectively, at different time points. GFP and *HTT* were under OK371-gal4 expression. (J) Average number of cell bodies counted at the tip of the L1 vein. (K) Average fluorescence of cell bodies at the tip of the L1 vein. Data were plotted as Mean $\pm$ SEM and statistical significance was calculated by two-way ANOVA and Tukey's multiple comparisons test. Scale bars = 20μm.

In this experiment the flies expressed *HTT*16QFL or *HTT*128QFL under the control of the OK371-Gal4 and the wings were dissected at multiple time points. The cell bodies at the tip of the L1 vein were counted and their fluorescence was measured. In the flies expressing *HTT*128QFL the levels of GFP fluorescence had dramatically decreased between 1 and 7 dpe, however this stayed consistent in the flies expressing *HTT*16QFL (Figure 3.5B-E). It was interesting to see that the cell body number declined in flies expressing *HTT*128QFL, but the axons remained intact and fluoresced strongly (Figure 3.5F-I). A two-way ANOVA revealed that genotype ($F_{1,79}$ = 44.68, $p < 0.0001$) and age ($F_{3,79}$ = 11.95, $p < 0.0001$) had a statistically significant effect on the number of the cell bodies. It also revealed that the interaction between age and genotype was significant ($F_{3,79}$ = 18.03, $p < 0.0001$). Post hoc Tukey's multiple comparisons test showed there was no statistical difference in cell body number of the *HTT*16QFL flies at 1 and 14 dpe ($p < 0.9999$) (Figure 3.5J). However, in flies expressing *HTT*128QFL the average number of cell bodies had decreased from 3.6 to 2.5 which was a significant decrease in the number of visible cell bodies over time ($p < 0.0001$) (Figure 3.5J). The *HTT*128QFL flies had significantly fewer visible cell bodies at the tip of the L1 vein than the *HTT*16QFL flies at 14 dpe ($p = 0.0026$). The number of visible cell bodies in the *HTT*128QFL flies kept decreasing as the flies aged with an average number of cell bodies of 0.6 in comparison to the average of the *HTT*16QFL flies which was 3.8 cell bodies at 21 dpe ($p < 0.0001$). These results show that sensory neurons in the wing are sensitive to pathogenic hu*HTT* expression and it indicates the use of the wing to study neurodegeneration in HD *Drosophila* models. These results also indicated that Wallerian degeneration is unlikely to be the cause of neurodegeneration in the sensory periphery neurons since the hallmark dying back of the axon was not observed.

3.3 Discussion

In all models investigated, the expression of mutant *HTT* with an expanded CAG repeat tract yielded disease-relevant phenotypes. Lifespan was significantly reduced, locomotor deficits were observed, HTT aggregates formed in the brain and neurodegeneration was visualised. This was consistent with previously published data regarding the models that were used. We further show that the wing model system can be used to directly study neurodegeneration caused by mutant HTT toxicity, and cell death was correlated with behavioural changes. A summary of the model phenotypes are depicted in Table 3.2.

We show that HTT aggregates form as early as 1 dpe when mutant *HTT* with a fluorescent tag is expressed, but 90% of the flies were still alive at 20 dpe. Locomotor deficits are also present at 7 dpe, however the lack of data at 1 dpe makes it difficult to compare the onset of a locomotor phenotype with HTT aggregation. The presence of aggregates without an immediate effect on lifespan suggests that HTT aggregation might initially be a neuroprotective process to prevent toxic mutant HTT oligomers from interfering with transcription, mitochondrial function and many other cellular processes. HTT aggregates continue to be present in the fly brain as the flies age. It has been shown that HTT aggregates inhibit axonal transport of various organelles in *Drosophila* larvae and adult flies (Gunawardena et al. 2003; Krench and Littleton 2013). Most of this work was conducted by overexpressing aggregate-prone mutant HTT in the eye or at neuromuscular junctions. It would be interesting to show axonal trafficking defects in the glutamatergic neurons of the wing as we would be able to identify the time point where HTT aggregates begin inhibiting axonal transport, and correlate this to the neurodegeneration phenotype in the wing.

In the full-length *HTT* model there is currently no evidence of HTT aggregate formation (Romero et al. 2008), which could be due to the detection methods, however there a significant locomotor deficit occurs at 7 dpe, which worsens as the flies age. There was an early loss of GFP signal in the *HTT*128QFL flies, prior to a significant decline of visible cell bodies, which aligned with the time point where the significant, but mild, locomotor changes had manifested. This suggests that this early neuronal phenotype has a physiological effect on neuronal function.

Interestingly, the median lifespan of the flies that pan-neuronally expressed *HTT*16QFL was longer than that of the flies that expressed GFP. There is evidence of the toxicity of GFP (Liu et al. 1999; Ansari et al. 2016), which may have accounted for this and should be considered when using this transgene as an expression control. The *HTT*25QCer flies had a different longevity profile compared to the *HTT*16Q flies, with the former dying progressively through the experimental time course. The median lifespan of the *HTT*16Q expressing flies was 68 days, whereas the medium lifespan of the *HTT*25QCer flies was 40 days. This suggests that longer non-pathological expansion could have a detrimental effect in the fly model and the CFP could also confer some toxicity as observed with the GFP (Liu et al. 1999). This is conceivable since the *Drosophila* homolog of the *HTT* gene does not have CAG expansion, hence the introduction of a CAG tract at any length may confer mild toxicity. However, the detrimental effect of *HTT*25QCer expression is not likely caused by aggregate formation as this was not observed for the *HTT*25QCer transgene. Interestingly, expressing *HTT*25QCer did not confer locomotor deficits and while the median lifespan did not differ greatly to the *HTT*96QCer flies, the survival curve was statistically significantly different. This also suggests that maximum lifespan should be considered in conjunction with median lifespan when examining the effect of mutant *HTT* expression in *Drosophila*. Since the differences in locomotor ability and HTT aggregation between *HTT*25Q and *HTT*96Q groups were robust, I conclude that fluorescently tagged HTT constructs are extremely useful for modelling aggregation and it negates the need to used antibodies to detect HTT in the brain. This means that there is more scope in future experiments for detecting other proteins with immunohistochemistry (IHC), such as indicators of cell death pathway activation or mitochondrial damage.

Driver	Model	Median Lifespan (days)	Locomotor Deficit	Neurodegeneration phenotype	Htt Aggregation
ELAV-Gal4	*HTT128QFL*	24	Present at 7 dpe		
	HTT16QFL	67	No		
	HTT96QCer	36	Present at 7 dpe		Yes
	HTT25QCer	40	No		No
OK371-Gal4	*HTT128QFL*	-	Present at 21 dpe	Cell bodies die before axons degenerate	
	HTT16QFL	-	No	Cell bodies die before axons degenerate	
	HTT96QCer	-	No	Cell bodies die before axons degenerate	Perinuclear and axonal aggregates
	HTT25QCer	-	No	No	No

Table 3.2 – A summary of the results from each assay for each *Drosophila* model and the driver that was used to express the human *HTT* constructs.

In the *Drosophila* field of HD research, an assay to measure neurodegeneration of the cell body, dendrite and axon directly has not yet been attempted, with most researchers utilising assays in the eye to investigate neurodegeneration associated with mutant HTT (Kirk et al. 1997; Lee et al. 2004; Jimenez-Sanchez et al. 2015; Pons et al. 2018; Vu et al. 2018). While the eye assays have been undoubtedly useful to investigate genetic modifiers of mutant HTT (Romero et al. 2008; Tamura et al. 2011; Besson et al. 2015), they have several limitations. GMR-Gal4 is not a neuron-specific driver and causes expression of transgenes in glia among other cell types (Ray and Lakhotia 2015). This means that neurodegeneration phenotypes observed could be due to a glial response to hu*HTT* expression rather than neuronal response alone, which could confound the results. The neurons in the fly eye cannot be visualised in detail as the dendrites, cell bodies and axons cannot be differentiated from one another. Another caveat is that the eye cannot be used for live-imaging. There are caveats of using the wing to investigate neurodegeneration, namely the neurons are glutamatergic instead of GABA-ergic like the MSNs of the striatum, and we have described the literature depicting the specific sensitivity of the MSNs to HTT toxicity (Morigaki and Goto 2017) (See Chapter 1.2.4). The neurons in the wing are peripheral sensory neurons, and while they are supported by glia, it is not the same environment as the *Drosophila* central nervous system. Both systems enable the study of neurodegeneration and HTT aggregation, but for the purpose of this project the wing neurodegeneration assay was preferable for studying the effect of toxic *HTT* expression on neuronal health.

Our experiments show that the expression of pathological *HTT* in glutamatergic neurons leads to neurodegeneration, but the fluorescence from the cell bodies fades prior to any signs of axonal degeneration. This lack of GFP signal in the cell bodies is apparent at 7 dpe, and while the cell bodies are visible enough to count, the fluorescence of the axons appears unchanged. I suggest that mutant HTT may have a global effect on reducing the amount of GFP produced. Mutant HTT has been shown to cause global translation repression (Eshraghi et al. 2021), which may account for such changes. The first indication of axonal degeneration is at 21 dpe where the fluorescence pattern of the axons changed from clear fluid lines to fragmented ones and the cell bodies were already absent. This suggests that the cell body is preferentially vulnerable to mutant *HTT*. This idea is further supported by

the localisation of the HTT aggregates in these neurons to the cell body. Enlargement and rupture of the cell body has also been observed *in vitro* (Mao et al. 2016), and it has been suggested that mutant HTT activates a unique form of necroptosis. This is in contrast to several previous papers that suggest apoptosis is the main cause of cell death (Portera-Cailliau et al. 1995; Saudou et al. 1998; Tang et al. 2005). Perhaps global translational repression affects the cell bodies preferentially. There have also been other findings which suggest that neurons degenerate by a gradual dying back from the terminal (Li et al. 2001). Our phenotype suggests that apoptosis or necrosis is likely to occur first, but cannot efficiently be distinguished based on morphology alone. Other forms of cell death such as parthanatos have not yet been explored in the context of HD and may play a role. It therefore remains to be determined exactly how mutant *HTT* causes neurodegeneration and the wing system may help us understand potential mechanisms.

The strengths of using OK371-gal4 is that the expression of *HTT* is limited to a subset of neurons yielding single cell resolution under microscope. Visualising neurons in the wing is a rapid process from dissection to microscope (which takes as little as a few minutes), that is useful as a quick screening tool. There is also the capacity to live-image neurons in the wing (Vagnoni and Bullock 2016). The wing system method could also be adapted using a method called MARCM which enables transgenes to be expressed in a random small set of cells (Luo and Wu 2007). This enables the investigation of lethal and non-lethal modifying genes without damaging the whole fly. The biggest advantage is that for the first time we can see how neurons die *in vivo* so we can determine whether the cell body or axons are most vulnerable to pathological *HTT*. By direct visualisation of neurons using the wing system, it may be possible to find out how they die through *Drosophila* genetic approaches.

Overexpressing p35 inhibits apoptosis by blocking caspase activity (LaCount et al. 2000). As a further experiment, we could express this in the mutant *HTT* expressing neurons of the wing and observed whether we can rescue the neurodegeneration. Necrosis is another potential cell death pathway that could be causing this degeneration phenotype. Neuronal necrosis can be caused by a number of factors such as ion imbalance (i.e. Ca^{2+} overload) and lack of oxygen from ischaemia (Syntichaki and Tavernarakis 2003). Combining the use of G-cAMP indicators and biochemical sensors for ATP with the wing system (Vagnoni and

Bullock 2018) we could potentially visualise necroptotic signals. During necrosis the membrane integrity of the cell is lost which causes the cell to swell and rupture, expelling its contents into the extracellular space (Proskuryakov et al. 2003). This might explain the debris that is seen following cell death. The JNK pathway has been associated with neuronal necrosis in *Drosophila*, so overexpressing or knocking down elements of that pathway may also yield some answers (Yang et al. 2013). These are all potential pathways that could be followed up to elucidate what is occurring to these neurons using the new wing study system to study mutant HTT toxicity.

Drosophila melanogaster is an ideal model organism for genetic screening due to their small genome, the large array of genetic tools available and the fact that they are a medium-throughput system. The results from this chapter show that all models with an expanded repeat had a detrimental effect on lifespan and locomotion in comparison to their expression controls when pan-neuronally expressed. The potential toxicity from CFP was considered when choosing a model to screen which results in cerulean tagged *HTT* flies not being used. The most appropriate model to use was the *HTT*128QFL flies. This model showed clear disease-relevant phenotypes in all assays performed, had no fluorescent tag, and it had the full-length human transgene making it more translatable to human disease. When picking the assay for the screen, I had to take into consideration whether a clear phenotype was seen, whether the assay was well-characterised, and the sample size needed to see a statistically significant difference. The RING assay is a well-characterised assay that has been used extensively in *Drosophila*-neurodegeneration studies. The sample size requirements are lower than lifespan and there was a clear staged decline in climbing ability between 7 and 14 dpe for the *HTT*128QFL flies (Figure 3.2). This would enable detection of damaging and protective transgenes. The RING assay combined with the *HTT*128QFL would be a rapid screening platform. Another benefit of this model is that it showed a clear neurodegeneration phenotype in the novel wing assay and a significant shortening of lifespan. Therefore, an in-depth characterisation of any candidates from the screen could be easily followed up with other assays using the same model. The screen and its results are described in Chapter 6.

3.4 Summary of Main Points

- Expression of human *HTT* with a pathological CAG length shortens lifespan and reduces climbing ability in accordance with existing literature.

- Between ages 7 dpe and 14 dpe the *HTT*128QFL expressing flies exhibited a significant locomotor deficit in comparison to *HTT*16QFL expressing flies.

- Cerulean fluorescently tagged pathological *HTT* forms aggregates as early as 1dpe when pan-neuronally expressed.

- HTT aggregates form intracellularly, localising mainly in the cell body, but also in the axon. They are not intranuclear.

- A novel wing assay was described wherein neurodegeneration of cell bodies prior to axonal degeneration was observed in conditions where pathological hu*HTT* was expressed.

- It was decided that the genetic screen investigating genetic modifiers of HD disease phenotypes would be carried out with *HTT*128QFL expressing flies and the RING Assay.

4. Investigating somatic instability of the CAG repeat tract of human *HTT* in *Drosophila* neurons

4.1 Introduction

The age at which motor symptoms develop in Huntington's disease (HD), is inversely correlated with the length of the expanded CAG tract in exon 1 of the *HTT* gene (Lee et al. 2012). However, this only accounts for 60% of the variability in the age at which motor symptoms onset (AMO), meaning the remaining 40% is due to heritable and/or environmental factors (Wexler et al. 2004). Multiple GWAS have been performed, examining the predicted age of motor symptom onset (according to their CAG repeat length) and comparing it to their actual AMO to find common genetic modifiers of disease onset (Lee et al. 2015; Moss et al. 2017; Lee et al. 2019). They indicated that multiple genes related to DNA repair pathways had statistically significant single nucleotide polymorphisms/variances (SNP/Vs) within their sequence or promoter regions suggesting that DNA repair pathways were most likely dysregulated in HD and could be affecting the *HTT* gene. One of the ways mutated DNA repair genes could be affecting the onset or progression of disease within an individual who has inherited a pathogenic *HTT* allele is by changing the CAG repeat tract length in somatic (non-germline) cells. The CAG repeat tract in mutant human *HTT* is unstable and has the propensity to expand or contract over a patient's lifespan (Swami et al. 2009). The instability in the CAG expansion is known as somatic instability as it occurs within post-mitotic cells, specifically post-mitotic neurons in the brain (Gonitel et al. 2008). This suggests the change in CAG number is due to DNA repair pathways rather than DNA replication as neurons are non-dividing cells (Kennedy and Shelbourne 2000). HD mouse models have shown that specific regions of the brain (for example, the striatum or the cortex) are more likely to exhibit somatic instability of the CAG repeat tract than others which could be why these areas are more vulnerable to mutant *HTT* in disease (Shelbourne et al. 2007). Knockout or knockdown of DNA repair genes has been proven to modulate the instability of the CAG repeat tract in mouse and cell models of HD (Manley et al. 1999; Pinto et al. 2013; Tomé et al. 2013; Goold et al. 2019). The composition of the CAG tract has also been shown to affect the AMO with CAA interruptions, which also codes for glutamine, seemingly stabilising the repeat tract and delaying AMO (Wright et al.

2019; McAllister et al. 2022). Somatic instability is important as it might drive disease onset and could therefore be a drug target to modulate disease progression.

For the scope of this project, the issue to address was can *Drosophila* be used to model somatic instability? Inter-generational instability of a CAG repeat tract has been reported in a *Drosophila* model of spinocerebellar ataxia (SCA) (Jung et al. 2011). They showed that expressing a protein with an expanded PolyQ tract affected the stability of a non-coding expanded CAG repeat construct in germline tissue. The change was small, with expansions equating to ±1-3 CAGs. Large changes to the CAG repeat tract in a mutant *HTT* allele have been observed between parent and offspring with expansion thought to be occurring in post-mitotic haploid cells (McMurray and Kortun 2003). They suggest that the CAG repeat expands in the late stages of spermatogenesis when the chromatin is condensing. In contrast to germline instability, somatic instability of the CAG repeat tract in mutant *HTT* is most prevalent in the striatum and cortex (Kennedy et al. 2003; Lee et al. 2011; Aviolat et al. 2019). In order to mimic the conditions in a HD patient brain the experiments in this chapter carried out were completed by expressing hu*HTT* constructs pan-neuronally (ELAV-Gal4) with DNA taken at different ages. Something to consider when investigating somatic instability in *Drosophila* was the homology of genes linked to somatic instability in HD. The table below displays the HD GWAS hits associated with DNA repair pathways and thought to be associated with somatic instability of the *HTT* CAG tract (Table 4.1).

Human Gene	*Drosophila* homolog	DIOPT Score
FAN1	---	---
MSH3	---	---
MLH1	Mlh1	14
EXO1	Tosca	11
BRCA2	Brca2	3
MSH2	Spellchecker1	14
MSH6	Msh6	13
PMS1	Pms2	3
PMS2	Pms2	13
LIG1	DNALig1	15

The HD GWAS found the most significant SNVs in or near the coding region for the gene *FAN1* which has endonuclease activity and acts in DNA interstrand cross-link repair and various other processes e.g. replication fork restart (Kratz et al. 2010; Liu et al. 2010; MacKay et al. 2010; Smogorzewska et al. 2010). *FAN1* mutants which ablate the endonuclease activity have been shown to increase the instability of the CAG repeat in HD iPSCs (McAllister et al. 2022). *Drosophila* do not have a homolog for *FAN1* (Table 4.1) and while *FAN1* expression has been shown to regulate CAG repeat stability of *HTT* (Goold et al. 2021), the expression of functioning FAN1 potentially protects against CAG expansion. Perhaps the homologs of modifiers that enhance repeat instability when expressed are more relevant to this investigation.

Mismatch repair (MMR) is a highly conserved process whereby incorrectly matched nucleotides that occur during DNA replication are corrected (Li 2008) (Figure 4.1). This process is crucial to prevent mutations from becoming permanent changes in dividing cells, but it is also used in neurons to maintain genomic stability (Fishel et al. 2007). Some proteins involved in MMR have been implicated in CAG repeat instability in HD and other repeat expansion disorders (Benn et al. 2020). GWAS highlighted significant SNVs in or near coding regions of *MSH3* that are thought to modify disease progression (Moss et al. 2017). *MLH1*, *MSH2*, and *PMS2* were also shown to have significant SNVs in or near their coding regions associated with modified disease onset (Table 4.1) (Lee et al. 2019). MMR is conserved in *Drosophila*, but its components are more limited than mammalian MMR (Figure 4.1). There is no *Drosophila* homolog for *MSH3* which limits the number of MutS complexes that can form during MMR, making it a simpler process than mammalian MMR (Sekelsky 2017) (Figure 4.1). Increased *MSH3* expression has been associated with increased somatic instability and earlier disease progression in HD (Flower et al. 2019). Abolishing *MLH1* expression in HD mouse models has been shown to reduce the instability of the CAG repeat tract (Pinto et al. 2013). This evidence shows MMR proteins are important for the

repeat instability of the CAG repeat tract of *HTT*, but we needed to test if these phenotypes could be replicated in *Drosophila* models of HD.
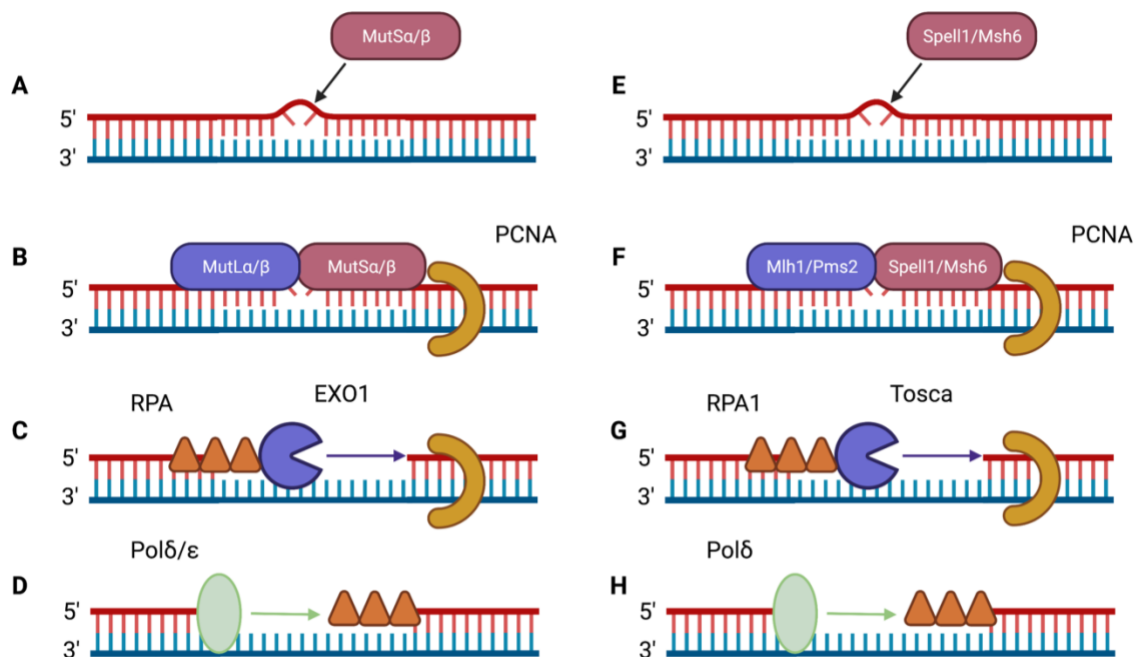
Figure 4.1 – A comparison of human and *Drosophila* MMR. Mammals: A) Recognition of mismatch by MutS complex comprised of MSH2 and MSH3/6. B) Recruitment of MutL complex which contains endonuclease activity that nicks the strand. MutL can be comprised of MLH1 and PMS1/PMS2. PCNA is also recruited and activates endonuclease activity. C) EXO1 is recruited to the mismatch site and excises the nucleotides surrounding the mismatch, moving in a 5'-3' direction. RPA molecules prevent the degradation of the single strand. D) The strand is resynthesised by DNA polymerase Polδ or Polε, which also resynthesises the strand in a 5'-3' direction. Drosophila: E) MutS complex comprised of MSH2 ortholog Spellchecker1 (Spell1) and Msh6 recognises the mismatch. This is homologous to the MutSα complex. F) Mlh1 and Pms2 form the MutL complex, orthologous to MutLα and it has conserved endonuclease activity. G) Tosca is orthologous to EXO1 and it excises the nucleotides adjacent to and within the mismatch site. H) Polδ facilitates resynthesis of the DNA strand and the mismatch is repaired. (Brooks et al. 1996; Li 2008; Do and LaRocque 2015; Sekelsky 2017; Gupta and Heinen 2019). (Created with Biorender).

4.1.1 Aims and hypothesis

I hypothesise that if there is an extensive pure CAG repeat tract in a transgenic human HTT *Drosophila* model then, if the flies can be aged long enough there will be somatic instability in the CAG repeat.

Aim 1) Choose an appropriate HD *Drosophila* model to study somatic instability.

Aim 2) Test whether the CAG repeat tract in a human *HTT* transgene can undergo somatic expansion when expressed in neurons in adult *Drosophila*.

4.1.2 Experimental design

It was necessary to sequence the *HTT* constructs that had been used Chapter 3 to confirm the CAG repeat tract length, the composition of the CAG tract (pure CAG or not), and to test whether any of the models could be used to test for somatic instability in *Drosophila*.

$$\female \quad ELAV-Gal4; \frac{Sp}{CyO}; \frac{+}{+} \qquad \times \qquad \male \quad w^-; \frac{UAS-GFP}{CyO}; \frac{UAS-HTT128QFL}{Tm3,sb,e}$$

$$\female \quad \frac{ELAV-gal4}{w^-}; \frac{UAS-GFP}{Sp}; \frac{UAS-HTT128QFL}{+}$$

$$\female \quad ELAV-Gal4; \frac{Sp}{CyO}; \frac{+}{+} \qquad \times \qquad \male \quad w^-; \frac{UAS-HTT16QFL}{CyO}; \frac{UAS-GFP}{Tm3,sb,e}$$

$$\female \quad \frac{ELAV-gal4}{w^-}; \frac{UAS-HTT16QFL}{Sp}; \frac{UAS-GFP}{+}$$
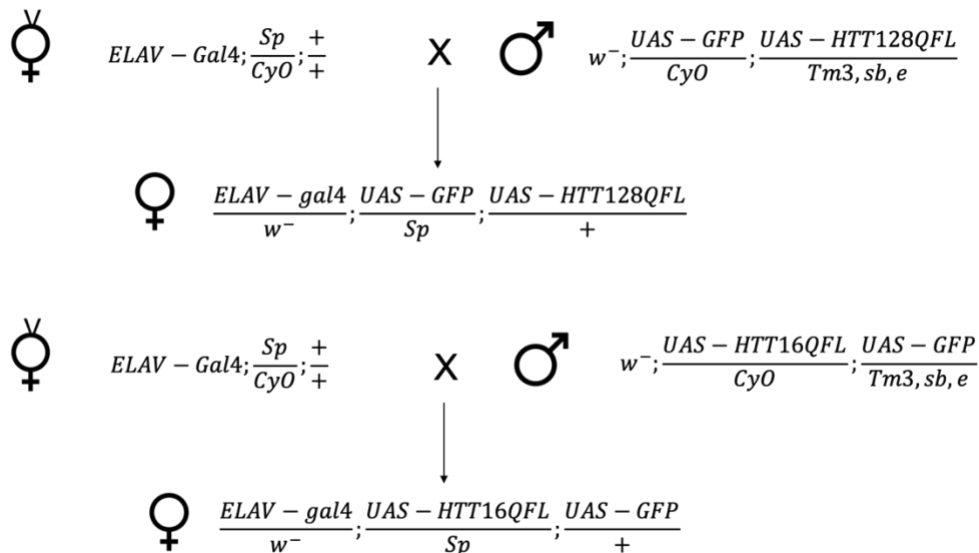
Crossing Scheme 4.1 – Pan-neuronal driver (ELAV-Gal4) carrying virgins are crossed with males carrying UAS-GFP and UAS-*HTT* with either 16 or 128 CAG repeats. The resulting progeny express GFP and full-length human *HTT* in all neurons.

Some constructs were lethal when expressed throughout development so to bypass this lethality the temperature sensitive expression control TubulinGal80^{TS} was used. The flies were raised at 18°C to inhibit the activity of Gal4 in neurons, thus blocking the expression of the hu*HTT* constructs during development. Once the flies eclosed they were moved to 30°C to allow for hu*HTT* expression.

$$\female \quad w^-; \frac{Tubulin\ Gal80^{TS}}{CyO}; \frac{ELAV-Gal4}{TM6,T6,Hu,e} \qquad \times \qquad \male \quad w^-; \frac{Sp}{CyO}; \frac{UAS-mRFP\ HTT138Q}{Tm3,sb,e}$$

$$\female \quad w^-; \frac{Tubulin-Gal80^{TS}}{Sp}; \frac{UAS-mRFP\ HTT138Q}{ELAV-Gal4}$$
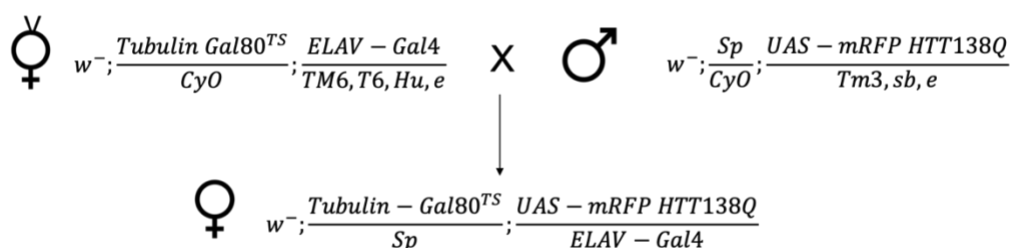
Crossing Scheme 4.2 – Temperature sensitive expression control (TubulinGal80^{TS}) combined with the pan-neuronal driver (ELAV-Gal4) ensured that the highly toxic human *HTT* constructs were not expressed in neurons during development.

For investigating whether somatic instability occurs in *Drosophila*, DNA had to be taken at various life stages of the flies expressing *HTT*. The timepoints chosen were 1 dpe which equated to one day of expression in the case of the *HTT*138Q-mRFP carrying flies, 7 dpe, and every 7 days until the flies died. Flies expressing *HTT*138Q-mRFP did not have a long lifespan so DNA was only taken up to 14 dpe.

4.2 Results

4.2.1 CAG tracts in the *HTT* constructs contain CAA interruptions

It was important to determine the exact sequences of the CAG tract of the *HTT* constructs that were being expressed in the HD *Drosophila* models. CAA interruptions in the CAG tract of *HTT* have been correlated with later disease onset in HD patients (McAllister et al. 2021). The exact nucleotides of the sequences would enable the choice of the best model to study somatic instability. A pure CAG tract containing ≥40 CAGs would be preferable as this would be disease relevant and it has been shown that a longer pure CAG tract increases the risk of somatic instability (Lee et al. 2019).

The CAG tracts of the full-length *HTT* constructs, the truncated *HTT* constructs, the mRFP-tagged hu*HTT* constructs and the cerulean fluorescently tagged *HTT* constructs were all sequenced by Sanger Sequencing (Figure 4.2, 4.3, 4.4 and Table 4.2); (details of primers and sequencing method can be found in Methods 2.3.8). The CAG tracts of the *HTT*128QFL and *HTT*128Qtrunc constructs were identical and contained 121 repeats instead of their listed 128 (Figure 4.2). The cDNA used for these models was donated by Michael R. Hayden and appears to be similar to the sequence used for the YAC128 mouse model which has been reported as containing between 119-121 repeats (Slow et al. 2003; Lee et al. 2004; Romero et al. 2008). They both contained several CAA interruptions which resulted in the longest pure CAG tract being composed of 39 CAGs. CAG repeat tract composition has been implicated in disease progression with pure *HTT* CAG tracts being associated with enhanced disease progression (Lee et al. 2019). Previous publications indicated that CAA interruptions result in a stable repeat tract (Gray et al. 2008; Pouladi et al. 2012; Wright et al. 2019), which led to these two constructs not being selected for investigating somatic instability.
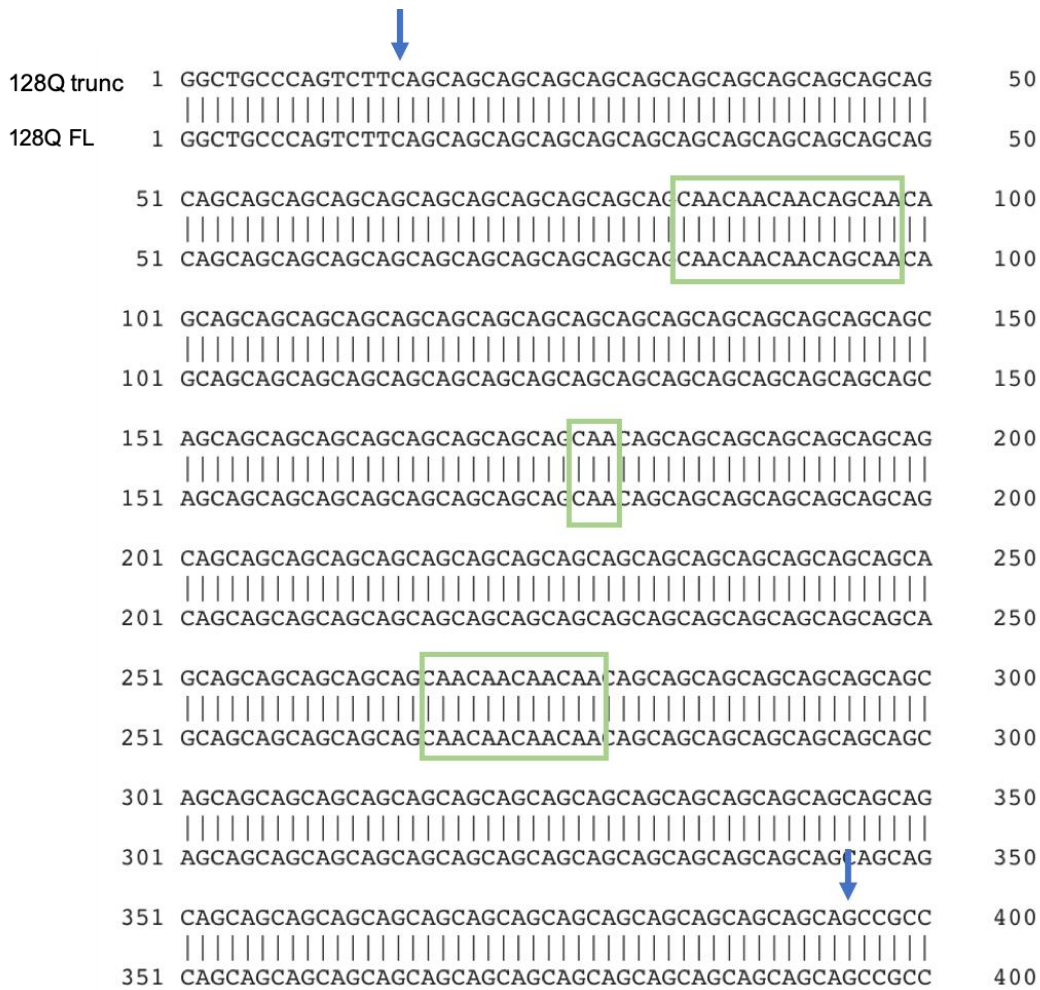
	Length (base pairs)	Similarity	Gaps
Alignment of CAG tracts	400	100.0%	0.0%

Figure 4.2 – Sequences of *HTT*128Q constructs reveal identical CAG sequence containing CAA interruptions. EMBOSS Needle Pairwise sequence alignment of CAG tracts of the *HTT*128Q truncated and *HTT*128Q full-length constructs show 100.0% similarity. Blue arrows indicate the start and end of the CAG repeat tract. Green boxes indicate identical CAA interruptions. Dash indicates a gap, line indicates similarity/identity, dot indicates mismatch between sequences.

The repeat tracts of the *HTT*96QCer flies and the *HTT*128Q flies did not align perfectly and pairwise sequence analysis showed that it had a 63.8% homology to the repeat tract of the *HTT*128Q flies (Figure 4.3 and Table 4.2). The *HTT*96QCer tract was a mixed CAG/CAA sequence that was 96 repeats in length, with 48 CAGs and 48 CAAs. This number was based on the first CAG that was observed in the sequence, however there is the possibility that the sequence began with a CAA. Due to the quality of the sequence the first base of potentially the first codon could not be confirmed and it was assigned given an "N", making the sequence NAA. The CAG repeat tract of the *HTT*96QCer fly contained a minisatellite that

repeated 16 times throughout the sequence: CAG-CAG-CAA-CAG-CAA-CAA. This sequence was similar to the mixed CAG/CAA sequence that was used to generate the 97Q BACHD mouse model which was CAA-CAG-CAG-CAA-CAG-CAA (Gray et al. 2008). Another source sites the sequence as it appeared in the HTT96Q fly (CAG-CAG-CAA-CAG-CAA-CAA), with an added CAA at the beginning of it (Pouladi et al. 2012). If the first triplet in the sequence was a CAA, then the sequence of the CAG repeat tract of the *HTT*96QCer fly would be identical to the CAG repeat tract of the BACHD mouse model. BACHD mice do not exhibit somatic or germline stability (Gray et al. 2008; Pouladi et al. 2012), because of their sequence homology, the *HTT*96QCer line was not selected to investigate somatic instability.

```
HTT128Q     1  CAGCAGCAGCAGCAGCAGCAGCAGCAGCAGCAGCAGCAGCAGCAGCAGCA  50
HTT96QCer   1  --------------------------------------------------   0

           51  GCAGCAGCAGCAGCAGCAGCAACAACAACAGCAACAGCAGCAGCAGCAGC  100
                                              |||||||||.||||||.|
            1  ------------------------------CAGCAGCAACAGCAAC       16

          101  AGCAGCAGCAGCAGCAGCAGCAGCAGCAGCAGCAGCAGCAGCAGCAGCAG  150
                |.|||||||||.||||||.||.|||||||||.||||||.||.|||||||||.|||
           17  AACAGCAGCAACAGCAACAACAGCAGCAACAGCAACAACAGCAGCAACAG  66

          151  CAGCAGCAGCAGCAACAGCAGCAGCAGCAGCAGCAGCAGCAGCAGCAGCA  200
                ||.||.|||||||||||||||.||.|||||||||.||||||.||.|||||||||
           67  CAACAACAGCAGCAACAGCAACAACAGCAGCAACAGCAACAACAGCAGCA  116

          201  GCAGCAGCAGCAGCAGCAGCAGCAGCAGCAGCAGCAGCAGCAGCAGCAGC  250
                .|||||.||.|||||||||.||||||.||.|||||||||.||||||.||.|||||
          117  ACAGCAACAACAGCAGCAACAGCAACAACAGCAGCAACAGCAACAACAGC  166

          251  AGCAACAACAACAACAGCAGCAGCAGCAGCAGCAGCAGCAGCAGCAGCAG  300
                |||||||.|||||||||||||||.||||||.||.|||||||||.||||||.||.
          167  AGCAACAGCAACAACAGCAGCAACAGCAACAACAGCAGCAACAGCAACAA  216

          301  CAGCAGCAGCAGCAGCAGCAGCAGCAGCAGCAGCAGCAGCAGCAGCAGCA  350
                |||||||||.||||||.||.|||||||||.||||||.||.|||||||||.|||||
          217  CAGCAGCAACAGCAACAACAGCAGCAACAGCAACAACAGCAGCAACAGCA  266

          351  GCAGCAGCAGCAGCAGCAGCAGCAGCAGCAG       381
                .||.|||||||||.||||||.||.
          267  ACAACAGCAGCAACAGCAACAA---------       288
```

	CAG tract length (base pairs)	CAG (triplet)	Similarity to *HTT*128Q	Gaps
*HTT*96QCer	288	96	63.8%	24.4%

Figure 4.3 –Pairwise sequence alignment of the CAG tract from the *HTT*128Q and *HTT*96QCer constructs.

EMBOSS Needle Pairwise sequence analysis shows these CAG repeat tracts have 63.8% similarity. Dash indicates a gap, line indicates similarity/identity, dot indicates mismatch between sequences.

The sequence of the *HTT*138Q-mRFP repeat tract included some CAA interruptions, but the composition and position of the CAA interruptions were different to the *HTT*128Q and the HTT96QCer constructs. For instance, the *HTT*138Q-mRFP construct contained a pure CAG tract of 57 repeats in comparison to the 39 repeats seen in the *HTT*128Q constructs. The *HTT*128Q constructs had one incidence of a single CAA interruption, whereas the CAA interruptions in the *HTT*138Q-mRFP construct always contained multiple adjacent CAAs. As the *HTT*138Q-mRFP construct had the longest pure CAG repeat tract and a pure CAG tract that exceeded 40 repeats it was selected to investigate somatic instability.

	Length (base pairs)	Similarity	Gaps
Alignment of CAG tracts	426	89.2%	10.6%

Figure 4.4 – Pairwise sequence alignment of the CAG tracts in the *HTT*138Q and *HTT*128Q constructs are not identical and show differing CAA interruptions. EMBOSS Needle Pairwise sequence analysis shows these CAG repeat tracts have 89.2% similarity. Green boxes indicate identical CAA interruptions. Orange boxes indicate gaps or differences in CAA interruption composition. Dash indicates a gap, line indicates similarity/identity, dot indicates mismatch between sequences.

Genotype	Listed number of repeats	Number of repeats according to Sanger sequencing	Number of CAA tract interruptions	Length of longest pure CAG tract
*HTT*128QFL	128	121	3	39
*HTT*16QFL	16	16	0	16
*HTT*128Q trunc	128	121	3	39
*HTT*0Q trunc	0	0	0	0
*HTT*96QCer	96	96-97?	-	2
*HTT*25QCer	25	25	0	25
*HTT*138Q-mRFP	138	142	3	57
*HTT*15Q-mRFP	15	15	0	15

Genotype	CAA interruption composition and position
*HTT*128QFL	CAA-CAA-CAA-CAG-CAA (23-27) CAA (54) CAA-CAA-CAA-CAA (84-87)
*HTT*128Q trunc	CAA-CAA-CAA-CAG-CAA (23-27) CAA (54) CAA-CAA-CAA-CAA (84-87)
*HTT*96QCer	NAA/CAA (1)? (CAG-CAG-CAA-CAG-CAA-CAA)$_{16}$
*HTT*138Q-mRFP	CAA-CAA-CAA-CAG-CAA (28-32) CAA-CAA-CAA-CAA (90-93) CAA-CAA-CAA-CAA-CAA (99-103)

Table 4.2 – A summary table of the sequence of the CAG tract of the *HTT* constructs in the HD fly models and the composition of the CAA interruptions. (n=1).

4.2.2 *Drosophila melanogaster* do not exhibit somatic instability in the expanded CAG tract of *HTT*

The absence of a *MSH3* homolog in the *Drosophila* genome reduced the probability of CAG expansion being observed, although there could be alternative pathways that dictate repeat expansion in HD. The sequencing data of the *HTT*138Q-mRFP line showed a pure CAG tract of 57 CAGs. The disease-causing threshold for HD is 40 CAGs and CAG repeat tracts in HD patients of this size have been shown to expand throughout their lifetime (Kacher et al. 2021). Because of this, we thought there might have been a possibility that somatic instability of the CAG repeat might have been observed in the *HTT*138Q-mRFP model. DNA was extracted from flies pan-neuronally expressing *HTT*138Q-mRFP at 1, 7 and 14 dpe and capillary electrophoresis was carried out to determine the CAG repeat tract length (Figure 4.5) (See Methods 2.3.7 for GeneScan details).

GeneScan detects the size of PCR fragments and the height of the peaks indicates the frequency that a fragment at a specific size was detected. A DNA ladder is used to accurately measure the size of the PCR fragments. The traces typically form a hedgehog plot, with a modal peak at the centre, indicating the size that most of the fragments were, with 2-3 peaks either size of the modal peak. These smaller peaks indicate fragments that are of similar size to the size at the modal peak. Peaks to the left of the modal peak indicate fragments of smaller size and peaks to the right of the modal peak indicate the sample contains fragments of a larger size. An indication of CAG repeat expansion would have been multiple peaks situated to the right of the modal peak as that would demonstrate the presence of PCR fragments containing CAG repeat tracts with a higher number of CAGs than the modal (Pinto et al. 2013; Flower et al. 2019). This can sometimes form into a second smaller hedgehog plot to the right of the modal peak. The traces for the distribution of the CAG repeat tract lengths replicated the classical hedgehog plot, with 2-3 peaks either side of the modal peak. The traces for the peaks representing fragments containing 134 CAGs and 135 CAGs were very similar in height in all of the traces, at each time point. This was all within the error of the system so it represented no real difference in the CAG repeat tract sizes of the PCR fragments generated from the *HTT*138Q-mRFP samples. These data show no evidence of somatic instability occurring in the neurons of *HTT*138Q-mRFP expressing flies.

138Q-mRFP *HTT*

1 Day PE

1 Week PE

2 Weeks PE

134 CAG
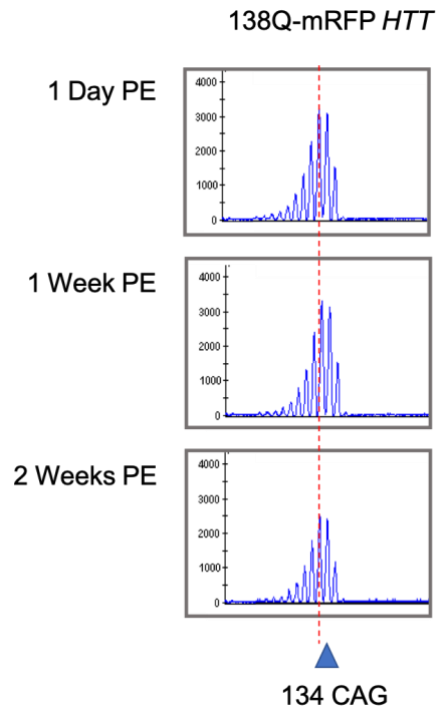
	Modal Peak		
Days Post Eclosion (dpe)	133	134	135
1	1	2	4
7		4	2
14		4	1

Figure 4.5 – *Drosophila melanogaster* expressing hu*HTT* with an expanded CAG tract do not exhibit somatic instability. Capillary electrophoresis (Genescan) traces of the distribution of CAG fragments of the HTT138Q mRFP-tagged construct that has been expressed for 1, 7 and 14 dpe. (n=5-7, n=1 DNA extracted from one fly). A summary table showing the size of the CAG repeat at the modal peak for each sample.

4.3 Discussion

Until these experiments, somatic instability of a CAG repeat tract had not been investigated in *Drosophila melanogaster*. There were factors suggesting that it would not occur, such as the lack of homologs for genes implicated in somatic instability in disease and the shortened lifespan of *Drosophila* when expressing toxic *HTT* pan-neuronally. CAA interruptions in all of the *HTT* sequences also indicated that somatic instability might not occur, due to their stabilising effect on CAG repeat tracts (Wright et al. 2019). We can conclude from this investigation that when an expanded CAG tract within *HTT* is expressed in post-mitotic neurons in *Drosophila* there is no indication of somatic instability. There was no shift in the peak pattern and no appearance of a second hedgehog plot with another modal peak, both denoting a lack of expansion (or contraction). These results indicate that *Drosophila* cannot be used as a model system to investigate somatic instability in the context of HD.

There are a number of factors that are likely to be contributing to the lack of somatic instability observed:

1) Shorter pure CAG tracts in the *HTT* genes
2) Presence of CAA interruptions in the *HTT* sequences
3) Lack of *MSH3* homolog
4) The lifespan of flies expressing mutant *HTT* was too short

The sequences of the CAG tracts of the *HTT* constructs in the *Drosophila* models revealed CAA interruptions throughout the repeat tract. Recent research has shown that the pure CAG tract is a larger determinant of disease progression rather than the poly-glutamine tract, indicating that CAA interruptions are protective in some way (Ciosi et al. 2019; Lee et al. 2019). Other research has shown that the presence of a penultimate CAA in the CAG repeat tract prevents earlier age of onset of disease and reduces somatic expansion in a HD patient cohort (Wright et al. 2019; McAllister et al. 2022). The BACHD mice, which has an extremely similar sequence to the HTT96QCer flies, and YAC128 mice both contain mixed CAG/CAA sequences and there is no evidence of somatic expansion in those models (Gray et al. 2008; Pouladi et al. 2012). With this information it is likely that the CAA interruptions that were found in the *HTT* sequences in the fly models were stabilising the repeat tract, thus reducing the chance of somatic instability occurring. In order to bypass this, a *HTT*

construct could be modified to remove the CAA interruptions in the CAG repeat tract and then expressed in *Drosophila*.

The lack of *Drosophila* homologs for genes that were most strongly associated with the somatic expansion of the CAG repeat in disease (i.e. *FAN1* and *MSH3*) could potentially have prevented the expansion of the CAG repeat tract in these fly models (Tomé et al. 2013; Lee et al. 2015; Goold et al. 2019). There are some human MMR genes that are associated with instability that have *Drosophila* orthologs (Table 4.1) and the pathway is highly conserved between humans and *Drosophila* (Figure 4.1). MutS complexes recognise the mismatch, MutL complexes facilitate the nicking of the strand and recruitment of exonucleases, and the strand is re-synthesised by DNA polymerases. The *Drosophila* pathway is much simpler, containing only one MutS and MutL heterodimer, comprised from MSH2-MSH6 and MLH1-PMS2 respectively, whereas the human pathway has the propensity to use MutS and MutL complexes composed of different subunits (Sekelsky 2017). While the expression of functioning *MLH1* and *MSH2* have both been implicated in destabilising the CAG repeat tract in the striatum and other tissues of HD mouse models (Manley et al. 1999; Wheeler et al. 2003; Pinto et al. 2013) this may not be occurring in the fly. Perhaps the mechanism of somatic instability of triplet repeat sequences is utilising MMR proteins outside of their canonical function.

In *Drosophila*, the pathway seems to be exclusively activated to fix mismatches that occur during DNA replication. Tosca, the *Drosophila* ortholog of *EXO1*, excises the strand containing the mismatch and is predominantly expressed in *Drosophila* female germline cells (Digilio et al. 1996). Instability of an expanded CAG repeat tract in *Drosophila* has previously been published, but it was an investigation into inter-generational instability within germline cells (Jung et al. 2011). Evidence suggests that higher rates of intergenerational instability of the *HTT* CAG repeat in human patients occurs from father to offspring in comparison to the mother who usually transmits a stable or contract *HTT* allele (Telenius et al. 1993; Trottier et al. 1994; Aziz et al. 2011). When this information is combined with the fact that Tosca primarily functions in female germline cells, it suggests that intergenerational instability of CAG repeats is not mediated by MMR machinery in the fly. It is likely that intergenerational and somatic instability have different mechanisms to

elicit repeat expansion. In these experiments *HTT* was expressed in post-mitotic neurons to replicate what occurs in human disease, however the lack of crucial MMR machinery associated with instability in conjunction with MMR potentially only occurring in germline cells probably accounts for CAG repeat instability not being observed. Perhaps expansion of a CAG tract can only be achieved by the intergenerational instability mechanism in *Drosophila*. In order to investigate whether MMR occurs in *Drosophila* neurons, biochemical assays that detect the activity of MMR proteins should be used.

Flies expressing pathogenic *HTT* pan-neuronally have a median lifespan of 20-36 days depending on the construct. This may not be enough time for somatic instability to occur. In a mouse knock-in model of HD the CAG repeat tract expressed in striatum expanded, on average, by 1 repeat per month (Lee et al. 2011). Expanding the CAG repeat tract *in vivo* appears to require more than the expected lifetime of a fly expressing *HTT*. When considering this timescale with regards to the lifespan of the fly, it was highly unlikely that somatic instability would be observed in our experiments. However, expressing *HTT* in a smaller-subset of neurons could decrease Htt toxicity in the fly brain, potentially increasing the flies' lifespan to an age whereby instability could be observed.

GeneScan is an accurate technique used to size fluorescently tagged PCR fragments by capillary electrophoresis. Regarding the sizing of CAG repeat tracts it is more accurate than Sanger sequencing, as expanded CAG repeats can sometimes be mis-read with more CAG's being recorded than are actually there. This was seen with the *HTT*138Q-mRFP construct where the sequencing data showed 142 repeats, but GeneScan traces displayed modal peaks at a fragment size indicating 134 repeats. GeneScan captures the range of CAG tract sizes which allows for identification of unstable constructs, whereas sequencing will just yield one (maximal) repeat tract length.

To summarise, when an expanded CAG repeat tract containing a pure CAG tract of 57 CAGs, but otherwise a mixed CAG/CAA sequence, is expressed in post-mitotic neurons in *Drosophila*, there appears to be no indication of somatic instability. Perhaps somatic instability could be observed if a model was created expressing *HTT* with a pure CAG tract in a small sub-set of neurons which could survive up to 2 months, however, in the scope and

timescale of this project it was not possible. There are also benefits to having a stable CAG repeat when conducting experiments as we can examine phenotypes without confounding the data by somatic expansions which are hard to control for. The escape response deficit that the flies exhibited in the previous results chapter is not a direct comparison to the motor symptoms that HD patients experience, but it may be a useful assay for detecting druggable targets unrelated to repeat instability. See Chapter 5 for the screen of potential genetic modifiers of HD.

4.4 Summary of Main Points

- All human *HTT* constructs with expanded CAG tracts contained CAA interruptions.

- *HTT*128Q full-length and truncated models contained identical repeat tract, which contains 121 repeats.

- *HTT*96QCer construct contained a minisatellite that repeats 16 times throughout the CAG repeat tract.

- *HTT*138Q-mRFP contained the longest pure CAG tract – 57 CAGs.

- There was no evidence for somatic instability in flies expressing *HTT*138QFL.

- Flies can be used to model and investigate HD without somatic instability of the CAG repeat tract confounding results.

5. Screening for genetic modifiers of HD phenotypes in *Drosophila melanogaster*

5.1 Introduction

In the previous results chapter it was established that when the toxic full-length human *HTT* construct containing 128Q's (*HTT*128QFL) was expressed pan-neuronally in *Drosophila*, they develop a robust locomotor deficit compared to flies expressing *HTT* with a short repeat tract (*HTT*16QFL). Their locomotor ability was measured by the Rapid Iterative Negative Geotaxis (RING) Assay which tests the escape response and overall motor performance of *Drosophila* (Gargano et al. 2005). The climbing deficit of the *HTT*128QFL expressing flies was significant at 7 days post eclosion (dpe) and it continued to worsen as the flies aged. It was decided that the RING assay and the *HTT*128QFL model would be used to screen for potential modifiers of this CAG expansion related phenotype.

Some of the genes selected for the screen were chosen from the multiple HD Genome Wide Association Studies (GWAS) which highlighted the involvement of DNA repair pathways in the onset of HD (Lee et al. 2015; Moss et al. 2017; Lee et al. 2019). From pathological studies it was further found that high levels of nuclear DNA damage can be detected in HD patient blood (Askeland et al. 2018). As referenced in previous chapters, the most significant SNPs with the largest effect sizes (up to 5 years/allele) were found in the gene *FAN1*. *FAN1* plays a role in inter-strand crosslink repair amongst other functions in humans (Thongtip et al. 2016), but it does not have a *Drosophila* homolog which meant it could not be screened. *MSH3* is another gene that has been implicated in disease progression (Moss et al. 2017; Flower et al. 2019), at least in the sense of CAG repeat instability. As with *FAN1*, *Drosophila* do not have a homolog for *MSH3*, however many other molecules in the DNA repair and maintenance pathways exist in the fly and may be relevant to HD pathogenesis which is why homologs for *PARP1*, *PARG*, *MRE11* and *XRCC1* were also assayed. The complete list of genes studied are detailed below (Table 5.1).

Human gene	Fly homolog	DIOPT Score	Function
MSH2	spellchecker1	14	DNA MMR
MSH6	Msh6	13	DNA MMR
EXO1	tosca	11	DNA MMR
PMS2	Pms2	13	DNA MMR
PARP1	Parp	13	NER, BER, chromosome stability
PARG	Parg	7	Regulates PARP1 activity
MRE11	mre11	15	DNA DSB repair
XRCC1	Xrcc1	11	DNA SSB Repair

Table 5.1 - List of the human and fly orthologs of the genes screened and their function. The *Drosophila* RNAi Screening Center Integrative Ortholog Prediction Tool (DIOPT) calculates a score which indicates how orthologous the genes are between the selected species. This tool uses a number of tools to indicate homology. The highest score is 15 (Hu et al. 2011).

The DNA Mismatch Repair (MMR) pathway is activated following DNA synthesis and in response to damage caused by exogenous agents in transcriptional events (Brooks et al. 1996). It corrects base-base mismatches made by DNA polymerases during the process (Iyer and Pluciennik 2021). Genes containing long repeat sequences, such as the trinucleotide CAG repeat in *HTT*, are prone to strand-slippage errors and these can form a variety of noncanonical conformations of DNA (Levinson and Gutman 1987). Non-canonical conformations of DNA form due to mismatches and the MMR processes these. MSH2 and MSH6 are two proteins in the MMR that form the heterodimer MutSα which recognises sites of mismatched nucleotides (Gupta and Heinen 2019). MSH2 has previously been implicated in exacerbating the expansion of the CAG repeat tract in the striatum of the HdhQ111/+ HD mouse model (Kovalenko et al. 2012). When the endogenous *Msh2* gene was deleted in the MSNs of HdhQ111/+ mice, CAG instability of the *HTT* gene was ablated in the striatum. In contrast, *MSH6* did not seem to have an effect on the somatic instability of the CAG repeat tract of *HTT* in the HdhQ111/+ mice (Dragileva et al. 2009). It was unclear how these two genes would affect the phenotype of the *HTT*128QFL expressing flies that have an interrupted CAG repeat expansion and do not exhibit repeat instability (as detailed in Chapter 4).

Another heterodimer involved in the MMR pathway is the MutLα complex which is canonically formed by MLH1 and PMS2 (Iyer and Pluciennik 2021). The MutLα complex is responsible for trapping the MutS complex at the mismatch site, and it enhances the recognition of the mismatch through this physical interaction with the MutS complex (Li 2008; Qiu et al. 2015). PMS2 exhibits endonuclease activity that introduces nicks into the DNA strand (Oers et al. 2010). Similarly, to MSH2 and MSH6, PMS2 has been associated with the stability of the CAG repeat tract in cell models of HD (Goold et al. 2021). FAN1 has been shown to interact with PMS2 and MLH1 in the MutLα complex conformation, and it is thought that this interaction stabilises the CAG repeat tract, allowing for canonical MMR without resulting in expansions (Goold et al. 2021). When FAN1 is not associated with the MutLα complex at the CAG repeat tract site, there may be a higher propensity for MMR resulting in CAG expansion. In Friedreich's Ataxia, it has been shown that *PMS2* knockdown resulted in large expansions of the GAA repeat tract in the frataxin gene, whereas *MSH2* and *MSH6* knockdown resulted in a reduction of somatic mutations in neuronal tissues of YG8 *FXN* GAA mice (Bourn et al. 2012). Somatic instability was not a read-out for the screen because the CAG tract in human *HTT* constructs does not expand when expressed in *Drosophila* neurons, but it was important to establish if these genes would affect other HD-related phenotypes. This made it difficult to predict the effect that knocking down these genes would have on the flies' locomotor phenotype.

Exonuclease 1 (EXO1) is a 5' exonuclease that excises the error containing strand that the MutL complex has nicked during MMR (Negishi 2016; Pećina-Šlaus et al. 2020). Unlike its upstream counterparts, EXO1 has not specifically been related to HD and somatic instability of the CAG repeat tract. It was included in the screen to fully assess whether any part of the MMR pathway would affect the locomotor function of the HD-flies.

Published literature indicates the components of the MMR pathway affect the instability of the CAG repeat tract, however given that repeat instability was not detected in our fly model (Chapter 4) it was important to investigate other DNA maintenance/repair pathways unrelated to CAG repeat instability. It is possible that more general DNA damage is important for pathogenesis, rather than solely mismatches (Browne et al. 1997; Castaldo et

al. 2018). Poly ADP-Ribose Polymerase 1 (PARP1) is a protein with major roles in DNA damage repair and chromosome stability (Ray Chaudhuri and Nussenzweig 2017). When DNA is damaged by reactive oxygen species (ROS) PARP1 is recruited to the site of DNA damage and when it binds to the DNA strand it is able to add poly ADP-ribose units to itself and target proteins (PARylation) (Huambachano et al. 2011). This reaction is dependent on the availability of NAD^+. The linear or branched chains of PAR recruit target proteins to the site of DNA damage, enabling DNA repair to occur (Amé et al. 2004). PAR has also been shown to bind to HTT (Maiuri and Truant 2018) which makes PARP1 an interesting candidate in this screen. PARP1 inhibitors are currently used to treat various forms of cancer, but they have also been tested in mouse models of HD, where treatment was shown to have neuroprotective effects (Cardinale et al. 2015; Paldino et al. 2020) (See Chapter 1.4.3 for more details). PARP1 hyperactivity has been associated with the cell death pathway, Parthanatos (David et al. 2009), which occurs in response to extremely high levels of DNA damage from UV, ROS, among other insults (See Chapter 1.2.5.4 for more details). As high levels of DNA damage have been recorded in HD human tissue and HD mouse models (Bogdanov et al. 2001; Illuzzi et al. 2009; Askeland et al. 2018; Castaldo et al. 2018), this may be occurring in the *HTT*128QFL *Drosophila* model as well. Thus, regulating endogenous *Parp* by reducing its expression with RNAi may be beneficial for the HD fly model. Based on data from the mouse models and the potential high levels of DNA damage in the *HTT*128QFL flies, we hypothesised that *Parp* knockdown in the *HTT*128QFL fly model would rescue the climbing deficit.

PARP1 activity is counteracted by Poly ADP-Ribose Glycohydrolase (PARG), which removes the chains of PAR from PARP1 and its targets with a specific hydrolytic reaction (Barkauskaite et al. 2015). The downregulation of *PARG* expression has not been extensively studied in HD, but a *Drosophila Parg* knockdown mutant was found to have neurodegenerative phenotypes, locomotor deficits and shortened lifespan (Hanai et al. 2004). Because of this, we hypothesised that *Parg* knockdown would worsen the locomotor phenotype of the *HTT*128QFL expressing flies.

X-ray repair cross-complementing protein 1 (XRCC1) is a DNA repair protein that is recruited to sites of single stranded breaks (SSBs) by PARP1 activity (London et al. 2015, Caldecott

2019). It functions as a scaffolding protein for multiple enzymes during the process of SSB repair including DNA polymerase (Polβ) and a DNA ligase (LIG3) (Thompson and West 2000; Almeida and Sobol 2007). Mutations in *XRCC1* in neurons have been reported to result in malfunctioning SSB repair which was associated with aberrant PARP1 activity, elevated levels of PAR and neurodegeneration, potentially by Parthanatos (Hoch et al. 2017; Adamowicz et al. 2021). Apart from PARylation its recruitment to the SSB, the exact function of XRCC1 has not been fully elucidated, but researchers have reported that in *XRCC1* deficient cells PARP1 remains trapped to the SSB site preventing Polβ and Lig3 from repairing the break (Demin et al. 2021). In cells with functioning XRCC1, PARP1 inhibitors also prevented SSB repair from occurring, leading to the hypothesis that XRCC1 is a PARP1 "anti-trapper" (Demin et al. 2021). In *XRCC1* deficient cancer cells PARP1 inhibitors have been used as a pharmacological cancer treatment as the combination of PARP1 inhibition and *XRCC1* deficiency yields synthetic lethality (Ali et al. 2020). This research demonstrates the important relationship that PARP1 and XRCC1 have in repairing SSBs and cellular health.

Evidence for XRCC1 interacting directly with huntingtin protein (HTT) has not been published, but ataxia-telangiectasia mutated kinase (ATM) a protein that stops SSBs from becoming DSBs by preventing DNA replication at SSB sites, has been reported to interact with HTT (Khoronenkova and Dianov 2015; Maiuri et al. 2017). This could mean that XRCC1 acts up or downstream of the HTT-ATM oxidative DNA damage response complex. Similarly, to *EXO1*, it is difficult to predict whether knocking down the expression of *XRCC1* could have an effect on the climbing ability of the *HTT*128QFL expressing flies.

Meiotic recombination 11 (MRE11) is a DNA nuclease that is recruited by PARP1 to sites of SSBs at stalled replication forks, with MRE11 foci having been shown as co-localising with PAR foci in U2OS cells (Bryant et al. 2009). MRE11 is a part of the MRN complex, with RAD50 and NBS1 (D'Amours and Jackson 2002). It responds to DSBs and regulates the repair by non-homologous end-joining (NHEJ) or homology directed repair (HDR) (Stracker and Petrini 2011). Mutations in *MRE11* have been shown to cause ataxia telangiectasia-like disorder (ATLD) which causes neurodegeneration and a pre-disposition for cancer (Stewart et al. 1999; Delia et al. 2004; Fernet et al. 2005; Hartlerode et al. 2018). Similarly to *XRCC1*, *MRE11* deficient endometrial cancer cells exhibit sensitivity to PARP1 inhibition, with PARP1

inhibitors incurring synthetic lethality of the cells *in vitro* (Koppensteiner et al. 2014). This highlights *MRE11*'s important role in DNA repair, but currently there is no strong link to *MRE11* and HD. In *Drosophila*, mre11 is required to stop telomere fusion and chromosome breakage from occurring (Ciapponi et al. 2004). As *MRE11* has such an important role in initiating the repair of DSBs and chromosome integrity, it is likely that knocking down *mre11* in *Drosophila* neurons will have a negative impact on the climbing ability of the *HTT*128QFL expressing flies.

5.1.1 Aims and hypothesis

I hypothesise that knocking down key DNA maintenance and repair genes in neurons of *Drosophila* with a *HTT*128QFL background will alter the locomotor deficit.

Aim 1) Screen DNA maintenance and repair genes by knocking down their expression in *Drosophila* neurons with a *HTT*128QFL background, using the RING Assay. We predict that reduced expression of these genes will worsen the locomotor phenotypes (indicating overall loss of CNS function).

Aim 2) Choose and verify appropriate candidate "hit" genes to characterise further in *Drosophila* models of HD.

5.1.2 Experimental Design

A reverse genetic screen was designed to investigate the effect of DNA maintenance and repair genes on the locomotor deficit observed in the *HTT*128QFL model. The native homologs for the human genes of interest had their expression reduced by RNA interference (RNAi) or null mutants. RNAi expression was regulated by the Gal4-UAS system. For the purpose of this screen RNAis were co-expressed with *HTT*128QFL in all neurons by ELAV-Gal4. Null-mutants were also crossed into the *HTT*128QFL flies to investigate the effect in a heterozygous background. All genotypes are listed in Chapter 2.1.2. All flies were reared at 25°C and the crossing scheme indicated below.

$$\female \quad \frac{ELAV-Gal4}{ELAV-Gal4}; \frac{Sp}{CyO}; \frac{+}{+} \qquad \times \qquad \male \frac{w^-}{Y}; \frac{RNAi}{RNAi}; \frac{+}{+}$$

$$\female \quad \frac{w^-}{w^-}; \frac{Sp}{CyO}; \frac{UAS-HTT128QFL}{Tm3,Sb,e} \qquad \times \qquad \male \frac{ELAV-Gal4}{Y}; \frac{RNAi}{CyO}; \frac{+}{+}$$

$$\female \quad \frac{ELAV-Gal4}{w^-}; \frac{RNAi}{Sp}; \frac{UAS-HTT128QFL}{+}$$
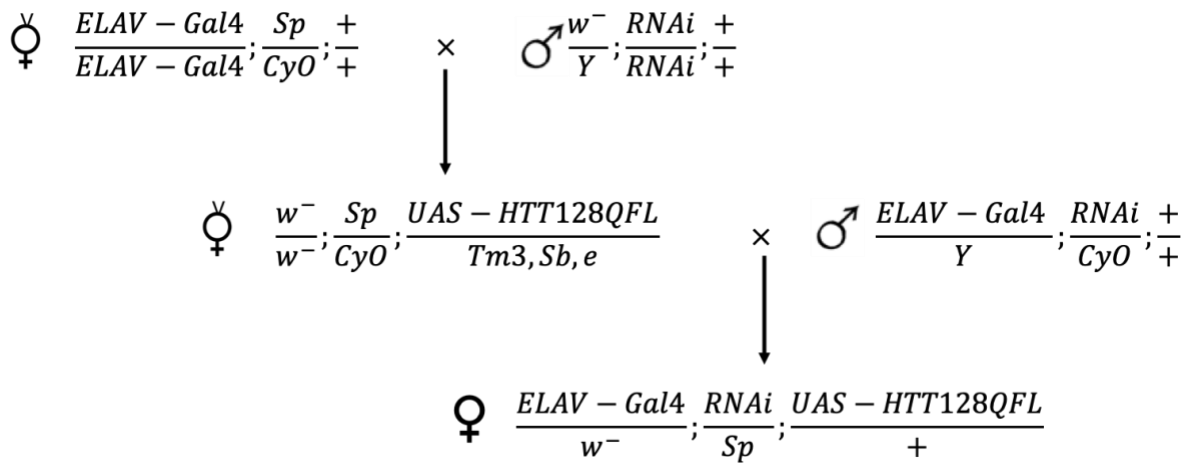
Crossing Scheme 5.1 - Pan-neuronal driver (ELAV-Gal4) carrying virgins are crossed with males carrying the RNAi for a gene of interest. The resulting progeny express an RNAi of the gene of interest in all neurons. The progeny are crossed with virgin females carrying mutant full-length *HTT*. The resulting progeny express pathogenic *HTT* and RNAi for the gene of interest in all neurons.
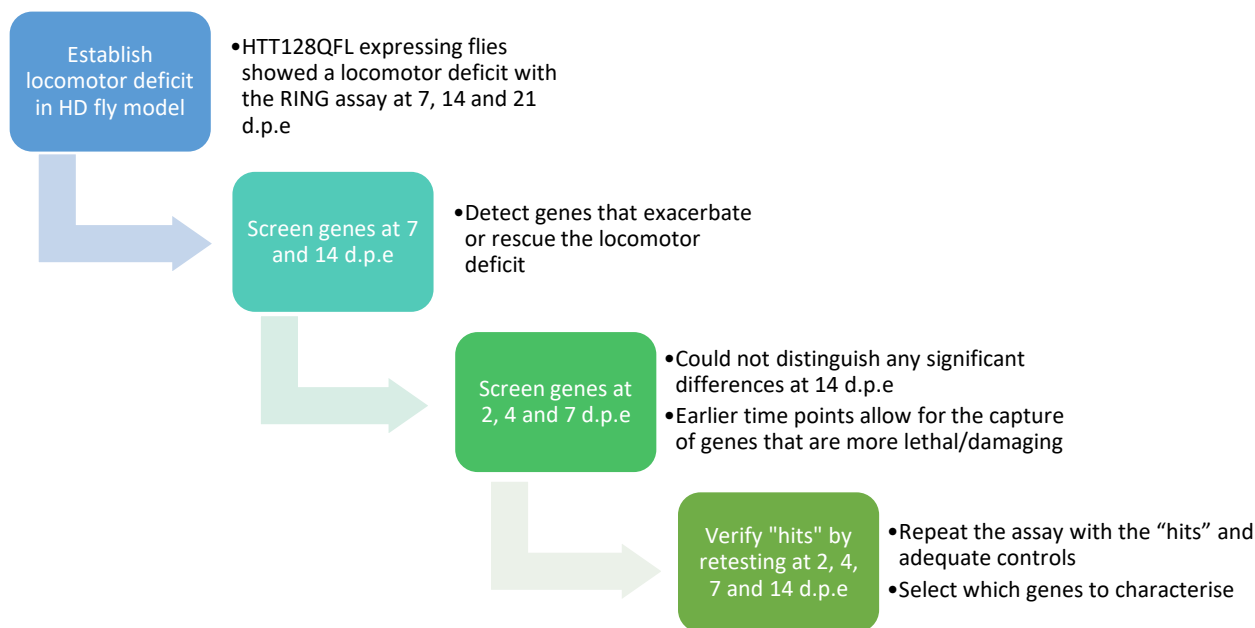
Figure 5.1 – A flow diagram of the development and modification of the screen.

Based on the findings from Chapter 4, I found a robust phenotype in locomotor ability at 7 dpe and this time point taken forward to the screen. For the purpose of the screen I also included a 2 and 4 dpe to detect potentially early modulation of more subtle changes. After the genes were assayed at 2, 4 and 7 dpe the most significant genes were re-tested at those timepoints and at a later stage (14 dpe). The RNAis that still had an effect on the locomotor phenotype post-verification were then assayed again in a wild-type background to confirm whether there was an interaction with *HTT* or the effect was solely due to the RNAi. The lifespan of the flies was also measured.

5.2 Results

5.2.1 *Msh6* knockdown ameliorates the locomotor deficit of *HTT*128QFL expressing flies

It was clear from the GWAS that MMR genes can have a significant role in HD onset (Lee et al. 2015) and progression (Moss et al. 2017). While those results and other published data hypothesise that MMR genes elicit their effect on disease onset and/or progression by driving somatic expansion of the CAG repeat tract, it was still important to test whether these genes could affect motor phenotypes as the modifiers could still be functioning through a different mechanism. The homologs for *MSH2* (*spellchecker1*), *MSH6* (*Msh6*), *EXO1* (*tosca*) *and PMS2* (*Pms2*) were assayed by RNAi in a mutant *HTT* expressing background (Figure 5.2).
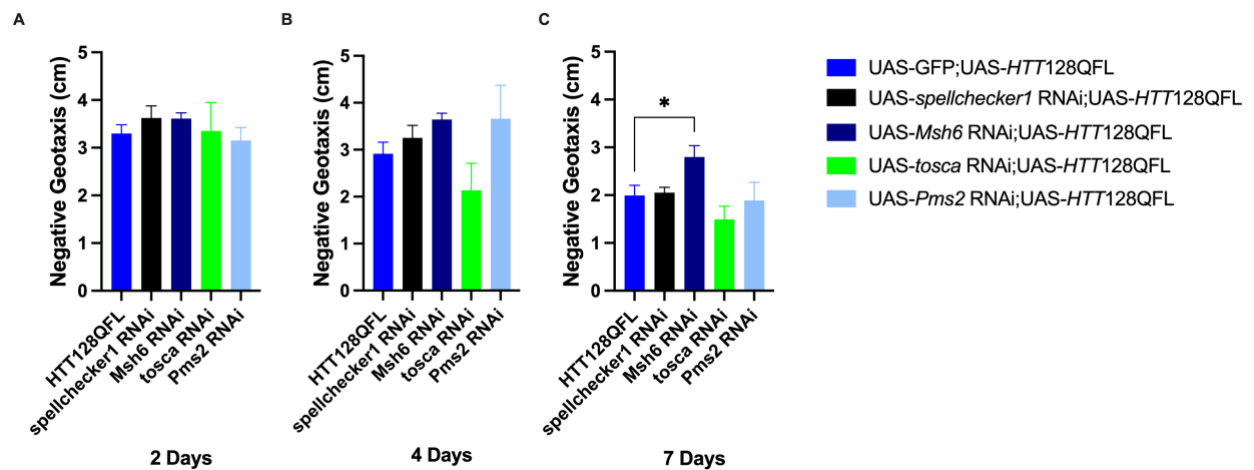
Figure 5.2 – Msh6 knockdown ameliorates the locomotor deficit of the HTT128QFL expressing flies. (A-C) The average distanced climbed by flies after 4 seconds at 2, 4 and 7 d.p.e. The flies pan-neuronally expressed an RNAi for spellchecker1, Msh6, tosca, or Pms2 with a HTT128QFL background. HTT128QFL flies expressed UAS-GFP as a UAS expression control. (HTT128QFL n=15-18, spell1 RNAi n=9-11, Msh6 RNAi n=10, tosca n=3-6, Pms2 RNAi n=3-6, n=1 the average distance climbed by flies in one vial averaged over 5 technical replicates). Data are plotted as Mean± SEM and statistical significance was calculated by One Way ANOVA and Dunnett's multiple comparison test.

At 2 dpe none of the MMR associated RNAi's had a significant effect on the climbing ability of the *HTT*128QFL expressing flies with *spellchecker1* (*spell1*) RNAi flies climbing to an average of 3.62 cm, *Msh6* to 3.61cm, *tosca* RNAi climbing to 3.35 cm, *Pms2* RNAi climbing to 3.15 cm, and *HTT*128QFL flies climbing to 3.30 cm (Figure 5.2A). A one-way ANOVA was performed to detect whether the MMR RNAi had an effect on the locomotor function of the

*HTT*128Q flies at 2 dpe. It revealed that there was not a statistically significant difference between the average negative geotaxis of the MMR RNAi's at 2 dpe.

At 4 dpe. *Spell1* RNAi flies climbed an average of 3.25 cm, *Msh6* RNAi climbed to an average of 3.65 cm, *Pms2* climbed to 3.66 cm, and *HTT*128QFL climbing to 2.91 cm (Figure 5.2B). A one-way ANOVA confirmed that MMR RNAi's did not have a statistically significant effect on the climbing ability of the *HTT*128QFL expressing flies although a trend was seen for the *Tosca* RNAi where flies seemingly climbed worse than the *HTT*128QFL control flies.

At 7 dpe *Spell1* knockdown, *tosca* knockdown and *Pms2* knockdown had no effect on the climbing ability of the *HTT*128QFL expressing flies with an average climbing distance of 2.05 cm, 1.49 cm, 1.89 cm, and 1.99 cm respectively (Figure 5.2C). However, *Msh6* knockdown had increased the climbing ability of the *HTT*128QFL with an average negative geotaxis of 2.80 cm in comparison to 1.99 cm. A one-way ANOVA showed a statistically significant effect in the climbing ability of at least two genotypes ($F_{4, 43}$ = 3.289, p = 0.0194), with post hoc Dunnett's multiple comparison's test confirming that *Msh6* knockdown significantly rescues the locomotor deficit of *HTT*128QFL flies at 7 dpe (p = 0.0406).

These findings show that knocking down the expression of the *Msh6* subunit of the MutSα complex ameliorate the *HTT*128QFL locomotor phenotype, but knocking down other genes involved in MMR does not have a significant effect.

5.2.2 *Parp* knockdown rescues the locomotor deficit of *HTT*128QFL expressing flies

After screening the genes in the MMR pathway, it was important to consider other aspects of DNA repair and maintenance. This included the *Drosophila* ortholog for *PARP1/2*, *Parp* and *Parg*. PARP1 tags DNA and DNA repair proteins with PAR-polymers to initiate repair and PARG catalyses the reaction that removes the PAR-polymers (Amé et al. 2004), and these were screened next.
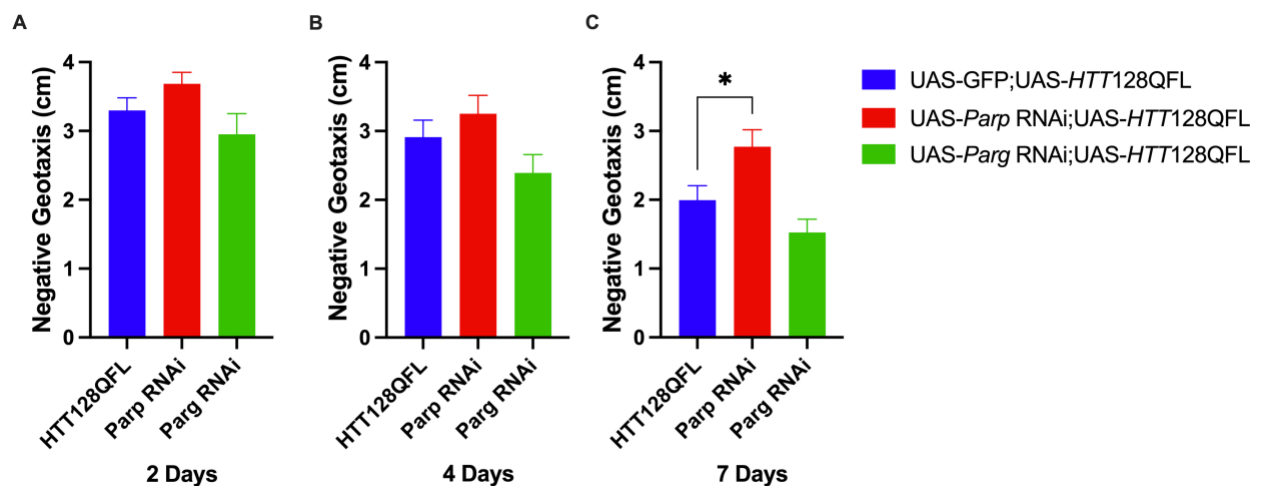
Figure 5.3 – *Parp* knockdown recues the locomotor deficit of the *HTT*128QFL expressing flies. (A-C) The average distanced climbed by flies after 4 seconds at 2, 4 and 7 dpe. The flies pan-neuronally expressed an RNAi for *Parp* or *Parg* with a *HTT*128QFL background. *HTT*128QFL flies expressed UAS-GFP as a UAS expression control. (*HTT*128QFL n=15-18, *Parp* RNAi n= 10-11, *Parg* RNAi n=7-8, n=1 the average distance climbed by flies in one vial averaged over 5 technical replicates). Data are plotted as Mean ± SEM and statistical significance was calculated by One Way ANOVA and Dunnett's multiple comparison test.

At 2 dpe there appeared to be no effect of knocking down either *Parp* or *Parg* on the locomotor function of the *HTT*128QFL expressing flies (Figure 5.3 A), however a one-way ANOVA was performed to assess statistical significance of *Parp* or *Parg* knockdown on the average negative geotaxis of *HTT*128QFL flies. The one-way ANOVA revealed that there was a statistically significant effect of the genotype on the locomotor function of *HTT*128QFL expressing flies ($F_{3, 30}$ = 3.259, p = 0.0351). However, post hoc tests revealed no specific differences between the groups.

 At 7 dpe the *Parg* RNAi had a slightly worsening effect on the climbing ability of the *HTT*128QFL expressing flies, with the average negative geotaxis of 1.53 cm and 1.99 cm respectively (Figure 5.3C). This difference was not statistically significant. However, at 7 dpe

the *Parp* RNAi led to an improved mean distance climbed by the *HTT*128QFL flies, increasing the average distance climbed from 1.99 cm to 2.77 cm. A one-way ANOVA confirmed that there was a significant effect of the genotype on the locomotor ability of the *HTT*128QFL flies ($F_{2, 32}$ = 5.979), and post hoc Dunnett's multiple comparison tests found that the mean distanced climbed was significantly different between the *Parp* RNAi flies and the *HTT*128QFL flies (p = 0.0348).

These findings show that knocking down *Parp* expression in neurons of *HTT*128QFL expressing flies rescues the locomotor phenotype and *Parg* knockdown trends towards worsening, but it was not statistically significant. This suggests that DNA maintenance pathways have a role in HD pathogenesis unrelated to CAG repeat instability.

5.2.3 *Xrcc1* knockdown yields early locomotor deficit which is lost as the flies age

As *Parp* knockdown yielded a rescue of the locomotor phenotype it was important to assess the effect that other downstream targets of *Parp* might have. *Parp* recruits *XRCC1* to sites of DNA damage, specifically to sites of single strand breaks. Reduced *XRCC1* expression has been shown to negatively impact SSB repair as it results in PARP1 DNA trapping which prevents other SSB repair proteins from accessing the SSB site (Demin et al. 2021). Assessing the effect of *XRCC1* knockdown on the locomotor function of *HTT*128QFL flies could implicate a role of PARP1 in HD progression.
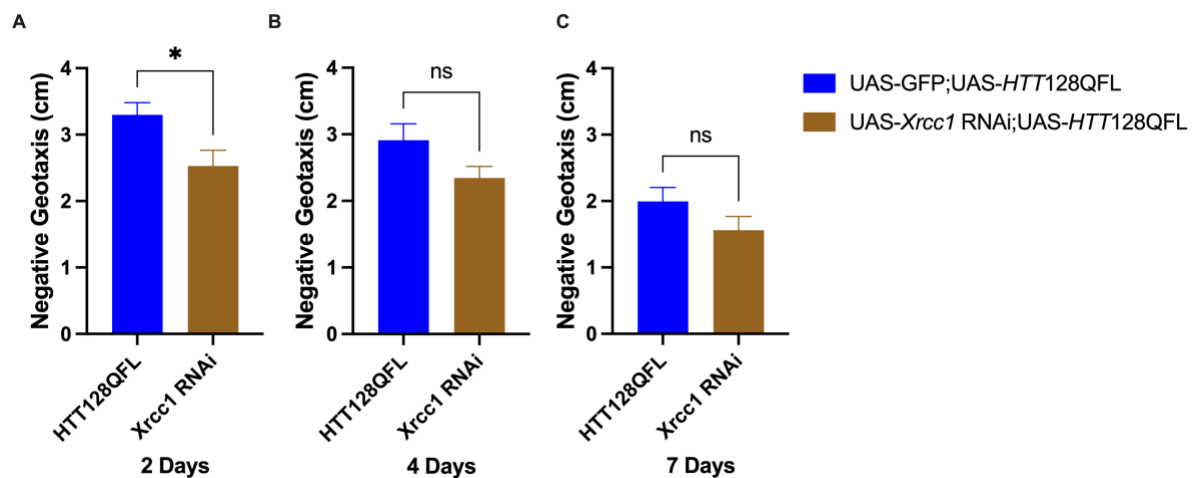
Figure 5.4 – *Xrcc1* knockdown yields early furthering of the locomotor deficit which is lost as the flies age. (A-C) The average distanced climbed by flies after 4 seconds at 2, 4 and 7 dpe. The flies pan-neuronally expressed an RNAi for *Xrcc1* with a *HTT*128QFL background. *HTT*128QFL flies expressed UAS-GFP as a UAS expression control. (*HTT*128QFL n=15-18, *Xrcc1* RNAi n=6-8, n=1 the average distance climbed by flies in one vial averaged over 5 technical replicates). Data are plotted as Mean ± SEM and statistical significance was calculated by Unpaired t test with Welch's correction.

The *Xrcc1* RNAi worsened the locomotor ability of the flies at 2 dpe with an average climbing distance of 2.53 cm in comparison to the *HTT*128QFL flies with an average distance climbed of 3.30 cm (Figure 5.4A). The average negative geotaxis was statistically significant between *XRCC1* RNAi flies (M = 2.527, SD = 0.671) and *HTT*128QFL flies (M = 3.298, SD = 0.713); $t_{15.22}$ = 2.570, p = 0.0212.

As the flies aged the *Xrcc1* had a slight worsening effect on the locomotor ability of the *HTT*128QFL flies but unpaired T-tests confirmed this was not statistically significant at 4 dpe (p = 0.722) and 7 dpe (p = 0.1603) (Figure 5.4B-C). This is similar to the slightly negative

effect that was observed with the Parg RNAi on the locomotor function of the HD flies. This is as predicted as reduced expression of *Xrcc1* and *Parg* could yield PARP1 hyperactivation and potentially parthanatos (David et al. 2009; Hoch et al. 2017; Demin et al. 2021). *Parp* knockdown significantly rescued the locomotor function of the HD flies, and two of its regulators had a slightly negative effect on the locomotor function of the HD flies. These results show that PARP1 could be an important modifier of HD progression.

5.2.4 *Mre11* knockdown significantly worsens the locomotor deficit of the *HTT*128QFL expressing flies

After observing the protective effect that *Parp* knockdown had on the locomotor phenotype, it was important to assess the effect of genes downstream of Parp activity to test whether they were also involved in the pathway. One of the target proteins Parp recruits to sites of DNA damage is mre11.
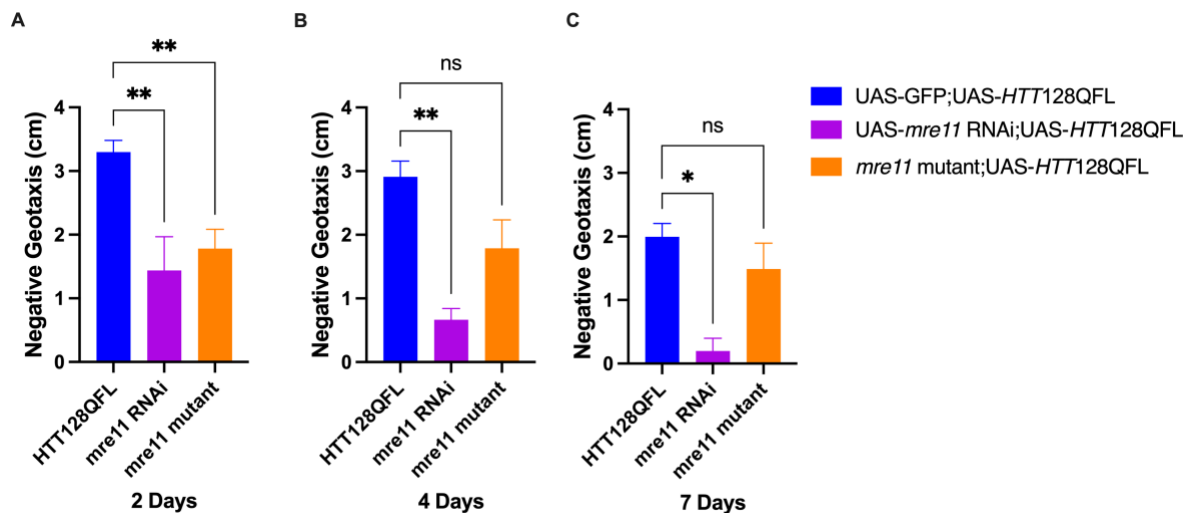
Figure 5.5 – *Mre11* knockdown by RNAi and heterozygous null mutation worsen the locomotor deficit of *HTT*128QFL expressing flies. (A-C) The average distanced climbed by flies after 4 seconds at 2, 4 and 7 dpe. The flies pan-neuronally expressed an RNAi for *mre11* or a heterozygous null mutant *mre11* with a *HTT*128QFL background. *HTT*128QFL flies expressed UAS-GFP as a UAS expression control. (*HTT*128QFL n=15-18, *mre11* RNAi n= 2-3, *mre11* mutant n=3-5, n=1 the average distance climbed by flies in one vial averaged over 5 technical replicates). Data are plotted as Mean ± SEM and statistical significance was calculated by One Way ANOVA and Dunnett's multiple comparison test.

An RNAi and heterozygous null allele mutant were used to investigate the effect of *mre11* knockdown on the climbing ability of the *HTT*128QFL flies. At 2 dpe an early damaging effect on the climbing ability of the *HTT*128QFL flies was observed when *mre11* expression was knocked down by RNAi and null mutant (Figure 5.5A). The *HTT*128QFL expressing flies could climb a distance of 3.30 cm whereas the *mre11* RNAi and mutant could only climb on average to 1.44 cm and 1.78 cm respectively. A one-way ANOVA confirmed there was a statistically significant effect of genotype on the locomotor ability of the *HTT*128QFL expressing flies ($F_{2, 18}$ = 11.85, p = 0.0005). Dunnett's test for multiple comparisons found the average negative geotaxis of the *mre11* RNAi and mutant were significantly worsening

the locomotor performance of the *HTT*128QFL expressing flies (RNAi p = 0.0047; mutant p = 0.0023).

At 4 and 7 dpe one-way ANOVA's were performed to assess whether there was a statistically significant effect of *mre11* knockdown on locomotor function. Both ANOVAs revealed there was a significant difference in the mean negative geotaxis of at least two groups (4 dpe, $F_{2, 23}$ = 7.899, p = 0.0024; 7 dpe, $F_{2, 19}$ = 4.341, p = 0.0280). Dunnett's multiple comparisons test found the effect of *mre11* RNAi continued to significantly reduce the locomotor ability of the *HTT*128QFL expressing flies at 4 and 7 dpe (4 dpe, p = 0.0028, 95% C.I. = 0.7710 to 3.727; 7 dpe, p =0.0188) (Figure 5.5B-C). While the *mre11* mutant flies only climbed to an average of 1.79 cm at 4 dpe in comparison to the 2.91 cm that *HTT*128QFL flies climbed, Dunnett's multiple comparison tests revealed it was not statistically significant, (p = 0.0675). At 7 dpe the *mre11* mutant flies climbed on average 1.49 cm and the *HTT*128Qflies climbed 1.99 cm. There was a slight reduction in climbing ability with the *mre11* mutant, but Dunnett's multiple comparisons test found this to not be statistically significant. These results show that *mre11* knockdown by RNAi has a more damaging effect on the locomotor ability of the *HTT*128QFL flies than when *mre11* expression is reduced by half in the case of the heterozygous null mutant. Overall, knocking down *mre11* expression was detrimental to the locomotor performance of flies expressing *HTT*128QFL, further supporting the notion that DNA damage response pathways play a role in HD pathogenesis.

5.2.5 Re-testing the screen hits verifies the protective effect of *Parp* knockdown and the damaging effect of *mre11* knockdown on the locomotor phenotype

It was important to verify that the effects the RNAi's had on the locomotor phenotype of the *HTT*128QFL expressing flies could be repeated. The genes *Parp*, *Parg* and *mre11* were chosen to assay again with expression controls, an RNAi control and the *HTT*16QFL line. These genes were chosen as they were all connected in their function; Parp as a DNA damage sensor, Parg as one of the two regulators of Parp assayed in the screen, and mre11 as a DNA damage repair protein that is recruited by Parp which had a more significant effect on the locomotor function of the HD flies than *Xrcc1* knockdown. The impact of the RNAis/mutants on the locomotor function of the *HTT*128QFL flies was replicated as before, but the sample size was increased and the locomotor function was also assessed at 14 dpe. This was done because we previously reported that the *HTT*128QFL expressing flies could barely climb at all at 14 dpe, so it was important to assess whether the *Parp* RNAi could rescue the locomotor phenotype at a later time point. The same RNAi and mutant lines that were used in the initial screen were used in the verification process.

The *Parp* RNAi rescue effect seen at 7 dpe was replicated with the *Parp* RNAi flies climbing on average 3.31 cm and the *HTT*128QFL flies only climbing 2.37 cm (Figure 5.6C) (Table 1). The results from Dunnett's multiple comparison test confirmed that the difference in climbing ability between *HTT*128QFl flies and *Parp* RNAi flies at 7 dpe was significant ($p = 0.0013$). As the *Parp* RNAi flies aged the rescue effect continued with a significant increase in the average distance climbed at 14 dpe in comparison to the *HTT*128QFL flies ($p < 0.0001$) (Table 5.2). At 14 dpe the *Parp* RNAi flies were able to climb to 2.14cm in comparison to the 0.31cm climbed on average by the *HTT*128QFL expressing flies (Figure 5.6D). These data verify that *Parp* knockdown can ameliorate the extremely severe climbing deficit of the *HTT*128QFL flies and this pathway should be investigated further.

The *mre11* RNAi and the null mutant of were also retested to verify their effect on locomotor function of the *HTT*128QFL flies. Dunnett's multiple comparisons tests showed that the climbing ability of the *mre11* knockdown flies was significantly worse than that of the *HTT*128QFL flies at 2, 4 and 7 dpe ($p < 0.0001$) (Figure 5.6 A-C) (Table 5.2). However, at 14 dpe the significance was lost for both *mre11* knockdown flies (RNAi, $p = 0.7902$; mutant, p

= 0.9998) (Table 5.2). The *mre11* mutant flies on average climbed to 0.35cm which was similar to the 0.31 cm climbed on average by the *HTT*128QFL flies (ns, p = 0.9989) (Figure 5.6D). The *mre11* RNAi flies were unable to climb as high as that with an average climbing distance of 0.02 cm, however the difference was not significant (ns, p = 0.7902) (Table 5.2). It is possible the *mre11* knockdown flies did not have a significant effect on the climbing ability at 14 dpe, because of the severity of the HD model locomotion at this time point, making any additive effects difficult to measure.
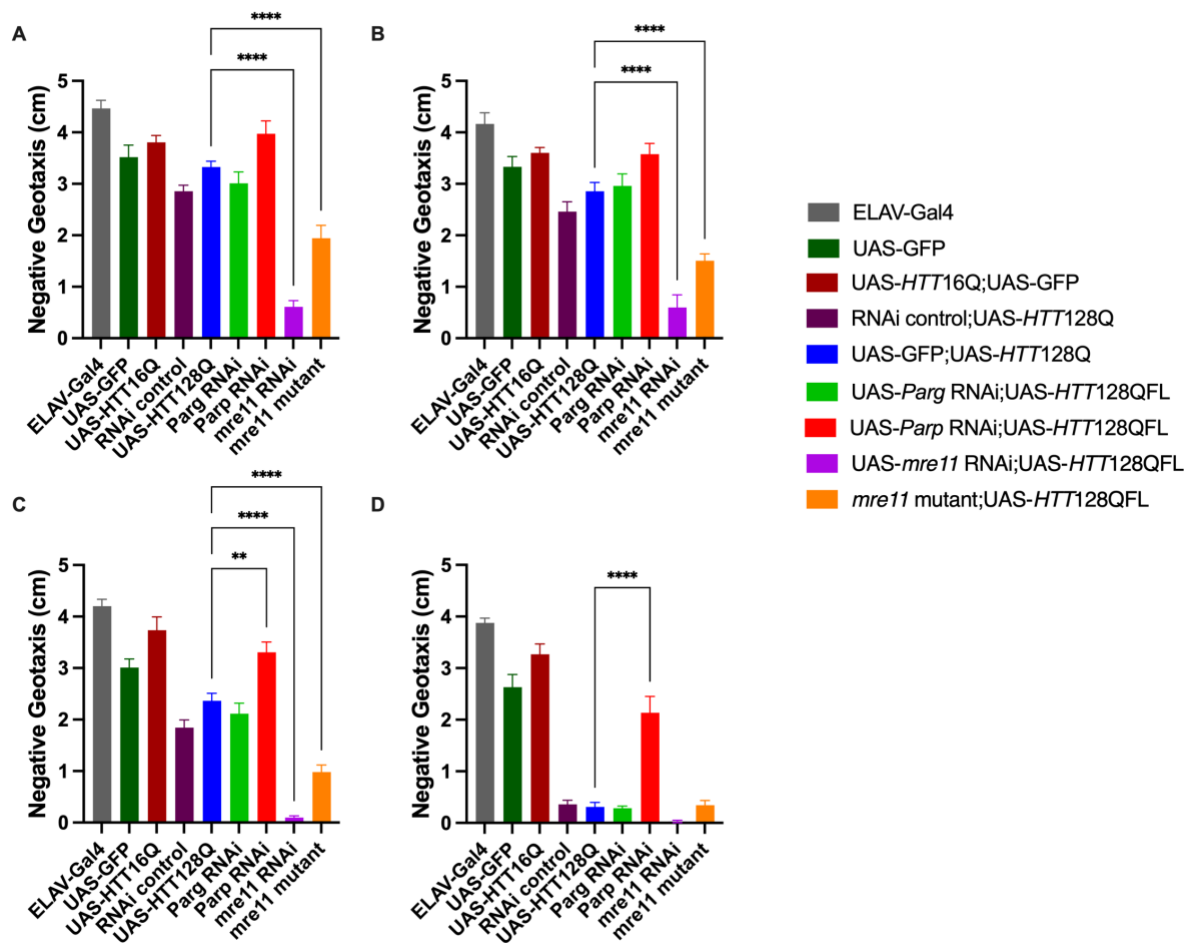
Figure 5.6 - *Parp* knockdown rescues the locomotor deficit and *mre11* knockdown worsens it. (A-D) The average distance climbed by flies after 4 seconds at 2, 4, 7 and 14 dpe. All genes, RNAis and mutants were expressed pan-neuronally by ELAV-Gal4. All RNAis, mutants and the RNAi control had a *HTT*128QFL background. *HTT*128QFL and *HTT*16QFL expressed a UAS-GFP as an expression control. (ELAV-Gal4 n=10, UAS-GFP n=10, *HTT*16QFL n=10, RNAi control n=10, *HTT*128QFL n=10, *Parg* RNAi n=10, *Parp* RNAi n=10, *mre11* RNAi n=8-10, *mre11* mutant n=10, n=1 the average distance climbed by flies in one vial averaged over 5 technical replicates). Data are plotted as Mean ± SEM and statistical significance was calculated by One Way ANOVA and Dunnett's multiple comparisons test. ns, p > 0.05; **, p = 0.0013; ****, p < 0.0001.

Genotype	2 dpe	4 dpe	7 dpe	14 dpe
RNAi control; *HTT*128QFL	ns, p = 0.3560	ns, p = 0.5840	ns, p = 0.1721	ns, p = 0.9997
Parg RNAi; *HTT*128QFL	ns, p = 0.7648	ns, p = 0.9994	ns, p = 0.8548	ns, p= 0.9999
Parp RNAi; *HTT*128QFL	ns, p = 0.0947	ns, p = 0.0614	**Significant rescue, p = 0.0013**	**Significant rescue, p < 0.0001**
mre11 RNAi; *HTT*128QFL	**Significant decline, p < 0.0001**	**Significant decline, p < 0.0001**	**Significant decline, p < 0.0001**	ns, p = 0.7902
mre11 mutant; *HTT*128QFL	**Significant decline, p < 0.0001**	**Significant decline, p < 0.0001**	**Significant decline, p < 0.0001**	ns, p = 0.9998

Table 5.2 – A summary of p values from the Dunnett's multiple comparisons tests when comparing the average negative geotaxis of UAS-GFP; *HTT*128QFL with the genotypes of interest at each time point. Significant results are in bold text.

An important result to note was that expressing the RNAi control line with the *HTT*128QFL had no significant effect on the locomotor ability of the *HTT*128QFL flies at any of the 4 time points (Table 5.2). *Parg* knockdown also had no significant effect on the climbing ability of the *HTT*128QFL flies at all the time points (Table 5.2). These data show that the insertion of the RNAi construct into the genome did not affect the locomotor ability of the *HTT*128QFL flies. They also show that *Parg* knockdown by RNAi had no significant effect on the locomotor phenotype of the *HTT*128QFL flies. For the purposes of this study it was not characterised further.

5.2.6 Age-dependent decrease in locomotor ability was observed in all genotypes

When verifying the hits from the screen the opportunity arose to observe the effect of ageing on the locomotor ability of the flies with multiple genetic backgrounds. The first publication detailing the RING Assay stated its purpose was to measure the age-related decline in locomotor function (Gargano et al. 2005). With this data we wanted to assess whether knockdown of genes of interest could affect the rate at which the locomotor deficit of the *HTT*128QFL flies changed over time.
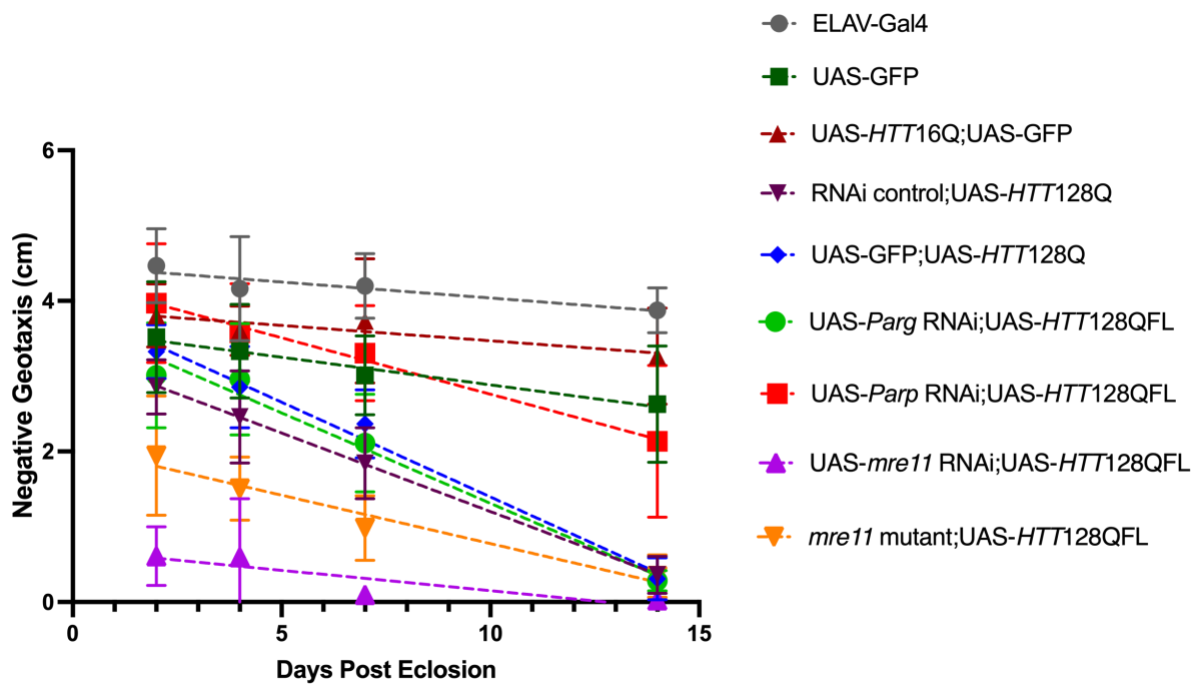
Figure 5.7 – UAS-GFP; *HTT*128QFL expressing flies had the steepest age-dependent decline in climbing performance. A line plot of the average distance climbed by the flies at 2, 4, 7 and 14 dpe and their linear regression. (ELAV-Gal4 n=10, UAS-GFP n=10, *HTT*16QFL n=10, RNAi control n=10, *HTT*128QFL n=10, *Parg* RNAi n=10, *Parp* RNAi n=10, *mre11* RNAi n=8-10, *mre11* mutant n=10). Data are plotted as Mean ± SEM and statistics were calculated by Simple linear regression.

Genotype	Slope	Significantly non-zero
ELAV-Gal4	-0.0425	Yes, p = 0.0177
GFP	-0.0733	Yes, p = 0.0027
*HTT*16QFL; GFP	-0.0408	Yes, p = 0.0495
RNAi control; *HTT*128QFL	-0.2087	Yes, p < 0.0001
UAS-GFP; *HTT*128QFL	-0.2517	Yes, p < 0.0001
Parg RNAi; *HTT*128QFL	-0.2400	Yes, p < 0.0001
Parp RNAi; *HTT*128QFL	-0.1498	Yes, p < 0.0001
mre11 RNAi; *HTT*128QFL	-0.0541	Yes, p = 0.0033
mre11 mutant; *HTT*128QFL	-0.1285	Yes, p < 0.0001

Table 5.3 – The slope and P values of the linear regression of the average climbing distance of the flies that were retested.

A line plot was created to observe the effect of ageing on the locomotor ability of all genotypes (Figure 5.7). A simple linear regression on all of the data showed that the climbing ability of all genotypes significantly decreased as the flies aged (Figure 5.7) and (Table 5.3). The UAS-GFP; *HTT*128QFL expressing flies had the steepest slope (-0.2517) with the most severe age-related decline, followed by the *Parg* RNAi flies (-0.2400), and the RNAi control flies (-0.2087). While the *mre11* mutant flies, *Parp* RNAi expressing flies and the *mre11* RNAi expressing flies had less steep slopes (-0.1285 and -0.1498 respectively), the change in their locomotor ability over time was still highly significant (p < 0.0001). The slope of the *mre11* RNAi expressing flies was the least steep (-0.0541) but still highly significant (p = 0.0033). The age-related decline seen for this was likely skewed because the *mre11* knockdown flies had a highly significant motor deficit at 1 dpe in comparison to the HTT128QFL control flies. Together this indicates that the effect of *mre11* and *Parp* knockdown both strongly relate to ageing and mutant huntingtin toxicity even at early stages.

5.2.7 *Mre11* and *Parp* RNAi significantly worsen the locomotor function of "WT" flies

Prior to choosing a HD pathogenesis modifying candidate to characterise further, it was paramount to assess whether the effects of the RNAi's were dependent or independent of *HTT*128QFL expression.

It was apparent that *mre11* knockdown alone was enough to yield a locomotor deficit. At the young age of 2 dpe the *mre11* RNAi flies merely climbed to an average of 0.92 cm (Figure 5.8). This decreased to 0.03 cm at 14 dpe. A two-way ANOVA showed both a genotype specific difference ($F_{3, 68}$ = 8.605, p < 0.0001) and an age specific difference ($F_{2, 68}$ = 208.4, p < 0.0001). Tukey's multiple comparisons test revealed the climbing ability of the *mre11* RNAi flies did not significantly decline between 2 and 14 dpe (p = 0.6743). Tukey's multiple comparisons test also showed that at each time point, *mre11* knockdown had a statistically significant worsening effect on the locomotor performance of the flies in comparison to flies carrying the pan-neuronal driver ELAV-Gal4 (2 dpe, p < 0.0001; 4 dpe, p < 0.0001; 7 dpe, p < 0.0001; 14 dpe, p < 0.0001). This data confirmed that the effect of *mre11* knockdown on the locomotor performance of the flies is independent of m*HTT* expression.

Between 2 and 7 dpe, the average distance climbed between ELAV-Gal4 flies and *Parp* RNAi flies was not statistically significant. At 2 dpe, ELAV-Gal4 flies climbed to an average of 4.47 cm and *Parp* RNAi flies averaged a negative geotaxis of 4.30 cm, and similar average distances were maintained at 4 dpe with the average distances climbed being 4.16 cm and 4.14 cm respectively. At 7 dpe there was a difference in their average distance climbed with ELAV-Gal4 flies climbing to an average of 4.20 cm and *Parp* RNAi flies climbing to an average of 3.09 cm, but this was shown by Tukey's multiple comparisons test to not be statistically significant. At 14 dpe The *Parp* RNAi flies climbed significantly less than the ELAV-Gal4 flies, reaching an average of 2.59 cm in comparison to 3.88 cm (p = 0.0154). Tukey's post hoc tests also revealed the climbing ability of the *Parp* RNAi flies significantly declined between 2 and 14 dpe (p = 0.0208). These results show that there is an age-dependent decrease in locomotor performance when *Parp* is knocked down in a non-HD background. This is opposite to our previous results which rescue m*HTT* associated locomotor phenotype. This suggests that a reduction in *Parp* is generally detrimental to neurons unless they are

expressing mutant *HTT* which makes the rescue effect of the locomotor phenotype in the *Parp* RNAi;*HTT*128QFL flies even greater.
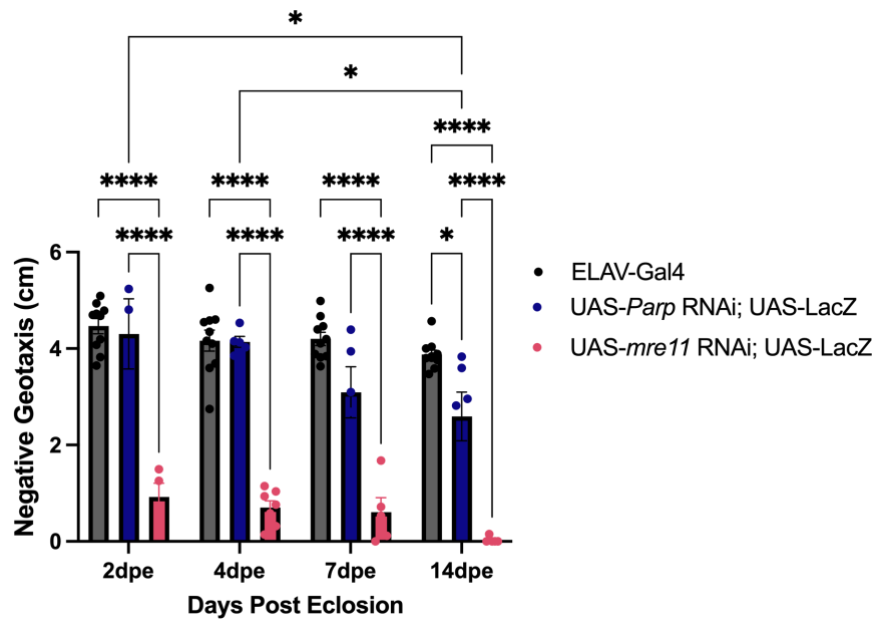
Figure 5.8 – The locomotor ability of *mre11* knockdown flies is reduced regardless of *HTT* expression. The average distanced climbed by flies after 4 seconds at 2, 4, 7 and 14 dpe. The flies pan-neuronally expressed an RNAi for *Parp* or *mre11*. LacZ was expressed as an expression control to compare to previous experiments. Flies expressing solely ELAV-Gal4 acted as a control. (ELAV-Gal4 n=10, *Parp* RNAi n= 3-6, *mre11* RNAi n=4-7, n=1 the average distance climbed by flies in one vial averaged over 5 technical replicates). Data are plotted as Mean $\pm$ SEM and statistical significance was calculated by Two Way ANOVA and Tukey's multiple comparison test. Ns, $p > 0.05$; *, $p = 0.0141\text{-}0.0208$; ****, $p < 0.0001$.

5.2.8 *Mre11* and *Parp* knockdown yield significantly decreased lifespan

The lifespan of the *Parp* and *mre11* RNAi flies was also measured in order to establish if knocking down the expression of either gene would have an effect on the lifespan of the fly. The Kaplan Meier plot below displays the survival percentage of the two RNAi lines and flies carrying pan-neuronal driver ELAV-Gal4 (Figure 5.9). The median lifespan for each genotype was calculated and the Log-rank (Mantel-Cox) test showed a significant difference in the survival curves (df = 2, p < 0.0001). The median lifespan of *mre11* RNAi flies was 9.5 days which was significantly shorter than the median lifespans of *Parp* RNAi and ELAV-Gal4 flies, 52 and 75 days respectively.
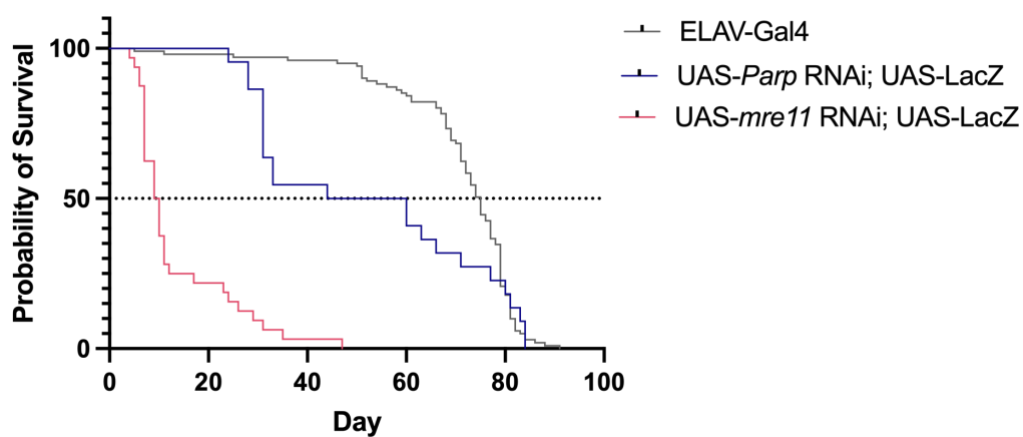
Figure 5.9 - *Mre11* knockdown significantly reduces *Drosophila* lifespan. Kaplan Meier plot displaying the percentage survivorship of flies with pan-neuronal knockdown of *Parp* or *mre11*, with a control line carrying only the pan-neuronal driver ELAV-Gal4. (ELAV-Gal4 n=101, *Parp* RNAi n = 24, *mre11* RNAi n= 34). Statistical significance was calculated by Log-rank (Mantel Cox) test.

Combining the observations from the RING and longevity assays, it was clear that *mre11* knockdown was detrimental to locomotion and survival, regardless of *HTT*128QFL expression. While *Parp* knockdown appeared to be damaging to lifespan and locomotor function, in comparison to flies carrying ELAV-Gal4, it did not have as significant effect as *mre11* knockdown. These results point to an interesting role for *Parp* expression in HD which will be further explored in the following results chapter.

5.3 Discussion

In Chapter 3 we found a significant locomotor deficit in flies expressing pathological hu*HTT* with the RING assay and this was chosen to screen potential modifiers. *Msh6* and *Parp* knockdown rescued the locomotor phenotype of the *HTT*128QFL flies, whereas *Xrcc1* and *mre11* knockdown exacerbated the phenotype. *Parp* and *mre11* knockdown lines were taken forward for retesting because they had opposing effects on the locomotor phenotype of the HTT128QFL flies and *mre11* is activated downstream of Parp (Ray Chaudhuri and Nussenzweig 2017) so we thought it would be interesting to verify two genes whose function was connected, although it is important to note that they do not always function together. *Msh6* was not taken forward to the verification stage as none of the other MMR genes yielded a significant result, and we wanted to separate the results from association with somatic instability. Since we did not find any evidence of somatic expansion of the CAG tract in Chapter 4, we suggest that these candidates may affect the level of DNA mutations overall, or have other effects on protein aggregation or neuronal survival.

Overall the RING assay proved useful to investigate several candidate genes via RNAi mediated knockdown. Perhaps more subtle effects of gene knockdown were lost because the analysis took a single N as an average of approximately 10 flies within one vial, rather than every fly separately, which would yield more statistical power. However, separate vials were necessary to control of repeated experiments. The Gal4-UAS system used to drive the RNAis and mutant *HTT* is also temperature dependent. Rearing experimental flies at 25°C was useful to get a screenable phenotype in our HD model and to get a robust genetic knockdown. Although the temperature could be changed to 29°C to potentially increase the level of knockdown, this may have increased the expression of mutant *HTT*, potentially increasing overall toxicity. To aid with screening speed, one RNAi was used per gene, however it is important to note that one RNAi may be insufficient to knockdown or have off-target effects, hence any significant findings must be validated. Overall, this reverse genetic screen is a useful tool to screen for new modifiers and in future, could be used to screen a larger number of genes, or a forward genetic screen.

Following the screen, changes to the locomotor deficit of the *HTT*128QFL flies from the *Parp* or *mre11* knockdown were then verified. However, in control flies that do not express mutant *HTT*, *mre11* knockdown continued to cause severe locomotor deficits and also a reduction of lifespan. *MRE11* mutations have been associated with human ataxia-telangiectasia-like disorder and *Mre11* knockout mice are embryonic lethal (Xiao and Weaver 1997). This showed that *mre*11 would not be a good candidate for further investigation as its neuronal expression levels clearly impacted overall CNS function and mortality regardless of genetic background, so the possibilities of it being a druggable target in HD is unlikely. We believe this is due to the important role that mre11 has in DNA DSB repair. DNA DSBs can be caused by high levels of ROS and with the knowledge that mitochondria become dysfunctional in HD (Chen et al. 2007; Carmo et al. 2018), and thus unable to reduce cellular ROS, DSBs could be building up in cells expressing mutant hu*HTT*. As mre11 is a major component of the MRN complex which acts in homologous recombination and non-homologous end-joining of DSBs (Rass et al. 2009), if *mre11* expression is significantly reduced then it is likely that DSBs may not be repaired and an accumulation of unrepaired lesions has been reported to result in cell death (Rulten and Caldecott 2013). In HD it would be preferable to treat the cause of ROS rather than target DSB repair as high levels of cellular ROS also impacts cellular health in ways unrelated to DNA.

There are a few publications that have investigated the role of *Parp* in HD. PARP1 inhibition was found to be neuroprotective in the R6/2 HD model mouse model when treated with INO-1001, a potent PARP1 inhibitor (Cardinale et al. 2015; Paldino et al. 2020). They both report that INO-1001 treatment led to increased lifespan and neuronal survival. INO-1001 inhibits PARP1 activity by competing with PARP1 for NAD$^+$, blocking the activity of the synthesised protein (Murai et al. 2012). In the screen RNAi-mediated *Parp* knockdown ameliorated the climbing ability which indicates neuroprotective effects, similar to those observed in mice given INO-1001. The neuroprotective effect of *Parp* RNAi-mediated knockdown will be investigated in Chapter 6. PARP1 inhibitors are currently being used in cancer treatment, so they have been approved for human treatment. Some PARP1 inhibitors have been shown to cross the blood brain barrier (BBB) (Mikule and Wilcoxen 2015; Chabot et al. 2017), which would be beneficial if they were to be considered for HD

treatment. Repurposing PARP1 inhibitors could be a streamlined approach to treating HD, however more characterisation of the *Parp* knockdown and inhibition must occur prior to testing this. We investigate the efficacy of several PARP1 inhibitors in Chapter 6.

To summarise, the screen discovered that *Parp* knockdown rescued the locomotor deficit of the *HTT*128QFL flies, whereas *mre11* knockdown exacerbated the motor phenotype. It was decided that *parp* knockdown would be characterised in other HD fly models to assess its potential effect on the lifespan, Htt aggregation in the brain and neurodegeneration in the wing and brain. In the upcoming chapter these data will be reported and discussed.

5.4 Summary of main points

- *Parp* knockdown rescues the locomotor phenotype of the *HTT*128QFL expressing flies at 7 and 14 dpe
- *Mre11* knockdown worsens the locomotor deficit of the *HTT*128QFL expressing flies at 2, 4 and 7 dpe
- The effect of *Mre11* knockdown appears to be independent of *HTT* expression.
- The effect of *Parp* knockdown will be further characterised in *Drosophila* models of HD

6. Modelling the role of *Parp* inhibition in *Drosophila* models of Huntington's disease

6.1 Introduction

In the previous chapter it was established that reducing *Parp* expression in the *HTT*128QFL model of Huntington's disease (HD) rescued the locomotor deficit of the *HTT*128QFL flies. As previously described, PARP1 is an enzyme responsible for the detection of sites of DNA damage and recruiting the necessary components of the repair pathway to the site of damage (Amé et al. 2004). The process by which PARP1 recruits these components requires post translational modifications known as PARylations, which entail covalently adding poly-ADP ribose groups to itself and its targets. This process requires NAD+. While its main roles are in the detection of sites of DNA damage and recruitment of DNA repair proteins, it is also involved in chromatin structure modulation, inflammatory responses and response to heat shock (Krishnakumar and Kraus 2010; Ray Chaudhuri and Nussenzweig 2017; Sinha et al. 2021).

Pharmacological *PARP*1 inhibitors are currently being used in targeted cancer therapies (Chen 2011). In BRCA2 or XRCC1 deficient cancer cells, PARP1 inhibition leads to cell death by means of synthetic lethality (Bryant et al. 2005; Farmer et al. 2005; Ali et al. 2020; Diéras et al. 2020). In humans, *PARP*1/2 inhibition or BRCA2/XRCC1 deficiency alone won't cause cell death, but when these events occur in tandem it results in cell death. This targeted approach is extremely effective in treating an array of cancers ranging from ovarian cancer to glioblastoma (Gupta et al. 2019). *PARP*1/2 inhibitors work by "trapping" *PARP*1/2 to a site of damaged DNA which prevents it from translocating to other sites of DNA damage and there is the possibility that some *PARP* inhibitors are able to block the crucial NAD+ site (Murai et al. 2014; Pommier et al. 2016). This would prevent PARP from PARylating itself and its targets. This culminates in lethal levels of DNA damage and genome instability, and ultimately cell death (Rouleau et al. 2010).

In the context of HD, PARP inhibition has been shown to ameliorate HD-related phenotypes in the R6/2 mouse model (Cardinale et al. 2015; Paldino et al. 2017). They survived longer, had reduced *HTT* aggregation and even selective sparing of medium spiny neurons in the

brain, demonstrating its neuroprotective qualities. R6/2 mice treated with a PARP1/2 inhibitor also displayed ameliorated behavioural phenotypes with increased rotarod performance, reduced hindlimb clasping and extended lifespan. The results from the Screen chapter which showed *Parp* knockdown rescued the locomotor deficit of flies expressing mutant human *HTT* complemented Paldino et al.'s R6/2 mouse data. It was also shown that inhibitor treatment was not toxic to the WT mice. The researchers examined the effect of PARP inhibition on cAMP response element-binding protein (CREB) and CREB binding protein (CBP) in the striatum and found that in MSNs where CREB was upregulated, PARP1 inhibition had a positive effect on their survival (Cardinale et al. 2015; Paldino et al. 2017).

Paldino et al. were able to demonstrate that the potent PARP1 inhibitor, INO-1001, was crossing the mouse blood brain barrier as they were able to detect changes to the striatal health of the R6/2 mice with INO-1001 treatment, even though it was given to the mice by intraperitoneal injection. Using inhibitors that could cross the *Drosophila* blood brain barrier (BBB) was integral as all studies up to this point have used the pan-neuronal driver ELAV-Gal4. Some PARP1 inhibitors that cross the mammalian BBB are Niraparib and Veliparib (Mikule and Wilcoxen 2015; Chabot et al. 2017; Gupta et al. 2019; Gada et al. 2021). Both have been tested to treat brain metastases from various types of cancer with varying degrees of success, with one study using liquid chromatography mass-spectrometry to confirm the presence of the inhibitors in the brain and at the site of the brain tumour in a xenograft tumour mouse model (Gada et al. 2021).

The *Drosophila* BBB is structured slightly differently to mammalian BBB with one of the main differences being that the *Drosophila* BBB is exclusively formed by a matrix of glia, whereas the mammalian BBB is formed by endothelial cells (Limmer et al. 2014). The external layer of the *Drosophila* BBB is comprised of perineurial glial cells connected to each other by gap junctions. Underneath the perineurial glial cells are the lamellae of subperineurial cells that form a flat endothelial-like sheet covering the entire nervous system. While the subperineurial glia are a different cell-type to the mammalian endothelial cells, they do share similar properties, namely that they are both polarised. The subperineurial layer allows for the uptake of nutrients and has complex septate junctions that prevent paracellular transport. The septate junctions function similarly to the tight junctions that

form between the endothelial cells in the mammalian BBB (Hindle and Bainton 2014). *Drosophila* treated with levodopa (L-DOPA), a dopamine pre-cursor used to treat Parkinson's disease, show increased dopamine levels in dopaminergic neurons and alter the connectivity of 5-HT neurons projecting to the mushroom bodies in comparison to untreated *Drosophila* (Cichewicz et al. 2017; Niens et al. 2017). These flies were incubated on food containing L-DOPA, meaning they ingested the drug and it was able to yield neurochemical changes in the brain. While PARP1 inhibitors may not have the same molecular structure as L-DOPA, it is promising that a drug known to cross the mammalian BBB has been shown to impact neurochemistry in the *Drosophila* brain, thus implicating its ability to cross the *Drosophila* BBB.

This chapter explores the characterisation of genetically reducing *Parp* expression and pharmacologically reducing Parp activity in order to gain insights into its role in the disease and assess it as a viable treatment for HD.

6.1.1 Aims and hypothesis

I hypothesise that inhibiting *Parp* either genetically or pharmacologically will rescue other HD-related phenotypes in the fly.

Aim 1) Characterise the effect of *Parp* RNAi on lifespan, locomotion, neurodegeneration and *HTT* aggregation in HD fly models.

Aim 2) Examine the effect of pharmacological inhibitors on HTT aggregation and locomotion.

Aim 3) Assess whether we can model PARP1 inhibition in HD patient-derived iPSCs

6.1.2 Experimental design

In order to investigate the effects of *Parp* knockdown in *Drosophila* HD models it was necessary to establish whether the RNAi constructs were specifically targeting endogenous *Parp* levels. This was done by quantitative PCR (qPCR), with primers designed to exclusively bind to endogenous *Parp* cDNA. Primer design can be found in Chapter 2.3.3. Both *Parp* RNAi's were driven by the pan-neuronal driver ELAV-Gal4 and RNA was extracted from the heads.

$$\female \; \frac{ELAV-Gal4}{ELAV-Gal4}; \frac{Sp}{CyO}; \frac{+}{+} \quad \times \quad \male \; \frac{w^-}{Y}; \frac{Parp\ RNAi\ 2}{Parp\ RNAi\ 2}; \frac{+}{+}$$

$$\downarrow$$

$$\female \; \frac{ELAV-Gal4}{w^-}; \frac{Parp\ RNAi\ 2}{Sp}; \frac{+}{+}$$

$$\female \; \frac{ELAV-Gal4}{ELAV-Gal4}; \frac{Sp}{CyO}; \frac{+}{+} \quad \times \quad \male \; \frac{w^-}{Y}; \frac{+}{+}; \frac{Parp\ RNAi\ 3}{Parp\ RNAi\ 3}$$

$$\downarrow$$

$$\female \; \frac{ELAV-Gal4}{w^-}; \frac{+}{Sp}; \frac{Parp\ RNAi\ 3}{+}$$
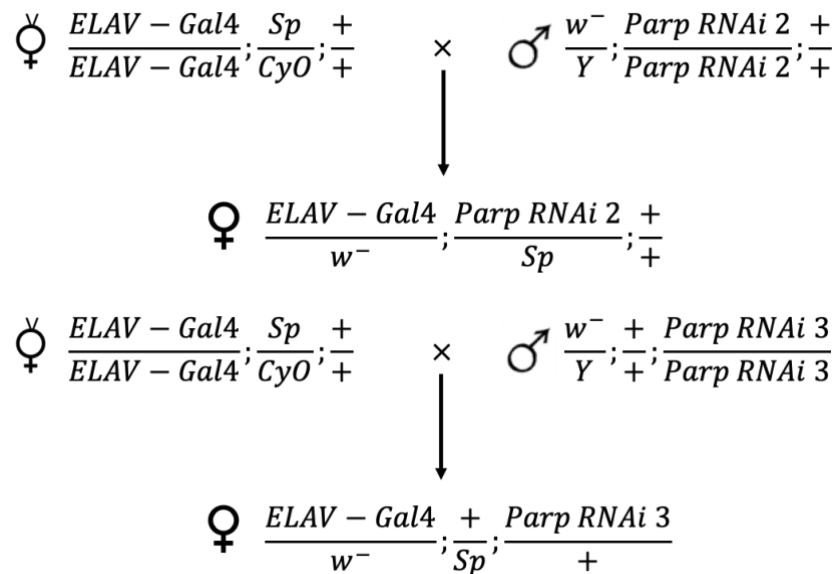
Crossing Scheme 6.1 - Pan-neuronal driver (ELAV-Gal4) carrying virgins are crossed with males carrying the *Parp* RNAi on the second and third chromosome. The resulting progeny express the *Parp* RNAi in all neurons.

The locomotor performance of the *HTT* expressing flies in both sets of *Parp* inhibition experiments was assessed as previously done in Chapters 3 and 5. The time points 2, 4, 7 and 14 dpe were used for the majority of experiments. Brains were dissected and prepared as outlined in Chapter 2.2.5, at 1, 7 and 14 dpe. Aggregate number and area calculations can be found in Chapter 2.6.2. These experiments were performed with the Cerulean-tagged *HTT* constructs, the crossing schemes can be found below.

$$\female\; \frac{ELAV-Gal4}{ELAV-Gal4}; \frac{Sp}{CyO}; \frac{+}{+} \qquad \times \qquad \male\; \frac{w^-}{Y}; \frac{UAS-HTT96QCer}{CyO}; \frac{Dr}{Tm3,Sb,e}$$

$$\male\; \frac{ELAV-Gal4}{Y}; \frac{UAS-HTT96QCer}{CyO}; \frac{+}{Tm3,Sb,e} \quad \times \female\; \frac{w^-}{w^-}; \frac{+}{+}; \frac{UAS-LacZ}{Tm6,Hu,e}$$

$$\female + \male\; \frac{ELAV-Gal4}{w^-/Y}; \frac{UAS-HTT96QCer}{+}; \frac{UAS-LacZ}{+}$$

$$\female\; \frac{ELAV-Gal4}{ELAV-Gal4}; \frac{Sp}{CyO}; \frac{+}{+} \qquad \times \qquad \male\; \frac{w^-}{Y}; \frac{UAS-HTT96QCer}{CyO}; \frac{Dr}{Tm3,Sb,e}$$

$$\male\; \frac{ELAV-Gal4}{Y}; \frac{UAS-HTT96QCer}{CyO}; \frac{+}{Tm3,Sb,e} \qquad \times \qquad \female\; \frac{w^-}{w^-}; \frac{UAS-Parp\;RNAi\;2}{UAS-Parp\;RNAi\;2}; \frac{+}{+}$$

$$\female + \male\; \frac{ELAV-Gal4}{w^-/Y}; \frac{UAS-HTT96QCer}{UAS-Parp\;RNAi\;2}; \frac{+}{+}$$
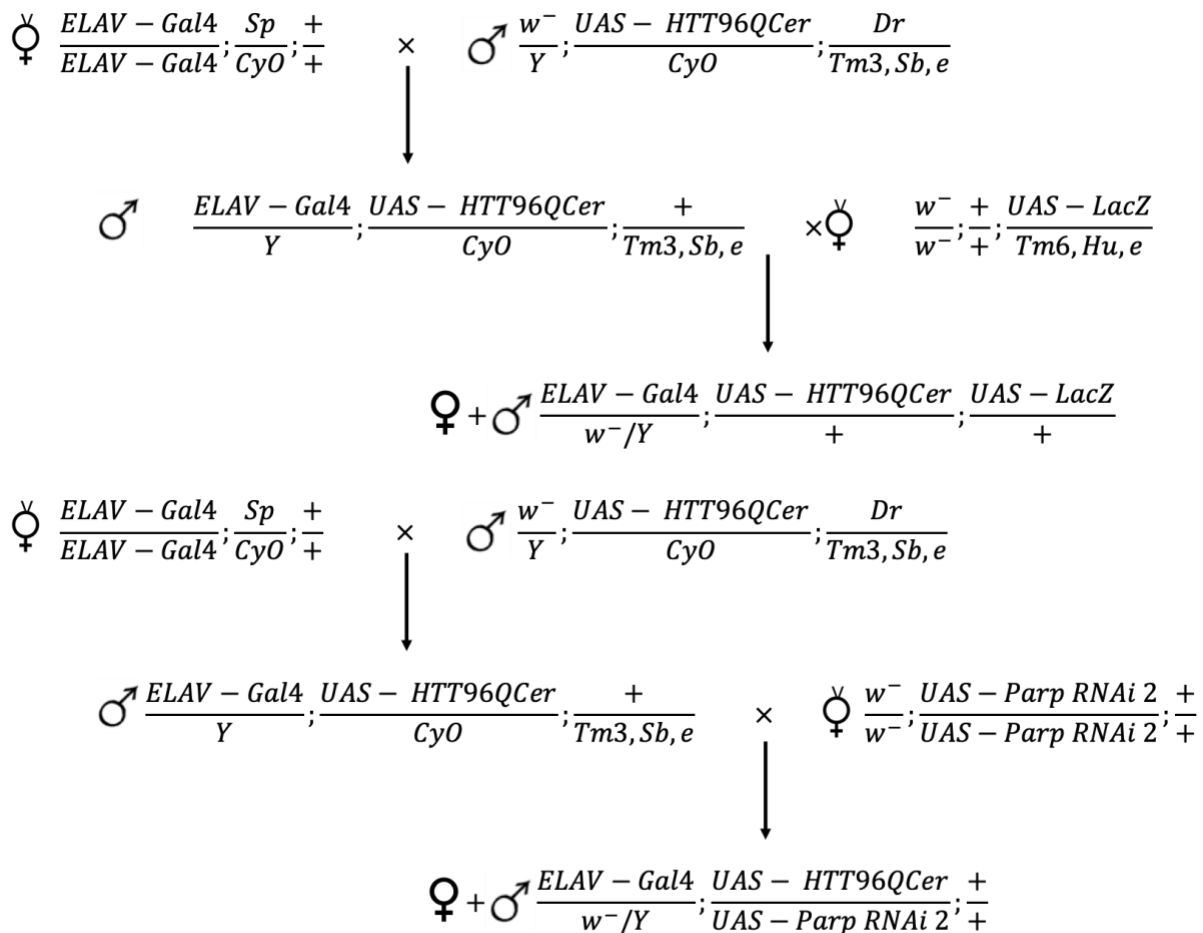
Crossing Scheme 6.2 - Pan-neuronal driver (ELAV-Gal4) carrying virgins were crossed with males carrying *HTT*96QCer construct. The progeny were crossed to flies either carrying the expression control LacZ or the *Parp* RNAi on the second chromosome. The progeny expressed *HTT*96QCer and LacZ or *Parp* RNAi 2 in all neurons.

For the PARP1 inhibitor experiments the inhibitors Niraparib and Veliparib were used at concentrations of 50 nM and 5 nM. DMSO was the vehicle control. Locomotor performance was measured by the RING Assay. HTT aggregate number and area were calculated. The crossing scheme for the experiment is included below.

$$\female\; \frac{ELAV-Gal4}{ELAV-Gal4}; \frac{Sp}{CyO}; \frac{+}{+} \qquad \times \qquad \male\; \frac{w^-}{Y}; \frac{UAS-HTT96QCer}{CyO}; \frac{+}{Tm3,Sb,e}$$

$$\female\; \frac{ELAV-Gal4}{w^-/Y}; \frac{UAS-HTT96QCer}{Sp}; \frac{+}{+}$$
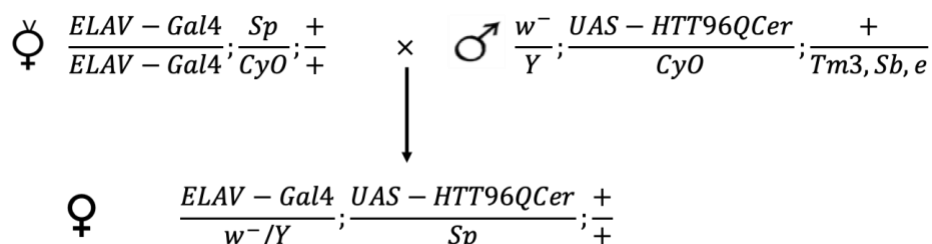
Crossing Scheme 6.3 - Pan-neuronal driver (ELAV-Gal4) carrying virgins were crossed with males carrying *HTT*96QCer construct. The progeny express *HTT*96QCer in all neurons.

Nuclear PAR and γ-H2AX levels were assessed in undifferentiated HD patient-derived iPSCs. They were treated with either E8 media, 1 mM KBrO3 or 10mM KBrO3 for 2 hours, then washed and fixed (4% PFA). Immunocytochemistry was performed with PAR antibody (Sigma Aldrich, MABE1016, 1:400), γ-H2AX antibody (Abcam, ab11174, 1:400) and Hoechst (Thermo Scientific, 62249, 1:12,000). See Chapter 2.4 for the details.

6.2 Results

6.2.1 Two independent *Parp* RNAi significantly reduce the expression of endogenous *Parp* RNA

Prior to investigating the role of *Parp* knockdown on previously established phenotypes, it was important to check that the expression of endogenous *Parp* RNA was significantly reduced. qPCR was performed to confirm this. The expression of endogenous Parp in the RNAi lines inserted on the 2nd chromosome (2) and 3rd chromosome (3) was compared to the RNA expression in the landing site control lines.
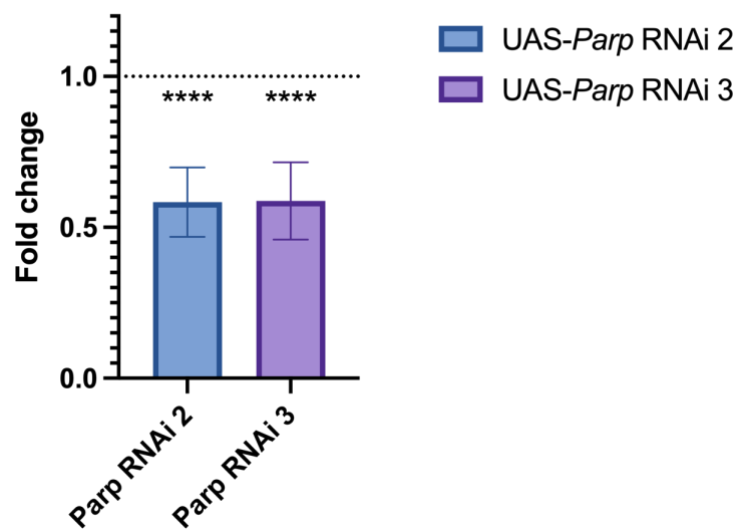
Figure 6.1 – Knockdown efficiency of endogenous *Parp* in fly heads expressing *Parp* RNAis. *Parp* RNAi lines were expressed by ELAV-Gal4 for 7 days. Total RNA from 8 fly heads was extracted and used to reverse transcribe cDNA. qPCR was performed to quantify *Parp* RNA levels normalised to the *rp49* reference mRNA. Values represent the level of normalised Parp mRNA in the *Parp* RNAi fly lines in comparison to their respective RNAi control line. Data are plotted as Mean ± SEM; pairwise fixed reallocation randomization test, **** $p < 0.0001$, (n = 3, n=1 the normalised *Parp* mRNA level from RNA extract from 8 fly heads).

Both *Parp* RNAi's used in this study were shown to significantly reduce the expression of *Parp* in the fly brain, when compared to RNAi control ($p < 0.0001$), (Figure 6.1). As both RNAi's significantly reduced the expression of *Parp* by 40%, either could be used for follow-up experiments. Endogenous Parp protein levels were not quantified.

6.2.2 *Parp* knockdown extends lifespans of *HTT* expressing flies

As the effect of *Parp* knockdown on the locomotor ability of the *HTT* expressing flies had already been established, it was important to assess whether other disease-like phenotypes would also be affected by neuronal *Parp* knockdown. Flies pan-neuronally expressing *HTT* with a pathological CAG repeat tract have been shown to have shorter lifespans than wild-type flies and flies expressing *HTT* with a non-pathological repeat (See Chapter 3). The effect of *Parp* knockdown was assessed in two different HD models. These experiments were performed with the *Parp* RNAi on the second chromosome (*Parp* RNAi 2) as it had previously been used in the screen (Chapter 5).
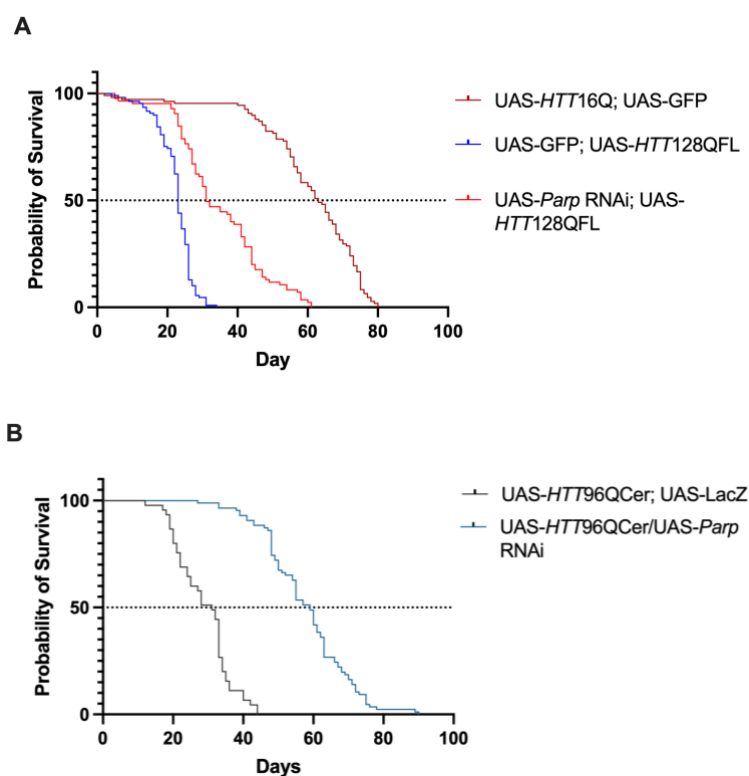
Figure 6.2 – Neuronal Parp knockdown lengthens lifespan of *HTT* expressing flies. (A) Kaplan Meier plot displaying the percentage survivorship of flies' pan-neuronally expressing full-length *HTT* constructs with and without *Parp* RNAi. *HTT*128QFL and *HTT*16QFL expressed UAS-GFP as an expression control. (*HTT*16QFL+UAS-GFP n=108, *HTT*128QFL+UAS-GFP n=109, *HTT*128QFL+*Parp* RNAi n=85). (B) Kaplan Meier plot displaying the percentage survivorship of flies' pan-neuronally expressing fluorescently tagged *HTT* constructs with and without *Parp* RNAi. *HTT*96QCer expressed UAS-LacZ as an expression control. (*HTT*96QCer+LacZ n=45, *HTT*96QCer+*Parp* RNAi n=86). Data are plotted as survival proportions at significant time points and statistical significance was calculated by Log-Rank Mantel-Cox test.

Parp knockdown in either the *HTT*128QFL or *HTT*96QCer lines led to a significant increase in median lifespan. The Log-Rank (Mantel-Cox) test showed the median lifespan of *HTT*128QFL

flies significantly extended from 23 days to 31 days (df = 1, p < 0.0001) when endogenous levels of *Parp* were knocked down (Figure 6.2A). This equates to a 34.8% increase in lifespan. The median lifespan of *HTT*96QCer flies also significantly extended from 31 days to 59 days (df = 1, p < 0.0001), (Figure 6.2B). This equated to a 90.3% increase in median lifespan, meaning the *Parp* RNAi nearly doubled the median lifespan of the *HTT*96QCer flies. The *Parp* RNAi in the *HTT*96QCer flies had a bigger effect on extending lifespan than it did in the *HTT*128QFL flies. This shows that *Parp* knockdown is having a significant rescuing effect on the lifespan of toxic hu-*HTT* expressing flies, regardless of the length of the CAG repeat and whether the construct is full-length, truncated or has a fluorescent tag.

The median lifespan of *HTT*16QFL expressing flies was significantly longer than the *HTT*128QFL+*Parp* RNAi flies (Figure 6.2A). At 63 days, the median lifespan of *HTT*16QFL flies was double the lifespan of the *HTT*128QFL+*Parp* RNAi flies. Even though the *Parp* RNAi may be significantly rescuing the lifespan phenotype of the *HTT*128QFL flies, it is by no means extending the lifespan to "healthy"/wild-type lengths. We show an example of the effect of *Parp* knockdown on the lifespan of flies expressing *HTT*16QFL later in this Chapter.

6.2.3 *Parp* knockdown rescues locomotor phenotype of other HD fly models

As knocking down *Parp* expression had an effect on the lifespan of *HTT*96QCer flies, it was important to assess whether *Parp* knockdown would also affect the locomotor ability of these flies. It has already been established that pan-neuronally expressing *HTT*96QCer yields a locomotor deficit in comparison to *HTT*25QCer expressing flies (see Chapter 3), hence I focused on the pathological *HTT*96QCer flies for the purpose of this *Parp* knockdown experiment.
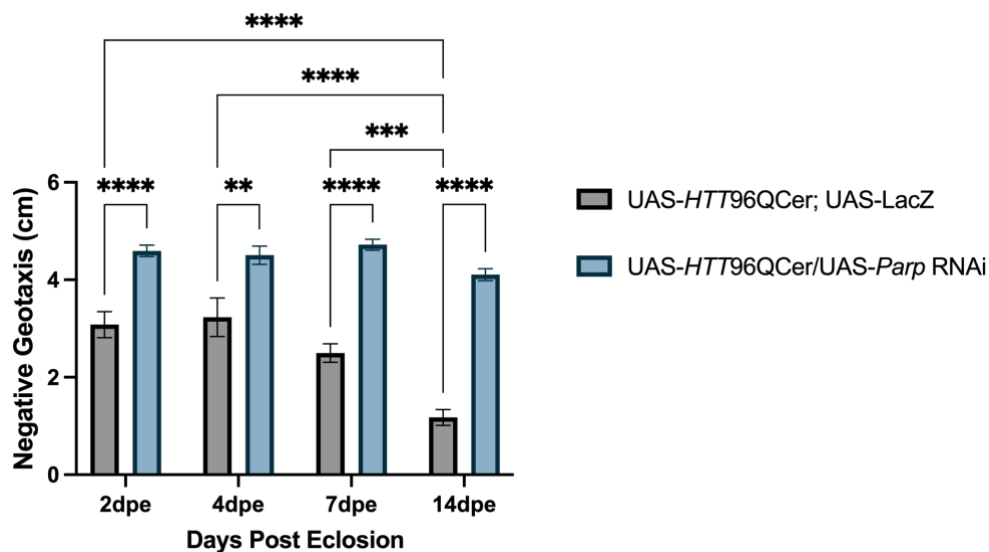
Figure 6.3 – Neuronal *Parp* knockdown rescues locomotor deficit of *HTT*96QCer expressing flies. The average distanced climbed by flies after 4 seconds at 2, 4, 7 and 14 dpe. The flies pan-neuronally expressed the *HTT* construct *HTT*96QCer with or without the *Parp* RNAi. The flies without the RNAi expressed LacZ as an expression control. (*HTT*96QCer;LacZ n=8-10, *HTT*96QCer/*Parp* RNAi n=9-11, n=1 the average distance climbed by flies in one vial averaged over 5 technical replicates). Data are plotted as Mean ± SEM and statistical significance was calculated by two-way ANOVA and Tukey's multiple comparisons tests. ns, p > 0.05; **, p = 0.001;, ***, p = 0.0005; ****, p < 0.0001.

It was clear that *Parp* knockdown was significantly rescuing the locomotor deficit of the *HTT*96QCer flies. two-way ANOVA confirmed that age ($F_{3,67}$ = 16.38, p < 0.0001) and genotype ($F_{1,67}$ = 194.2, p < 0.0001) significantly affected the locomotor ability of the flies (Figure 3), and that the interaction between age and genotype was significant ($F_{3,67}$ = 6.743, p = 0.0005). Post hoc Tukey's multiple comparisons tests confirmed that at 2 dpe *Parp* knockdown already had a statistically significant effect on the locomotor ability of the *HTT*96QCer flies, with the *Parp* RNAi flies climbing to 4.59 cm, whereas the *HTT*96QCer flies

without *Parp* knockdown only reached an average of 3.08 cm (p < 0.0001). At 4 dpe the *Parp* knockdown flies climbed to an average of 4.51 cm and *HTT*96QCer+LacZ flies only climbed to an average of 3.23 cm (p = 0.0015), however the climbing ability of the *HTT*96QCer+LacZ flies was not statistically different between 2 and 4 dpe (p = 0.9996). At 7 dpe the climbing ability of the *HTT*96QCer+LacZ started to decline, with flies only being able to climb an average of 2.50 cm. In comparison to this, the *Parp* RNAi flies climbed an average of 4.72 cm, which was significantly higher than the flies without *Parp* knockdown at this time point (p = 0.0001). This trend continued at 14 dpe with the climbing ability of the *HTT*96QCer+LacZ reducing further to an average of 1.18 cm which was significantly lower than the average distance climbed by the *Parp* RNAi flies at this time point (p < 0.0001).

As the flies aged, there continued to be a difference in their locomotor abilities, with the flies carrying the *Parp* RNAi continuing to climb better than those without. The locomotor ability of the *HTT*96QCer+LacZ flies significantly declined over time, specifically between 7 dpe and 14 dpe (p = 0.0004), whereas the *Parp* RNAi flies showed no significant difference in climbing ability as they aged. These findings show that knocking down *Parp* expression in the neurons of *HTT*96QCer flies rescues the locomotor deficit, similarly to that seen in the *HTT*128QFL model in Chapter 5.

6.2.4 *Parp* knockdown rescues HTT aggregate phenotype

One of the hallmarks of HD is the aggregation of huntingtin protein (HTT) in the striatum and other regions of the brain. It has already been established that neuronal expression of hu-*HTT* constructs with pathological repeats leads to high numbers of HTT aggregates within the *Drosophila* brain and peripheral neurons, from as young as 1 dpe (See Chapter 3.2.3 and 3.2.4). As *Parp* knockdown had lengthened the lifespan and rescued the locomotor phenotypes of two *Drosophila* models of HD with expanded CAG repeat tracts, it was imperative to investigate whether *Parp* knockdown would have an effect on the number of HTT aggregates in the *Drosophila* brain. Two RNAi's for *Parp* were used in this experiment to verify any effect observed on the HTT aggregates.

The flies expressing *HTT*25QCer;LacZ showed no evidence of HTT aggregate formation at 1, 7 and 14 dpe (Figure 6.4A-D), while aggregates were clearly observed in the brains of flies expressing *HTT*96QCer;LacZ (Figure 6.4E-H). At 1 dpe *HTT*96QCer;LacZ fly brains had an average of 224.1 aggregates per brain section at 63X magnification. The average aggregate number in orthogonal projections of brain sections from *HTT*96QCer;LacZ flies increased to 477.89 aggregates at 7 dpe, and increased further to an average of 943.7 aggregates at 14 dpe. Two-way ANOVA revealed that age ($F_{2, 63}$ = 17.80, p < 0.0001) and genotype ($F_{2, 63}$ = 105.0, p < 0.0001) had a statistically significant effect on the number of HTT aggregates in the brain sections. This was calculated using the macro described in Chapter 2.6.1. It also revealed that there was a statistically significant interaction between age and genotype ($F_{4, 63}$ = 13.85, p < 0.0001). Post hoc Tukey's multiple comparisons test showed that the increase in HTT aggregate number of the *HTT*96QCer;LacZ flies between 1 and 7dpe, and subsequently 7 and 14 dpe was statistically significant (1 to 7 dpe, p = 0.0035);(7 to 14 dpe, p <0.0001).

Both *Parp* RNAis exhibited significantly lower numbers of HTT aggregates in comparison to the *HTT*96QCer;LacZ flies (Figure 6.4Q). At 1 dpe *HTT*96QCer/*Parp* RNAi 2 flies exhibited an average of 10.8 aggregates which was 20 times lower than the number of aggregates observed in the *HTT*96QCer;LacZ flies (p = 0.0342). The flies carrying *Parp* RNAi 3 had even fewer aggregates, with an average of 1.7 aggregates at 1 dpe (p = 0.0100). There was no

significant difference between the average number of aggregates of both *Parp* RNAi flies at 1 dpe.

This difference in average aggregate number continued to increase as the flies aged. At 7 dpe the average number of aggregates in the selected brain region of the *HTT*96QCer/*Parp* RNAi 2 flies was 58.7 aggregates, and the average number of aggregates for *HTT*96QCer;*Parp* RNAi 3 flies was 25.7 aggregates, both of which were significantly lower than *HTT*96QCer;LacZ at 477.89 aggregates (*Parp* RNAi 2, p < 0.0001);(*Parp* RNAi 3, p <0.0001). At 14 dpe the average number of aggregates per brain region imaged of the *HTT*96QCer/*Parp* RNAi 2 flies increased to 83.8 aggregates and the *HTT*96QCer;*Parp* RNAi 3 fly brains increased slightly to an average of 29.0 aggregates counted per brain region. Both average aggregate numbers increased, but they were not statistically significant from their average aggregate number at 7 dpe. These were still both statistically significantly lower than the average number of aggregates for the *HTT*96QCer;LacZ flies at 14 dpe (*Parp* RNAi 2, p < 0.0001);(*Parp* RNAi 3, p <0.0001). These data show that knocking down endogenous *Parp* expression in the *HTT*96QCer fly model significantly reduces the number of HTT aggregates in the brain.

As the number of aggregates decreased when endogenous *Parp* levels were reduced, it was important to check whether the area of the aggregates differed between the genotypes (Figure 6.4R) as age-associated increases in HTT aggregate area have been observed in a Q175 mouse model (Carty et al. 2015). The average area of the aggregates for all genotypes increases with time. 2-way ANOVA revealed there was a statistically significant effect of age ($F_{2,57}$ = 17.03, p < 0.0001) and genotype ($F_{2,57}$ = 5.975, p = 0.0044) on the area of the aggregates and that the interaction was statistically significant ($F_{4,57}$ = 5.431, p = 0.0009). Post hoc Tukey's multiple comparisons test confirmed that flies carrying *Parp* RNAi 3 had average aggregate areas that were significantly smaller than *HTT*96QCer;LacZ flies at 1 dpe (p = 0.0038). However, as the flies aged between 1 and 14 dpe, the average area of the aggregates in the *Parp* RNAi 3 flies significantly increased (p = 0.0001). While the average aggregate area of flies carrying *Parp* RNAi 2 appeared smaller than that of the *HTT*96QCer;LacZ flies, it did not significantly differ from them at any time point. These data

show that while *Parp* knockdown may affect aggregate area early on in the lifespan of the *HTT*96QCer flies, it does not affect the average area of the aggregates as the flies age.

HTT96QCer;
Parp RNAi 3   HTT96QCer/
Parp RNAi 2   HTT96QCer;LacZ   HTT25QCer;LacZ

10X   1dpe   63X   10X   7dpe   63X

138
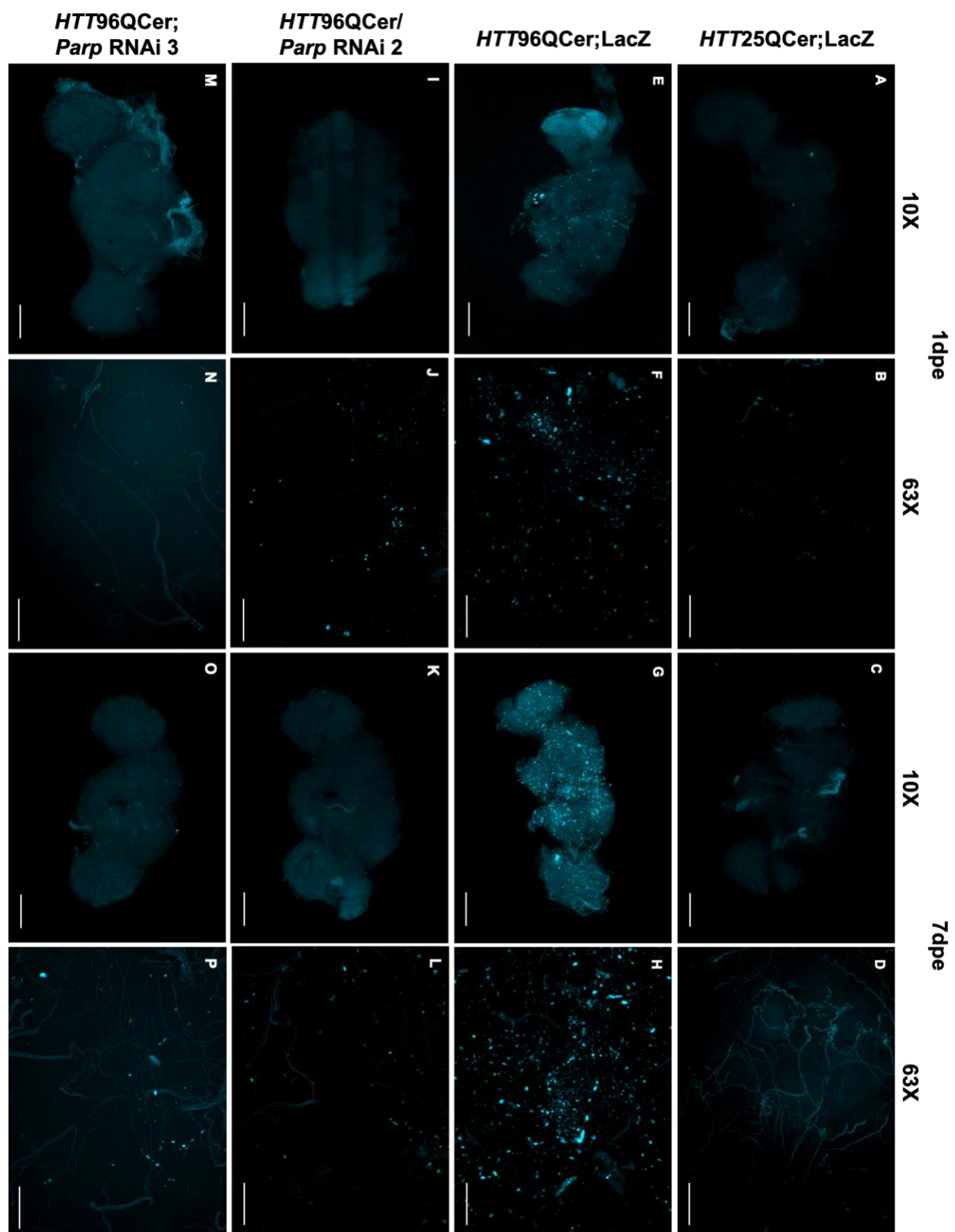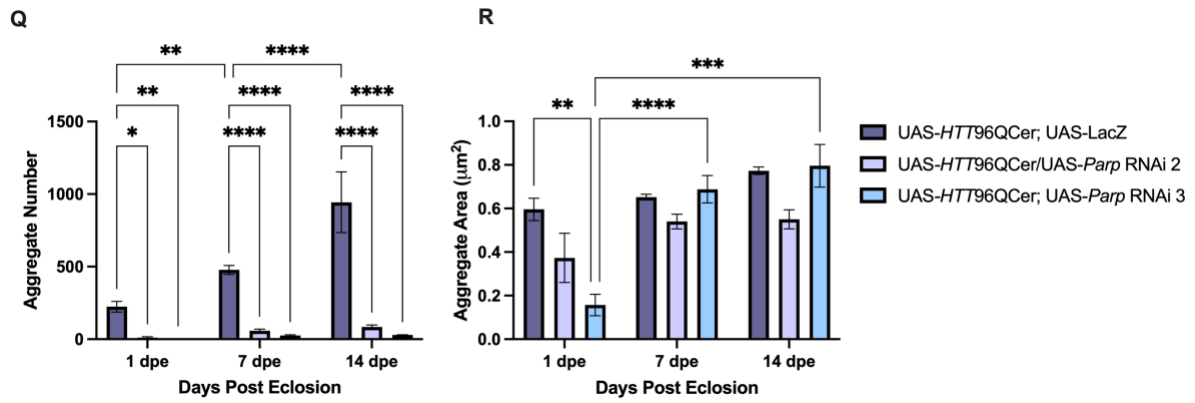
Figure 6.4 - *Parp* knockdown significantly reduces number of *HTT* aggregates in *Drosophila* brains. (A-D) Orthogonal projections of *Drosophila* brains from flies expressing *HTT*25QCer+LacZ at 1 dpe and 7 dpe at 10X and 63X magnification. (E-H) Orthogonal projections of *Drosophila* brains from flies expressing *HTT*96QCer+LacZ at 1 dpe and 7 dpe at 10X and 63X magnification. (I-L) Orthogonal projections of *Drosophila* brains from flies expressing *HTT*96QCer+*Parp* RNAi (II) at 1 dpe and 7 dpe at 10X and 63X magnification. (M-P) Orthogonal projections of Drosophila brains from flies expressing *HTT*96QCer+*Parp* RNAi (III) at 1 dpe and 7 dpe at 10X and 63X magnification. (Q) Average number of HTT aggregates per orthogonal projection of the fly brain at 63X magnification. (R) Average area of the HTT aggregates counted per orthogonal projection. (*HTT*96QCer;LacZ n=5-9, *HTT*96QCer/*Parp* RNAi n=8-10, *HTT*96QCer;*Parp* RNAi n=2-11, n=1 the average from two orthogonal projections of one fly brain. Data are plotted as Mean ± SEM and statistical significance was calculated by two-way ANOVA and Tukey's multiple comparisons test. Scale bar 100 μm at 10X, 20μm at 63X. ns, $p > 0.05$; *, $p = 0.035$; **, $p = 0.01\text{-}0.0038$; ***, $p = 0.0009$; ****, $p < 0.0001$.

6.2.5 *Parp* knockdown does not affect neurodegeneration in the wing

In Chapter 3, a new assay was created to assess the effect of expressing toxic *HTT* on the viability of sensory neurons in the wing. It was found that expressing mutant *HTT* with an expanded repeat tract reduced the fluorescent signal in the cell body, seemingly showing signs of neurodegeneration, without axonal degeneration. As *Parp* knockdown had rescued multiple phenotypes it was important to assess whether *Parp* knockdown would affect neurodegeneration in the wing. As 21 dpe was the time point where there was the most significant effect on the number of cell bodies and fluorescence, it was the time point picked to measure the effect of *Parp* RNAi on neurodegeneration in the wing in these experiments.
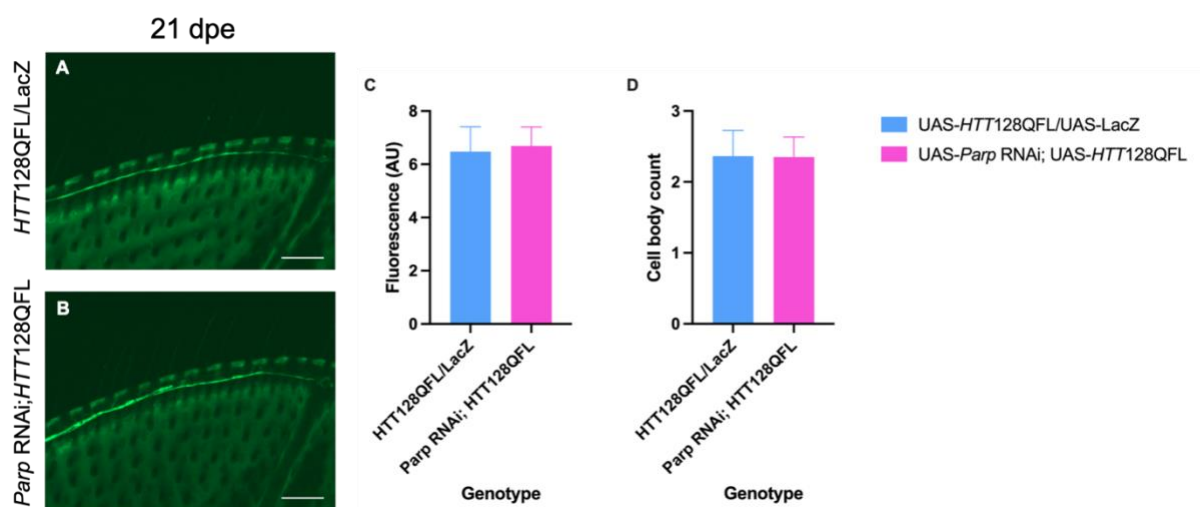
Figure 6.5 - *Parp* knockdown does not alter cell body fluorescence and number of *HTT*128QFL L1 vein neurons. (A) A representative image of the glutamatergic neurons at the tip of the L1 vein from a *HTT*128QFL/LacZ fly at 21dpe. (B) A representative image of the glutamatergic neurons at the tip of the L1 vein from a *Parp* RNAi; *HTT*128QFL fly at 21dpe. (C) Average fluorescence of the cell bodies of the glutamatergic neurons at the tip of the L1 vein. (D) Average cell body number counted at the tip of the L1 vein. (*HTT*128QFL/LacZ n=11, *Parp* RNAi;*HTT*128QFL n=20, n=1 one wing). Data are plotted as Mean $\pm$ SEM and statistical significance was calculated by unpaired t test. Scale bar = 20 μm.

There was no significant difference in the cell body number and cell body fluorescence of *HTT*128QFL flies with and without *Parp* knockdown (Figure 6.5A-B). Unpaired t tests confirmed that *Parp* expression did not significantly affect the average cell body fluorescence (t_{29} = 0.1755, p = 0.8619) and average cell body number (t_{29} = 0.02913, p = 0.9770) of neurons in the wings of *HTT*128QFL flies at 21 dpe (Figure 6.5C-D). These data

show that *Parp* knockdown does not rescue the viability of peripheral cell bodies of neurons expressing pathological hu*HTT*.

6.2.6 *Parp* knockdown does not affect lifespan, but improves locomotor performance in *HTT*16QFL flies

Previously, we showed that when *Parp* was knocked down pan-neuronally in WT flies there was a reduction in the locomotor performance and median lifespan of the *Parp* knockdown flies in comparison to control (Chapter 4). We assessed whether knocking down *Parp* would have a similar effect in the *HTT*16QFL flies, that have a non-pathological CAG repeat. In these experiments LacZ and GFP were expressed in conjunction with *HTT*16QFL to act as expression controls for the *Parp* RNAi line.
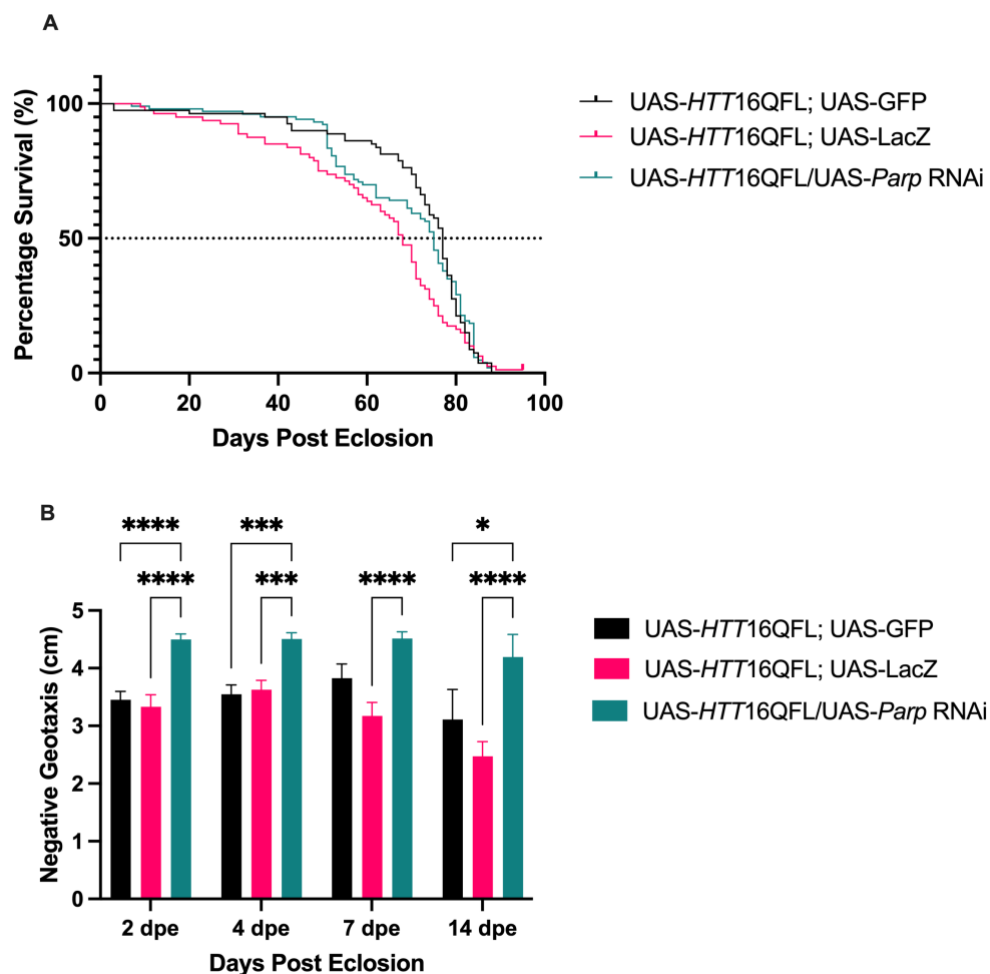
Figure 6.6 - *Parp* knockdown does not inhibit lifespan and locomotion of *HTT*16QFL flies. (A) Kaplan Meier plot displaying the percentage survivorship of flies' pan-neuronally expressing full-length healthy *HTT* constructs with and without *Parp* RNAi. *HTT*16QFL expressed UAS-GFP and UAS-LacZ as expression controls. Data are plotted as survival proportions at significant time points and statistical significance was calculated by Log-Rank Mantel-Cox test. (B) The average distanced climbed by flies after 4 seconds at 2, 4, 7 and 14 dpe. The flies pan-neuronally expressed the *HTT* construct *HTT*16QFL with or without the *Parp* RNAi. The flies without the RNAi expressed LacZ or GFP as an expression control. (*HTT*16QFL;UAS-GFP n=3-9, *HTT*16QFL;UAS-LacZ n=4-

Knocking down *Parp* expression did not conclusively affect the lifespan of the *HTT*16QFL expressing flies (Figure 6.6A). The median lifespan of the *HTT*16QFL/*Parp* RNAi flies was 75 days which was only 2 days lower than the median lifespan of the *HTT*16QFL;UAS-GFP flies at 77 days. Log-Rank Mantel-Cox test revealed the difference in median lifespan was not statistically significant (Figure 6.6A). However, the median lifespan of the flies expressing *HTT*16QFL;UAS-LacZ was significantly lower than the other two genotypes with a median lifespan of 68 days (df = 2, p = 0.0393). While this difference in lifespan was significant, 68 days is still an above average lifespan for *Drosophila melanogaster* (Linford et al. 2013). When compared to the *HTT*16QFL;UAS-GFP flies, *Parp* knockdown did not have a significant effect on the lifespan of the *HTT*16QFL flies. However, when compared to the other control line (*HTT*16QFL;UAS-LacZ), *Parp* knockdown was shown to significantly extend the lifespan of the *HTT*16QFL expressing flies. These results show that *Parp* knockdown does not worsen the lifespan of *HTT*16QFL expressing flies, and may even extend the lifespan depending on the control line used.

The climbing ability of the *HTT*16QFL flies was significantly affected by *Parp* knockdown (Figure 6.6B). Two-way ANOVA revealed that both age ($F_{3,76}$ = 4.538, p = 0.0056) and genotype ($F_{2,76}$ = 47.30, p < 0.0001) significantly affected the locomotor function of the *HTT*16QFL expressing flies. Post hoc Tukey's multiple comparisons tests confirmed statistically significant increases in locomotor function when *Parp* expression was reduced. At 2 dpe *HTT*16QFL/*Parp* RNAi flies climbed significantly higher than *HTT*16QFL;UAS-GFP (p < 0.0001) and *HTT*16QFL;UAS-LacZ flies (p < 0.0001), reach an average distance climbed of 4.50 cm in comparison to 3.45 cm and 3.33 cm respectively. This trend continued at 4 dpe, but at 7 dpe the difference between *HTT*16QFL/*Parp* RNAi flies and *HTT*16QFL;UAS-GFP flies was not statistically significant (p = 0.0609) even though *HTT*16QFL/*Parp* RNAi flies climbed an average of 0.69 cm higher than *HTT*16QFL;UAS-GFP flies. However, at 14 dpe the statistical significance was restored. *HTT*16QFL/*Parp* RNAi flies climbed to an average of 4.19 cm, whereas *HTT*16QFL;UAS-GFP climbed to an average of 3.11 cm (p = 0.0148) and

*HTT*16QFL;UAS-LacZ climbed to an average of 2.47 cm (p < 0.0001). Interestingly, even though there was a difference of 0.64 cm in the average distance climbed by *HTT*16QFL;UAS-GFP and *HTT*16QFL;UAS-LacZ, this was not statistically significant (p = 0.2178). These results show that *Parp* knockdown can increase the locomotor function of flies carrying full-length hu*HTT* with a non-pathological repeat.

6.2.7 *Parp* levels are significantly reduced in *HTT*16QFL flies, but not in *HTT*128QFL flies

We wanted to establish if endogenous *Parp* RNA levels were different in the *HTT*128QFL model, in comparison to control, to see if that might explain why the *Parp* RNAi elicited its effects. Hyperactivation of *Parp* is associated with cell death, so one theory was that *PARP* might have been transcriptionally upregulated in the *HTT*128QFL model and the RNAi merely brought the endogenous *Parp* levels down to a healthy/physiological level which rescued the lifespan and locomotor deficits. A qPCR assessing the endogenous *Parp* levels in *HTT*128QFL and *HTT*16QFL 7-day old mature fly brains was performed to test this theory.
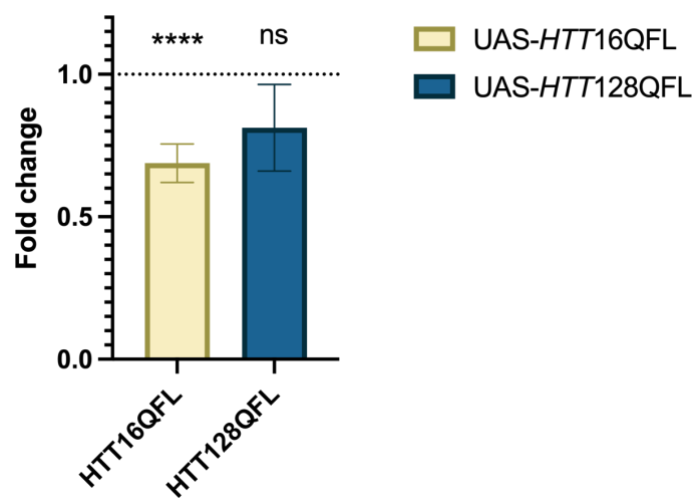
Figure 6.7 - Endogenous *Parp* expression is significantly reduced in *HTT*16QFL flies, but not in *HTT*128QFL flies. UAS-*HTT*16QFL and UAS-*HTT*128QFL were expressed by ELAV-Gal4 for 7 days. Total RNA from 8 fly heads was extracted and used to reverse transcribe cDNA. qPCR was performed to quantify *Parp* RNA levels normalised to the *rp49* reference mRNA. Values represent the level of normalised *Parp* mRNA in the HD fly lines in comparison to ELAV-Gal4 control. Data are plotted as Mean $\pm$ SEM; pairwise fixed reallocation randomization test, **** $p < 0.0001$, ns = not significant, (n = 3, n=1 the normalised *Parp* mRNA level from RNA extract from 8 fly heads).

It was apparent that flies expressing *HTT*16QFL pan-neuronally had lower levels of *Parp* expression than ELAV-Gal4 control flies and the *HTT*128QFL flies (Figure 6.7). *Parp* mRNA expression was significantly reduced by 32% ($p < 0.0001$), in comparison to the levels observed in the ELAV-Gal4 control flies. While there appeared to be a slight reduction in the expression of *Parp* in the *HTT*128QFL flies of about 20% in comparison to control, it was not statistically significant ($p = 0.1667$). *Parp* mRNA expression does not differ between flies expressing pathological huHTT and control, which suggests that Parp may be eliciting its

effects at a protein level. When these results are combined with the lifespan and locomotor data from Chapter 3 and Figure 6.6, it demonstrates that a reduced level of *Parp* expression does not inhibit lifespan and locomotion of flies expressing hu*HTT* with a non-pathological CAG repeat. This is in contrast to the findings from Chapter 5 where *Parp* RNAi expression significantly reduced the lifespan and locomotor function in comparison to control. Perhaps the expression of human *HTT* modulates the potential toxicity of reduced neuronal Parp expression.

6.2.8 PARP1 inhibitor treatment rescues locomotor phenotype

After showing that genetically knocking down *Parp* expression rescued several disease-related phenotypes in the HD fly models, we wanted to see if similar effects could be replicated using pharmacological PARP1 inhibitors. The *HTT*96QCer fly model was chosen for these experiments as locomotor and HTT aggregate data could be collected. The flies were incubated with food treated with the PARP1 inhibitors Niraparib and Veliparib, or DMSO (vehicle) throughout their entire lifespan, and their locomotor function was assayed at 2, 4 and 7 dpe.
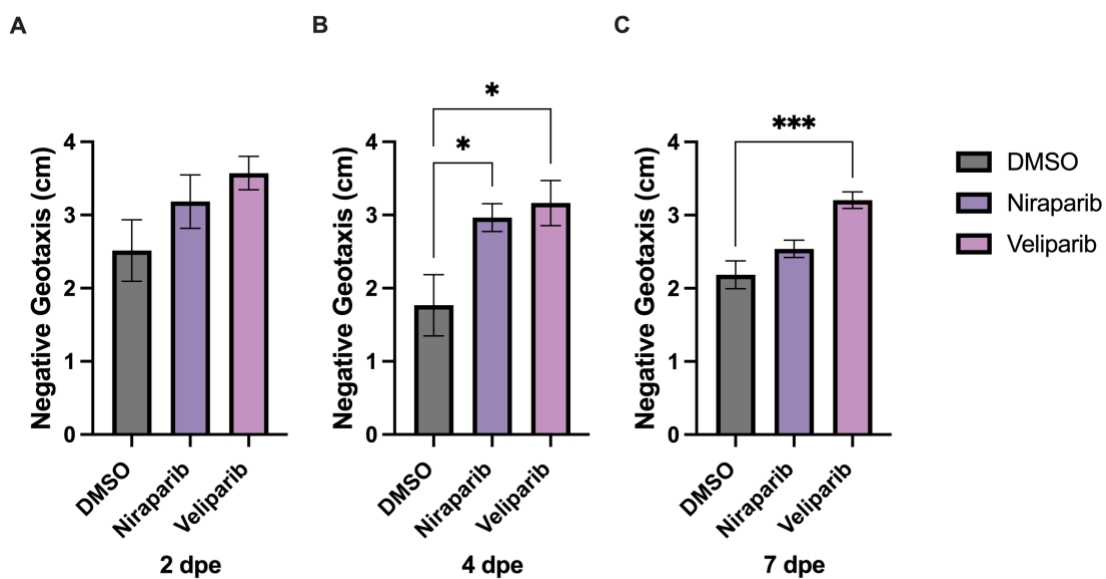
Figure 6.8 – PARP1 inhibitor treatment rescues locomotor phenotype of *HTT*96QFL flies. (A-C) The average distance climbed by flies expressing *HTT*96QFL at 2, 4 and 7 dpe. Flies were treated with either DMSO (vehicle), 50 nM Niraparib or 5 nM Veliparib. (DMSO n= 2-3, Niraparib n=5-6, Veliparib n=4-5, n=1 the average distance climbed by flies in one vial averaged over 5 technical replicates). Data are plotted as Mean $\pm$ SEM and statistical significance was calculated by one-way ANOVA and Dunnett's multiple comparisons tests. ns, p > 0.05; *, p = 0.0438-0.0262; ***, p = 0.0008.

Both PARP1 inhibitor treatments significantly increased the average climbing distance of the flies (Figure 6.8). At 4 dpe and 7 dpe, one-way ANOVA's confirmed that the PARP1 inhibitor treatment significantly affected the climbing ability of the *HTT*96QCer flies at 4 dpe ($F_{2,8}$ = 5.009, p = 0.0389) and 7 dpe ($F_{2,11}$ = 13.76, p = 0.0010). Post hoc Dunnett's multiple comparisons test revealed that at 4 dpe, Niraparib (p = 0.0438) and Veliparib (p = 0.0262) significantly increased the locomotor performance of the *HTT*96QFL flies, in comparison to DMSO control. At 7 dpe Veliparib treated flies climbed an average of 3.21cm which was significantly higher than the climbing ability of the DMSO treated flies at 2.18 cm (p =

0.0008). These data show that PARP1 inhibitor treatment rescues the locomotor deficit of *HTT*96QCer flies.

6.2.9 PARP1 inhibitors do not change the number of Htt aggregates in the brain

The benefit of using the *HTT*96QCer model for the PARP1 inhibitor experiment was the ability to study multiple phenotypes that the inhibitors could be affecting. The impact of the *Parp* RNAi's on the HTT aggregate number in the *HTT*96QCer model was interesting, so it was key that we assessed whether the HTT aggregates were affected by the PARP1 inhibitors.
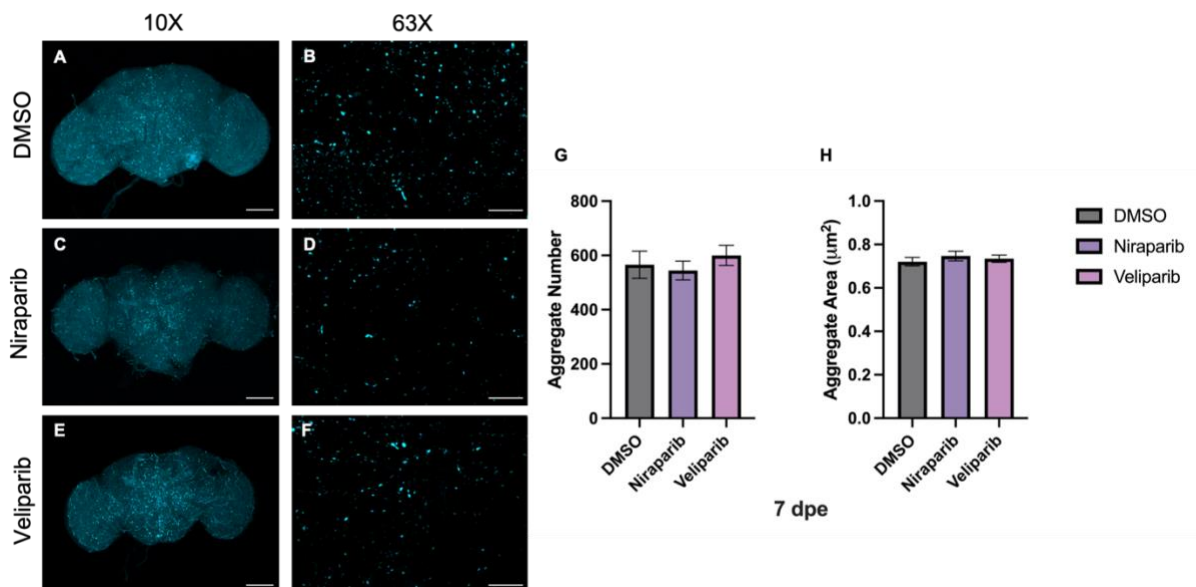
Figure 6.9 – HTT aggregate number and area do not change with PARP1 inhibitor treatment at 7 dpe. (A-F) Orthogonal projections of *Drosophila* brains from flies expressing *HTT*96QCer at 7 dpe at 10X and 63X magnification. The flies had been treated with DMSO (vehicle), Niraparib or Veliparib. (G) Average number of aggregates per orthogonal projection of the fly brain at 63X magnification. (H) Average area of the aggregates counted per orthogonal projection at 63X. (DMSO n=9, Niraparib n=17, Veliparib n=17, n=1 two orthogonal projections from each side of the central brain of one fly). Data were plotted as Mean ± SEM and statistical significance was calculated by one-way ANOVA and Tukey's multiple comparisons tests. Scale bar 100μm at 10X, 20 μm at 63X.

There was no significant effect of the PARP1 inhibitor treatment on the number of aggregates or the area of the aggregates that formed in the fly brain at 7 dpe (Figure 6.9A-F). The average number of HTT aggregates in a section of the fly brain (at 63X magnification) from a fly treated with DMSO (vehicle) was 565.9. The average number of HTT aggregates from Niraparib treated flies was 544.4 and the average number of HTT aggregates from Veliparib treated flies was 599.9. One-way ANOVA was performed to assess whether the PARP1 inhibitor treatment would have a statistically significant effect on the number of HTT aggregates at 7dpe, and there were not any differences ($F_{2,40}$ = 0.6026, p = 0.5523), (Figure

6.9G). The area of the HTT aggregates was also extremely similar with vehicle treated flies having aggregates with an average of 0.72 μm^2, Niraparib treated flies having an average aggregate area of 0.75 μm^2 and Veliparib treated flies having an average aggregate area of 0.74 μm^2. A one-way ANOVA demonstrated that PARP1 inhibitor treatment did not have a significant effect on the area of the HTT aggregates ($F_{2,40}$ = 0.6026, p = 0.5523), (Figure 6.9H). These results show that PARP1 inhibitor treatment did not affect the size or number of HTT aggregates despite the neuroprotective effect on motor phenotypes.
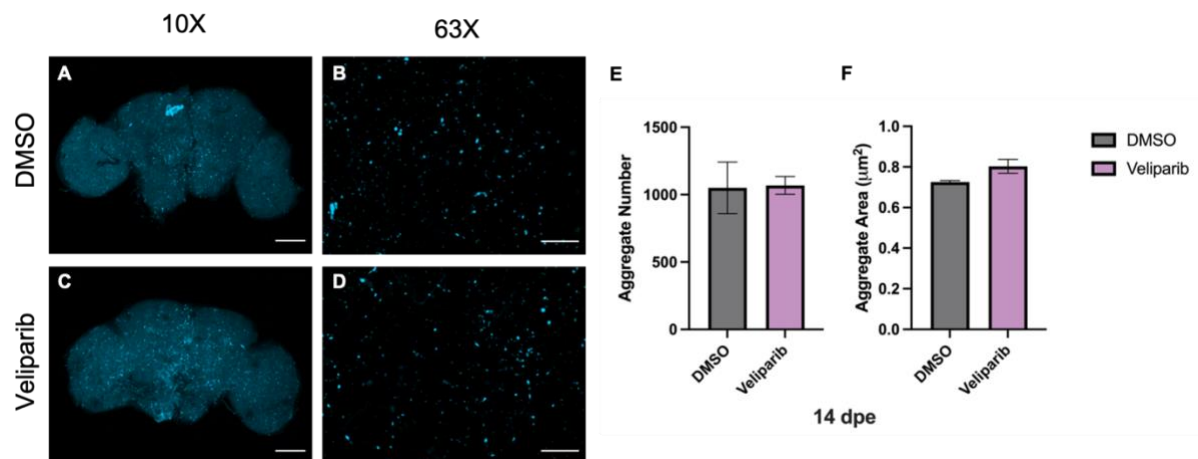
Figure 6.10 – HTT aggregate number and area do not change with Veliparib treatment at 14 dpe. (A-D) Orthogonal projections of *Drosophila* brains from flies expressing *HTT*96QCer at 14 dpe at 10X and 63X magnification. The flies had been treated with DMSO (vehicle) or Veliparib. (E) Average number of aggregates per orthogonal projection of the fly brain at 63X magnification. (F) Average area of the aggregates counted per orthogonal projection at 63X. (DMSO n=4, Veliparib n=4, n=1 two orthogonal projections from each side of the central brain of one fly). Data were plotted as Mean ± SEM and statistical significance was calculated by unpaired t tests. Scale bar 100 μm at 10X, 20μm at 63X.

There was no significant difference in between the HTT aggregate number and area of DMSO and Veliparib treated at 14 dpe (Figure 6.10A-D). The average number of HTT aggregates in the DMSO treated flies was 1051 and the average number of HTT aggregates in the Veliparib treated flies was 1069. The mean aggregate area for the vehicle treated flies was 0.73 μm^2 and for the Veliparib treated flies it was 0.80 μm^2. An unpaired t test revealed PARP1 inhibitor treatment had no statistically significant effect on the aggregate number ($t_{3.70}$ = 0.08917, p = 0.9336) or the aggregate area ($t_{3.25}$ = 2.210, p = 0.1070). This data confirms that Veliparib treatment at 5 nM does not ameliorate the size and number of HTT aggregates.

6.2.10 Nuclear γ-H2AX intensity of HD-patient derived iPSCs increases with $KBrO_3$ treatment, but nuclear PAR intensity does not differ

It was important to assess whether the beneficial impact of *Parp* knockdown that was observed in *Drosophila*, could be emulated in other disease models. Hence, I assessed PARP1 activity in HD patient-derived iPSCs and controls. These cells were derived from fibroblasts of a HD patient whose pathogenic *HTT* allele contained a CAG repeat tract of 109 CAGs (11b11) (Donaldson 2019). An isogenic control was created by reducing the CAG tract to a length of 22 CAGs by CRISPR processing (2h1) (Donaldson 2019). Previously these cells have been differentiated into neurons and used to model CAG repeat instability, but in these experiments we used undifferentiated iPSCs. The cells were exposed to oxidative stress to induce DNA damage which would theoretically activate PARP1. This was done by treating the iPSCs with potassium bromate ($KBrO_3$) to increase reactive oxygen species (ROS) levels. PAR and γ-H2AX antibodies were used to indicate the presence of PARP1 activity and DNA DSBs, respectively.

Average nuclear PAR intensity of the 2h1 cells was slightly higher than the nuclear PAR intensity in the 11b11 cells which seemed most apparent in the E8 treated condition with no $KBrO_3$ present (Figure 6.11 A-D, M-P, Y). A two-way ANOVA revealed genotype had a statistically significant effect on the nuclear PAR fluorescence ($F_{1,58}$ = 5.961, p = 0.0177), however $KBrO_3$ treatment did not and the interaction between $KBrO_3$ treatment and genotype was also not statistically significant. Post hoc Tukey's multiple comparison tests did not find any relevant significant differences. Nuclear γ-H2AX intensity clearly increased with the 10 mM $KBrO_3$ treatment in both genotypes. Initially the γ-H2AX signal was only saturated in specific cells, seemingly cells undergoing replication as the Hoechst signal was lacking in those sites. However, with the $KBrO_3$ treatment the γ-H2AX signal became more diffuse throughout the colonies for both genotypes. Two-way ANOVA showed that $KBrO_3$ treatment had a statistically significant effect on the nuclear γ-H2AX intensity ($F_{2,58}$ = 104.5, p < 0.0001), but genotype didn't and there was not a statistically significant interaction between treatment and genotype. Post hoc Tukey's multiple comparisons tests showed a significant upregulation in nuclear γ-H2AX signal for both cell lines when they were treated with 10 mM $KBrO_3$ in comparison to 1 mM $KBrO_3$ (2h1, p < 0.0001); (11b11, p < 0.0001).

However, there was no significant difference in the nuclear γ-H2AX intensity between E8 media treated cells and 1 mM KBrO$_3$ treated cells. These results show evidence that high levels of DSBs are occurring in response to KBrO$_3$ treatment at higher concentrations, but the lack of change in nuclear PAR levels indicates PARP1 activity is not increased. While PARP1 activity is most commonly associated with SSBs, it does have a role in recruiting proteins to sites of DSBs (i.e. MRE11). In the case of these undifferentiated HD-patient derived cells it could be that PARP1 does not appear to play a significant role in recruiting the DSB repair machinery to the sites of DNA damage.
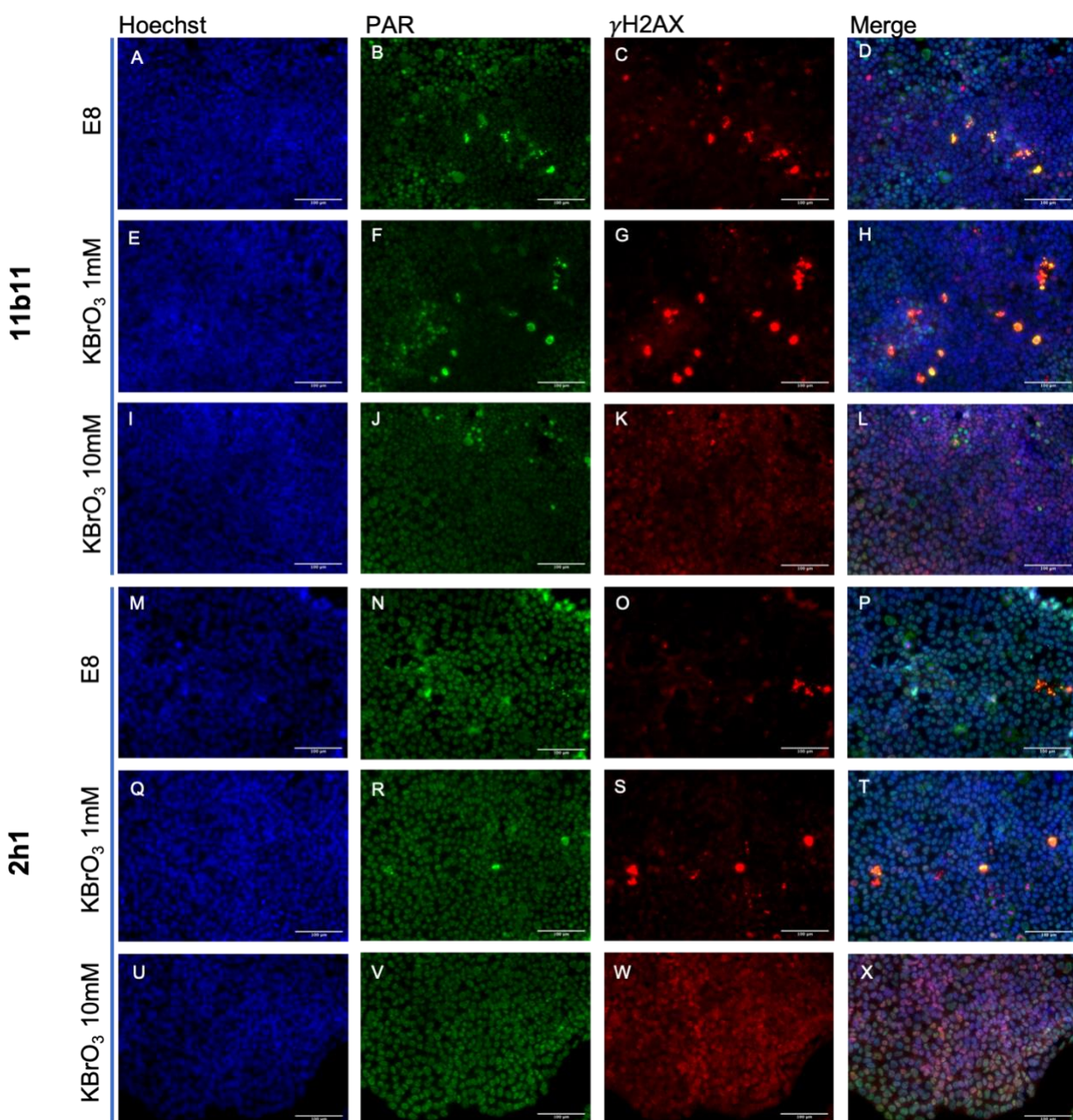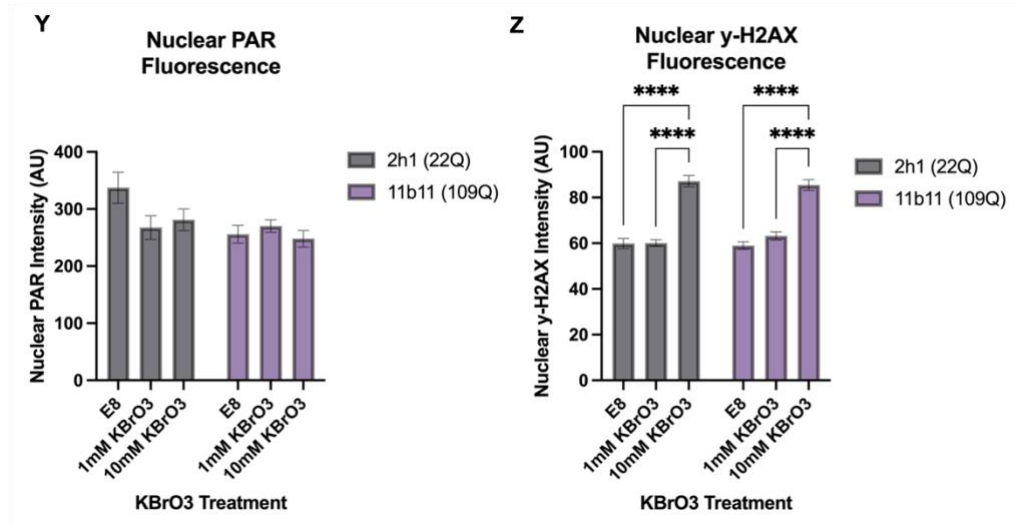
Figure 6.11 – Nuclear PAR fluorescence does not increase with KBrO$_3$ treatment, but γ-H2AX does. iPSCs were derived from a HD patient. 11b11 cells expressed a pathological *HTT* allele containing 109 CAGs. 2h1 cells were an isogenic line whereby a toxic number of CAGs had been removed to yield a *HTT* allele containing 22 CAGs. (A-L) Representative images of PAR and γ-H2AX immunofluorescence in 11b11 undifferentiated iPSCs expressing HTT109Q. They were subjected to three different treatments, no KBrO$_3$ (E8 media), 1 mM KBrO$_3$ and 10 mM KBrO$_3$. Images were taken at 20X magnification and then zoomed in. Scale bar indicates 100 μm. (M-X) Representative images of PAR and γ-H2AX immunofluorescence in 2h1 undifferentiated iPSCs expressing HTT22Q. They were subjected to three different treatments, no KBrO$_3$ (E8 media), 1 mM KBrO$_3$ and 10 mM KBrO$_3$. Images were taken at 20X magnification and then zoomed in. Scale bar indicates 100 μm. (Y) Average nuclear PAR fluorescence in a colony of iPSCs. (Z) Average nuclear γ-H2AX fluorescence in a colony of iPSCs.

6.3 Discussion

Reducing Parp activity by RNAi or pharmacological inhibition ameliorates HD-related phenotypes in *Drosophila* models of HD. Lifespan, locomotion and HTT aggregation were all significantly impacted by reducing *Parp* activity. The results reflect the PARP1 inhibitor work that was performed in the R6/2 mouse model by Paldino et al. and reinforce the idea that PARP1 inhibitors could be used to treat some symptoms of HD (Cardinale et al. 2015; Paldino et al. 2017; Paldino et al. 2020). However, it is still unclear how PARP1 inhibition mediated the phenotypic changes. The conservation of the protective effect of PARP1 inhibition between mice and flies opens the door for future mechanistic experiments to better understand disease pathways.

Parp RNAi

Fly model	Median Lifespan	Locomotion	Htt Aggregation	Neurodegeneration
HTT16QFL	No change	Significantly improves	-	-
HTT128QFL	Significantly improves	Significantly improves	-	No change
HTT96QCer	Significantly improves	Significantly improves	Significantly reduces	-
Parp RNAi 2; LacZ	Significant decline	Significant decline	-	-

Table 6.1 – A summary of the phenotypic changes when *Parp* expression is knocked down by RNAi in the HD fly models.

Parp knockdown increased the lifespan and rescued the locomotor deficit of the *HTT*128QFL and *HTT*96QCer fly models (Table 6.1). Both constructs were expressed pan-neuronally so one can assume that the effects observed were due to *Parp* knockdown somehow improving the function of the nervous system. Paldino et al. showed that the striatum from *PARP*1 inhibited R6/2 mice had upregulated levels of CREB and BDNF (Cardinale et al. 2015; Paldino et al. 2017). They hypothesised that because those two proteins were upregulated, apoptosis was being inhibited in the treated R6/2 mice. In order to investigate this in the HD fly models, TUNEL staining could be performed in the fly brains, which would detect fragmented DNA which is indicative of apoptosis (Vasudevan and Ryoo 2016). *Drosophila* researchers have also assessed the expression of apoptosis specific proteins such as cleaved

caspase-3, cleaved dcp-1, hid, DIAP-1, among others, to indicate whether apoptosis is occurring in *Drosophila* tissue (Vasudevan and Ryoo 2016). Genetic manipulation of apoptosis factors in fly HD models may uncover mechanisms behind the extension of the lifespan and rescue of the locomotor deficit. If apoptosis is ruled out as a leading cause of neurodegeneration in the HD fly models it is possible to do forward and reverse genetic screens to find potential modifiers in an unbiased way (Lewis and Smith 2016).

One of the most interesting findings was the effect of the *Parp* RNAi's on the HTT aggregate number in the brains of *HTT*96QCer expressing flies. The reduction of HTT aggregates in the brains of the *HTT*96QCer flies with *Parp* RNAi's was an unexpected result with a 10-fold reduction in HTT aggregates at 14 dpe. However, there was not enough time to follow-up with experiments to fully characterise it and the pathway by which it occurred. Previous research regarding changes in HTT aggregation have indicated that PIN1 expression can modulate HTT aggregation (Miller et al. 2012; Agostoni et al. 2016; Carnemolla et al. 2017). PIN1 and PARP1 have already been shown to relate to each other as PIN1 inhibitors have been tested in tandem with PARP1/2 inhibitors to target BRCA1 proficient cancer tumours (Luo et al. 2020). PIN1 is a prolyl-isomerase and it regulates DSB repair (Steger et al. 2013) and DSBs are recognised by PARP1 and the PARylation at the DSB recruits target proteins (e.g. MRE11) to the repair site (Caron et al. 2019). In Carnemolla at al.'s paper they describe how the overexpression of PIN1 reduces the number of HTT aggregates in HEK293 cells that have been co-transfected with a GFP-tagged pathological HTT construct and PIN1. The same lab had previously published that PIN1 loss in the HdhQ111 knock-in mice caused an increase in HTT aggregate load in the mouse striatum (Agostoni et al. 2016). They propose that PIN1 overexpression is mediating the degradation of soluble HTT by the activating the proteasome through a yet undefined pathway, which in turn breaks down soluble mutant HTT. This could potentially be modulated upstream by PARP1 activity/expression, and other research has indicated how differential ubiquitination can affect the degradation of mutant HTT fragments by the proteasome (Bhat et al. 2014), however it remains to be determined if PIN1 affects the ubiquitination status of HTT.

There is the possibility that while PARP1 activity is upstream of PIN1 in DSB repair, they may not be connected in the in the scope of HTT aggregation. PIN1 has multiple targets which

could be affecting HTT aggregation via a pathway that is unrelated to DSB Repair. However, the pathway Carnemolla et al. proposed to be activated by overexpression of PIN1 could still be affected by PARP1 activity. In HEK293 cells, Topoisomeras1 (TOP1) has been shown to undergo PARylation, which enables it to contact DNA so it can form DNA-protein crosslinks during DNA repair (Sun et al. 2021). Once recruited to the site of DNA damage and the crosslinks between TOP1 and DNA have formed, the PAR polymers attached to TOP1 are hydrolysed by PARG. After this TOP1 is ubiquitinated and it is degraded by the proteasome. However, if the PAR polymers are not removed from TOP1, TOP1 can still be ubiquitinated, but the proteasome is incapable of degrading it (Sun et al. 2021). Sun et al. showed that when PARG was inhibited, TOP1 remained in a PARylated state and the proteasome could not access the ubiquitin and degrade TOP1. Perhaps this same mechanism is responsible for the lack of degradation of HTT by the proteasome. If HTT can be PARylated by Parp, then this could explain why reducing *Parp* expression led to a reduction in HTT aggregation. There may have been enhanced HTT degradation in the brain. The *Parp* RNAi's reduced Parp expression by 40%, which could be the threshold to replicate the effect observed by Sun et al. with TOP1. As *Parp* expression in the *HTT*96QCer flies was reduced, this could have reduced PARylation of mutant HTT and enabled clearance of the soluble mutant HTT prior to aggregate formation. The RNAis reduced *Parp* expression throughout development which could explain why the number of HTT aggregates was dramatically reduced at just 1 dpe. In the *HTT*96QCer flies without the *Parp* RNAi, the HTT protein could potentially be PARylated to the levels required to inhibit proteasomal degradation which would explain the large number of HTT aggregates (Figure 6.12).
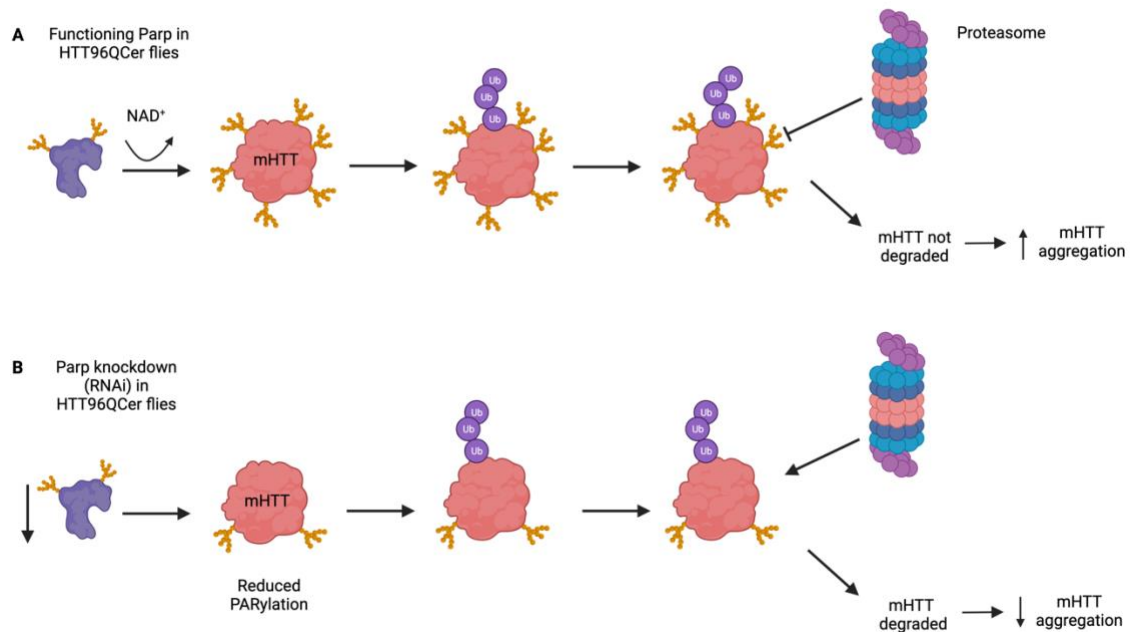
Figure 6.12 - Illustration of how _Parp_ knockdown might affect mHTT protein aggregation in _Drosophila._ (A) Parp PARylates mutant HTT (mHTT), utilising NAD+. PARylated mHTT is ubiquitinylated, but the proteasome cannot access mHTT to breakdown due to the PARylated state. This results in mHTT not being broken down and an increase in mHTT aggregation. (B) When _Parp_ expression is inhibited by RNAi, mHTT is less PARylated. mHTT is ubiquitinylated and due to the lower levels of PARylation, the proteasome can access the ubiquitin signal and mHTT. mHTT is degraded by the proteasome leading to lower levels of mHTT aggregation. (Created with Biorender).

Maiuri and Truant have published some data which shows HTT can be PARylated and a HTT IP showed many PARylated proteins including PARP1 interacting with HTT (Maiuri and Truant 2018). They have discovered a potential PAR-binding domain (Barba Bazan et al. 2018), and they also have some data that shows that when cells were treated with veliparib this increased the interaction of HTT to PARP1 and PARylated proteins. Interestingly, PARP1 has been shown to be activated by pre-formed fibril (PFF) α-synuclein in Parkinson's disease (PD) (Kam et al. 2018). PARylated PFF α-synuclein increased the neurotoxicity of the fibrils by 25-fold and increased PAR levels have been reported in the CSF of PD patients (Kam et al. 2018). This could partially explain why there was less toxicity in the _Parp_ RNAi flies, in comparison to the flies without _Parp_ knockdown. Some ways to assess this relationship in the fly could be to treat flies with proteasome inhibitors and measure its effect on HTT aggregate number. This could be done with flies expressing _HTT_96QCer with and without the _Parp_ RNAi, and the brains could be stained for ubiquitin to test if the aggregates co-localise with the ubiquitin.

Another example of PAR binding to a disease-relevant protein in a neurodegenerative disorder is TDP-43 in Amyotrophic Lateral Sclerosis (ALS) and Frontotemporal Dementia (FTD). In ALS and FTD, TDP-43 becomes hyperphosphorylated and delocalises from the nucleus to the cytoplasm where it forms aggregates (Suk and Rousseaux 2020). This study showed that inhibiting tankyrase, a member of the PARP family (Kim 2018), reduced the number of TDP-43 foci in the cytoplasm in mammalian cells (McGurk et al. 2018). When endogenous tankyrase expression was reduced in a fly model expressing human TDP-43 there was a significant reduction in the degeneration of the eye. Upregulation of tankyrase expression in the same fly model resulted in increased degeneration of the eye. It would be interesting to assess whether reducing tankyrase expression would have an effect on the HTT aggregation phenotype observed in the *HTT*96QCer model. If reduced tankyrase expression did modulate the number of HTT aggregates then one could infer that the PARylation state of HTT is critical for HTT aggregation kinetics. It would also implicate other PARP proteins as potential therapeutic targets, in case there are issues with the toxicity of inhibiting PARP1.

In the same study PAR was shown to co-immunoprecipitate with TDP-43 which affected liquid-liquid phase separation of TDP-43 and its cellular localisation (McGurk et al. 2018). The PAR binding domain was found to be located in the nuclear localisation sequence which likely explained the change in cellular localisation. It would be interesting to examine the loci of the predicted HTT PAR-binding domain to see if it is localised near any of HTT's protein interacting domains. This could infer pathways that are affected by the PARylation state of HTT, i.e. ubiquitination. The data from this study demonstrates another example of how PARylation affects protein aggregation in neurodegenerative diseases, and how regulating PAR levels could ameliorate disease.

There was also a screen which assayed inhibitors and agonists for several proteins (EGFR tyrosine kinase, Caspase-1 and others) in *Drosophila* and PC-12 cell model which found some compounds that rescued HTT aggregation and neurodegeneration (Desai et al. 2006). These publications show that a multitude of pathways can affect HTT aggregation highlighting the complexity of HTT and its multiple interactors.

In Chapter 3 the use of the neurodegeneration assay which assessed the number and fluorescence of the cell bodies at the tip of the L1 vein was described. In this chapter it was used to assess whether *Parp* knockdown would have an effect on the cell body number and fluorescence and it did not end up rescuing this particular phenotype. We hypothesised that the cell death pathway in response to *HTT*128QFL expression in these glutamatergic neurons was not Wallerian degeneration due to the survival of the axons. Hyperactivity of PARP1 has been associated with necrosis as it results in NAD+ depletion and subsequent ATP depletion which causes cell death (Ha and Snyder 1999; Ying and Padanilam 2016). Perhaps the *Parp* RNAi did not have an effect on the cell body number and fluorescence phenotypes because Parp is not hyperactivated in this *HTT*128QFL model, however we only assessed *Parp* RNA levels so we would have to quantify protein expression to confirm this. The qPCR results from Figure 6.7 show that *Parp* expression in the *HTT*128QFL model was not significantly different to that of control flies (ELAV-Gal4), and perhaps the ATP levels of the glutamatergic neurons are being depleted some other way. As previously discussed in Chapter 3, more experiments need to be done to confirm the type of cell death. Primarily the health of the cell body needs to be confirmed, which can be done using a UAS-redstinger which indicates the presence of a cell body. Once this has been performed then more experiments can be designed which will be tailored to the pathway the results reveal.

Genotype	Relative change in *Parp* RNA expression in comparison to control
Parp RNAi 2	Significant 40% decrease
Parp RNAi 3	Significant 40% decrease
*HTT*16QFL	Significant 40% decrease
*HTT*128QFL	No significant difference to control

Table 6.2 – The relative *Parp* expression in various fly lines in comparison to their control. The relative expression of *Parp* mRNA in the *Parp* RNAi lines was compared to their respective RNAi control lines. The relative expression of *Parp* mRNA in the *HTT* lines was compared to flies carrying the ELAV-Gal4 driver.

One of the unexpected results was that the flies expressing *HTT*16QFL had lower endogenous *Parp* expression in comparison to control, whereas the *Parp* RNA expression of the *HTT*128QFL expressing flies was not (Table 6.2). It is unclear why the endogenous *Parp* RNA levels were lower, but we previously alluded to the fact that we hadn't assessed Parp protein expression. Even though there was a significant effect of the *Parp* knockdown on

locomotor function of *HTT*128QFL flies at 7 dpe, it may have been better to assess endogenous *Parp* RNA levels at a disease-relevant time point such as 21 dpe when we observed the cell body degeneration, but also initial stages of axonal degeneration. Ideally, we would have examined Parp enzymatic activity however currently the available commercial kits are only suitable for human studies. Regardless of the reason for lower endogenous *Parp* RNA levels in the *HTT*16QFL flies, further knockdown of *Parp* does not reduce the lifespan or inhibit the locomotor function of the *HTT*16QFL expressing flies, so low levels of *Parp* RNA do not seem to be neurotoxic. This brings into question the idea of neuronal homeostasis of PARylation and when does too much or too little become toxic? High levels of PARylation can result in Parthanatos, but low levels of PAR could result in reduced DNA repair which is also toxic. It is possible that even though *Parp* RNA levels in the *HTT*128QFL flies are higher, that Parp protein may be hyperactive so it is important to find a way to assess PARylation kinetics in *Drosophila* models of HD.

The iPSCs were used as a translatable model as the cells were originally derived from HD-patient fibroblasts. Nuclear PAR levels did not change with $KBrO_3$ treatment even though DSBs were occurring, which was indicated by the increase in nuclear γ-H2AX fluorescence. To improve this experiment and make it more disease-relevant and related to the fly data we would use differentiated neurons instead of undifferentiated iPSCs. All of the fly experiments were conducted with flies expressing hu*HTT* in neurons, so assessing PAR levels in differentiated neurons would be more relevant to this work. It would have been beneficial to use a molecule that specifically causes SSBs as PARP1 is more readily activated by the presence of SSBs. Another condition might be to stain for PARP1 to assess the localisation of the protein when the cells are exposed to ROS. Assessing the cytoplasmic PAR intensity would have been a useful metric as increased levels of cytoplasmic PAR can initiate the cell death pathway Parthanatos. There are commercial kits that assess PARP1 enzymatic activity which could also be used to investigate the activity of PARP1 in HD cell lines with and without ROS induced cellular stress. Some experiments with PARP1 inhibitors mirroring the PARP inhibitor experiment in the flies would have been useful for drawing comparisons between the two models. As with the staining in the *Drosophila* brain, it would have also been useful to stain for indicators of cell survival and perform live-dead assays. There is always the potential to perform more experiments, but the key future experiments include

modelling PAR and PARP1 expression in neurons differentiated from these iPSCs to closer relate the findings to the disease.

A reduction of *Parp* expression results in a reduction of HTT aggregates, increased lifespan and an amelioration of locomotor performance, but does this mean pharmacological inhibitors of PARP1 should be used to treat HD? PARP1 inhibitors are currently being used to treat some types of cancer, targeting tumours that are deficient in specific DNA repair proteins such as BRCA2 and XRCC1 (Bryant et al. 2005; Farmer et al. 2005; Ali et al. 2020). PARP1 inhibitors work by trapping PARP1 to the DNA at a damaged site, during this time PARP1 is unable to PARylate itself or its targets which inhibits DNA repair from occurring (Pommier et al. 2016). When this is combined with BRCA2/XRCC1 deficiency it results in synthetic lethality. While this mechanism is beneficial in cancer treatment because the primary goal is to kill cancer cells, trapping PARP1 to DNA in neurons may not be the desired outcome if we wanted to regulate PARP1 activity in HD MSNs. This will be discussed further in the General Discussion (See Chapter 7.2).

When the *HTT*96QCer flies were treated with Veliparib and Niraparib there was a significant increase in locomotor performance, however no effect was observed on the number of HTT aggregates. This could be related to the concentration of the inhibitors in the food, considering only one dose was tested per inhibitor. Changes to the locomotor performance may be easier to achieve and require a lower dose than changes to the HTT aggregate number, and as only one dose was tested, repeating the experiments with multiple doses may clarify this. Niraparib and veliparib have both been shown to cross the mammalian BBB (Mikule and Wilcoxen 2015; Chabot et al. 2017; Gada et al. 2021), but one of the reasons for a lack of difference in HTT aggregate number could be due to the drugs not crossing the *Drosophila* BBB. The structure of the *Drosophila* and mammalian BBB's are structurally similar, but perhaps the *Drosophila's* glia-based BBB is a tougher barrier for the inhibitors to pass through. There is evidence for PARP1 inhibitors crossing the mammalian BBB when xenograft cancer mice were treated with PARP1 inhibitors. The researchers quantified the PARP1 inhibitor levels in the brain using liquid chromatography mass-spectrometry, which identified traces of the inhibitor in the brain and the metastasised brain tumour (Gada et al. 2021). This technique has been used to characterise the proteome of the *Drosophila* brain

(Kuznetsova et al. 2019) and to analyse monoamines in *Drosophila* brain tissue (Davla et al. 2021), which means there is the potential for it to be used to quantify PARP1 inhibitor levels in the brains of the hu*HTT* expressing flies. This could confirm whether the inhibitors had crossed the brain barrier and thus indicate whether the observed changes in locomotor function were related to changes in CNS function.

6.4 Summary of Main Points

- Knocking down endogenous *Parp* levels in *Drosophila* brain extends the lifespan, rescues the locomotor phenotype and reduces the HTT aggregate number of multiple hu-*HTT* expressing flies.

- Pharmacological inhibitors of human PARP1/2 rescue the locomotor phenotype of hu-*HTT* expressing flies, but does not rescue the HTT aggregate phenotype.

- HD-patient derived iPSCs display DNA damage to oxidative stress but are not affected by PARP1/2 inhibition.

7. General Discussion

7.1 Summary of Findings

The aims of this project included characterising disease-like phenotypes in *Drosophila* models of HD, screening for modifiers of a specific phenotype and then characterising a hit in *Drosophila* and iPSCs. Somatic instability of the human CAG repeat tract in *Drosophila* neurons was also assessed. I found that when you express mutant human *HTT* with a pathological CAG repeat tract the flies have shorter lifespans, develop locomotor deficits, and exhibit cell-body specific neurodegeneration and HTT aggregation. All of these phenotypes demonstrated the utility of using *Drosophila* melanogaster as a medium throughput model system for HD. We found the CAG repeat tract in the HD fly models was stable which was most likely due to the transgenes containing CAA interruptions and lack of MSH3. While screening for modifiers of the locomotor deficit of the *HTT*128QFL flies we found that *Parp* knockdown rescued the locomotor deficit significantly, so it was chosen for further characterisation. *Parp* knockdown was characterised using RNAi and pharmacological PARP1 inhibitors in the fly. Using RNAi, we found that reducing *Parp* expression rescued the lifespan deficit of multiple *Drosophila* models, increased the locomotor function and significantly reduced the number of HTT aggregates in the brain. Small molecule PARP1 inhibitors, approved for human use in treating certain types of cancer, did not ameliorate the HTT aggregate number in the brain, but did rescue the locomotor phenotype of the HD flies. These results suggest the possibility of PARP1 as a new therapeutic target for treating HD.

7.2 *Drosophila melanogaster* as a model system for Huntington's disease

We and previous researchers have shown that expressing mutant hu*HTT* in *Drosophila* neurons reduces lifespan, yields locomotor deficits, causes mutant HTT aggregation and results in neurodegeneration. All of these factors are hallmarks of the human disease which enables the comparison of modifiers of those phenotypes to potential modifiers of the human disease. *Drosophila* as a model system has a lot of beneficial tools that can be manipulated for in-depth study of HD.

The benefits of using *Drosophila* for investigating HD are their short life cycle that can be easily manipulated by temperature, a small genome, a well-characterised central nervous system and there are numerous genetic tools that can be used to study disease. As with most neurodegenerative diseases, it is greatly discussed as to whether mutant protein aggregates are neuroprotective or neurotoxic. Fortunately, the *Drosophila* is a model system in which this could be investigated. We have shown that HTT aggregation can be measured at a single-cell level and there are many unique genetic tools that the fly has that can be taken advantage of to study this. The binary expression system Gal4-UAS can be used in tandem with the QF2-QUAS system to express and inhibit a vast number of genes to aid investigations such as HTT aggregation. The RNAi libraries enable epistasis experiments which map genes to specific pathways, in this instance we would examine *Parp* knockdown in tandem with components of the UPS system which would be one way of assessing whether PARylation of HTT affects its ability to be degraded by the proteasome. *Drosophila* also provide the ability to visualise peripheral neurons at a single cell resolution using a quick dissection of the wing (Neukomm et al. 2014; Soares et al. 2014). This could streamline the process of screening modifiers of neurodegeneration in several diseases, not just HD. While there are limitations with this method, (i.e. proof cell body is dying/dead), this would be an efficient way to search for modifiers of neurodegeneration through forward or reverse screening. Other methods to assess neurodegeneration include utilising the eye of the *Drosophila* and assessing the number and or structure of the ommatidia (Tamura et al. 2011; Yang et al. 2013). All of these methods provide insight into the many beneficial ways *Drosophila* can be used to investigate HD and other neurodegenerative diseases.

Model	HTT Gene length	HTT CAG length	Lifespan deficit	Locomotor deficit	HTT Aggregates	Somatic CAG instability	Striatal volume loss
HTT128QFL (fly)	Full-length	121 repeats Mixed CAG/CAA	Present: 23 days	Present	Not observed	No	N/A
HTT96QCer (fly)	Exon1	96 repeats Mixed CAG/CAA	Present: 36 days	Present	Present	No	N/A
YAC128 (mouse)	Full-length	125 repeats Mixed CAG/CAA	No	Present	Present	No	Present
BACHD (mouse)	Full-length	97 repeats Mixed CAG/CAA	No	Present	Present	No	Present
R6/1 (mouse)	Exon1	116 CAGs	Can live up to 1 year	Present	Present	Present	Present
R6/2 (mouse)	Exon1	116-293 CAGs	Present: 14-15 weeks	Present	Present	Present	Present
BAC-CAG (mouse)	Exon1	~120 repeats Pure CAG	-	Present	Present	Present	Present
HdhQ111 (mouse)	Knock-in	111 repeats Pure CAG	-	Present	Present	Present	Present

Table 7.1 – A comparative table of HD-like phenotypes in fly and selected mouse models of HD. (Mangiarini et al. 1997; Wheeler et al. 2000; Slow et al. 2003; Wheeler et al. 2003; Li et al. 2005; Van Raamsdonk et al. 2005; Gray et al. 2008; Pouladi et al. 2012; Larson et al. 2015; Yhnell et al. 2016; Goodliffe et al. 2020; Gu et al. 2022).

A table was created to compare the HD-like phenotypes observed in this project to a selection of commonly used HD mouse models, as there are some elements of HD that *Drosophila* currently cannot model (Table 7.1). One of the hallmarks of HD is the somatic instability of the CAG repeat tract of the *HTT* gene. When *HTT* is expressed in *Drosophila* neurons, the CAG repeat tract does not exhibit any signs of somatic instability. CAA

interruptions are a common feature in the CAG repeat tracts of the *HTT* transgenes of *Drosophila* models of HD, similar to existing mouse models (YAC128 and BACHD) (Gray et al. 2008; Pouladi et al. 2012) (Table 7.1). It is hypothesised that CAA interruptions stabilise CAG repeat tracts and are potentially neuroprotective for HD patients (McAllister et al. 2022). The age of the flies is another issue as somatic instability of the CAG repeat tract probably occurs over the patients lifespan with most instability found in post-mortem tissue (Kacher et al. 2021), whereas flies have an average lifespan of 60 days without toxic *HTT* expression. *Drosophila* also lack homologs for genes associated with somatic instability such as *FAN1* and *MSH3* (Moss et al. 2017; Sekelsky 2017; Goold et al. 2019; Goold et al. 2021). Fortunately, there are several mouse models that are available to model somatic instability which include the transgenic R6/2 model and BAC-CAG model as well as the HdhQ111 knock-in model (Table 7.1). These mouse models also display locomotor and HTT aggregation phenotypes like the *Drosophila* models but do not exhibit somatic instability of the CAG repeat tract in the *HTT* gene. This demonstrates somatic instability does not need to occur in order to be a good model of HD. While somatic instability could not be investigated in the fly, it was advantageous for the screen as we could examine elements of the MMR and other potential modifiers which are associated with somatic instability, and assess if they affected CNS function in a HD model in the absence of somatic instability.

Endogenous *Drosophila Htt* does not contain the disease-causing CAG repeat tract which resides in exon1 of the human gene. In order to tackle this obstacle, CRISPR technology could be used to insert a CAG repeat tract into the endogenous *Drosophila Htt* gene. The HdhQ111 knock-in mouse model was created by inserting human exon1 of *HTT* with an expanded CAG repeat tract and 268 base pairs of intron 1 which replaces 124 base pairs of mouse intron 1 (Wheeler et al. 1999). Perhaps a similar technique could be used in *Drosophila* as modifying the endogenous gene so that it contained a pure CAG repeat tract would allow for research to test if somatic instability could occur in *Drosophila*. Another change that this could bring about is a delay in the disease-related phenotypes that were observed, as the edited endogenous *Htt* would be expressed at endogenous levels. This would possibly give a more realistic model of the disease than overexpressing the transgene, however phenotypes may be more subtle and harder to detect and the short lifespan of the fly could also limit the detection of disease-related phenotypes.

Alternatively, we could insert the *HTT* UAS constructs into the *Drosophila* genome via site-directed mutagenesis rather than random insertion with a P-element (Banga and Boyd 1992). To the best of my knowledge all existing *HTT* UAS constructs are randomly inserted into the genome, making comparisons between expanded and non-expanded conditions challenging. While the random insertion of the *HTT* UAS constructs into the fly genome did not yield lethality or negative effects on the lifespan and health of the flies, it would be beneficial to control which loci the construct is inserted into.

7.3 PARP1 as a therapeutic target for HD

We previously discussed the potential mechanisms of how Parp knockdown ameliorated the HD-related phenotypes in *Drosophila*. PARylation of specific proteins has been associated with inhibiting protein degradation by the UPS (Sun et al. 2021), which could potentially be occurring in HD with toxic HTT. It has been established that PAR binds to full-length HTT (Maiuri and Truant 2018), so the PARylation state of HTT could be preventing its degradation. This could lead to the build-up of HTT aggregates that the proteasome cannot process (Figure 6.12 and 7.1). There is evidence suggesting PARylation drives the toxicity of α-synuclein fibrils in Parkinson's disease and PARP1 deletion reduces this toxicity (Kam et al. 2018), so PARP1 could be driving toxicity of mHTT in a similar way. High levels of PARP1 have been observed in post-mortem brain tissue of HD patients (Vis et al. 2005), but future experiments need to establish the enzymatic activity of PARP1 and PARG in HD patients and animal models as this may give more insight than levels of immunofluorescence. PARP1 may not need to be hyperactive to have negative effects in HD as physiological levels of PARP1 could be enough to PARylate HTT to an extent where it cannot be degraded by the UPS. The activity of PARG should also be established as it is one of the few enzymes that has the ability to hydrolyse the glycosidic ribose-ribose bonds that bind PAR polymers to their targets (Slade et al. 2011). If PARG activity is reduced in HD patients or animal models then PARylation levels could become dysregulated, which could lead to the lack of HTT breakdown as described above.

The mechanism of neurodegeneration in the medium spiny neurons in HD is not known. As PARP1/Parp inhibition/knockdown has been shown to be neuroprotective in HD mouse models (Cardinale et al. 2015; Paldino et al. 2017; Paldino et al. 2020) and rescues HD-like phenotypes in HD *Drosophila* models there is the potential that PARP1/Parp is hyperactivated in these systems and the inhibition or downregulation of expression reduces PARP1/Parp activity. PARP1 hyperactivation triggers the cell death pathway, Parthanatos (David et al. 2009; Fatokun et al. 2014). PARP1 hyperactivation and subsequently Parthanatos occurs in response to high levels of DNA damage (Wang et al. 2009) which has been associated with HD pathogenesis and has been shown more broadly in other neurodegenerative conditions such as AD and PD (Bogdanov et al. 2001; Rulten and Caldecott 2013; Askeland et al. 2018; Castaldo et al. 2018; Lin et al. 2020; Gonzalez-Hunt and Sanders 2021) (Table 7.1). If Parthanatos is a cause of neurodegeneration in HD, then inhibiting PARP1 may reduce striatal cell death. More work needs to be done to establish the mechanism of neurodegeneration in HD and whether PARP1 inhibition can protect against it.
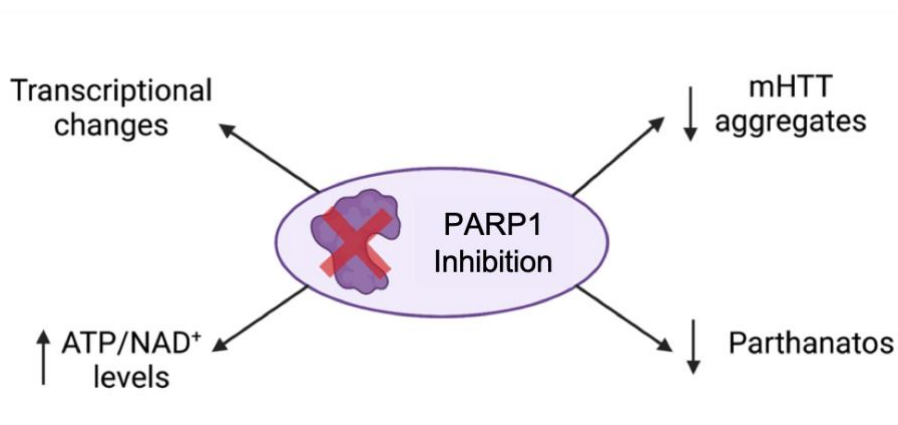
Figure 7.1 – The potential downstream effects of PARP1 inhibition in HD.

One of the hypothesised early pathogenic mechanisms in HD is mitochondrial dysfunction. Mutant HTT monomers and oligomers have been shown to interact with mitochondria directly and indirectly (via the dysregulation of transcription) (Shirendeb et al. 2011; Carmo et al. 2018; Lloret and Beal 2019). NAD^+ is required for ATP production in the mitochondria and it is also required for the PARylation activity of PARP1. If PARP1 is hyperactive in HD then a likely consequence is the depletion of NAD^+ and subsequently ATP. With mitochondrial dysfunction already being a hallmark of early pathogenesis of HD, reducing the metabolic requirements of the cell by inhibiting PARP1 may slow the damage to the

mitochondria in HD. The combination of a reduction of mHTT in the neurons, due to the previously described PARylation/proteasome hypothesis, and reduced NAD$^+$ load could potentially prevent or slow mitochondrial dysfunction.

It has been suggested that PARP1 positively and negatively regulates transcription by PARylating histone proteins, which modifies chromatin structure and by directly interacting with promoter regions of genes (Kraus and Lis 2003; Schiewer and Knudsen 2014; Azad et al. 2018). *Parp* knock-out *Drosophila* larvae exhibited large-scale expression changes in 602 genes with genes coding for transcription factors being downregulated and genes coding for the cytochrome P450 family, which act in oxidoreduction, being upregulated (Bordet et al. 2020). HTT has also been shown to regulate the transcription of various genes, but most notably in HD is the evidence suggesting mHTT downregulates *BDNF* transcription (Zuccato et al. 2003; Zuccato and Cattaneo 2007; Zuccato et al. 2011). The PARP1 inhibitor INO-1001 has been tested in R6/2 mice to assess whether PARP1 inhibition would be a useful strategy for treating HD (Cardinale et al. 2015; Paldino et al. 2017) and one of the effects they saw was an increase in the immunoreactivity of BDNF and its transcriptional activator phosphorylated CREB in the striatum in comparison to untreated R6/2 mice. They showed that the transcription regulator CREB-binding protein (CBP) is sequestered to mHTT aggregates in the cytoplasm, which potentially prevents it from translocating to the nucleus, thus inhibiting its activity as a transcriptional activator. R6/2 mice treated with INO-1001 showed a reduction of the sequestration of CBP to mHTT aggregates, which when combined with the evidence of increased BDNF and CREB immunoreactivity in INO-1001 treated R6/2 mice striatum, demonstrate that PARP1 is possibly interacting with HTT-related transcription. While *Parp* knockout in *Drosophila* larvae affected the expression of a large number of genes, inhibiting PARP1 may not have such a significant effect as the inhibitors may not completely block PARP1 activity. The existing literature and our data exemplify reasons for following-up PARP1 as a therapeutic target for HD. The usefulness of PARP1 inhibitor treatment must be discussed alongside other emerging treatment options for HD patients.

Currently there are several antisense oligonucleotides (ASOs) that are in various stages of clinical trials for the treatment of HD. ASOs are short, single stranded oligonucleotides that

target mRNA of specific proteins in order to modify protein expression (Rinaldi and Wood 2018; Di Fusco et al. 2019). Protein expression is modified by RNase H-mediated degradation of the mRNA (Silva et al. 2020). ASOs have proven their value to the medical world as they are currently being used to treat diseases such as Duchenne muscular dystrophy and Familial Amyloid Neuropathies (Roberts et al. 2020). ASOs are seen as a viable method for treating HD due to the toxic gain of function phenotypes that mutant *HTT* exhibits during the course of the disease (Lane et al. 2018). These "Huntingtin-lowering" approaches function on the idea that decreasing *HTT* mRNA levels would reduce the levels of toxic *HTT* protein, thus affecting the some of its gain of function properties and the levels of HTT aggregation. In HD the target is *HTT* mRNA and the most developed ASO is Tominersen which targets both the mutant and healthy *HTT* mRNA (Tabrizi et al. 2019b). Unfortunately, the Tominersen trial was halted in March 2021 because the drug was ineffective and might even have made some patients worse at the higher doses (Tabrizi et al. 2022). The trial will not be restarted but there are plans for a smaller Phase II trial in a subset of patients with very mild symptoms only (Ionis Pharmaceuticals Inc., 2022). This is not the only HD ASO trial that has been hit with challenges, with Wave Life Sciences redesigning their *HTT* ASO to improve the chemistry (Wave Life Sciences, 2021). This is because they did not see knockdown of HTT during their initial trial, unlike in the Tominersen trial where good knockdown was observed. Targeting *HTT* mRNA is a difficult task and while the ASO trials targeting *HTT* are a valid therapeutic approach and will hopefully treat the disease effectively in the near future, perhaps an ASO targeting *MSH3* would be a viable option as decreased expression of MSH3 could limit somatic expansions (Tomé et al. 2013; Flower et al. 2019) potentially slowing disease progression. It is likely that multiple complementary approaches will be used to treat the disease in the future.

We have shown the beneficial effects of genetic *Parp* knockdown in the fly brain on several disease-related phenotypes, perhaps an ASO trial targeting PARP1 could be another strategy for treating HD. Before this is investigated, PARP1 inhibition must be further characterised in flies, human cell models and other animal models of HD. If the results remain consistent, in that PARP1 inhibition is neuroprotective in the HD models, then PARP1 inhibitors could be trialled on HD patients. As there are PARP1 inhibitors in current treatments for cancer, it would probably be best to prioritise an inhibitor that has been proven to cross the blood

brain barrier such as Veliparib and Niraparib. It is possible that in the future small molecule PARP1 inhibitors could be used in combination therapy with ASOs to maximise therapeutic outcomes.

One thing to consider with PARP1 inhibition is that pharmacological inhibitors of PARP1/2 are currently used to target DNA-repair deficient cancer cells (i.e. BRCA2/XRCC1 deficient cells) (Bryant et al. 2005; Sandhu et al. 2010; Ali et al. 2020; Boussios et al. 2020; Diéras et al. 2020; Diéras et al. 2020). HD patients have lower incidences of cancer diagnoses (McNulty et al. 2018), but there is also evidence of higher levels of DNA damage in HD patient blood and HD mouse model brain tissue in comparison to controls (Bogdanov et al. 2001; Askeland et al. 2018; Castaldo et al. 2018). Inhibiting PARP1, which is a key enzyme in the DNA damage response, may result in DNA damage remaining unrepaired, genetic mutations and potentially cancer.

7.4 Future Directions

Parp inhibition is clearly having an effect in the *Drosophila* HD models, however there is still a lot of work to be done to fully characterise the mechanisms by which it is affecting the disease-like phenotypes that were observed. Due to time constraints, the PARP1 inhibitor experiment was limited in its drug concentrations, sample size and time points. This would be the first experiment to be modified and repeated. Two objectives need to be reached; verify that the PARP1 inhibitors are improving locomotor function of the *HTT*96QCer flies; and assess whether the PARP1 inhibitors are crossing the blood brain barrier (BBB). Once these two objectives have been met then the mechanism by which *Parp* inhibition is ameliorating the phenotypes needs to be assessed.

PARylation of HTT is potentially impacting its ability to be broken down by the proteasome, as excessive PARylation could be preventing the proteasome from accessing or recognising the ubiquitinylated sites on HTT. In order to test this IHC could be performed on the brains of *HTT*96QCer expressing flies to assess whether PAR co-localises with mHTT aggregates. This could be repeated with the *Parp* RNAi and/or the PARP1 inhibitors to assess whether the localisation or amount of PAR immunofluorescence changes. We have mentioned

previously the genetic tool kit of the fly and how it can be best utilised to measure different outcomes. Potentially RNAi or UAS constructs for elements of the ubiquitin-proteasome system could be used in epistasis experiments to investigate the mechanism of mHTT degradation. It would be useful to replicate these results in cellular models of HD as live-imaging techniques with fluorescently tagged HTT, PAR and/or proteasomes could be used to assess their localisation and interaction in healthy cells in comparison to cells expressing mHTT.

PARP1/Parp hyperactivation and Parthanatos would also need to be investigated. Establishing Parp protein levels in *Drosophila* models of HD might indicate the activation of the protein, but optimising the PAR antibody staining in the brain would also denote Parp activity. I suggest expressing pathological *HTT* in a small subset of neurons in the brains of *Drosophila*, and then assessing PAR immunofluorescence throughout the entire brain. If there is a higher level of PAR fluorescence in the region where *HTT* is expressed, then it could indicate hyperactivation of Parp protein. Indicators of NAD+ levels would also help elucidate Parp activity as Parp requires NAD+ to PARylate itself and its targets, thus higher levels of NAD+ in the neurons expressing *HTT* could suggest higher levels of Parp activity. This could be coupled with staining for the mitochondrial protein AIF which is released from the mitochondria in response PAR translocating from the nucleus to the cytoplasm. If AIF staining was couple with fluorescently tagged mitochondria, then we could assess the localisation of AIF in these neurons with colocalization of AIF and mitochondrial fluorescence indicating Parthanatos is not occurring. If we can establish Parp activity in *Drosophila* and other animal and cellular models of HD, we could be a step closer to understanding its role in HD pathogenesis.

7.5 Concluding Remarks

Huntington's disease is a monogenic disorder but data now suggests that multiple genes may modify the age at which motor symptoms onset. While no significant SNPs from the HD GWAS were associated with the *PARP1* locus not all genes contain genetic variation that is detected in GWAS. It appears that modifying homologous PARP1 expression/activity does ameliorate HD-like symptoms in the HD fly models. More research clearly needs to be done

to understand the mechanisms by which PARP1 inhibition is eliciting these effects and whether we can repurpose existing drugs for the treatment of HD.

8. References

Adamowicz, M. et al. 2021. XRCC1 protects transcription from toxic PARP1 activity during DNA base excision repair. *Nature Cell Biology* 23(12), pp. 1287–1298. doi: 10.1038/s41556-021-00792-w.

Agostoni, E. et al. 2016. Effects of Pin1 Loss in HdhQ111 Knock-in Mice. *Frontiers in Cellular Neuroscience* 10. Available at: https://www.frontiersin.org/article/10.3389/fncel.2016.00110.

Ali, A.A.E. et al. 2012. The zinc-finger domains of PARP1 cooperate to recognise DNA strand-breaks. *Nature structural & molecular biology* 19(7), pp. 685–692. doi: 10.1038/nsmb.2335.

Ali, R. et al. 2020. PARP1 blockade is synthetically lethal in XRCC1 deficient sporadic epithelial ovarian cancers. *Cancer Letters* 469, pp. 124–133. doi: 10.1016/j.canlet.2019.10.035.

Almeida, K.H. and Sobol, R.W. 2007. A unified view of base excision repair: lesion-dependent protein complexes regulated by post-translational modification. *DNA repair* 6(6), pp. 695–711. doi: 10.1016/j.dnarep.2007.01.009.

Al-Ramahi, I. et al. 2006. CHIP Protects from the Neurotoxicity of Expanded and Wild-type Ataxin-1 and Promotes Their Ubiquitination and Degradation *. *Journal of Biological Chemistry* 281(36), pp. 26714–26724. doi: 10.1074/jbc.M601603200.

Amé, J.-C. et al. 2004. The PARP superfamily. *BioEssays* 26(8), pp. 882–893. doi: https://doi.org/10.1002/bies.20085.

Andrade, M.A. and Bork, P. 1995. HEAT repeats in the Huntington's disease protein. *Nature Genetics* 11(2), pp. 115–116. doi: 10.1038/ng1095-115.

Ansari, A.M. et al. 2016. Cellular GFP Toxicity and Immunogenicity: Potential Confounders in in Vivo Cell Tracking Experiments. *Stem Cell Reviews and Reports* 12(5), pp. 553–559. doi: 10.1007/s12015-016-9670-8.

Arama, J. et al. 2015. GABAA receptor activity shapes the formation of inhibitory synapses between developing medium spiny neurons. *Frontiers in Cellular Neuroscience* 9. Available at: https://www.frontiersin.org/article/10.3389/fncel.2015.00290.

Arrasate, M. et al. 2004. Inclusion body formation reduces levels of mutant huntingtin and the risk of neuronal death. *Nature* 431(7010), pp. 805–810. doi: 10.1038/nature02998.

Askeland, G. et al. 2018. Increased nuclear DNA damage precedes mitochondrial dysfunction in peripheral blood mononuclear cells from Huntington's disease patients. *Scientific Reports* 8(1), pp. 1–9. doi: 10.1038/s41598-018-27985-y.

Aslesh, T. and Yokota, T. 2020. Development of Antisense Oligonucleotide Gapmers for the Treatment of Huntington's Disease. In: Yokota, T. and Maruyama, R. eds. *Gapmers: Methods and Protocols*. Methods in Molecular Biology. New York, NY: Springer US, pp. 57–67. Available at: https://doi.org/10.1007/978-1-0716-0771-8_4.

Atwal, R.S. et al. 2007. Huntingtin has a membrane association signal that can modulate huntingtin aggregation, nuclear entry and toxicity. *Human Molecular Genetics* 16(21), pp. 2600–2615. doi: 10.1093/hmg/ddm217.

Augood, S.J. et al. 1996. Reduction in enkephalin and substance P messenger RNA in the striatum of early grade Huntington's disease: A detailed cellularin situ hybridization study. *Neuroscience* 72(4), pp. 1023–1036. doi: 10.1016/0306-4522(95)00595-1.

Aviolat, H. et al. 2019. Assessing average somatic CAG repeat instability at the protein level. *Scientific Reports* 9(1), pp. 1–14. doi: 10.1038/s41598-019-55202-x.

Azad, G.K. et al. 2018. PARP1-dependent eviction of the linker histone H1 mediates immediate early gene expression during neuronal activation. *Journal of Cell Biology* 217(2), pp. 473–481. doi: 10.1083/jcb.201703141.

Aziz, N.A. et al. 2011. Parent-of-origin differences of mutant HTT CAG repeat instability in Huntington's disease. *European Journal of Medical Genetics* 54(4), pp. e413-418. doi: 10.1016/j.ejmg.2011.04.002.

Babcock, D.T. and Ganetzky, B. 2015. Transcellular spreading of huntingtin aggregates in the Drosophila brain. *Proceedings of the National Academy of Sciences of the United States of America* 112(39), pp. E5427–E5433. doi: 10.1073/pnas.1516217112.

Báez-Mendoza, R. and Schultz, W. 2013. The role of the striatum in social behavior. *Frontiers in Neuroscience* 7, p. 233. doi: 10.3389/fnins.2013.00233.

Banga, S.S. and Boyd, J.B. 1992. Oligonucleotide-directed site-specific mutagenesis in Drosophila melanogaster. *Proceedings of the National Academy of Sciences* 89(5), pp. 1735–1739. doi: 10.1073/pnas.89.5.1735.

Barba Bazan, C. et al. 2018. ROS-Specific Huntingtin Interactions: Measuring poly ADP ribose levels in HD cells. Available at: https://zenodo.org/record/1464979.

Barkauskaite, E. et al. 2015. Structures and Mechanisms of Enzymes Employed in the Synthesis and Degradation of PARP-Dependent Protein ADP-Ribosylation. *Molecular Cell* 58(6), pp. 935–946. doi: 10.1016/j.molcel.2015.05.007.

Bates, G.P. et al. 2015. Huntington disease. *Nature Reviews Disease Primers* 1(April), pp. 1–21. doi: 10.1038/nrdp.2015.5.

Becher, M.W. et al. 1998. Intranuclear Neuronal Inclusions in Huntington's Disease and Dentatorubral and Pallidoluysian Atrophy: Correlation between the Density of Inclusions andIT15CAG Triplet Repeat Length. *Neurobiology of Disease* 4(6), pp. 387–397. doi: 10.1006/nbdi.1998.0168.

Beglinger, L.J. et al. 2014. Results of the Citalopram to Enhance Cognition in Huntington Disease Trial. *Movement disorders : official journal of the Movement Disorder Society* 29(0 3), pp. 401–405. doi: 10.1002/mds.25750.

Benn, C.L. et al. 2020. Drugging DNA Damage Repair Pathways for Trinucleotide Repeat Expansion Diseases. *Journal of Huntington's Disease* , pp. 1–18. doi: 10.3233/JHD-200421.

Bergonzoni, G. et al. 2021. D1R- and D2R-Medium-Sized Spiny Neurons Diversity: Insights Into Striatal Vulnerability to Huntington's Disease Mutation. *Frontiers in Cellular Neuroscience* 15. Available at: https://www.frontiersin.org/article/10.3389/fncel.2021.628010.

Besson, M.T. et al. 2015. Enhanced Neuronal Glucose Transporter Expression Reveals Metabolic Choice in a HD Drosophila Model. *PLOS ONE* 10(3), p. e0118765. doi: 10.1371/journal.pone.0118765.

Bhat, K.P. et al. 2014. Differential ubiquitination and degradation of huntingtin fragments modulated by ubiquitin-protein ligase E3A. *Proceedings of the National Academy of Sciences* 111(15), pp. 5706–5711. doi: 10.1073/pnas.1402215111.

Bloomington Drosophila Stock Center. [no date]. Available at: https://bdsc.indiana.edu/information/recipes/molassesfood.html.

Bogdanov, M.B. et al. 2001. Increased oxidative damage to DNA in a transgenic mouse model of Huntington's disease. *Journal of Neurochemistry* 79(6), pp. 1246–1249. doi: 10.1046/j.1471-4159.2001.00689.x.

Bordet, G. et al. 2020. Poly(ADP-ribose) polymerase 1 in genome-wide expression control in Drosophila. *Scientific Reports* 10(1), p. 21151. doi: 10.1038/s41598-020-78116-5.

Bottje, W.G. 2019. Oxidative metabolism and efficiency: the delicate balancing act of mitochondria. *Poultry Science* 98(10), pp. 4223–4230. doi: 10.3382/ps/pey405.

Bourn, R.L. et al. 2012. Pms2 Suppresses Large Expansions of the (GAA·TTC)n Sequence in Neuronal Tissues. *PLoS ONE* 7(10). doi: 10.1371/journal.pone.0047085.

Boussios, S. et al. 2020. Poly (ADP-Ribose) Polymerase Inhibitors: Talazoparib in Ovarian Cancer and Beyond. *Drugs in R&D* 20(2), pp. 55–73. doi: 10.1007/s40268-020-00301-8.

Brand, H. and Perrimon, N. 1993. Targeted gene expression as a means of altering cell fates and generating dominant phenotypes. *Development* 118, pp. 401–415.

Brandt, J. et al. 2002. Neuropsychological manifestations of the genetic mutation for Huntington's disease in presymptomatic individuals. *Journal of the International Neuropsychological Society: JINS* 8(7), pp. 918–924. doi: 10.1017/s1355617702870060.

Brooks, P.J. et al. 1996. *DNA Mismatch Repair and DNA Methylation in Adult Brain Neurons*., pp. 939–945.

Browne, S.E. et al. 1997. Oxidative damage and metabolic dysfunction in Huntington's disease: Selective vulnerability of the basal ganglia. *Annals of Neurology* 41(5), pp. 646–653. doi: 10.1002/ana.410410514.

Bryant, H.E. et al. 2005. Specific killing of BRCA2-deficient tumours with inhibitors of poly(ADP-ribose) polymerase. *Nature* 434(7035), pp. 913–917. doi: 10.1038/nature03443.

Bryant, H.E. et al. 2009. PARP is activated at stalled forks to mediate Mre11-dependent replication restart and recombination. *The EMBO Journal* 28, pp. 2601–2615. doi: 10.1038/emboj.2009.206.

Butterworth, N.J. et al. 1998. Trinucleotide (CAG) repeat length is positively correlated with the degree of DNA fragmentation in Huntington's disease striatum. *Neuroscience* 87(1), pp. 49–53. doi: 10.1016/S0306-4522(98)00129-8.

Caldecott, K.W. 2019. XRCC1 protein; Form and function. *DNA Repair* 81, p. 102664. doi: 10.1016/j.dnarep.2019.102664.

Cardinale, A. et al. 2015. PARP-1 Inhibition Is Neuroprotective in the R6/2 Mouse Model of Huntington's Disease. *PloS one* 10(8), pp. e0134482–e0134482. doi: 10.1371/journal.pone.0134482.

Carmo, C. et al. 2018. Mitochondrial Dysfunction in Huntington's Disease. In: Nóbrega, C. and Pereira de Almeida, L. eds. *Polyglutamine Disorders*. Advances in Experimental Medicine and Biology. Cham: Springer International Publishing, pp. 59–83. Available at: https://doi.org/10.1007/978-3-319-71779-1_3.

Carnemolla, A. et al. 2017. PIN1 Modulates Huntingtin Levels and Aggregate Accumulation: An In vitro Model. *Frontiers in Cellular Neuroscience* 11. Available at: https://www.frontiersin.org/article/10.3389/fncel.2017.00121.

Caron, M.-C. et al. 2019. Poly(ADP-ribose) polymerase-1 antagonizes DNA resection at double-strand breaks. *Nature Communications* 10(1), p. 2954. doi: 10.1038/s41467-019-10741-9.

Carty, N. et al. 2015. Characterization of HTT Inclusion Size, Location, and Timing in the zQ175 Mouse Model of Huntington´s Disease: An In Vivo High-Content Imaging Study. *PLOS ONE* 10(4), p. e0123527. doi: 10.1371/journal.pone.0123527.

Castaldo, I. et al. 2018. DNA damage signatures in peripheral blood cells (PBMC) as biomarkers in prodromal Huntington's disease. *Annals of Neurology* , p. ana.25393-ana.25393. doi: 10.1002/ana.25393.

Cepeda, C. et al. 2014. The Role of Dopamine in Huntington's Disease. *Progress in brain research* 211, pp. 235–254. doi: 10.1016/B978-0-444-63425-2.00010-6.

Chabot, P. et al. 2017. Veliparib in combination with whole-brain radiation therapy for patients with brain metastases from non-small cell lung cancer: results of a randomized, global, placebo-controlled study. *Journal of Neuro-Oncology* 131(1), pp. 105–115. doi: 10.1007/s11060-016-2275-x.

Chen, A. 2011. PARP inhibitors: its role in treatment of cancer. *Chinese Journal of Cancer* 30(7), pp. 463–471. doi: 10.5732/cjc.011.10111.

Chen, C.-M. et al. 2007. Increased oxidative damage and mitochondrial abnormalities in the peripheral blood of Huntington's disease patients. *Biochemical and Biophysical Research Communications* 359(2), pp. 335–340. doi: 10.1016/j.bbrc.2007.05.093.

Chen, J. et al. 2013. Dopamine imbalance in Huntington's disease: a mechanism for the lack of behavioral flexibility. *Frontiers in Neuroscience* 7. Available at: https://www.frontiersin.org/article/10.3389/fnins.2013.00114.

Chen, M. et al. 2016. The Aggregation Free Energy Landscapes of Polyglutamine Repeats. *Journal of the American Chemical Society* 138(46), pp. 15197–15203. doi: 10.1021/jacs.6b08665.

Chen, S. et al. 2001. Polyglutamine aggregation behavior in vitro supports a recruitment mechanism of cytotoxicity. *Journal of Molecular Biology* 311(1), pp. 173–182. doi: 10.1006/jmbi.2001.4850.

Chery, J. 2016. RNA therapeutics: RNAi and antisense mechanisms and clinical applications. *Postdoc journal : a journal of postdoctoral research and postdoctoral affairs* 4(7), pp. 35–50.

Chuhma, N. et al. 2011. Functional Connectome of the Striatal Medium Spiny Neuron. *The Journal of Neuroscience* 31(4), pp. 1183–1192. doi: 10.1523/JNEUROSCI.3833-10.2011.

Ciapponi, L. et al. 2004. The Drosophila Mre11/Rad50 complex is required to prevent both telomeric fusion and chromosome breakage. *Current biology: CB* 14(15), pp. 1360–1366. doi: 10.1016/j.cub.2004.07.019.

Cicchetti, F. et al. 2000. Chemical anatomy of striatal interneurons in normal individuals and in patients with Huntington's disease. *Brain Research Reviews* 34(1), pp. 80–101. doi: 10.1016/S0165-0173(00)00039-4.

Cichewicz, K. et al. 2017. A New Brain Dopamine Deficient Drosophila and its Pharmacological and Genetic Rescue. *Genes, brain, and behavior* 16(3), pp. 394–403. doi: 10.1111/gbb.12353.

Ciosi, M. et al. 2019. A genetic association study of glutamine-encoding DNA sequence structures, somatic CAG expansion, and DNA repair gene variants, with Huntington disease clinical outcomes. *EBioMedicine* 48, pp. 568–580. doi: 10.1016/j.ebiom.2019.09.020.

Coleman, M.P. and Freeman, M.R. 2010. Wallerian Degeneration, Wld S , and Nmnat. *Annual Review of Neuroscience* 33(1), pp. 245–267. doi: 10.1146/annurev-neuro-060909-153248.

Cooper, J.K. et al. 1998. Truncated N-Terminal Fragments of Huntingtin with Expanded Glutamine Repeats form Nuclear and Cytoplasmic Aggregates in Cell Culture. *Human Molecular Genetics* 7(5), pp. 783–790. doi: 10.1093/hmg/7.5.783.

Costa, V. et al. 2010. Mitochondrial fission and cristae disruption increase the response of cell models of Huntington's disease to apoptotic stimuli. *EMBO Molecular Medicine* 2(12), pp. 490–503. doi: 10.1002/emmm.201000102.

Costa, V. and Scorrano, L. 2012. Shaping the role of mitochondria in the pathogenesis of Huntington's disease. *The EMBO Journal* 31(8), pp. 1853–1864. doi: 10.1038/emboj.2012.65.

Damiano, M. et al. 2010. Mitochondria in Huntington's disease. *Biochimica et Biophysica Acta (BBA) - Molecular Basis of Disease* 1802(1), pp. 52–61. doi: 10.1016/j.bbadis.2009.07.012.

D'Amours, D. and Jackson, S.P. 2002. The Mre11 complex: At the crossroads of DNA repair and checkpoint signalling. *Nature Reviews Molecular Cell Biology* 3(5), pp. 317–327. doi: 10.1038/nrm805.

Davenport, C.B. and Muncey, E.B. 1916. Huntington's chorea in relation to heredity and eugenics. *American Journal of Psychiatry* 73(2), pp. 195–222. doi: 10.1176/ajp.73.2.195.

David, K.K. et al. 2009. Parthanatos, A messenger of death. *Frontiers in Bioscience* 14(3), pp. 1116–1128. doi: 10.2741/3297.

Davla, S. et al. 2021. *A rapid and reliable multiplexed LC-MS/MS method for simultaneous analysis of six monoamines from brain tissues*. Neuroscience. Available at: http://biorxiv.org/lookup/doi/10.1101/2021.05.24.445477.

Dé Ric Saudou, F. and Humbert, S. 2016. The Biology of Huntingtin. doi: 10.1016/j.neuron.2016.02.003.

Dehay, B. and Bertolotti, A. 2006. Critical role of the proline-rich region in Huntingtin for aggregation and cytotoxicity in yeast. *The Journal of biological chemistry* 281(47), pp. 35608–15. doi: 10.1074/jbc.M605558200.

Delia, D. et al. 2004. MRE11 mutations and impaired ATM-dependent responses in an Italian family with ataxia-telangiectasia-like disorder. *Human Molecular Genetics* 13(18), pp. 2155–2163. doi: 10.1093/hmg/ddh221.

Demin, A.A. et al. 2021. XRCC1 prevents toxic PARP1 trapping during DNA base excision repair. *Molecular Cell* 81, pp. 3018-3030.e5. doi: 10.1016/j.molcel.2021.05.009.

Desai, U.A. et al. 2006. Biologically active molecules that reduce polyglutamine aggregation and toxicity. *Human Molecular Genetics* 15(13), pp. 2114–2124. doi: 10.1093/hmg/ddl135.

Deshmukh, A.L. et al. 2021. FAN1, a DNA Repair Nuclease, as a Modifier of Repeat Expansion Disorders. *Journal of Huntington's Disease* 10(1), pp. 95–122. doi: 10.3233/JHD-200448.

Di Fusco, D. et al. 2019. Antisense Oligonucleotide: Basic Concepts and Therapeutic Application in Inflammatory Bowel Disease. *Frontiers in Pharmacology* 10. Available at: https://www.frontiersin.org/article/10.3389/fphar.2019.00305.

Diéras, V. et al. 2020. Veliparib with carboplatin and paclitaxel in BRCA-mutated advanced breast cancer (BROCADE3): a randomised, double-blind, placebo-controlled, phase 3 trial. *The Lancet Oncology* 21(10), pp. 1269–1282. doi: 10.1016/S1470-2045(20)30447-2.

DiFiglia, M. et al. 1997. Aggregation of Huntingtin in Neuronal Intranuclear Inclusions and Dystrophic Neurites in Brain. *Science* 277(5334), pp. 1990–1993. doi: 10.1126/science.277.5334.1990.

Digilio, F.A. et al. 1996. *Tosca: A Drosophila Gene Encoding a Nuclease Specifically Expressed in the Female Germline*.

Do, A.T. and LaRocque, J.R. 2015. The role of Drosophila mismatch repair in suppressing recombination between diverged sequences. *Scientific Reports* 5(1), p. 17601. doi: 10.1038/srep17601.

Donaldson, J.J. 2019. *Huntingtin CAG repeat expansions in induced pluripotent stem cell models of Huntington's Disease*. phd, Cardiff University. Available at: https://orca.cardiff.ac.uk/129860/.

Donnelly, K.M. et al. 2020. Phagocytic glia are obligatory intermediates in transmission of mutant huntingtin aggregates across neuronal synapses. *eLife* 9, pp. 1–1. doi: 10.7554/eLife.58499.

Dragileva, E. et al. 2009. Intergenerational and striatal CAG repeat instability in Huntington's disease knock-in mice involve different DNA repair genes. *Neurobiology of disease* 33(1), pp. 37–47. doi: 10.1016/j.nbd.2008.09.014.

Dragunow, M. et al. 1995. In situevidence for DNA fragmentation in Huntington's disease striatum and Alzheimer's disease temporal lobes. *NeuroReport* 6(7), pp. 1053–1057.

Drouet, V. et al. 2014. Allele-Specific Silencing of Mutant Huntingtin in Rodent Brain and Human Stem Cells. *PLOS ONE* 9(6), p. e99341. doi: 10.1371/journal.pone.0099341.

Duff, K. et al. 2007. Psychiatric Symptoms in Huntington's Disease before Diagnosis: The Predict-HD Study. *Biological Psychiatry* 62(12), pp. 1341–1346. doi: 10.1016/j.biopsych.2006.11.034.

Ehrlich, M.E. 2012. Huntington's Disease and the Striatal Medium Spiny Neuron: Cell-Autonomous and Non-Cell-Autonomous Mechanisms of Disease. *Neurotherapeutics* 9(2), pp. 270–284. doi: 10.1007/s13311-012-0112-2.

Elmore, S. 2007. Apoptosis: A Review of Programmed Cell Death. *Toxicologic Pathology* 35(4), pp. 495–516. doi: 10.1080/01926230701320337.

Eshraghi, M. et al. 2021. Mutant Huntingtin stalls ribosomes and represses protein synthesis in a cellular model of Huntington disease. *Nature Communications* 12(1), p. 1461. doi: 10.1038/s41467-021-21637-y.

Estrada Sánchez, A.M. et al. 2008. Excitotoxic Neuronal Death and the Pathogenesis of Huntington's Disease. *Archives of Medical Research* 39(3), pp. 265–276. doi: 10.1016/J.ARCMED.2007.11.011.

Evans, S.J. et al. 2013. Prevalence of adult Huntington's disease in the UK based on diagnoses recorded in general practice records. *Journal of Neurology, Neurosurgery & Psychiatry* 84(10), pp. 1156–1160. doi: 10.1136/jnnp-2012-304636.

Fang, Y. and Bonini, N.M. 2015. Hope on the (fruit) fly: The Drosophila wing paradigm of axon injury. *Neural Regeneration Research* 10(2), pp. 173–175. doi: 10.4103/1673-5374.152359.

Farmer, H. et al. 2005. Targeting the DNA repair defect in BRCA mutant cells as a therapeutic strategy. *Nature* 434(7035), pp. 917–921. doi: 10.1038/nature03445.

Fatokun, A.A. et al. 2014. Parthanatos: mitochondrial-linked mechanisms and therapeutic opportunities. *British Journal of Pharmacology* 171(8), pp. 2000–2016. doi: 10.1111/bph.12416.

Fernet, M. et al. 2005. Identification and functional consequences of a novel MRE11 mutation affecting 10 Saudi Arabian patients with the ataxia telangiectasia-like disorder. *Human Molecular Genetics* 14(2), pp. 307–318. doi: 10.1093/hmg/ddi027.

Fire, A. et al. 1998. Potent and specific genetic interference by double-stranded RNA in Caenorhabditis elegans. *Nature* 391(6669), pp. 806–811. doi: 10.1038/35888.

Fishel, M.L. et al. 2007. DNA repair in neurons: So if they don't divide what's to repair? *Mutation Research - Fundamental and Molecular Mechanisms of Mutagenesis* 614(1–2), pp. 24–36. doi: 10.1016/j.mrfmmm.2006.06.007.

Flower, M. et al. 2019. MSH3 modifies somatic instability and disease severity in Huntington's and myotonic dystrophy type 1. *Brain* 142(7), pp. 1876–1886. doi: 10.1093/brain/awz115.

Frank, S. 2014. Treatment of Huntington's Disease. *Neurotherapeutics* 11(1), pp. 153–160. doi: 10.1007/s13311-013-0244-z.

Fricker, M. et al. 2018. Neuronal cell death. *Physiological Reviews* 98(2), pp. 813–880. doi: 10.1152/physrev.00011.2017.

Gada, K. et al. 2021. Tissue distribution and brain penetration of niraparib in tumor bearing mouse models and its clinical relevance. *Journal of Clinical Oncology* 39(15_suppl), pp. e15066–e15066. doi: 10.1200/JCO.2021.39.15_suppl.e15066.

Gargano, J.W. et al. 2005. Rapid iterative negative geotaxis (RING): a new method for assessing age-related locomotor decline in Drosophila. *Experimental Gerontology* 40(5), pp. 386–395. doi: 10.1016/J.EXGER.2005.02.005.

Gauthier, L.R. et al. 2004. Huntingtin Controls Neurotrophic Support and Survival of Neurons by Enhancing BDNF Vesicular Transport along Microtubules. *Cell* 118(1), pp. 127–138. doi: 10.1016/j.cell.2004.06.018.

Gerfen, C.R. et al. 1990. D1 and D2 Dopamine Receptor-regulated Gene Expression of Striatonigral and Striatopallidal Neurons. *Science* 250(4986), pp. 1429–1432. doi: 10.1126/science.2147780.

Giampà, C. et al. 2013. Systemic Delivery of Recombinant Brain Derived Neurotrophic Factor (BDNF) in the R6/2 Mouse Model of Huntington's Disease. *PLoS ONE* 8(5), p. e64037. doi: 10.1371/journal.pone.0064037.

Giralt, A. et al. 2011. Conditional BDNF release under pathological conditions improves Huntington's disease pathology by delaying neuronal dysfunction. *Molecular Neurodegeneration* 6, p. 71. doi: 10.1186/1750-1326-6-71.

Goldberg, Y.P. et al. 1996. Cleavage of huntingtin by apopain, a proapoptotic cysteine protease, is modulated by the polyglutamine tract. *Nature Genetics* 13(4), pp. 442–449. doi: 10.1038/ng0896-442.

Gonitel, R. et al. 2008. DNA instability in postmitotic neurons. *Proceedings of the National Academy of Sciences of the United States of America* 105(9), pp. 3467–3472. doi: 10.1073/pnas.0800048105.

Gonzalez-Hunt, C.P. and Sanders, L.H. 2021. DNA damage and repair in Parkinson's disease: Recent advances and new opportunities. *Journal of Neuroscience Research* 99(1), pp. 180–189. doi: 10.1002/jnr.24592.

Goodliffe, J. et al. 2020. Structural and functional features of medium spiny neurons in the BACHDΔN17 mouse model of Huntington's Disease. *PLOS ONE* 15(6), p. e0234394. doi: 10.1371/journal.pone.0234394.

Goold, R. et al. 2019. FAN1 modifies Huntington's disease progression by stabilizing the expanded HTT CAG repeat. *Human molecular genetics* 28(4), pp. 650–661. doi: 10.1093/hmg/ddy375.

Goold, R. et al. 2021. FAN1 controls mismatch repair complex assembly via MLH1 retention to stabilize CAG repeat expansion in Huntington's disease. *Cell Reports* 36(9), p. 109649. doi: 10.1016/j.celrep.2021.109649.

Goula, A.-V. et al. 2012. Transcription Elongation and Tissue-Specific Somatic CAG Instability. Pearson, C. E. ed. *PLoS Genetics* 8(11), pp. e1003051–e1003051. doi: 10.1371/journal.pgen.1003051.

Graham, R.K. et al. 2006. Cleavage at the Caspase-6 Site Is Required for Neuronal Dysfunction and Degeneration Due to Mutant Huntingtin. *Cell* 125(6), pp. 1179–1191. doi: 10.1016/j.cell.2006.04.026.

Gray, M. et al. 2008. Full-Length Human Mutant Huntingtin with a Stable Polyglutamine Repeat Can Elicit Progressive and Selective Neuropathogenesis in BACHD Mice. *The Journal of Neuroscience* 28(24), pp. 6182–6195. doi: 10.1523/JNEUROSCI.0857-08.2008.

Graybiel, A.M. and Grafton, S.T. 2015. The striatum: Where skills and habits meet. *Cold Spring Harbor Perspectives in Biology* 7(8), pp. a021691–a021691. doi: 10.1101/cshperspect.a021691.

Greenspan, Ralph.J. 1997. *Fly Pushing*. New York: Cold Spring Harbor Laboratory Press.

Gu, X. et al. 2022. Uninterrupted CAG repeat drives striatum-selective transcriptionopathy and nuclear pathogenesis in human Huntingtin BAC mice. *Neuron* 110(7), pp. 1173-1192.e7. doi: 10.1016/j.neuron.2022.01.006.

Guedes-Dias, P. et al. 2016. Mitochondrial dynamics and quality control in Huntington's disease. *Neurobiology of Disease* 90, pp. 51–57. doi: 10.1016/j.nbd.2015.09.008.

Guillotin, D. and Martin, S.A. 2014. Exploiting DNA mismatch repair deficiency as a therapeutic strategy. *Experimental Cell Research* 329(1), pp. 110–115. doi: 10.1016/J.YEXCR.2014.07.004.

Gunawardena, S. et al. 2003. Disruption of Axonal Transport by Loss of Huntingtin or Expression of Pathogenic PolyQ Proteins in Drosophila. *Neuron* 40, pp. 25–40. doi: 10.1016/S0896-6273(03)00594-4.

Gupta, D. and Heinen, C.D. 2019. The mismatch repair-dependent DNA damage response: Mechanisms and implications. *DNA Repair* 78, pp. 60–69. doi: 10.1016/j.dnarep.2019.03.009.

Gupta, S.K. et al. 2019. PARP Inhibitors for Sensitization of Alkylation Chemotherapy in Glioblastoma: Impact of Blood-Brain Barrier and Molecular Heterogeneity. *Frontiers in Oncology* 8, p. 670. doi: 10.3389/fonc.2018.00670.

Gusella, J.F. et al. 1983. A polymorphic DNA marker genetically linked to Huntington's disease. *Nature* 306(5940), pp. 234–238. doi: 10.1038/306234a0.

Gusella, J.F. and MacDonald, M.E. 2009. Huntington's disease: the case for genetic modifiers. *Genome medicine* 1(8), p. 80. doi: 10.1186/gm80.

Gutekunst, C.-A. et al. 1999. Nuclear and Neuropil Aggregates in Huntington's Disease: Relationship to Neuropathology. *Journal of Neuroscience* 19(7), pp. 2522–2534. doi: 10.1523/JNEUROSCI.19-07-02522.1999.

Ha, H.C. and Snyder, S.H. 1999. Poly(ADP-ribose) polymerase is a mediator of necrotic cell death by ATP depletion. *Proceedings of the National Academy of Sciences* 96(24), pp. 13978–13982. doi: 10.1073/pnas.96.24.13978.

Hackam, A.S. et al. 1999. Evidence for both the nucleus and cytoplasm as subcellular sites of pathogenesis in Huntington's disease in cell culture and in transgenic mice expressing mutant huntingtin. *Philosophical Transactions of the Royal Society B: Biological Sciences* 354(1386), pp. 1047–1055.

Hanai, S. et al. 2004. Loss of poly(ADP-ribose) glycohydrolase causes progressive neurodegeneration in Drosophila melanogaster. *Proceedings of the National Academy of Sciences of the United States of America* 101(1), pp. 82–6. doi: 10.1073/pnas.2237114100.

Hannon, G.J. 2002. RNA interference. *Nature* 418(6894), pp. 244–251. doi: 10.1038/418244a.

Hansson, O. et al. 1999. Transgenic mice expressing a Huntington's disease mutation are resistant to quinolinic acid-induced striatal excitotoxicity. *Proceedings of the National Academy of Sciences* 96(15), pp. 8727–8732. doi: 10.1073/pnas.96.15.8727.

Hansson, O. et al. 2001. Resistance to NMDA toxicity correlates with appearance of nuclear inclusions, behavioural deficits and changes in calcium homeostasis in mice transgenic for exon 1 of

the huntington gene. *European Journal of Neuroscience* 14(9), pp. 1492–1504. doi: 10.1046/j.0953-816x.2001.01767.x.

Harjes, P. and Wanker, E.E. 2003. The hunt for huntingtin function: interaction partners tell many different stories. *Trends in Biochemical Sciences* 28(8), pp. 425–433. doi: 10.1016/S0968-0004(03)00168-3.

Hartlerode, A.J. et al. 2018. Reversible mislocalization of a disease-associated MRE11 splice variant product. *Scientific Reports* 8(1), pp. 10121–10121. doi: 10.1038/s41598-018-28370-5.

Hayden, M.R. 1983. Reflections on the history of Huntington's chorea. *Trends in Neurosciences* 6, pp. 122–124. doi: 10.1016/0166-2236(83)90062-0.

Hindle, S.J. and Bainton, R.J. 2014. Barrier mechanisms in the Drosophila blood-brain barrier. *Frontiers in Neuroscience* 8. Available at: https://www.frontiersin.org/article/10.3389/fnins.2014.00414.

Hoch, N.C. et al. 2017. XRCC1 mutation is associated with PARP1 hyperactivation and cerebellar ataxia. *Nature* 541(7635), pp. 87–91. doi: 10.1038/nature20790.

Hoshino, M. et al. 2006. Transcriptional repression induces a slowly progressive atypical neuronal death associated with changes of YAP isoforms and p73. *The Journal of Cell Biology* 172(4), pp. 589–604. doi: 10.1083/jcb.200509132.

Hsieh, P. and Yamane, K. 2008. DNA mismatch repair: Molecular mechanism, cancer, and ageing. *Mechanisms of Ageing and Development* 129(7–8), pp. 391–407. doi: 10.1016/j.mad.2008.02.012.

Hsu, Y.-T. et al. 2018. Insights into GABAAergic system alteration in Huntington's disease. *Open biology* 8(12). doi: 10.1098/rsob.180165.

Hu, Y. et al. 2011. An integrative approach to ortholog prediction for disease-focused and other functional studies. *BMC Bioinformatics* 12, p. 357. doi: 10.1186/1471-2105-12-357.

Huambachano, O. et al. 2011. Double-stranded DNA Binding Domain of Poly(ADP-ribose) Polymerase-1 and Molecular Insight into the Regulation of Its Activity*. *Journal of Biological Chemistry* 286(9), pp. 7149–7160. doi: 10.1074/jbc.M110.175190.

Huang, R.-C. 2018. The discoveries of molecular mechanisms for the circadian rhythm: The 2017 Nobel Prize in Physiology or Medicine. *Biomedical Journal* 41(1), p. 5. doi: 10.1016/J.BJ.2018.02.003.

Huntington, G. 1872. On Chorea. *The Medical and Surgical Reporter of Philadelphia* 26(15), pp. 317–321.

Iennaco, R. et al. 2022. The evolutionary history of the polyQ tract in huntingtin sheds light on its functional pro-neural activities. *Cell Death & Differentiation* 29(2), pp. 293–305. doi: 10.1038/s41418-021-00914-9.

Illuzzi, J. et al. 2009. DNA breakage and induction of DNA damage response proteins precede the appearance of visible mutant huntingtin aggregates. *Journal of Neuroscience Research* 87(3), pp. 733–747. doi: 10.1002/jnr.21881.

Ionis Pharmaceuticals Inc. 2022. Ionis' partner to evaluate tominersen for Huntington's disease in new Phase 2 trial. Available at: https://ir.ionispharma.com/news-releases/news-release-details/ionis-partner-evaluate-tominersen-huntingtons-disease-new-phase.

Iyer, J. et al. 2016. Quantitative assessment of eye phenotypes for functional genetic studies using Drosophila melanogaster. *G3: Genes, Genomes, Genetics* 6(5), pp. 1427–1437. doi: 10.1534/g3.116.027060.

Iyer, R.R. and Pluciennik, A. 2021. DNA Mismatch Repair and its Role in Huntington's Disease. *Journal of Huntington's Disease* 10(1), pp. 75–94. doi: 10.3233/JHD-200438.

Jackson, G.R. et al. 1998. Polyglutamine-Expanded Human Huntingtin Transgenes Induce Degeneration of Drosophila Photoreceptor Neurons. *Neuron* 21(3), pp. 633–642. doi: 10.1016/S0896-6273(00)80573-5.

Jana, N.R. et al. 2001. Altered proteasomal function due to the expression of polyglutamine-expanded truncated N-terminal huntingtin induces apoptosis by caspase activation through mitochondrial cytochrome c release. *Human Molecular Genetics* 10(10), pp. 1049–1059. doi: 10.1093/hmg/10.10.1049.

Jauhar, S. and Ritchie, S. 2010. Psychiatric and behavioural manifestations of Huntington's disease. *Advances in Psychiatric Treatment* 16(3), pp. 168–175. doi: 10.1192/apt.bp.107.005371.

Jayaraman, A. and Reynolds, R. 2022. Diverse pathways to neuronal necroptosis in Alzheimer's disease. *European Journal of Neuroscience* , pp. 1–14. doi: 10.1111/ejn.15662.

Jimenez-Sanchez, M. et al. 2015. SiRNA screen identifies QPCT as a druggable target for Huntington's disease. *Nature Chemical Biology* 11(5), pp. 347–354. doi: 10.1038/nchembio.1790.

Johri, A. and Beal, M.F. 2012. Antioxidants in Huntington's disease. *Biochimica et Biophysica Acta (BBA) - Molecular Basis of Disease* 1822(5), pp. 664–674. doi: 10.1016/j.bbadis.2011.11.014.

Juenemann, K. et al. 2013. Expanded Polyglutamine-containing N-terminal Huntingtin Fragments Are Entirely Degraded by Mammalian Proteasomes. *The Journal of Biological Chemistry* 288(38), pp. 27068–27084. doi: 10.1074/jbc.M113.486076.

Juenemann, K. et al. 2015. Detection of ubiquitinated huntingtin species in intracellular aggregates. *Frontiers in Molecular Neuroscience* 8. Available at: https://www.frontiersin.org/article/10.3389/fnmol.2015.00001.

Jung, J. et al. 2011. Defining genetic factors that modulate intergenerational CAG repeat instability in Drosophila melanogaster. *Genetics* 187(1), pp. 61–71. doi: 10.1534/genetics.110.121418.

Jung, J. and Bonini, N. 2007. CREB-Binding Protein Modulates Repeat Instability in a Drosophila Model for PolyQ Disease. *Science* 315(5820), pp. 1857–1859. doi: 10.1126/science.1139517.

Kacher, R. et al. 2021. Propensity for somatic expansion increases over the course of life in Huntington disease. Orr, H. T. et al. eds. *eLife* 10, p. e64674. doi: 10.7554/eLife.64674.

Kachian, Z.R. et al. 2019. Suicidal ideation and behavior in Huntington's disease: Systematic review and recommendations. *Journal of Affective Disorders* 250, pp. 319–329. doi: 10.1016/J.JAD.2019.03.043.

Kalchman, M.A. et al. 1996. Huntingtin Is Ubiquitinated and Interacts with a Specific Ubiquitin-conjugating Enzyme *. *Journal of Biological Chemistry* 271(32), pp. 19385–19394. doi: 10.1074/jbc.271.32.19385.

Kaltenbach, L.S. et al. 2007. Huntingtin Interacting Proteins Are Genetic Modifiers of Neurodegeneration. *PLoS Genetics* 3(5), pp. 0689–0708. doi: 10.1371/journal.pgen.0030082.

Kam, T.-I. et al. 2018. Poly (ADP-ribose) Drives Pathologic α-Synuclein Neurodegeneration in Parkinson's Disease. *Science (New York, N.Y.)* 362(6414), p. eaat8407. doi: 10.1126/science.aat8407.

Katow, H. et al. 2021. Involvement of Huntingtin in Development and Ciliary Beating Regulation of Larvae of the Sea Urchin, Hemicentrotus pulcherrimus. *International Journal of Molecular Sciences* 22(10), p. 5116. doi: 10.3390/ijms22105116.

Kelly, S.M. et al. 2017. Dissection and Immunofluorescent Staining of Mushroom Body and Photoreceptor Neurons in Adult Drosophila melanogaster Brains. *Journal of Visualized Experiments* (129). doi: 10.3791/56174.

Kennedy, L. et al. 2003. Dramatic tissue-specific mutation length increases are an early molecular event in Huntington disease pathogenesis. *Human Molecular Genetics* 12(24), pp. 3359–3367. doi: 10.1093/hmg/ddg352.

Kennedy, L. and Shelbourne, P.F. 2000. Dramatic mutation instability in HD mouse striatum: does polyglutamine load contribute to cell-specific vulnerability in Huntington's disease? *Human Molecular Genetics* 9(17), pp. 2539–2544. doi: 10.1093/HMG.

Keryer, G. et al. 2011. Ciliogenesis is regulated by a huntingtin-HAP1-PCM1 pathway and is altered in Huntington disease. *Journal of Clinical Investigation* 121(11), pp. 4372–4382. doi: 10.1172/JCI57552.

Khoronenkova, S.V. and Dianov, G.L. 2015. ATM prevents DSB formation by coordinating SSB repair and cell cycle progression. *Proceedings of the National Academy of Sciences* 112(13), pp. 3997–4002. doi: 10.1073/pnas.1416031112.

Kiechle, T. et al. 2002. Cytochrome C and caspase-9 expression in Huntington's disease. *NeuroMolecular Medicine* 1(3), pp. 183–195. doi: 10.1385/NMM:1:3:183.

Kim, M.K. 2018. Novel insight into the function of tankyrase (Review). *Oncology Letters* 16(6), pp. 6895–6902. doi: 10.3892/ol.2018.9551.

Kim, Y.E. et al. 2016. Soluble Oligomers of PolyQ-Expanded Huntingtin Target a Multiplicity of Key Cellular Factors. *Molecular Cell* 63(6), pp. 951–964. doi: 10.1016/j.molcel.2016.07.022.

Kingwell, K. 2021. Double setback for ASO trials in Huntington disease. *Nature Reviews Drug Discovery* 20(6), pp. 412–413. doi: 10.1038/d41573-021-00088-6.

Kirk, K.E. et al. 1997. *SUMO Modification of Huntingtin and Huntington's Disease Pathology*.

Kirkwood, S.C. et al. 2001. Progression of Symptoms in the Early and Middle Stages of Huntington Disease. *Archives of Neurology* 58(2), pp. 273–278. doi: 10.1001/archneur.58.2.273.

Koch, E.T. and Raymond, L.A. 2019. Dysfunctional striatal dopamine signaling in Huntington's disease. *Journal of Neuroscience Research* 97(12), pp. 1636–1654. doi: 10.1002/jnr.24495.

Koppensteiner, R. et al. 2014. Effect of MRE11 loss on PARP-inhibitor sensitivity in endometrial cancer In Vitro. *PLoS ONE* 9(6), pp. 100041–100041. doi: 10.1371/journal.pone.0100041.

Koushika, S.P. et al. 1996. ELAV, a Drosophila neuron-specific protein, mediates the generation of an alternatively spliced neural protein isoform. *Current biology : CB* 6(12), pp. 1634–41. doi: 10.1016/S0960-9822(02)70787-2.

Kovalenko, M. et al. 2012. Msh2 Acts in Medium-Spiny Striatal Neurons as an Enhancer of CAG Instability and Mutant Huntingtin Phenotypes in Huntington's Disease Knock-In Mice. *PLoS ONE* 7(9). Available at: https://www.ncbi.nlm.nih.gov/pmc/articles/PMC3436885/.

Kratz, K. et al. 2010. Deficiency of FANCD2-Associated Nuclease KIAA1018/FAN1 Sensitizes Cells to Interstrand Crosslinking Agents. *Cell* 142(1), pp. 77–88. doi: 10.1016/j.cell.2010.06.022.

Kraus, W.L. and Lis, J.T. 2003. PARP Goes Transcription. *Cell* 113(6), pp. 677–683. doi: 10.1016/S0092-8674(03)00433-1.

Kremer, B. et al. 1994. A Worldwide Study of the Huntington's Disease Mutation: The Sensitivity and Specificity of Measuring CAG Repeats. *New England Journal of Medicine* 330(20), pp. 1401–1406. doi: 10.1056/NEJM199405193302001.

Krench, M. and Littleton, J.T. 2013. Modeling Huntington disease in Drosophila: Insights into axonal transport defects and modifiers of toxicity. *Fly* 7(4), pp. 229–36. doi: 10.4161/fly.26279.

Krishnakumar, R. and Kraus, W.L. 2010. The PARP Side of the Nucleus: Molecular Actions, Physiological Outcomes, and Clinical Targets. *Molecular Cell* 39(1), pp. 8–24. doi: 10.1016/j.molcel.2010.06.017.

Kuemmerle, S. et al. 1999. Huntington aggregates may not predict neuronal death in Huntington's disease. *Annals of Neurology* 46(6), pp. 842–849.

Kuznetsova, K.G. et al. 2019. Brain Proteome of Drosophila melanogaster Is Enriched with Nuclear Proteins. *Biochemistry. Biokhimiia* 84(1), pp. 71–78. doi: 10.1134/S0006297919010097.

LaCount, D.J. et al. 2000. Caspase inhibitor P35 and inhibitor of apoptosis Op-IAP block in vivo proteolytic activation of an effector caspase at different steps. *Journal of Biological Chemistry* 275(21), pp. 15657–15664. doi: 10.1074/jbc.M000791200.

Lane, R.M. et al. 2018. Translating Antisense Technology into a Treatment for Huntington's Disease. In: Precious, S. V. et al. eds. *Huntington's Disease*. Methods in Molecular Biology. New York, NY: Springer, pp. 497–523. Available at: https://doi.org/10.1007/978-1-4939-7825-0_23.

Langbehn, D. et al. 2004. A new model for prediction of the age of onset and penetrance for Huntington's disease based on CAG length. *Clinical Genetics* 65(4), pp. 267–277. doi: 10.1111/j.1399-0004.2004.00241.x.

Langelier, M.-F. et al. 2012. Structural basis for DNA-dependent poly(ADP-ribosyl)ation by human PARP-1. *Science (New York, N.Y.)* 336(6082), pp. 728–732. doi: 10.1126/science.1216338.

Larson, E. et al. 2015. Age-, tissue- and length-dependent bidirectional somatic CAG•CTG repeat instability in an allelic series of R6/2 Huntington disease mice. *Neurobiology of Disease* 76, pp. 98–111. doi: 10.1016/j.nbd.2015.01.004.

Lee, J.-M. et al. 2011. Quantification of Age-Dependent Somatic CAG Repeat Instability in Hdh CAG Knock-In Mice Reveals Different Expansion Dynamics in Striatum and Liver. Nollen, E. A. A. ed. *PLoS ONE* 6(8), p. e23647. doi: 10.1371/journal.pone.0023647.

Lee, J.-M. et al. 2012. CAG repeat expansion in Huntington disease determines age at onset in a fully dominant fashion. *Neurology* 78(10), pp. 690–695. doi: 10.1212/WNL.0b013e318249f683.

Lee, J.-M. et al. 2015. Identification of Genetic Factors that Modify Clinical Onset of Huntington's Disease. *Cell* 162(3), pp. 516–526. doi: 10.1016/J.CELL.2015.07.003.

Lee, J.-M. et al. 2019. CAG Repeat Not Polyglutamine Length Determines Timing of Huntington's Disease Onset. *Cell* 178(4), pp. 887-900.e14. doi: 10.1016/j.cell.2019.06.036.

Lee, W.-C.M. et al. 2004. Cytoplasmic aggregates trap polyglutamine-containing proteins and block axonal transport in a Drosophila model of Huntington's disease. *Proceedings of the National Academy of Sciences of the United States of America* 101(9), pp. 3224–9. doi: 10.1073/pnas.0400243101.

Lei, W. et al. 2004. Evidence for Differential Cortical Input to Direct Pathway versus Indirect Pathway Striatal Projection Neurons in Rats. *The Journal of Neuroscience* 24(38), pp. 8289–8299. doi: 10.1523/JNEUROSCI.1990-04.2004.

Lesinskienė, S. et al. 2020. Juvenile Huntington's disease: two case reports and a review of the literature. *Journal of Medical Case Reports* 14(1), p. 173. doi: 10.1186/s13256-020-02494-7.

Levinson, G. and Gutman, G.A. 1987. Slipped-strand mispairing: a major mechanism for DNA sequence evolution. *Molecular Biology and Evolution* 4(3), pp. 203–221. doi: 10.1093/oxfordjournals.molbev.a040442.

Lewis, E.A. and Smith, G.A. 2016. Using Drosophila models of Huntington's disease as a translatable tool. *Journal of Neuroscience Methods* 265, pp. 89–98. doi: 10.1016/J.JNEUMETH.2015.07.026.

Leyva, M.J. et al. 2010. Identification and Evaluation of Novel Small Molecule Pan-Caspase Inhibitors in Huntington's Disease Models. *Chemistry & biology* 17(11), pp. 1189–1200. doi: 10.1016/j.chembiol.2010.08.014.

Li, G.-M. 2008. Mechanisms and functions of DNA mismatch repair. *Cell Research* 18(1), pp. 85–98. doi: 10.1038/cr.2007.115.

Li, H. et al. 2001. Huntingtin aggregate-associated axonal degeneration is an early pathological event in Huntington's disease mice. *Journal of Neuroscience* 21(21), pp. 8473–8481. doi: 10.1523/jneurosci.21-21-08473.2001.

Li, J.Y. et al. 2005. The use of the R6 transgenic mouse models of Huntington's disease in attempts to develop novel therapeutic strategies. *NeuroRx : the journal of the American Society for Experimental NeuroTherapeutics* 2(3), pp. 447–64. doi: 10.1602/neurorx.2.3.447.

Li, S.-H. et al. 2000. Intranuclear huntingtin increases the expression of caspase-1 and induces apoptosis. *Human Molecular Genetics* 9(19), pp. 2859–2867. doi: 10.1093/hmg/9.19.2859.

Li, Z. et al. 1999. A putative Drosophila homolog of the Huntington's disease gene. *Human molecular genetics* 8(9), pp. 1807–15. doi: 10.1093/hmg/8.9.1807.

Liévens, J.C. et al. 2008. AKT-sensitive or insensitive pathways of toxicity in glial cells and neurons in Drosophila models of Huntington's disease. *Human Molecular Genetics* 17(6), pp. 882–894. doi: 10.1093/hmg/ddm360.

Limmer, S. et al. 2014. The Drosophila blood-brain barrier: development and function of a glial endothelium. *Frontiers in Neuroscience* 8. Available at: https://www.frontiersin.org/article/10.3389/fnins.2014.00365.

Lin, T.-H. et al. 2021. TSG101 negatively regulates mitochondrial biogenesis in axons. *Proceedings of the National Academy of Sciences* 118(20), p. e2018770118. doi: 10.1073/pnas.2018770118.

Lin, X. et al. 2020. Contributions of DNA Damage to Alzheimer's Disease. *International Journal of Molecular Sciences* 21(5), p. 1666. doi: 10.3390/ijms21051666.

Lin, Y. et al. 2009. TRANSCRIPTION DESTABILIZES TRIPLET REPEATS. *Molecular carcinogenesis* 48(4), pp. 350–361. doi: 10.1002/mc.20488.

Lin, Y. and Wilson, J.H. 2011. Transcription-induced DNA toxicity at trinucleotide repeats. *Cell Cycle* 10(4), pp. 611–618. doi: 10.4161/cc.10.4.14729.

Lin, Y.-H. et al. 2019. Expression of Human Mutant Huntingtin Protein in Drosophila Hemocytes Impairs Immune Responses. *Frontiers in Immunology* 10. Available at: https://www.frontiersin.org/article/10.3389/fimmu.2019.02405.

Linford, N.J. et al. 2013. Measurement of Lifespan in Drosophila melanogaster. *Journal of Visualized Experiments* (71), pp. e50068–e50068. doi: 10.3791/50068.

Liu, H.S. et al. 1999. Is green fluorescent protein toxic to the living cells? *Biochemical and Biophysical Research Communications* 260(3), pp. 712–717. doi: 10.1006/bbrc.1999.0954.

Liu, T. et al. 2010. FAN1 Acts with FANCI-FANCD2 to Promote DNA Interstrand Cross-Link Repair. *Science* 329(5992), pp. 693–696. doi: 10.1126/science.1192656.

Llobet Rosell, A. and Neukomm, L.J. 2019. Axon death signalling in Wallerian degeneration among species and in disease. *Open Biology* 9(8), p. 190118. doi: 10.1098/rsob.190118.

Lloret, A. and Beal, M.F. 2019. PGC-1α, Sirtuins and PARPs in Huntington's Disease and Other Neurodegenerative Conditions: NAD+ to Rule Them All. *Neurochemical Research* 44(10), pp. 2423–2434. doi: 10.1007/s11064-019-02809-1.

London, R.E. 2015. The structural basis of XRCC1-mediated DNA repair. *DNA repair* 30, pp. 90–103. doi: 10.1016/j.dnarep.2015.02.005.

Luo, L. and Wu, J.S. 2007. A protocol for mosaic analysis with a repressible cell marker (Marcm) in drosophila. *Nature Protocols* 1(6), pp. 2583–2589. doi: 10.1038/nprot.2006.320.

Luo, M.-L. et al. 2020. Inactivation of the Prolyl Isomerase Pin1 Sensitizes BRCA1-Proficient Breast Cancer to PARP Inhibition. *Cancer research* 80(14), pp. 3033–3045. doi: 10.1158/0008-5472.CAN-19-2739.

Ma, B. et al. 2010. Localization of BDNF mRNA with the Huntington's disease protein in rat brain. *Molecular Neurodegeneration* 5(1), p. 22. doi: 10.1186/1750-1326-5-22.

Ma, Y. et al. 2006. Prevalence of off-target effects in Drosophila RNA interference screens. *Nature* 443(7109), pp. 359–363. doi: 10.1038/nature05179.

MacKay, C. et al. 2010. Identification of KIAA1018/FAN1, a DNA Repair Nuclease Recruited to DNA Damage by Monoubiquitinated FANCD2. *Cell* 142(1), pp. 65–76. doi: 10.1016/j.cell.2010.06.021.

Mahr, A. and Aberle, H. 2006. The expression pattern of the Drosophila vesicular glutamate transporter: A marker protein for motoneurons and glutamatergic centers in the brain. *Gene Expression Patterns* 6(3), pp. 299–309. doi: 10.1016/j.modgep.2005.07.006.

Maiuri, T. et al. 2013. The huntingtin N17 domain is a multifunctional CRM1 and Ran-dependent nuclear and cilial export signal. *Human Molecular Genetics* 22(7), pp. 1383–1394. doi: 10.1093/hmg/dds554.

Maiuri, T. et al. 2017. Huntingtin is a scaffolding protein in the ATM oxidative DNA damage response complex. *Human Molecular Genetics* 26(2), pp. 395–406. doi: 10.1093/hmg/ddw395.

Maiuri, T. and Truant, R. 2018. ROS-specific Huntingtin Interactions: In vitro poly-ADP ribose binding assays. Available at: https://zenodo.org/record/1411460.

Mangiarini, L. et al. 1996. Exon 1 of the HD Gene with an Expanded CAG Repeat Is Sufficient to Cause a Progressive Neurological Phenotype in Transgenic Mice. *Cell* 87, pp. 493–506. doi: 10.1016/S0092-8674(00)81369-0.

Mangiarini, L. et al. 1997. Instability of highly expanded CAG repeats in mice transgenic for the Huntington's disease mutation. *Nature Genetics* 15(2), pp. 197–200. doi: 10.1038/ng0297-197.

Manley, K. et al. 1999. Msh2 deficiency prevents in vivo somatic instability of the CAG repeat in Huntington disease transgenic mice. *Nature Genetics* 23(4), pp. 471–473. doi: 10.1038/70598.

Mao, Y. et al. 2016. Targeting TEAD/YAP-transcription-dependent necrosis, TRIAD, ameliorates Huntington's disease pathology. *Human Molecular Genetics* 25(21), pp. 4749–4770. doi: 10.1093/hmg/ddw303.

Marquette, A. et al. 2021. Membrane Interactions Accelerate the Self-Aggregation of Huntingtin Exon 1 Fragments in a Polyglutamine Length-Dependent Manner. *International Journal of Molecular Sciences* 22(13), p. 6725. doi: 10.3390/ijms22136725.

Martinez-Vicente, M. et al. 2010. Cargo recognition failure is responsible for inefficient autophagy in Huntington's disease. *Nature Neuroscience* 13(5), pp. 567–576. doi: 10.1038/nn.2528.

Masnata, M. et al. 2019. Demonstration of prion-like properties of mutant huntingtin fibrils in both in vitro and in vivo paradigms. *Acta Neuropathologica* 137(6), pp. 981–1001. doi: 10.1007/s00401-019-01973-6.

McAllister, B. et al. 2021. Timing and Impact of Psychiatric, Cognitive, and Motor Abnormalities in Huntington Disease. *Neurology* 96(19), pp. e2395–e2406. doi: 10.1212/WNL.0000000000011893.

McAllister, B. et al. 2022. Exome sequencing of individuals with Huntington's disease implicates FAN1 nuclease activity in slowing CAG expansion and disease onset. *Nature Neuroscience* 25(4), pp. 446–457. doi: 10.1038/s41593-022-01033-5.

McGill, J.K. and Beal, M.F. 2006. PGC-1α, a New Therapeutic Target in Huntington's Disease? *Cell* 127(3), pp. 465–468. doi: 10.1016/j.cell.2006.10.023.

McGuire, S.E. et al. 2003. Spatiotemporal rescue of memory dysfunction in Drosophila. *Science (New York, N.Y.)* 302(5651), pp. 1765–8. doi: 10.1126/science.1089035.

McGurk, L. et al. 2018. Poly (ADP-ribose) prevents pathological phase separation of TDP-43 by promoting liquid demixing and stress-granule localization. *Molecular cell* 71(5), pp. 703-717.e9. doi: 10.1016/j.molcel.2018.07.002.

McMurray, C.T. and Kortun, I.V. 2003. Repair in haploid male germ cells occurs late in differentiation as chromatin is condensing. *Chromosoma* 111(8), pp. 505–508. doi: 10.1007/s00412-003-0238-4.

McNulty, P. et al. 2018. Reduced Cancer Incidence in Huntington's Disease: Analysis in the Registry Study. *Journal of Huntington's Disease* 7(3), pp. 209–222. doi: 10.3233/JHD-170263.

Migliore, S. et al. 2019. Genetic Counseling in Huntington's Disease: Potential New Challenges on Horizon? *Frontiers in Neurology* 10. Available at: https://www.frontiersin.org/article/10.3389/fneur.2019.00453 [Accessed: 13 May 2022].

Mikule, K. and Wilcoxen, K. 2015. The PARP inhibitor, niraparib, crosses the blood brain barrier in rodents and is efficacious in a BRCA2-mutant intracranial tumor model. *Molecular Cancer Therapeutics* 14(12_Supplement_2), p. B168. doi: 10.1158/1535-7163.TARG-15-B168.

Miller, J. et al. 2010. Quantitative relationships between huntingtin levels, polyglutamine length, inclusion body formation, and neuronal death provide novel insight into huntington's disease molecular pathogenesis. *Journal of Neuroscience* 30(31), pp. 10541–10550. doi: 10.1523/JNEUROSCI.0146-10.2010.

Miller, J.P. et al. 2012. A Genome-Scale RNA–Interference Screen Identifies RRAS Signaling as a Pathologic Feature of Huntington's Disease. *PLOS Genetics* 8(11), p. e1003042. doi: 10.1371/journal.pgen.1003042.

Milnerwood, A.J. et al. 2010. Early Increase in Extrasynaptic NMDA Receptor Signaling and Expression Contributes to Phenotype Onset in Huntington's Disease Mice. *Neuron* 65(2), pp. 178–190. doi: 10.1016/j.neuron.2010.01.008.

Morigaki, R. and Goto, S. 2017. Striatal Vulnerability in Huntington's Disease: Neuroprotection Versus Neurotoxicity. *Brain Sciences* 7(6), p. 63. doi: 10.3390/brainsci7060063.

Moss, D.J.H. et al. 2017. Identification of genetic variants associated with Huntington's disease progression: a genome-wide association study. *The Lancet Neurology* 16(9), pp. 701–711. doi: 10.1016/S1474-4422(17)30161-8.

Murai, J. et al. 2012. Differential trapping of PARP1 and PARP2 by clinical PARP inhibitors. *Cancer research* 72(21), pp. 5588–5599. doi: 10.1158/0008-5472.CAN-12-2753.

Murai, J. et al. 2014. Stereospecific PARP trapping by BMN 673 and comparison with olaparib and rucaparib. *Molecular cancer therapeutics* 13(2), pp. 433–443. doi: 10.1158/1535-7163.MCT-13-0803.

Naito, M.G. et al. 2020. Sequential activation of necroptosis and apoptosis cooperates to mediate vascular and neural pathology in stroke. *Proceedings of the National Academy of Sciences* 117(9), pp. 4959–4970. doi: 10.1073/pnas.1916427117.

Negishi, T. 2016. Genome Stability in Drosophila: Mismatch Repair and Genome Stability. In: *Genome Stability: From Virus to Human Application*. Elsevier Inc., pp. 155–161. doi: 10.1016/B978-0-12-803309-8.00010-0.

Neueder, A. et al. 2017. The pathogenic exon 1 HTT protein is produced by incomplete splicing in Huntington's disease patients. *Scientific Reports* 7(1), p. 1307. doi: 10.1038/s41598-017-01510-z.

Neukomm, L.J. et al. 2014. Rapid in vivo forward genetic approach for identifying axon death genes in Drosophila. *Proceedings of the National Academy of Sciences of the United States of America* 111(27), pp. 9965–70. doi: 10.1073/pnas.1406230111.

Neveklovska, M. et al. 2012. Deletion of the huntingtin proline-rich region does not significantly affect normal huntingtin function in mice. *Journal of Huntington's disease* 1(1), pp. 71–87. doi: 10.3233/JHD-2012-120016.

Niens, J. et al. 2017. Dopamine Modulates Serotonin Innervation in the Drosophila Brain. *Frontiers in Systems Neuroscience* 11. Available at: https://www.frontiersin.org/article/10.3389/fnsys.2017.00076.

Oers, J.M.M. van et al. 2010. PMS2 endonuclease activity has distinct biological functions and is essential for genome maintenance. *Proceedings of the National Academy of Sciences* 107(30), pp. 13384–13389. doi: 10.1073/pnas.1008589107.

Okamoto, S. et al. 2009. Balance between synaptic versus extrasynaptic NMDA receptor activity influences inclusions and neurotoxicity of mutant huntingtin. *Nature Medicine* 15(12), pp. 1407–1413. doi: 10.1038/nm.2056.

Paldino, E. et al. 2017. Selective Sparing of Striatal Interneurons after Poly (ADP-Ribose) Polymerase 1 Inhibition in the R6/2 Mouse Model of Huntington's Disease. *Frontiers in Neuroanatomy* 11. Available at: https://www.frontiersin.org/articles/10.3389/fnana.2017.00061/full.

Paldino, E. et al. 2020. Modulation of Inflammasome and Pyroptosis by Olaparib, a PARP-1 Inhibitor, in the R6/2 Mouse Model of Huntington's Disease. *Cells* 9(10). Available at: https://www.ncbi.nlm.nih.gov/pmc/articles/PMC7602058/.

Panov, A.V. et al. 2002. Early mitochondrial calcium defects in Huntington's disease are a direct effect of polyglutamines. *Nature Neuroscience* 5(8), pp. 731–736. doi: 10.1038/nn884.

Pardiñas, A.F. et al. 2017. Identification of genetic variants associated with Huntington's disease progression: a genome-wide association study. *Articles Lancet Neurol* 16, pp. 701–712. doi: 10.1016/S1474-4422(17)30161-8.

Pasparakis, M. and Vandenabeele, P. 2015. Necroptosis and its role in inflammation. *Nature* 517(7534), pp. 311–320. doi: 10.1038/nature14191.

Paulsen, J. et al. 2001. Neuropsychiatric aspects of Huntington's disease. *Journal of Neurology, Neurosurgery, and Psychiatry* 71(3), pp. 310–314. doi: 10.1136/jnnp.71.3.310.

Paulsen, J.S. et al. 2008. Detection of Huntington's disease decades before diagnosis: the Predict-HD study. *Journal of Neurology, Neurosurgery & Psychiatry* 79(8), pp. 874–880. doi: 10.1136/jnnp.2007.128728.

Paulsen, J.S. et al. 2013. Cognitive decline in prodromal Huntington Disease: implications for clinical trials. *Journal of Neurology, Neurosurgery & Psychiatry* 84(11), pp. 1233–1239. doi: 10.1136/jnnp-2013-305114.

Pearce, M.M.P. et al. 2015. Prion-like transmission of neuronal huntingtin aggregates to phagocytic glia in the Drosophila brain. *Nature Communications* 6(1), pp. 6768–6768. doi: 10.1038/ncomms7768.

Pearce, M.M.P. and Kopito, R.R. 2018. Prion-Like Characteristics of Polyglutamine-Containing Proteins. *Cold Spring Harbor Perspectives in Medicine* 8(2), p. a024257. doi: 10.1101/cshperspect.a024257.

Pećina-Šlaus, N. et al. 2020. Mismatch Repair Pathway, Genome Stability and Cancer. *Frontiers in Molecular Biosciences* 7. Available at: https://www.frontiersin.org/articles/10.3389/fmolb.2020.00122/full.

Pfaffl, M.W. et al. 2002. Relative expression software tool (REST©) for group-wise comparison and statistical analysis of relative expression results in real-time PCR. *Nucleic Acids Research* 30(9), p. e36.

Picon, C. et al. 2021. Neuron-specific activation of necroptosis signaling in multiple sclerosis cortical grey matter. *Acta Neuropathologica* 141(4), pp. 585–604. doi: 10.1007/s00401-021-02274-7.

Pinto, R.M. et al. 2013. Mismatch Repair Genes Mlh1 and Mlh3 Modify CAG Instability in Huntington's Disease Mice: Genome-Wide and Candidate Approaches. Zeitlin, S. O. ed. *PLoS Genetics* 9(10), p. e1003930. doi: 10.1371/journal.pgen.1003930.

Pocas, G.M. et al. 2015. Alpha-Synuclein modifies mutant huntingtin aggregation and neurotoxicity in Drosophila. *Human Molecular Genetics* 24(7), pp. 1898–1907. doi: 10.1093/hmg/ddu606.

Pommier, Y. et al. 2016. Laying a trap to kill cancer cells: PARP inhibitors and their mechanisms of action. *Science Translational Medicine* . Available at: https://www.science.org/doi/abs/10.1126/scitranslmed.aaf9246.

Pons, M. et al. 2018. Identification of TCERG1 as a new genetic modulator of TDP-43 production in Drosophila. *Acta neuropathologica communications* 6(1), p. 138. doi: 10.1186/s40478-018-0639-5.

Portera-Cailliau, C. et al. 1995. *Evidence for Apoptotic Cell Death in Huntington Disease and Excitotoxic Animal Models*., pp. 3775–3787.

Pouladi, M.A. et al. 2012. Marked differences in neurochemistry and aggregates despite similar behavioural and neuropathological features of Huntington disease in the full-length BACHD and YAC128 mice. *Human Molecular Genetics* 21(10), pp. 2219–2232. doi: 10.1093/hmg/dds037.

Pringsheim, T. et al. 2012. The incidence and prevalence of Huntington's disease: a systematic review and meta-analysis. *Movement Disorders: Official Journal of the Movement Disorder Society* 27(9), pp. 1083–1091. doi: 10.1002/mds.25075.

Proskuryakov, S.Y. et al. 2003. Necrosis: A specific form of programmed cell death? *Experimental Cell Research* 283(1), pp. 1–16. doi: 10.1016/S0014-4827(02)00027-7.

Purice, M.D. et al. 2016. Delayed glial clearance of degenerating axons in aged Drosophila is due to reduced PI3K/Draper activity. *Nature communications* 7, p. 12871. doi: 10.1038/ncomms12871.

Qiu, R. et al. 2015. MutL traps MutS at a DNA mismatch. *Proceedings of the National Academy of Sciences* 112(35), pp. 10914–10919. doi: 10.1073/pnas.1505655112.

Quarrell, O.W.J. et al. 2007. Reduced penetrance alleles for Huntington's disease: a multi-centre direct observational study. *Journal of medical genetics* 44(3), p. e68. doi: 10.1136/jmg.2006.045120.

Quarrell, O.W.J. et al. 2013. Managing juvenile Huntington's disease. *Neurodegenerative disease management* 3(3), p. 10.2217/nmt.13.18. doi: 10.2217/nmt.13.18.

Quigley, J. 2017. Juvenile Huntington's Disease: Diagnostic and Treatment Considerations for the Psychiatrist. *Current Psychiatry Reports* 19(2), pp. 9–9. doi: 10.1007/s11920-017-0759-9.

Ramdzan, Y.M. et al. 2017. Huntingtin Inclusions Trigger Cellular Quiescence, Deactivate Apoptosis, and Lead to Delayed Necrosis. *Cell Reports* 19(5), pp. 919–927. doi: 10.1016/j.celrep.2017.04.029.

Rao, J. 2005. CHAPTER D1 - Clinical and Pathological Characteristics of Huntington Disease. In: LeDoux, M. ed. *Animal Models of Movement Disorders*. Burlington: Academic Press, pp. 299–307. Available at: https://www.sciencedirect.com/science/article/pii/B9780120883820500268.

Rass, E. et al. 2009. Role of Mre11 in chromosomal nonhomologous end joining in mammalian cells. *Nature Structural & Molecular Biology* 16(8), pp. 819–824. doi: 10.1038/nsmb.1641.

Ravi, D. et al. 2009. A network of conserved damage survival pathways revealed by a genomic RNAi screen. *PLoS Genetics* 5(6). doi: 10.1371/journal.pgen.1000527.

Ray Chaudhuri, A. and Nussenzweig, A. 2017. The multifaceted roles of PARP1 in DNA repair and chromatin remodelling. *Nature Reviews Molecular Cell Biology* 18(10), pp. 610–621. doi: 10.1038/nrm.2017.53.

Ray, M. and Lakhotia, S.C. 2015. The commonly used eye-specific sev-GAL4 and GMR-GAL4 drivers in Drosophila melanogaster are expressed in tissues other than eyes also. *Journal of Genetics* 94(3), pp. 407–416. doi: 10.1007/s12041-015-0535-8.

Ray, P.D. et al. 2012. Reactive oxygen species (ROS) homeostasis and redox regulation in cellular signaling. *Cellular signalling* 24(5), pp. 981–990. doi: 10.1016/j.cellsig.2012.01.008.

Raymond, L.A. 2003. Excitotoxicity in Huntington disease. *Clinical Neuroscience Research* 3(3), pp. 121–128. doi: 10.1016/S1566-2772(03)00054-9.

Reimers, J.M. et al. 2014. BDNF contributes to both rapid and homeostatic alterations in AMPA receptor surface expression in nucleus accumbens medium spiny neurons. *European Journal of Neuroscience* 39(7), pp. 1159–1169. doi: 10.1111/ejn.12422.

Richard, I.A. et al. 2022. Beyond PARP1: The Potential of Other Members of the Poly (ADP-Ribose) Polymerase Family in DNA Repair and Cancer Therapeutics. *Frontiers in Cell and Developmental Biology* 9. Available at: https://www.frontiersin.org/article/10.3389/fcell.2021.801200.

Riguet, N. et al. 2021. Nuclear and cytoplasmic huntingtin inclusions exhibit distinct biochemical composition, interactome and ultrastructural properties. *Nature Communications* 12(1), p. 6579. doi: 10.1038/s41467-021-26684-z.

Rinaldi, C. and Wood, M.J.A. 2018. Antisense oligonucleotides: the next frontier for treatment of neurological disorders. *Nature Reviews Neurology* 14(1), pp. 9–21. doi: 10.1038/nrneurol.2017.148.

Roberts, T.C. et al. 2020. Advances in oligonucleotide drug delivery. *Nature Reviews Drug Discovery* 19(10), pp. 673–694. doi: 10.1038/s41573-020-0075-7.

Robles-Murguia, M. et al. 2019. Tissue-specific alteration of gene expression and function by RU486 and the GeneSwitch system. *npj Aging and Mechanisms of Disease* 5(1), pp. 1–5. doi: 10.1038/s41514-019-0036-8.

Romero, E. et al. 2008. Suppression of Neurodegeneration and Increased Neurotransmission Caused by Expanded Full-Length Huntingtin Accumulating in the Cytoplasm. *Neuron* 57(1), pp. 27–40. doi: 10.1016/J.NEURON.2007.11.025.

Rosas-Arellano, A. et al. 2018. Molecular Sciences The Tiny Drosophila Melanogaster for the Biggest Answers in Huntington's Disease. doi: 10.3390/ijms19082398.

Rouleau, M. et al. 2010. PARP inhibition: PARP1 and beyond. *Nature reviews. Cancer* 10(4), pp. 293–301. doi: 10.1038/nrc2812.

Rüb, U. et al. 2015. The Neuropathology of Huntington´s disease: classical findings, recent developments and correlation to functional neuroanatomy. *Advances in Anatomy, Embryology, and Cell Biology* 217, pp. 1–146.

Rulten, S.L. and Caldecott, K.W. 2013. DNA strand break repair and neurodegeneration. *DNA Repair* 12(8), pp. 558–567. doi: 10.1016/j.dnarep.2013.04.008.

Ruocco, H.H. et al. 2006. Clinical presentation of juvenile Huntington disease. *Arquivos de Neuro-Psiquiatria* 64, pp. 5–9. doi: 10.1590/S0004-282X2006000100002.

Sahoo, B. et al. 2016. Folding Landscape of Mutant Huntingtin Exon1: Diffusible Multimers, Oligomers and Fibrils, and No Detectable Monomer. *PLOS ONE* 11(6), p. e0155747. doi: 10.1371/journal.pone.0155747.

Sameni, S. et al. 2020. Number and molecular brightness analysis reveals Htt25Q protein aggregation upon the uptake of Htt97Q aggregates. *Biochemical and Biophysical Research Communications* 522(1), pp. 133–137. doi: 10.1016/j.bbrc.2019.10.041.

Sandhu, S.K. et al. 2010. First-in-human trial of a poly(ADP-ribose) polymerase (PARP) inhibitor MK-4827 in advanced cancer patients (pts) with antitumor activity in BRCA-deficient and sporadic ovarian cancers. *Journal of Clinical Oncology* 28(15_suppl), pp. 3001–3001. doi: 10.1200/jco.2010.28.15_suppl.3001.

Sang, T.-K. et al. 2005. Inactivation of Drosophila Apaf-1 related killer suppresses formation of polyglutamine aggregates and blocks polyglutamine pathogenesis. *Human Molecular Genetics* 14(3), pp. 357–372. doi: 10.1093/hmg/ddi032.

Sapp, E. et al. 1995. Evidence for a preferential loss of enkephalin immunoreactivity in the external globus pallidus in low grade Huntington's disease using high resolution image analysis. *Neuroscience* 64(2), pp. 397–404. doi: 10.1016/0306-4522(94)00427-7.

Saudou, F. et al. 1998. Huntingtin Acts in the Nucleus to Induce Apoptosis but Death Does Not Correlate with the Formation of Intranuclear Inclusions. *Cell* 95(1), pp. 55–66. doi: 10.1016/S0092-8674(00)81782-1.

Saudou, F. and Humbert, S. 2016. The Biology of Huntingtin. *Neuron* 89(5), pp. 910–926. doi: 10.1016/J.NEURON.2016.02.003.

Sawa, A. et al. 1999. Increased apoptosis of Huntington disease lymphoblasts associated with repeat length-dependent mitochondrial depolarization. *Nature Medicine* 5(10), pp. 1194–1198. doi: 10.1038/13518.

Sawa, A. et al. 2003. Mechanisms of neuronal cell death in Huntington's disease. *Cytogenetic and Genome Research* 100(1–4), pp. 287–295. doi: 10.1159/000072864.

Sayre, L.M. et al. 2008. Oxidative Stress and Neurotoxicity. *Chemical Research in Toxicology* 21(1), pp. 172–188. doi: 10.1021/tx700210j.

Schiewer, M.J. and Knudsen, K.E. 2014. Transcriptional roles of PARP-1 in cancer. *Molecular cancer research : MCR* 12(8), pp. 1069–1080. doi: 10.1158/1541-7786.MCR-13-0672.

Schipper-Krom, S. et al. 2014. Dynamic recruitment of active proteasomes into polyglutamine initiated inclusion bodies. *FEBS letters* 588(1), pp. 151–159. doi: 10.1016/j.febslet.2013.11.023.

Schulte, J. and Littleton, J.T. 2011. The biological function of the Huntingtin protein and its relevance to Huntington's Disease pathology. *Current trends in neurology* 5, pp. 65–78.

Schuster, S. et al. 2019. Antiviral RNAi in Insects and Mammals: Parallels and Differences. *Viruses* 11(5), p. 448. doi: 10.3390/v11050448.

Sekelsky, J. 2017. DNA repair in Drosophila: Mutagens, models, and missing genes. *Genetics* 205(2), pp. 471–490. doi: 10.1534/genetics.116.186759.

Sepers, M.D. and Raymond, L.A. 2014. Mechanisms of synaptic dysfunction and excitotoxicity in Huntington's disease. *Drug Discovery Today* 19(7), pp. 990–996. doi: 10.1016/J.DRUDIS.2014.02.006.

Shehadeh, J. et al. 2006. Striatal neuronal apoptosis is preferentially enhanced by NMDA receptor activation in YAC transgenic mouse model of Huntington disease. *Neurobiology of Disease* 21(2), pp. 392–403. doi: 10.1016/j.nbd.2005.08.001.

Shelbourne, P.F. et al. 2007. Triplet repeat mutation length gains correlate with cell-type specific vulnerability in Huntington disease brain. *Human Molecular Genetics* 16(10), pp. 1133–1142. doi: 10.1093/hmg/ddm054.

Shen, K. et al. 2016. Control of the structural landscape and neuronal proteotoxicity of mutant Huntingtin by domains flanking the polyQ tract. *eLife* 5, p. e18065. doi: 10.7554/eLife.18065.

Shiraishi, R. et al. 2014. Systematic Analysis of Fly Models with Multiple Drivers Reveals Different Effects of Ataxin-1 and Huntingtin in Neuron Subtype-Specific Expression. Pandey, U. ed. *PLoS ONE* 9(12), p. e116567. doi: 10.1371/journal.pone.0116567.

Shirendeb, U. et al. 2011. Abnormal mitochondrial dynamics, mitochondrial loss and mutant huntingtin oligomers in Huntington's disease: implications for selective neuronal damage. *Human molecular genetics* 20(7), pp. 1438–55. doi: 10.1093/hmg/ddr024.

Silva, A.C. et al. 2020. Antisense oligonucleotide therapeutics in neurodegenerative diseases: the case of polyglutamine disorders. *Brain* 143(2), pp. 407–429. doi: 10.1093/brain/awz328.

Sinha, S. et al. 2021. PARP1-modulated chromatin remodeling is a new target for cancer treatment. *Medical Oncology* 38(10), p. 118. doi: 10.1007/s12032-021-01570-2.

Slade, D. et al. 2011. The structure and catalytic mechanism of a poly(ADP-ribose) glycohydrolase. *Nature* 477(7366), pp. 616–622. doi: 10.1038/nature10404.

Slepko, N. et al. 2006. Normal-repeat-length polyglutamine peptides accelerate aggregation nucleation and cytotoxicity of expanded polyglutamine proteins. *Proceedings of the National Academy of Sciences of the United States of America* 103(39), pp. 14367–14372. doi: 10.1073/pnas.0602348103.

Slow, E.J. et al. 2003. Selective striatal neuronal loss in a YAC128 mouse model of Huntington disease. *Human Molecular Genetics* 12(13), pp. 1555–1567. doi: 10.1093/hmg/ddg169.

Smith, G.A. et al. 2019. Glutathione S-Transferase Regulates Mitochondrial Populations in Axons through Increased Glutathione Oxidation. *Neuron* 103(1), pp. 52-65.e6. doi: 10.1016/j.neuron.2019.04.017.

Smith, M.A. et al. 2000. Motor Disorder in Huntington's Disease Begins as a Dysfunction in Error Feedback Control. *Nature* 403(6769), pp. 544–549. doi: 10.1038/35000576.

Smogorzewska, A. et al. 2010. A genetic screen identifies FAN1, a Fanconi anemia associated nuclease necessary for DNA interstrand crosslink repair. *Molecular cell* 39, pp. 36–47. doi: 10.1016/j.molcel.2010.06.023.

Snowden, J.S. 2017. The Neuropsychology of Huntington's Disease. *Archives of Clinical Neuropsychology* 32(7), pp. 876–887. doi: 10.1093/arclin/acx086.

Soares, L. et al. 2014. Axon injury and regeneration in the adult drosophila. *Scientific Reports* 4. doi: 10.1038/srep06199.

Squitieri, F. et al. 1994. DNA haplotype analysis of Huntington disease reveals clues to the origins and mechanisms of CAG expansion and reasons for geographic variations of prevalence. *Human Molecular Genetics* 3(12), pp. 2103–2114. doi: 10.1093/hmg/3.12.2103.

Srinivas, U.S. et al. 2019. ROS and the DNA damage response in cancer. *Redox Biology* 25, p. 101084. doi: 10.1016/j.redox.2018.101084.

Stamatakou, E. et al. 2018. Huntington's Disease. 1780, pp. 17–29. doi: 10.1007/978-1-4939-7825-0.

Stanley, C.B. et al. 2011. Structural Formation of Huntingtin Exon 1 Aggregates Probed by Small-Angle Neutron Scattering. *Biophysical Journal* 100(10), pp. 2504–2512. doi: 10.1016/j.bpj.2011.04.022.

Steffan, J.S. et al. 2001. Histone deacetylase inhibitors arrest polyglutamine-dependent neurodegeneration in Drosophila. *Nature* 413(6857), pp. 739–743. doi: 10.1038/35099568.

Steffen, J.D. et al. 2016. Fluorescent sensors of PARP-1 structural dynamics and allosteric regulation in response to DNA damage. *Nucleic Acids Research* 44(20), pp. 9771–9783. doi: 10.1093/nar/gkw710.

Steger, M. et al. 2013. Prolyl Isomerase PIN1 Regulates DNA Double-Strand Break Repair by Counteracting DNA End Resection. *Molecular Cell* 50(3), pp. 333–343. doi: 10.1016/j.molcel.2013.03.023.

Stewart, G.S. et al. 1999. The DNA Double-Strand Break Repair Gene hMRE11 Is Mutated in Individuals with an Ataxia-Telangiectasia-like Disorder. *Cell* 99(6), pp. 577–587. doi: 10.1016/S0092-8674(00)81547-0.

Stoker, T.B. et al. 2022. Huntington's disease: diagnosis and management. *Practical Neurology* 22(1), pp. 32–41. doi: 10.1136/practneurol-2021-003074.

Stout, J.C. et al. 2011. Neurocognitive signs in prodromal Huntington disease. *Neuropsychology* 25(1), pp. 1–14. doi: 10.1037/a0020937.

Stracker, T.H. and Petrini, J.H.J. 2011. The MRE11 complex: starting from the ends. *Nature Reviews Molecular Cell Biology* 12(2), pp. 90–103. doi: 10.1038/nrm3047.

Suk, T.R. and Rousseaux, M.W.C. 2020. The role of TDP-43 mislocalization in amyotrophic lateral sclerosis. *Molecular Neurodegeneration* 15(1), p. 45. doi: 10.1186/s13024-020-00397-1.

Sun, Y. et al. 2021. PARylation prevents the proteasomal degradation of topoisomerase I DNA-protein crosslinks and induces their deubiquitylation. *Nature Communications* 12(1), p. 5010. doi: 10.1038/s41467-021-25252-9.

Swami, M. et al. 2009. Somatic expansion of the Huntington's disease CAG repeat in the brain is associated with an earlier age of disease onset. *Human molecular genetics* 18(16), pp. 3039–47. doi: 10.1093/hmg/ddp242.

Syntichaki, P. and Tavernarakis, N. 2003. The biochemistry of neuronal necrosis: Rogue biology? *Nature Reviews Neuroscience* 4(8), pp. 672–684. doi: 10.1038/nrn1174.

Tabrizi, S.J. et al. 2013. Predictors of phenotypic progression and disease onset in premanifest and early-stage Huntington's disease in the TRACK-HD study: analysis of 36-month observational data. *The Lancet Neurology* 12(7), pp. 637–649. doi: 10.1016/S1474-4422(13)70088-7.

Tabrizi, S.J. et al. 2019a. Huntingtin Lowering Strategies for Disease Modification in Huntington's Disease. *Neuron* 101(5), pp. 801–819. doi: 10.1016/j.neuron.2019.01.039.

Tabrizi, S.J. et al. 2019b. Targeting Huntingtin Expression in Patients with Huntington's Disease. *New England Journal of Medicine* . Available at: https://www.nejm.org/doi/10.1056/NEJMoa1900907 [Accessed: 11 May 2021].

Tabrizi, S.J. et al. 2022. Potential disease-modifying therapies for Huntington's disease: lessons learned and future opportunities. *The Lancet Neurology* 21(7), pp. 645–658. doi: 10.1016/S1474-4422(22)00121-1.

Takano, H. and Gusella, J.F. 2002. The predominantly HEAT-like motif structure of huntingtin and its association and coincident nuclear entry with dorsal, an NF-kB/Rel/dorsal family transcription factor. *BMC Neuroscience* 3, p. 15. doi: 10.1186/1471-2202-3-15.

Tamura, T. et al. 2011. Ku70 alleviates neurodegeneration in Drosophila models of Huntington's disease. *PloS one* 6(11), p. e27408. doi: 10.1371/journal.pone.0027408.

Tan, Z. et al. 2015. Huntington's disease cerebrospinal fluid seeds aggregation of mutant huntingtin. *Molecular Psychiatry* 20(11), pp. 1286–1293. doi: 10.1038/mp.2015.81.

Tang, T.-S. et al. 2005. Disturbed Ca2+ signaling and apoptosis of medium spiny neurons in Huntington's disease. *Proceedings of the National Academy of Sciences* 102(7), pp. 2602–2607. doi: 10.1073/pnas.0409402102.

Tao, M. et al. 2019. Structure of Membrane-Bound Huntingtin Exon 1 Reveals Membrane Interaction and Aggregation Mechanisms. *Structure* 27(10), pp. 1570-1580.e4. doi: 10.1016/j.str.2019.08.003.

Tartari, M. et al. 2008. Phylogenetic Comparison of Huntingtin Homologues Reveals the Appearance of a Primitive polyQ in Sea Urchin. *Molecular Biology and Evolution* 25(2), pp. 330–338. doi: 10.1093/molbev/msm258.

Taylor, R.C. et al. 2008. Apoptosis: controlled demolition at the cellular level. *Nature Reviews Molecular Cell Biology* 9(3), pp. 231–241. doi: 10.1038/nrm2312.

Telenius, H. et al. 1993. Molecular analysis of juvenile Huntington disease: the major influence on (CAG)n repeat length is the sex of the affected parent. *Human Molecular Genetics* 2(10), pp. 1535–1540. doi: 10.1093/hmg/2.10.1535.

Thaker, H.M. and Kankel, D.R. 1992. Mosaic analysis gives an estimate of the extent of genomic involvement in the development of the visual system in Drosophila melanogaster. *Genetics* 131(4), pp. 883–894.

The Huntington's Disease Collaborative Research Group 1993. A Novel Gene Containing a Trinucleotide Repeat That Is Expanded and Unstable on Huntington's Disease Chromosomes. *Cell* 72, pp. 971–983.

Thomas, B.J. and Wassarman, D.A. 1999. A fly's eye view of biology. *Trends in Genetics* 15(5), pp. 184–190. doi: 10.1016/S0168-9525(99)01720-5.

Thompson, L.H. and West, M.G. 2000. XRCC1 keeps DNA from getting stranded. *Mutation Research/DNA Repair* 459(1), pp. 1–18. doi: 10.1016/S0921-8777(99)00058-0.

Thompson, L.M. et al. 2009. IKK phosphorylates Huntingtin and targets it for degradation by the proteasome and lysosome. *Journal of Cell Biology* 187(7), pp. 1083–1099. doi: 10.1083/jcb.200909067.

Thongtip, S. et al. 2016. Fan1 deficiency results in DNA interstrand cross-link repair defects, enhanced tissue karyomegaly, and organ dysfunction. *Genes & Development* 30, pp. 645–659. doi: 10.1101/gad.276261.115.

Tian, L. et al. 2009. Distinct Nucleotide Binding/Hydrolysis Properties and Molar Ratio of MutSα and MutSβ Determine Their Differential Mismatch Binding Activities. *The Journal of Biological Chemistry* 284(17), pp. 11557–11562. doi: 10.1074/jbc.M900908200.

Tomé, S. et al. 2013. MSH3 Polymorphisms and Protein Levels Affect CAG Repeat Instability in Huntington's Disease Mice. Barsh, G. S. ed. *PLoS Genetics* 9(2), p. e1003280. doi: 10.1371/journal.pgen.1003280.

Trottier, Y. et al. 1994. Instability of CAG repeats in Huntington's disease: Relation to parental transmission and age of onset. *Journal of Medical Genetics* 31(5), pp. 377–382. doi: 10.1136/jmg.31.5.377.

Trushina, E. and McMurray, C.T. 2007. Oxidative stress and mitochondrial dysfunction in neurodegenerative diseases. *Neuroscience* 145(4), pp. 1233–1248. doi: 10.1016/j.neuroscience.2006.10.056.

Uhlén, M. et al. 2015. Tissue-based map of the human proteome. *Science* 347(6220), p. 1260419. doi: 10.1126/SCIENCE.1260419.

Vagnoni, A. and Bullock, S.L. 2016. A simple method for imaging axonal transport in aging neurons using the adult Drosophila wing. *Nature Protocols* 11(9), pp. 1711–1723. doi: 10.1038/nprot.2016.112.

Vagnoni, A. and Bullock, S.L. 2018. A cAMP/PKA/Kinesin-1 Axis Promotes the Axonal Transport of Mitochondria in Aging Drosophila Neurons. *Current Biology* 28(8), pp. 1265-1272.e4. doi: 10.1016/j.cub.2018.02.048.

Van Raamsdonk, J.M. et al. 2005. Loss of wild-type huntingtin influences motor dysfunction and survival in the YAC128 mouse model of Huntington disease. *Human Molecular Genetics* 14(10), pp. 1379–1392. doi: 10.1093/hmg/ddi147.

Vasudevan, D. and Ryoo, H.D. 2016. Detection of Cell Death in Drosophila Tissues. *Methods in molecular biology (Clifton, N.J.)* 1419, pp. 131–144. doi: 10.1007/978-1-4939-3581-9_11.

Venkatraman, P. et al. 2004. Eukaryotic Proteasomes Cannot Digest Polyglutamine Sequences and Release Them during Degradation of Polyglutamine-Containing Proteins. *Molecular Cell* 14(1), pp. 95–104. doi: 10.1016/S1097-2765(04)00151-0.

Verma, M. et al. 2022. Excitotoxicity, calcium and mitochondria: a triad in synaptic neurodegeneration. *Translational Neurodegeneration* 11(1), p. 3. doi: 10.1186/s40035-021-00278-7.

Vilinsky, I. and Johnson, K.G. 2012. Electroretinograms in Drosophila: a robust and genetically accessible electrophysiological system for the undergraduate laboratory. *Journal of undergraduate neuroscience education : JUNE : a publication of FUN, Faculty for Undergraduate Neuroscience* 11(1), pp. A149-57.

Vis, J.C. et al. 2005. Expression pattern of apoptosis-related markers in Huntington's disease. *Acta Neuropathologica* 109(3), pp. 321–328. doi: 10.1007/s00401-004-0957-5.

Vonsattel, J.-P. et al. 1985. Neuropathological Classification of Huntington's Disease. *Journal of Neuropathology & Experimental Neurology* 44(6), pp. 559–577. doi: 10.1097/00005072-198511000-00003.

Vu, A. et al. 2018. Polyglutamine repeat proteins disrupt actin structure in Drosophila photoreceptors. *Molecular and Cellular Neuroscience* 93, pp. 10–17. doi: 10.1016/J.MCN.2018.08.005.

Wagner, A.S. et al. 2018. Self-assembly of Mutant Huntingtin Exon-1 Fragments into Large Complex Fibrillar Structures Involves Nucleated Branching. *Journal of Molecular Biology* 430(12), pp. 1725–1744. doi: 10.1016/J.JMB.2018.03.017.

Wang, X. and Ge, P. 2020. Parthanatos in the pathogenesis of nervous system diseases. *Neuroscience* 449, pp. 241–250. doi: 10.1016/j.neuroscience.2020.09.049.

Wang, Y. et al. 2009. Poly(ADP-ribose) signals to mitochondrial AIF: A key event in parthanatos. *Experimental Neurology* 218(2), pp. 193–202. doi: 10.1016/j.expneurol.2009.03.020.

Watts, J.K. and Corey, D.R. 2012. Gene silencing by siRNAs and antisense oligonucleotides in the laboratory and the clinic. *The Journal of pathology* 226(2), pp. 365–379. doi: 10.1002/path.2993.

Wave Life Sciences 2021. Wave Life Sciences Announces Initiation of Dosing in Phase 1b/2a SELECT-HD Clinical Trial of WVE-003 in Huntington's Disease. Available at: https://ir.wavelifesciences.com/news-releases/news-release-details/wave-life-sciences-announces-initiation-dosing-phase-1b2a-select.

Weiss, K.R. et al. 2012. Huntingtin aggregation kinetics and their pathological role in a Drosophila Huntington's disease model. *Genetics* 190(2), pp. 581–600. doi: 10.1534/genetics.111.133710.

Weiss, K.R. and Littleton, J.T. 2016. Characterization of axonal transport defects in Drosophila Huntingtin mutants. *Journal of neurogenetics* 30(3–4), pp. 212–221. doi: 10.1080/01677063.2016.1202950.

Wellington, C.L. et al. 1998. Caspase Cleavage of Gene Products Associated with Triplet Expansion Disorders Generates Truncated Fragments Containing the Polyglutamine Tract *. *Journal of Biological Chemistry* 273(15), pp. 9158–9167. doi: 10.1074/jbc.273.15.9158.

Wexler, N.S. et al. 2004. Venezuelan kindreds reveal that genetic and environmental factors modulate Huntington's disease age of onset. *Proceedings of the National Academy of Sciences of the United States of America* 101(10), pp. 3498–503. doi: 10.1073/pnas.0308679101.

Wheeler, V.C. et al. 1999. Length-dependent gametic CAG repeat instability in the Huntington's disease knock-in mouse. *Human Molecular Genetics* 8(1), pp. 115–122. doi: 10.1093/HMG.

Wheeler, V.C. et al. 2000. Long glutamine tracts cause nuclear localization of a novel form of huntingtin in medium spiny striatal neurons in HdhQ92 and HdhQ111 knock-in mice. *Human Molecular Genetics* 9(4), pp. 503–513. doi: 10.1093/hmg/9.4.503.

Wheeler, V.C. et al. 2003. Mismatch repair gene Msh2 modifies the timing of early disease in HdhQ111 striatum. *Human Molecular Genetics* 12(3), pp. 273–281. doi: 10.1093/hmg/ddg056.

Wheeler, V.C. and Dion, V. 2021. Modifiers of CAG/CTG Repeat Instability: Insights from Mammalian Models. *Journal of Huntington's Disease* 10(1), pp. 123–148. doi: 10.3233/JHD-200426.

Wild, E.J. and Tabrizi, S.J. 2017. Therapies targeting DNA and RNA in Huntington's disease. *The Lancet Neurology* 16(10), pp. 837–847. doi: 10.1016/S1474-4422(17)30280-6.

Wilson, C.J. 2009. Striatum: Internal Physiology. In: Squire, L. R. ed. *Encyclopedia of Neuroscience*. Oxford: Academic Press, pp. 563–572. Available at: https://www.sciencedirect.com/science/article/pii/B9780080450469013012.

Wright, G.E.B. et al. 2019. Length of Uninterrupted CAG, Independent of Polyglutamine Size, Results in Increased Somatic Instability, Hastening Onset of Huntington Disease. *American Journal of Human Genetics* 104(6), pp. 1116–1126. doi: 10.1016/j.ajhg.2019.04.007.

Xiao, Y. and Weaver, D.T. 1997. Conditional gene targeted deletion by Cre recombinase demonstrates the requirement for the double-strand break repair Mre11 protein in murine embryonic stem cells. *Nucleic Acids Research* 25(15), pp. 2985–2991. doi: 10.1093/nar/25.15.2985.

Xie, Y. et al. 2010. BDNF Overexpression in the Forebrain Rescues Huntington's Disease Phenotypes in YAC128 Mice. *The Journal of Neuroscience* 30(44), pp. 14708–14718. doi: 10.1523/JNEUROSCI.1637-10.2010.

Xu, T. et al. 2018. Molecular mechanism and therapy application of necrosis during myocardial injury. *Journal of Cellular and Molecular Medicine* 22(5), pp. 2547–2557. doi: 10.1111/jcmm.13575.

Yager, L.M. et al. 2015. The ins and outs of the striatum: Role in drug addiction. *Neuroscience* 301, pp. 529–541. doi: 10.1016/j.neuroscience.2015.06.033.

Yamamoto, S. et al. 2014. A drosophila genetic resource of mutants to study mechanisms underlying human genetic diseases. *Cell* 159(1), pp. 200–214. doi: 10.1016/j.cell.2014.09.002.

Yamanishi, E. et al. 2017. A novel form of necrosis, TRIAD, occurs in human Huntington's disease. *Acta Neuropathologica Communications* 5(1), p. 19. doi: 10.1186/s40478-017-0420-1.

Yang, D. et al. 2010. Expression of Huntington's disease protein results in apoptotic neurons in the brains of cloned transgenic pigs. *Human Molecular Genetics* 19(20), pp. 3983–3994. doi: 10.1093/hmg/ddq313.

Yang, W. et al. 2002. Aggregated polyglutamine peptides delivered to nuclei are toxic to mammalian cells. *Human Molecular Genetics* 11(23), pp. 2905–2917. doi: 10.1093/hmg/11.23.2905.

Yang, Y. et al. 2013. Neuronal necrosis and spreading death in a Drosophila genetic model. *Cell Death and Disease* 4(7), pp. e723–e723. doi: 10.1038/cddis.2013.232.

Yano, H. et al. 2014. Inhibition of mitochondrial protein import by mutant huntingtin. *Nature Neuroscience* 17(6), pp. 822–831. doi: 10.1038/nn.3721.

Yao, Y. et al. 2015. A striatal-enriched intronic GPCR modulates huntingtin levels and toxicity. Ramaswami, M. ed. *eLife* 4. Available at: https://doi.org/10.7554/eLife.05449.

Yhnell, E. et al. 2016. A Longitudinal Motor Characterisation of the HdhQ111 Mouse Model of Huntington's Disease. *Journal of Huntington's Disease* 5(2), pp. 149–161. doi: 10.3233/JHD-160191.

Ying, Y. and Padanilam, B.J. 2016. Regulation of necrotic cell death p53, PARP1 and Cyclophilin D - overlapping pathways of regulated necrosis? *Cellular and molecular life sciences : CMLS* 73(11–12), pp. 2309–2324. doi: 10.1007/s00018-016-2202-5.

Yohrling, G. et al. 2020. Prevalence of Huntington's Disease in the US (954). *Neurology* 94(15 Supplement). Available at: https://n.neurology.org/content/94/15_Supplement/954.

Yu, Y. et al. 2021a. Parp mutations protect from mitochondrial toxicity in Alzheimer's disease. *Cell Death & Disease* 12(7), p. 651. doi: 10.1038/s41419-021-03926-y.

Yu, Z. et al. 2021b. Necroptosis: A Novel Pathway in Neuroinflammation. *Frontiers in Pharmacology* 12. Available at: https://www.frontiersin.org/article/10.3389/fphar.2021.701564.

Zhang, H. et al. 2008. Full length mutant huntingtin is required for altered Ca2+ signaling and apoptosis of striatal neurons in the YAC mouse model of Huntington's disease. *Neurobiology of disease* 31(1), pp. 80–88. doi: 10.1016/j.nbd.2008.03.010.

Zhao, B. et al. 2010. The Hippo–YAP pathway in organ size control and tumorigenesis: an updated version. *Genes & Development* 24(9), pp. 862–874. doi: 10.1101/gad.1909210.

Zheng, J. et al. 2018. A Mitochondria-Associated Oxidative Stress Perspective on Huntington's Disease. *Frontiers in Molecular Neuroscience* 11. Available at: https://www.frontiersin.org/article/10.3389/fnmol.2018.00329.

Zhou, F.-M. 2020. Chapter 25 - The striatal medium spiny neurons: what they are and how they link with Parkinson's disease. In: Martin, C. R. and Preedy, V. R. eds. *Genetics, Neurology, Behavior, and Diet in Parkinson's Disease*. Academic Press, pp. 395–412. Available at: https://www.sciencedirect.com/science/article/pii/B9780128159507000254.

Zuccato, C. et al. 2003. Huntingtin interacts with REST/NRSF to modulate the transcription of NRSE-controlled neuronal genes. *Nature Genetics* 35(1), pp. 76–83. doi: 10.1038/ng1219.

Zuccato, C. et al. 2011. Brain-derived neurotrophic factor in patients with Huntington's disease. *PloS One* 6(8), p. e22966. doi: 10.1371/journal.pone.0022966.

Zuccato, C. and Cattaneo, E. 2007. Role of brain-derived neurotrophic factor in Huntington's disease. *Progress in Neurobiology* 81(5), pp. 294–330. doi: 10.1016/j.pneurobio.2007.01.003.